ORNL-3160

Contract No. W-7405-eng-26

METALLURGY DIVISION ANNUAL PROGRESS REPORT

for Period Ending May 31, 1961

J. H Frye, Jr., Director
W. D. Manly, Associate Director
J. E. Cunningham, Assistant Director

DATE ISSUED

AUG 17 1961

OAK RIDGE NATIONAL LABORATORY
Oak Ridge, Tennessee
operated by
UNION CARBIDE CORPORATION
for the
U. S. ATOMIC ENERGY COMMISSION

DISCLAIMER

METALLURGY DIVISION ANNUAL PROGRESS REPORT

SUMMARY

PART I. FUNDAMENTAL METALLURGY

The Fundamental Research Section of the Metallurgy Division is composed of eight groups whose interests include a wide range of metallurgy and metal physics and chemistry. Studies of crystal structures, phase transformations, radiation damage, order-disorder phenomena, oxidation, crystal growth, molten-salt media, mechanical deformation, preferred orientation, and alloy theory are being carried out.

1. Theory of Alloying

The Theory of Alloying Group studies alloy models and the basic factors which control solid solubilities, thermodynamics, and electrical properties of alloys. During the year a theory of axial ratios of hexagonal metals was extended, and the effect of various solutes on the axial ratio of zirconium was found to be consistent with the theory. The α/β boundaries in the cadmium-zirconium system were observed to be in agreement with a prediction calculated from thermodynamic properties derived from vapor pressures. Specific-heat investigations of α-Zr-Ag alloys were continued in the temperature range 1–4°K, and improvements were made in the accuracy of the calorimeter. To begin Fermi surface studies by means of oscillatory phenomena and studies of the effect of various solutes on the zirconium transition from the superconducting to the normal state, superconductivity magnets are now under development. Particular attention has been given to the compound Nb_3Sn clad with niobium. An iron-core electromagnet with superconducting coils of this material was made, and fields of 23,000 gauss were achieved.

2. X-Ray Studies of Crystalline Defects

Certain diffraction research is carried out in the X-Ray Studies of Crystalline Defects Group. Here line-broadening and diffuse-scattering measurements are of main interest. At present, work is being done on short-range order in alloys and on the structure of very thin oxide films grown on copper.

3. Reactions at Metal Surfaces

The oxidation research referred to above is being done in collaboration with the Reactions at Metal Surfaces Group. This group is concerned with the factors that determine the degree of protectiveness of oxide films grown on metals. It has been found that severe strains exist in the films grown on several metals, and indications are that such strains play an important role in destroying the protective character of the films. Measurements of the optical anisotropy of Cu_2O films grown on copper have been made and have been correlated with the x-ray diffraction research mentioned above. Studies of the oxidation of tantalum and the sulfurization of tantalum have been carried out also.

4. Crystal Physics

The Crystal Physics Group is interested in the growth processes of single crystals of high-temperature materials. Efforts are being made to grow crystals of a number of oxides (including those of uranium and thorium) and certain rare-earth nitrides. A valuable by-product of the activities of this group is that it will be a source of special single crystals of controlled quality and purity for other research groups at the Laboratory.

5. Spectroscopy of Ionic Media

Though at present the Spectroscopy of Ionic Media Group is primarily engaged in the study of the absorption spectra of molten salts, it will soon extend its activities to include work on crystalline solids. To that end, the growth of large single crystals of high perfection and purity has been started. Crystals of KCl and $NaNO_3$ have already been successfully produced. As in

the case of the Crystal Physics Group, this source of special materials will benefit other research programs at the Laboratory.

During the past year measurements of the absorption spectrum of bismuth in $BiCl_3$ melts have shown that probably two solute species are present in the melt. This work considerably narrows the possible specific species which may exist. Dilute solutions of bismuth in $BiBr_3$ melts, $BiCl_3$-KCl melts, and ionic nitrate melts have also been investigated.

6. Deformation of Crystalline Solids

A calorimeter for the measurement of the energy stored in metals during deformation was constructed and placed in operation during the past year by the Deformation of Crystalline Solids Group. The calorimeter is capable of operating over a range of temperatures, and satisfactory results have been obtained for alloys for which the quantity of energy stored is large. Further refinements will probably be necessary for making precision measurements on pure metals.

7. Structure of Metals

The Structure of Metals Group continued its investigation of low-temperature phase transformations in cerium. Work done in collaboration with the X-Ray Diffraction Group has identified the temperature intervals in which three different crystalline forms of cerium exist between room temperature and 4.2°K for samples given different mechanical treatment. It has been shown, with the help of the Neutron Diffraction Group of the Physics Division, that a change in the electronic configuration of cerium occurs for one of these crystalline forms. Preferred-orientation measurements were made on 3% Si–Fe and on aluminum, and twinning studies of vanadium and niobium were carried out. This group also measured, by diffraction techniques, deformation-stacking fault probabilities in lead, some lead alloys, aluminum, thorium, and cerium and is engaged in a study of the effect of impurities on the rate of recrystallization of metals.

8. X-Ray Diffraction

The X-ray Diffraction Group, in addition to its own research problems, functions as a general service laboratory for the division. A large number of routine analyses such as parameter measurements, orientation measurements, phase identifications, and stress determinations have been done as a service activity. Problems of a more than routine nature include an effort to understand the nature of radiation damage in BeO, a study of aging transformations in Zr-Nb, Zr-Cr, Zr-V, and U-Nb alloys, and a study of ordering in Cu-Au alloys. Crystal-structure investigations of $LuMnO_3$ and of certain phases in binary oxide systems containing BeO are also being carried out.

PART II. LONG-RANGE APPLIED METALLURGY

9. Physical Properties Studies

The Physical Properties Group continued studies of methods of determining thermal conductivity and the influence of the chemical and physical state of UO_2 on thermal conductivity. A thermal comparator was built and was calibrated and put into operation at temperatures of 50 to 600°C. The influence of grain size on thermal conductivity is being studied in this apparatus. Radial heat-flow equipment was modified so that data accurate to ±5% can be achieved for temperatures to 800°C.

10. Sintering Studies

The Sintering Studies Group has found a rough correlation between sinterability of ThO_2 and surface area, crystallite size, and immersion density for powders prepared by different methods but calcined at the same temperature. A change in the calcination temperature resulted in no correlation with those factors. The factor most consistent with sinterability was particle integrity under strong agitation. Preliminary studies of weld-neck growth between thoria spheres indicate that a plastic-flow mechanism may be the rate-controlling factor at 1800°C. Sintering rate studies show a peak and a minimum in the densification rate at 1000 and 1200°C, respectively. The diffusion coefficients of oxygen and thorium in ThO_2 are being determined.

11. Solid Reaction Studies

The Solid Reaction Studies Group has developed techniques for determining the diffusion of solid fission products in fuel and cladding materials. Preliminary data have been obtained for Zr^{95}, Nb^{95}, and Sr^{85} in zirconium and in uranium dioxide. The diffusion coefficients of Al^{26} and Mn^{54} were determined in high-purity aluminum from 500 to

650°C. Beryllium was found to react with uranium monocarbide in the range 700 to 1000°C, with the formation of UBe_{13}. There appears to be a marked increase in the rate of reaction between 750 and 800°C.

12. Zirconium Alloy Research

The Zirconium Alloy Research Group has obtained transformation data on iodide zirconium, Zircaloy-2, Zr–15% Nb, Zr–15% Nb–2% Mo, Zr-Mo, Zr-Cu, and Zr-Pd alloys by resistivity measurements during heating and cooling cycles and during isothermal treatments. Oxidation-rate measurements by a newly developed differential rate technique have shown that the oxidation of iodide zirconium and Zircaloy-2 in pure oxygen is not a smooth function of time. Optical equipment and methods are being developed for the study of oxide films *in situ*. The methods promise to give information useful for the characterization of oxides formed under varying conditions.

PART III. REACTOR METALLURGY

13. Ceramics Technology

Tests of SiC, Si-SiC, and pyrolytic-carbon coatings on graphite sleeves for the Experimental Gas-Cooled Reactor (EGCR) fuel elements showed that only the first two provided satisfactory oxidation resistance at 600°C and that a special isotropic grade of base graphite is required. Chemical tests showed that the increase in the thermal-neutron absorption cross section σ_a of the coated sleeves is primarily due to the silicon. Mechanical tests on sleeves that were found by eddy-current testing to be defective indicated that such sleeves, despite their defects, are acceptable for reactor use.

Unfueled graphite components with a bulk density of 2.09 g/cm^3 were produced, by using natural graphite and phenol-formaldehyde type binders. Satisfactory fueled graphite pellets containing pyrolytic-carbon-coated UC_2-UC particles were prepared by dry blending, cold pressing at 90,000 psi, and firing to 1000°C in argon.

A program directed toward the use of coated-particle fuel elements (particularly UC_2 and UC_2-ThC_2 coated with pyrolytic carbon) was initiated. Irradiation tests in the LITR and ORR were designed, and experimental techniques for pre- and postirradiation examinations were developed.

A wide variety of UO_2 shapes were prepared to specified dimensional and density requirements, by using ceramic-grade oxide powder. Varying the length of sintering time in hydrogen at 1750°C provided control over the extent of grain growth; argon was observed to be an effective grain-growth inhibitor. Preliminary studies of the oxygen-uranium system showed that oxygen loss in UO_{2+x} was significant at temperatures as low as 1450°C in a hydrogen-free atmosphere.

A method was developed for characterizing spheroidal UO_2 particles for use in metallic dispersion-type fuel elements. By embedding known weights of particles into known weights of epoxy resins, density determinations reproducible to ±0.01 g/cm^3 were obtained. Prolonged etching in nitric acid left an organic skeleton replica of the open pores of the particles. Consideration of the density and the amount of open porosity allowed for a critical evaluation of the usefulness of spheroidal particles.

Studies showed that Experimental Gas-Cooled Reactor (EGCR) UO_2 fuel pellets rapidly attain equilibrium with atmospheric moisture at a concentration of 23 to 30 ppm of moisture and that a moisture content of 10 ppm can be achieved at 25°C by mechanical evacuation pumping preceding the helium back-fill and end-closure steps during fuel element fabrication.

Particle-size distribution was found to be a primary factor controlling the density achieved during vibratory compaction of fused uranium-thorium oxide in fuel element tubes. By use of selected proportions of various size fractions of fused oxide, a density of 8.94 g/cm^3 was obtained; with only coarse and fine particles, the maximum density was 8.68 g/cm^3. Continuous size distributions compacted to densities between 8.54 and 8.74 g/cm^3. With dense oxides prepared by a sol-gel technique, density variations from 8.49 to 8.86 g/cm^3 were observed. For a given oxide and particle-size distribution, the average deviation of the density of a set of vibratorily compacted elements varied by only 0.2 to 0.6% of the average density.

The control problems associated with the preparation of a ThO_2 powder to be used for forming domed-end cylinders proved to be so difficult that the method was abandoned and an alternative method was developed. By use of a slightly modified slurry-type oxide, cubes were pressed

with the aid of a Carbowax binder. The green cubes were tumbled dry to essentially spherical shape, fired to 1350°C, polished by wet tumbling, and then fired to 1800°C to produce $\frac{1}{8}$-in. spheres with a density of 9.5 g/cm^3. The spheres were free of cracks and laminations.

Slow cooling (20°C/min) of a CaO-BeO mixture (40 mole % CaO, 60 mole % BeO) from 1500 to 1300°C produced a two-phase structure of BeO and CaO, while rapid cooling (160°C/sec) over the range of 1500 to 850°C produced $Ca_2Be_3O_5$ as an intermediate phase. This compound could not be produced by long heating of oxide mixtures at subsolidus temperature or by slow cooling and long soaking at various temperatures. An intermediate compound, $2BeO{\cdot}Y_2O_3$, was obtained by quenching melted mixtures of that system, but no such behavior was noted in the BeO-Eu_2O_3 system. The eutectic composition in the latter system is at approx 12 wt % BeO and 1425°C. An intermediate compound was observed in the BeO-SrO system. By using a porous plate of BeO as an absorber for the very fluid eutectic liquids encountered in these systems, and a thin wafer of mixed oxides, it was possible to establish the eutectic temperatures and compositions in the BeO-MgO, BeO-CeO_2, and BeO-ZrO_2 systems. Thermogravimetric studies were begun for the uranium-oxygen system at temperatures up to 2000°C under controlled oxygen pressures.

When pure BeO bodies that had been cold pressed without binder were sintered in hydrogen at 1750°C, a density of 95% of theoretical was obtained; bodies pressed with the aid of organic binders sintered to only 85 to 88% of theoretical. Grain growth was produced in high-density pieces by prolonged heating in hydrogen at 1750°C, but not in low-density pieces nor in air at 1500°C.

Beryllium oxide bodies containing up to 30 vol % of UO_2 or UO_2-ThO_2 mixtures were cold pressed from powders (submicron-size particles) without binders and sintered in argon at 1750°C to 95% of theoretical density. When larger particles, 150 to 250 μ, were used, cracking and nonuniform shrinkage were observed. These effects were minimized but not eliminated by adjusting the shrinkage of the UO_2, by slowing the rate of removal of the organic binder by means of a preliminary heating period, and by adjusting the heating rate during sintering.

A radial heat-flow apparatus constructed for use in studying the thermal conductivity of nuclear ceramics generated data with a precision of ±2% and an accuracy of at least ±5%, between room temperature and 800°C. Slight discontinuities in the thermal conductivity of INOR-8 were observed at 450 and 680°C. Specimens of UO_2 were fabricated and were characterized for thermal-conductivity studies to 1500°C in this apparatus.

Differential thermal analysis of Eu_2O_3 heated to 1200°C gave no evidence for the cubic-to-monoclinic transformation, but x-ray diffraction analysis of the heated material showed both phases to be present after heating. Holding the monoclinic phase at 950°C for 100 hr failed to convert any of the oxide to the cubic phase.

The sintering behavior of various rare-earth oxides was studied in hydrogen and in oxygen atmospheres at 1300, 1500, and 1600°C. Wide variations in final sintered densities were observed for the various oxides, with no correlation being found between sintered density and atomic number or crystal form. Low density values were measured for Gd_2O_3, CeO_2, Nd_2O_3, Tb_4O_7, Dy_2O_3, Ho_2O_3, and Er_2O_3 at 1600°C, while approximately theoretical density was achieved with Pr_6O_{11} and Sm_2O_3 at 1300°C.

Fansteel 82 alloy (32½% Ta, ¾% Zr, 66¾% Nb) did not react with Al_2O_3, BeO, or ZrO_2 at temperatures up to 2000–2100°C. Severe reaction of this alloy with various materials was observed as follows: beryllium at 1465°C, UC at 1355°C, TiO_2 at 1775°C, graphite and MgO at 1800 to 1900°C, and ThO_2 or UO_2 between 2000 and 2100°C.

14. Corrosion Engineering

An experimental program has been in progress to evaluate the compatibility of stainless and low-alloy steels under extended exposures to helium contaminated by CO and CO_2 in the temperature range 1100 to 1500°F. Steels containing 7% or more chromium in these tests exhibited relatively light oxide films and correspondingly low weight gains at impurity concentrations up to 1.0 vol % CO_2 and 0.25 vol % CO. The oxidation rates of these materials showed little dependence on impurity concentrations or ratios. Lower alloy materials exposed at 1100°F were severely oxidized by helium containing mixtures of CO_2 and CO as low as 100 ppm each. The extent of

oxidation of the latter materials increased as a function of impurity concentration.

Studies of the interdiffusion of graphite and type 304 stainless steel in direct contact have indicated that bonding of these materials may take place at 1300°F and at contact pressures as low as 500 psi. Pretreatment of the type 304 stainless steel surfaces by oxidation or copperplating successfully inhibits such bonding.

The corrosion properties of Inconel and INOR-8 during prolonged exposures to fluoride salt mixtures have been under study in forced-convection loops operating from one to two years. Results of these loop experiments, operated at maximum temperatures of 1200 to 1300°F, have indicated very low corrosion rates for INOR-8 but substantial corrosion losses for the higher chromium Inconel. INOR-8 loops normally showed only a thin intermetallic surface film following salt exposure, although one salt containing 20 mole % UF_4 resulted in shallow surface pitting along hot-leg surfaces. Inconel loops exhibited subsurface void formation to depths as great as 24 mils at the point of maximum salt temperature.

15. Fuels Evaluation

The fission-gas-retention properties of ceramic fuel bodies composed of dispersions of UO_2 in BeO, UC_2 particles coated with pyrolytic carbon, and a solid solution of 5 wt % UO_2 in ThO_2 were determined. From the properties the applicability of these fuels to the Experimental Gas-Cooled Reactor (EGCR) or advanced gas-cooled reactors can be evaluated. A study was also made of the basic phenomena governing the irradiation behavior of dispersion fuels.

The neutron-activation method was used to determine the fission-gas-retention properties of the ceramic fuels. It involves low-temperature irradiations followed by heat treatments ex-pile, during which the rates of release of Xe^{133} are measured.

Results of tests on bulk UO_2 at 1400°C showed that there is a good correlation between D' values and BET (nitrogen) surface areas. A value of the diffusion coefficient for Xe^{133} in bulk UO_2 of 7.5×10^{-16} cm^2/sec was computed from data obtained at 1400°C.

The mechanism of release of Xe^{133} from 30 vol % UO_2 in BeO was found to be diffusion at temperatures in the range 1200 to 1600°C. A high rate of release was observed at 1800°C, which was attributed to rapid grain growth and phase redistribution.

Studies on UC_2 particles coated with pyrolytic carbon by the Minnesota Mining and Manufacturing Company showed that the coatings retained Xe^{133} very well at temperatures up to 1825°C. At 2050°C and above, the coatings ruptured and released a large fraction of the Xe^{133} contained in the particles.

The mechanism of release of Xe^{133} from 5 wt % UO_2–ThO_2 was observed to be the same as that from bulk UO_2. However, ThO_2 is less volatile than UO_2; therefore the temperature at which sublimation is the controlling step in the release process is approximately 400°C higher in ThO_2 than in bulk UO_2.

A failure analysis of dispersion fuel elements indicated that low-temperature tests on dispersions of boron carbide particles in copper should lead to an understanding of UO_2–stainless steel fuel elements at elevated temperatures.

16. Materials Compatibility

Studies have been initiated to determine the equilibrium solubility of oxygen in liquid potassium, the most efficient methods of reducing the oxygen content of potassium, and the effect of oxygen contamination of potassium on its elevated-temperature corrosiveness.

Compatibility tests in refluxing-potassium capsule systems indicate that iron-base alloys have better corrosion resistance than nickel- or cobalt-base alloys. Results for type 316 stainless steel loops containing boiling potassium show attacks of less than 2 mils after 3000 hr of operation.

Seven high-temperature alloys were exposed to static air for 100 hr at 1800 and 2000°F. Inconel and Haynes alloy No. 25 were the most oxidation-resistant alloys of those tested.

Mass transfer between stainless steel and niobium in the Nb–Na–stainless steel system was investigated for temperatures in the range from 1500 to 1800°F. Nitrogen and carbon transferred from the stainless steel to the niobium. Substantial changes in the mechanical properties of niobium were observed in dissimilar-metal tests conducted with this alloy.

The vapor pressure of NaK (43.7 wt % K) was determined in the temperature range 1520 to 1832°F.

A radiographic technique was used to determine the distribution of fused salt in low-permeability graphite. Salt pickup at 1300°F and 150 psig was limited to shallow (<50 mils) surface permeation.

The quantity of salt that can be forced into graphite may be increased by prior heating of the graphite in air, which probably enlarges the pores of the graphite.

The density and resistance to salt permeation under pressure are apparently decreased for a particular grade of graphite as the size of the fabricated piece is increased. The shape of the fabricated piece also modifies these characteristics.

A relatively constant quantity of uranium (as UO_2) per unit bulk volume of AGOT graphite precipitated from an $LiF\text{-}BeF_2\text{-}UF_4$ mixture when equal quantities of the salt were exposed for 100 hr to different volumes of graphite at 1300°F. Additions of ZrF_4 and ThF_4 to fluoride salts were found to prevent the precipitation of UO_2 in salt-graphite systems.

Treating graphite with molten fluoride salts removed some of the oxygen contamination from the graphite. Exposure of graphite to the thermal decomposition products of ammonium bifluoride appeared to remove all the oxygen contamination.

INOR-8 specimens exposed for 14,000 hr to $LiF\text{-}BeF_2\text{-}UF_4$ in contact with bare graphite at 1300°F were unattacked, and the room-temperature and 1250°F tensile properties of the alloy were unaltered.

Studies on corrosion problems associated with various fuel processing systems, particularly the fluoride volatility process, are summarized.

17. Mechanical Properties

Research has been concerned with obtaining information and data for the solution of reactor design problems. The effort has included study of the mechanical properties of materials in-pile, investigation of the variables that affect the deformation and fracture of materials at elevated temperature, and development of new testing techniques which extend the capability of the group in the above areas.

The apparatus that was designed to allow simulation of the thermal and mechanical environment of the Experimental Gas-Cooled Reactor (EGCR) fuel element was successfully used to study the effects of external pressure and thermal cycling on the performance of the fuel element. Results of these experiments were correlated quite satisfactorily with effects observed in irradiation experiments on fuel elements.

The properties of type 304 stainless steel and Inconel in the presence and absence of irradiation are being investigated in conjunction with the Solid State Division. The temperature dependence of the irradiation effect on the stress rupture of type 304 stainless steel was determined in the range 1300 to 1600°F. The possible effect of the helium generated in Inconel from the $B^{10}(n,\alpha)$ reaction in-pile was studied at 1500°F. The results thus far do not conclusively prove that the observed irradiation effects on the stress-rupture life of Inconel are caused by this reaction.

Brazing of the midplane spacer on the EGCR fuel element was observed to cause abnormal grain growth during the thermal cycle needed to braze with GE-81 alloy. Studies indicated that the stress-rupture properties were adversely affected by this type of structure. The use of a lower brazing temperature afforded by a copper braze solved this problem.

Experimental and analytical work began on the general problem of the buckling of shells under external pressure. This problem is of interest because the primary failure criterion for the EGCR loops may be that of buckling.

The spectrum of mechanical properties of graphite in EGCR moderator blocks has been determined. The variations in properties were found to be a function of position in the block. The outside surfaces generally appear to be stronger. Attempts to measure a creep rate in graphite by careful experimental techniques under various conditions of loading showed that at temperatures up to 1100°F graphite does not exhibit time-dependent deformation.

The general-mechanical-properties research on the effects of environment and fatigue has continued to progress. The effects of hydrogen on the creep properties of high-temperature alloys have been under detailed investigation. The effects of CO_2 on stainless steels are being investigated, and the carburization observed is being studied by means of C^{14} tracer techniques and autoradiography. The mechanisms by which interstitials affect the properties of niobium and its alloys are being studied by two methods. One is by observing

the mechanical-property changes which occur, and the second is by investigating the interstitial interactions by use of internal friction.

Correlations between cyclic and monotonic creep fatigue have been obtained. Several theories for low-temperature fatigue have been tested against results obtained at elevated temperatures. Preliminary investigation of the effects of combined stresses on fatigue has been undertaken.

Several in-pile experiments have been performed to investigate the swelling of beryllium due to the $Be^9(n,2n)$ and (n,α) reactions which produce helium in the metal. In-pile and out-of-pile tube-burst experiments at 600 and 700°C on beryllium indicate that the stress-rupture properties of beryllium in-pile are strongly affected by the integrated flux.

The effect of stress state on the deformation and fracture of Zircaloy-2 is being investigated. It has been determined that Hill's method of weighting the principal shears may be used to describe the mechanical anisotropy.

18. Metal Forming and Casting

Fabrication work was directed toward developing materials for three potential areas of application: (1) low-temperature reactors (60 to 180°F), (2) medium-temperature reactors (400 to 1100°F), and high-temperature systems (>1100°F).

In the low-temperature reactor field, postirradiation examinations of aluminum-base fuels developed for applications in which the uranium is limited to 20% enrichment of the U^{235} isotope were almost completed. The results revealed that at exposures as high as 6.5×10^{20} fissions/cc (60% burnup of U^{235} atoms) dispersions of U_3O_8 and UAl_3 did not exhibit any gross dimensional changes. On the other hand, dispersions of UC_2 did not show acceptable behavior.

Despite inherent limitations at elevated temperatures, aluminum-base materials have been selected as the structural material for fuel element construction in the design of high-neutron-flux reactors. Type 6061 aluminum, for example, is the reference cladding material for the High-Flux Isotope Reactor (HFIR). Recent development work culminating in the manufacture of the 171-plate and 369-plate fuel elements for the criticality test program indicated that fabrication of these rather complex elements is possible. Fuel plates with a variation in uranium content across the plate width were prepared by using a 24 wt % U–Al alloy as well as a dispersion of 26 wt % U_3O_8 in aluminum. In the latter, 0.07 wt % B_4C was added homogeneously as a burnable poison. The composite fuel plates were formed to the specified involute shapes to close tolerances. The main problem encountered was pronounced blistering of the fuel plates during roll cladding. The technical feasibility of mechanically assembling the plates into the required unit with exceedingly close dimensional control was demonstrated.

Stainless steel continues to be an attractive cladding material for medium-temperature reactors, and studies have progressed on swage-clad UO_2 rods as well as on dispersions of UO_2 in stainless steel. The discovery that fused-and-ground UO_2 contains appreciable quantities of nitrogen was a significant contribution. It appears that this impurity must be kept to a minimum in order to eliminate potential swelling in swage-clad rods during brazing into fuel bundles, or later while under irradiation. In applications requiring high specific power, dispersions of UO_2 in stainless steel continue to show promise, and a program for developing fabrication techniques for dispersing 36 wt % spherical UO_2 in rather thick stainless steel plates has been successfully completed. Incorporation of the burnable poison in this fuel system has been utilized to advantage but has been plagued with erratic losses of boron during fabrication. Studies have been completed, and a topical report is in press which shows that the loss is related to the oxygen as well as to the hydrogen present in the conventional heat-treating atmospheres. It was concluded that vacuum treatments would be required to eliminate losses.

In the development of stainless-clad plate-type neutron absorbers, postirradiation examination of 3 wt % B^{10}–Fe material was completed, with the conclusion that the limit of B^{10} burnup prior to the onset of swelling is 5%. It was demonstrated by the manufacture of a full-size absorber section for test in the SM-1 reactor that plates can be economically made with variations in boron throughout the thickness. The test is designed to extend the burnup limit from 5 to 25%. The first irradiation results on 30 wt % dispersions of Eu_2O_3 in stainless steel showed that no microstructural or dimensional changes occurred after exposures as high as 9×10^{20} *nvt*.

In the development of high-temperature materials, investigations revealed that stoichiometric UC can be arc melted and cast into sound shapes without disturbing the stoichiometry. Careful mold design was necessary to minimize the exposure time of molten UC to graphite in order to prevent the formation of UC_2. Irradiation tests are planned on this product as part of the research in the advanced material development for the EGCR.

Investigations in the arc-melting of niobium alloys showed that it was possible to remelt, without significant contamination, material that had been purified by electron-beam melting. Niobium alloys containing from 64 to 1800 ppm nitrogen were reproducibly prepared and used for ductility studies. Those containing up to 420 ppm nitrogen were very ductile, but beyond this value a very rapid decrease in ductility occurred.

19. Metallography

Improved metallographic techniques have been developed for the evaluation of the microstructure of uranium-rich molybdenum alloys and zirconium-base alloys containing copper. The procedures are different, but involve electrolytic polishing and etching as well as either vacuum cathodic etching or etching by means of conventional chemical immersion. Optically flat surfaces are produced which, on examination, give sufficient resolution and detail for reliable grain-size determinations, phase identification, and analysis of microporosity.

Several innovations are being utilized to facilitate the metallographic processing of cold and hot specimens of both metal and ceramic materials. An embedment technique involving the use of a lead peroxide–boric acid glass finds application in the examination of ThO_2 particles. A prepolymer of diallyl phthalate in the form of a milled glass-fiber resin shows promise as a metallographic mounting material for handling radioactive samples. A new cloth with superior polishing and wearing characteristics, compared with standard silk or nylon, is being tested.

Cursory observation of metallographic mounts reveals that uranium dicarbide is more stable than uranium carbide on long exposure to room-temperature air.

The hot-hardness characteristics of several reactor materials of construction have been investigated. Hardness data at elevated temperature are presented for 1100- and 3003-grade aluminum alloys, type 502 stainless steel, and 29 wt % Mo–Ni alloy in the annealed and aged condition. Similar data are plotted for thorium and several thorium-base alloys.

20. Nondestructive Test Development

Standard industrial testing practices are usually not adequate for the more stringent requirements in the nuclear industry. Therefore considerable effort has been directed toward the development of improved techniques for the various testing problems posed by nuclear technology. These have included studies in the use of ultrasonics, electromagnetics, penetrating radiation, and other methods.

In the past year, most of the ultrasonic development work was directed toward studies of ultrasonic testing of thin metal sections and the properties of ultrasound, with particular emphasis on the detection of nonbonded areas. This included the evaluation of braze bonds of stainless steel tubing and sheath-to-copper disks, the inspection of flat-plate fuel elements, and the testing of the bond in duplex and triplex tubing.

Electromagnetic or eddy-current studies have included the development of new techniques and equipment for the measurement of such dimensions as interplate and interrod coolant-channel spacing. A prototype eddy-current test system with a wide choice of operating frequency has been constructed for use on test problems which are very frequency-sensitive. Studies are in progress to measure the magnetic field associated with different test-coil configurations to facilitate the design of new test systems.

One phase of the penetrating-radiation program has been the investigation of low-voltage radiographic conditions for the radiography of thin sections of steel, aluminum, and beryllium. X-ray attenuation coefficients have been measured by scintillation spectrometry on various alloys associated with power, compact, and research reactors. Further gamma-absorption studies are being directed toward the measurement of fuel-loading density in swaged and vibratorily compacted fuel rods. Work is continuing on the assay of U^{235}, by using the self-emitted gamma irradiation and scintillation spectrometry.

Most of the development of nondestructive tests for the evaluation of problem materials has been directed toward beryllium, graphite, and graphite coatings. Among the most useful test methods for

graphite have been low-voltage radiography and eddy currents. These two methods along with ultrasonics and penetrants have found applications for the inspection of beryllium.

Development work in support of the Gas-Cooled Reactor Program included the inspection of coatings on graphite, the remote inspection of experimental-loop through-tube weldments, and the nondestructive evaluation of beryllium tubing.

A series of studies was conducted to determine the applicability of nondestructive testing techniques to the measurement or evaluation of certain desired properties in the core B Fermi fuel element. The problems were the measurement of clad thickness, detection of nonbond, detection of core inhomogeneity, and measurement of coolant-channel spacing.

A large number of fuel plates were inspected for the first critical assembly of the High-Flux Isotope Reactor (HFIR), by using newly developed ultrasonic, radiographic, and eddy-current techniques.

21. Physical Metallurgy

In physical metallurgy, two problem areas have been investigated: the study of gas-metal reactions and the study of alloy stability.

Oxidation and carburization experiments on type 304 stainless steel were carried out as part of the Experimental Gas-Cooled Reactor (EGCR) project. The oxidation rates of type 304 stainless steel in CO_2-CO atmospheres up to 982°C were found to depend on the oxide which formed on the metal. When protective oxides formed, the reaction rates were insensitive to the concentration and the composition of the gases; however, when nonprotective oxides formed, the reaction rates depended on P_{CO_2}/P_{CO}. Carburization of the alloy depended mainly on temperature, time, and $(P_{CO})^2/P_{CO_2}$.

Research to understand the accelerated corrosion of beryllium in gaseous environments is part of the program on the development of advanced-type fuel elements for gas-cooled reactors. Beryllium reacts with high-temperature CO_2 to form BeO and Be_2C. In atmospheres of $H_2O(g)$ the metal is oxidized and decarburized; in hydrogen atmospheres it is decarburized. The oxidation reactions resulted in the formation of protective oxide films, and the decarburization reaction caused an accelerated rate of grain-boundary oxidation. The temperatures investigated were 550–725°C.

Because of a combination of low capture cross section and elevated-temperature strength, niobium-base alloys are attractive materials for use as cladding for fuel elements and for various structural components of a reactor system. Lack of oxidation resistance is the main obstacle to general use of this class of alloys, and development work has continued in attempts to understand better the oxidation mechanism in order to solve the problem through alloying. In addition, efforts are directed toward an engineering solution through cladding of these alloys with metals which afford oxidation protection.

Niobium alloys that exhibit decreased oxidation rates at 1000 and 1200°C at atmospheric pressure oxidized at a faster rate than the unalloyed metal at low pressures. The reaction rates for niobium and its alloys in low-pressure air were an order of magnitude lower than in an equivalent pressure of pure oxygen.

The poor oxidation resistance of niobium at elevated temperatures is also a major drawback associated with its use for construction of a reactor coolant system. The use of triplex tubing, however, offers a promising approach toward protecting the niobium and overcoming the reliability problem in air heat exchangers or radiator applications.

Aging reactions observed in annealed Nb–1% Zr alloys were determined to be due to the precipitation of a phase which ultimately becomes ZrO_2. Correlations between the aging response, the oxygen content of the alloy, and the annealing temperatures were developed.

The use of alloy fuels for fast reactors of the Fermi type depends to some extent on the strength and stability of the alloy system. The transformations occurring in γ-stabilized U-Mo alloys weaken or strengthen the alloy, depending on the molybdenum content. The strongest alloy at 550°C appears to be U–13% Mo. The rate of transformation from γ to $\alpha + \gamma'$ decreases with increasing molybdenum content. This rate is accelerated by an order of magnitude when cold work precedes the transformation heat treatment.

INOR-8, which has been selected to contain fluoride melts for the Molten-Salt Reactor Experiment, is a solid-solution alloy, except for carbides, up to 1092°C. Intermetallic compounds were observed in alloys containing 20% Mo–10% Cr–10% Fe and in 18% Mo–8% Cr–8% Fe. An ordering reaction which becomes significant at 540°C

causes an increase in the specific heat of INOR-8. A decrease in the values of the specific heat above 610°C is attributed to a disordering reaction.

22. Postirradiation Examination

The gamma spectrometer with its associated collimator recently installed in the hot cells located in Building 4501 has proved to be a valuable nondestructive tool for postirradiation examination of various test components. For example, the newly designed collimator provided sufficient resolution and definition to allow identification of specific gamma emitters retained in the first in-pile thoria slurry loop after operation and drainage of the slurry, which also contained small quantities (additives) of uranium and palladium in D_2O. Moreover, the equipment was successfully used in locating a plug noted during operation of the first UO_2SO_4 solution loop tested in the ORR HN-1 facility and, hence, greatly facilitated the subsequent cutup operation for corrosion evaluation. Spectral measurements on a cermet composed of a Eu_2O_3 dispersion in stainless steel, which is under consideration as a control material for application in the Pressurized Water Reactor Program of the Army, showed the equipment to have real potential in performing nondestructive burnup analysis.

In-cell examination of four in-pile slurry autoclaves revealed that a significant quantity of fines had been produced during irradiation of thoria spheres under static conditions. In one instance, a black, vitreous deposit, having an apparent bulk density of approx 1, was found at the liquid-vapor interface region of the autoclave.

In order to assist corrosion evaluation, two remote-replication techniques are being successfully utilized to obtain topographical information on the surfaces of materials exposed to various media. Reliable replicas of the internal surfaces of autoclaves after in-pile testing are being produced by centrifugally casting a thin section of RTV silicone rubber with a modified curing agent, while the cellulose acetate technique is giving good results on reproducing the topography of metallographically polished and etched specimens.

The application of the Questar telescope, which was used for macroscopic examination of the interior of the HRE-2 core vessel, has been extended to allow inspection of the interior surfaces of the fluorinator and hydrofluorinator vessels after service in the Volatility Pilot Plant of the Chemical Technology Division.

The X-Ray Diffraction Group has collaborated with the Philips Electronics Company in the design and construction of a diffractometer for the examination of radioactive samples for the HRLEL facility.

A remote scanning tank was designed and fabricated for the ultrasonic inspection of high-level irradiated components in the HRLEL. Further remote measurements were made of the wall thickness of the core vessel of Homogeneous Reactor Experiment No. 2.

23. Powder Metallurgy and Fuel Cycle

Fuels composed of uranium carbide bonded with uranium silicide, which offer the advantages of excellent fabricability, high uranium density, and low thermal-neutron-absorption cross section, have been fabricated by conventional pressing and sintering techniques. Bodies cemented with 5, 10, and 15 wt % USi_2 were consolidated to a density of 97% of theoretical by firing for 2 hr at 1650°C. The constitution of the bodies after firing was determined by x-ray diffraction analysis to be UC plus α USi_2.

Exploratory studies to determine the effects of alloying on the high-temperature properties of thorium point to a number of interesting alloys. Hot hardness at 600°C shows a fourfold increase over that for unalloyed thorium when 4 wt % indium is added, and a threefold increase is noted with a 5 wt % zirconium addition. At 750°C, these improvements are even larger. At 400°C, a Th–0.2 wt % Be–0.2 wt % C alloy appears promising, giving a $3\frac{1}{2}$-fold increase in hot hardness. Limited hot-tensile tests tend to confirm these strengthening effects.

Plate composites of 25 vol % UO_2 dispersed in depleted U–15 wt % Mo with molybdenum cladding have been successfully roll clad at 1150°C, giving a sound core structure and good metallurgical bonding at the clad-core interface. Fuel cores also were made by using 20 vol % UC as the dispersoid. These fertile-matrix dispersion fuels offer promise of high burnup and thermal performance with excellent breeding gain for fast-reactor application.

Structurally sound and strong alloy rods ($\frac{3}{16}$ in. in diameter, U–10 to 15 wt % Mo) have been fabricated from both elemental and prealloyed powders

by rotary swaging at 1050°C, with a reduction in area of about 60%.

A refractory-type borosilicate glass (containing 4 wt % B_2O_3) was examined as a potential poison for Army Package Power Reactor type fuel application. Pressing and plate fabrication studies, in which the borated glass together with UO_2 was incorporated in a type 347 stainless steel matrix, showed the glass to possess remarkable resistance to stringering and to reaction with the other core constituents. Because the borosilicate glass retained its boron during fabrication and has good irradiation stability, it is tentatively adjudged superior to poisons previously tested.

In early fuel-core fabrication studies on the HFIR (High-Flux Isotope Reactor) Project, a procedure was developed for cold-pressing powders ($Al-U_3O_8-B_4C$) into a symmetrical, straight-taper geometry. Good dimensional control, density, homogeneity, and reproducibility were achieved.

A process was developed for making a mock target for the HFIR critical experiment. Methods for batch blending UO_2, silver, and aluminum in the proportions designated to simulate the neutron-absorption properties of the actual target materials were determined. Also, pressing procedures were established for producing cores of controlled density, homogeneity, and isotope inventory.

To evaluate materials for the "gray" section of a prospective HFIR control element, pressing and compatibility studies were conducted on Mn, Ta, W, TaC, and WC in aluminum matrix powder. Whereas the tantalum-aluminum, TaC-Al, and WC-Al systems pressed satisfactorily, the tantalum-aluminum system appears to be the most promising on the basis of both fabricability and compatibility. Evaluations indicated compacts of tantalum-aluminum to be dimensionally stable for 500 hr at 600°C and to have been hot roll-clad successfully in an aluminum sheathing.

24. Welding and Brazing

The developmental projects carried out are primarily project connected and, consequently, vary quite widely in scope. The development of suitable joining techniques for unique and unusual materials of interest in reactor technology comprises a major effort. The development of satisfactory beryllium welding and brazing procedures has been accomplished to the extent that in-pile beryllium radiation capsules have been successfully fabricated, as have over 200 high-temperature tube-burst capsules. Welding studies on niobium in the form of Nb–1% Zr alloy have been concentrated on the study of the high-temperature aging phenomenon occurring in welds in this alloy, and methods for circumventing the phenomenon have been developed. Brazing alloys which readily wet and flow on niobium have also been developed, with the base metals for these alloys being titanium and zirconium.

A weld-cracking problem associated with one heat of INOR-8 has been investigated, and it is thought to result from an improper melting practice used by the vendor. Good weldability has been demonstrated for heats made with improved procedures. A nickel-base alloy, INCO BP-85, has been found to be a suitable filler metal for welding stainless steels to ferritic steels for high-temperature cyclic service. Procedures have been developed which appear to be applicable for fabricating reactor shells and vaned assemblies from Zircaloy-2.

Suitable procedures are being developed for fabricating fuel elements and other components of interest in the various reactor projects. For the HFIR project, a critical element of aluminum alloy was successfully fabricated by welding. Fuel elements of stainless steel have been successfully built to extremely close tolerances as a support effort for the Fermi Reactor Project. Procedures have been developed for fabricating complex, instrumented stainless steel fuel elements for the Gas-Cooled Reactor Program. Techniques have also been determined for repeatedly opening and closing quick-disconnect-type joints using solidified-metal seals.

CONTENTS

Part I

FUNDAMENTAL METALLURGY

1. THEORY OF ALLOYING

LATTICE CONSTANTS OF α-ZIRCONIUM ALLOYS[1]

J. O. Betterton, Jr. D. S. Easton

The axial ratios of close-packed hexagonal metals and alloys, according to theories of Jones[2,3] and Goodenough,[4] depend upon the electronic energy for cases where the Fermi surface is nearly spherical (i.e., s-type bands) and where the electrostatic interaction of the valency electrons and the ions and the exchange interaction between ions can be neglected. Magnesium and its alloys[5] and the noble-metal brasses[6] appear to agree with this hypothesis. A shear in the crystal structure will necessarily produce a shear in the Brillouin zone. With this shear, the electronic energies of those states of the Fermi surface near a zone face are altered so that a force is exerted on the zone face much like that of surface tension.

The d electrons in zirconium are unlikely to have spherical energy contours in k space, and as an added complication, an overlapping of five different bands of electrons is likely to be present.

The perturbation of the d-electron states near the zone boundary is assumed to reduce their energy, and the $E(k)$ surface is assumed to be lowest at the center of the {0002} face and to rise to a maximum value at the center of the $\{10\bar{1}0\}$ faces. Should this d band contain somewhat less than two electrons, the $1/a$ distances would be distorted from values corresponding to ideal close packing to smaller $1/a$ distances by the attractive interaction of the electrons and the zone face. Other factors being equal, the axial ratio would be reduced as is observed in α-zirconium. Theoretical calculations by Lehman[7] on a similar hexagonal metal, titanium, and calculations on other transition metals[8,9] show d bands with $E(k)$ surfaces of this type and a small number of electrons in the overlapping s-p band.

Overlap of the first d band to form another band is assumed to occur with a minimum energy on the {0002} face. As the average number of electrons in zirconium is increased by alloying, this overlap would tend to reduce $1/c$ distances and expand the axial ratios. If the number of electrons in the new band is small, the effects should be large initially and diminish with still further additions.

The effects on the lattice parameters of the B-subgroup elements, Ag, Cd, In, Sn, and Sb, in the same long period as zirconium, are in substantial agreement with this model. Because these solutes all have about the same atomic size, the a dimensions follow approximately a common curve. The c spacings, in marked contrast with the a dimensions, change in a systematic manner with the valency of the solute added. Assuming that 1, 2, 3, 4, and 5 electrons, respectively, are contributed to the alloy by the solute atoms Ag, Cd, In, Sn, and Sb, the effect of the increased valency is to rotate the c-dimension curve upward.

The relationship to the shear strain in the modified Jones theory is seen more clearly in terms of axial ratios, since the effects of slight volume changes in the alloys are eliminated. The variation of the axial ratio is in general not quite linear with composition, and the present theory fits better at lower concentrations. The situation

---

[1]Paper presented at 1961 Annual Meeting of the AIME, St. Louis, Mo., Feb. 26–Mar. 1; abstract published in *J. Metals* 13, 86 (1961).

[2]H. Jones, *Proc. Roy. Soc. (London)* **147A**, 396 (1934).

[3]H. Jones, *Phil. Mag.* **41**, 663 (1950).

[4]J. Goodenough, *Phys. Rev.* **89**, 282 (1953).

[5]G. V. Raynor, *The Physical Metallurgy of Magnesium and Its Alloys*, Pergamon, New York, 1959.

[6]J. B. Massalski and H. W. King, *Acta Met.* **8**, 684 (1960).

[7]G. W. Lehman and T. G. Berlincourt, *Final Report on Research on Electron Energy States in Transition Metals*, AI-1889 (February 1957).

[8]M. F. Manning and M. I. Chodorow, *Phys. Rev.* **56**, 787 (1939).

[9]G. C. Fletcher, "Density of States Curve for the 3d Electrons in Nickel," *Proc. Phys. Soc.* **A65**, 192 (1952).

may be shown more clearly as the derivative of the axial ratio-concentration curves in the dilute alloy region, as shown in Fig. 1.1. Three essential parts of the alloying effect on the axial ratio are shown by this graph. First, the intercept of the curve represents a valency-independent term by which α-zirconium is restored to ideal close packing by dilution of the zirconium atoms. Titanium and hafnium do not produce this effect since both elements in their hexagonal form have electronic structures and axial ratios similar to those of zirconium. Secondly, the electrons from each of the B-subgroup solutes increase the rate of expansion of the axial ratio in proportion to their number. Finally, absence of atomic size factor effects is indicated by the data for In and Ga and for Ti and Hf. This type of behavior, when

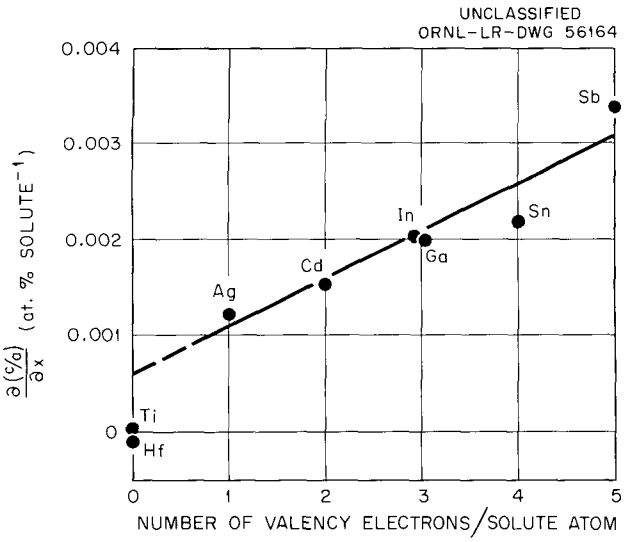

Fig. 1.1. Changes of the Axial Ratio with 1 at. % Additions.

the rate of change is proportional to valency, indicates two things. First, since each electron has an equal effect, it implies that zirconium itself has nearly zero s-p type electrons. Secondly, this behavior would be expected from the Jones theory and the present model, giving a direct relationship between the Brillouin zone and the position of the Fermi surface in an alloy. For a band structure which is rigid for a small amount of alloying, the Fermi surface should shift in approximate proportion to the number of electrons added. The changes in axial ratio would then be proportional to extra electrons contributed by the solute.

In addition to the B-subgroup solutes mentioned above, the effects on the α-zirconium lattice constants of Ce, Nd, and Pd were measured. Each of these slightly soluble elements expand the axial ratio. Solubilities are Pd < 0.2, Ce < 0.33, and Nd > 0.33 at. % at 800°C. It is believed that s and d electrons of the rare earths Ce and Nd, and some of the d electrons of the transition element Pd transfer to the zirconium band structure. Since Ce and Nd are equal in changing the ratio c/a, and in raising the α/β transition temperature,[10] the $4f$ electrons would appear to be too low in energy to leave the rare-earth ion. In this way, Ce and Nd should have effective metallic valencies of three, equivalent to the trivalent chemical valencies. The observed effects are somewhat larger.

SPECIFIC HEATS OF ZIRCONIUM ALLOYS[11]

G. D. Kneip, Jr. J. O. Scarbrough
J. O. Betterton, Jr.

The specific heats of dilute alloys of silver, indium, and tin in zirconium were found to consist of an electronic and a vibrational term and to obey Eq. (1) over the temperature range 1.2 to 4.5°K:

$$C = \alpha T + \beta T^3 . \qquad (1)$$

No evidence of phase transitions was found except for the two highest-composition tin alloys, which undergo a superconducting transformation at approx 1.25°K. All these solutes raise the coefficient of the electronic term and lower the Debye temperature.

Because of the proximity of the atomic levels, it seems reasonable to assume that the band structure of zirconium is similar to that of the other transition metals and consists of narrow d bands with a high density of states overlapped by a broad s band containing few electrons. If it is assumed that the s and d bands can be treated

[10] L. Ianniello and A. A. Burr, "Effect of Some Rare Earth Elements on the HCP-BCC Transformation of Zirconium," paper presented at 1961 Annual Meeting of AIME, St. Louis, Mo., Feb. 26–Mar. 1; abstract published in *J. Metals* 13, 68 (1961).

[11] G. D. Kneip and J. O. Betterton, Jr., pp 357–58 in *Proceedings of the VII International Conference on Low Temperature Physics* (G. M. Graham and A. C. Hollis Hallett, eds.), University of Toronto Press, 1961.

independently, then the density of electronic states as determined by the specific heat is the sum of the s and d densities. Although tin, like zirconium, has four electrons outside of completed shells, the addition of tin to zirconium raises the specific heat rapidly, so that the common conduction band in the alloy must not contain four electrons per atom, or else the relative positions of the s and d bands must shift during alloying.

If it is assumed that the bands do not shift during alloying and that the zirconium d electrons are tightly bound and do not penetrate into the atomic polyhedra of the solute atoms, then, for small solute concentrations, the change in the density of states and hence the electronic specific heat can be shown to be a linear function of solute concentrations, as is experimentally observed. According to this model, the change in the Fermi level which occurs during alloying is dependent upon the solute valence and the number of s electrons in zirconium. Thus, any properties which depend explicitly on the Fermi surface are independent of the total number of d electrons. The change in the coefficient of the electronic specific heat with alloying, then, should be a linear function of the solute valence, as is experimentally observed and shown in Fig. 1.2.

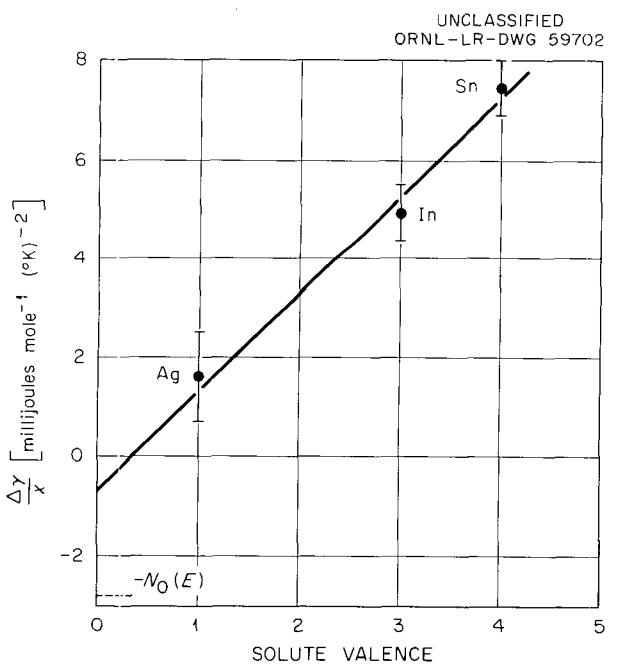

Fig. 1.2. Rate of Change of the Electronic Coefficient of the Specific Heat of Zirconium Alloys as a Function of Solute Valence.

Although the experimental results are in substantial agreement with this simple isotropic two-band model, certain discrepancies exist. First, $\Delta\gamma/x$ should be equal to the negative of the density of d states of pure zirconium when the solute valence is equal to the number of s electrons in zirconium. Although the number of s electrons cannot be uniquely determined without independently evaluating the density of d states, it is reasonable to assume (1) that the number of s electrons is small, (2) that the d states contribute approximately two-thirds of the total specific heat in the pure metal, and thus (3) that the curve of Fig. 1.2 should pass through $\Delta\gamma/x = -2$ for some positive value of the solute valence. Second, the slope of the density-of-states curve can be determined from the slope of the curve shown in Fig. 1.2, and, from this and the density of states of the pure metal, an estimate can be made of the number of d electrons. Both the number of d electrons and the width of the d band found in this way are unexpectedly small. The small number of d electrons may indicate that in zirconium a new d-band overlap has just occurred. The axial ratio change with alloying is in agreement with the overlapping d bands, and supporting evidence for the small number of electrons in one band is found in the Hall coefficient of zirconium.[12] The extremely narrow d band, however, is not consistent with a width of approx 1 ev from the x-ray "L" emission spectra.[13] It is perhaps remarkable that such a single model can adequately represent the major features of the alloying process for these highly anisotropic zirconium alloys.

At these low temperatures, only the long-wavelength phonons are excited; therefore, the lattice specific heat and hence the Debye temperature is determined by elastic waves whose wavelength is several atomic distances. For this case, the alloy should be considered to be an isotropic solid whose vibrational properties are dependent upon the average interatomic force constants and the average atomic mass. Since the mean atomic mass is nearly constant for these alloys, the linear dependence of the Debye temperatures on

[12] T. G. Berlincourt, *Phys. Rev.* 114, 969 (1959).

[13] C. H. Shaw and E. L. Jossem, *Soft X-Ray Spectra of Metals and Alloys*, final report, RF Project 471, Ohio State University Research Foundation (December 1959).

the solute concentration may be interpreted as due to changes in the elastic constants. The more rapid change in the Debye temperature for the silver alloys than for either the indium or tin alloys indicates that, for these systems, factors other than the electronic energy are important in determining the elastic constants.

VAPOR PRESSURES IN THE CADMIUM-ZIRCONIUM SYSTEM

J. O. Betterton, Jr. J. H. Frye, Jr.
D. S. Easton

In previous work[14] on the thermodynamic properties of the α and β phases of the Cd-Zr system, the α/β phase boundaries were calculated from the pressures, and a maximum in the $(\alpha + \beta)$ region was predicted that was not then observed in the phase diagram. Recent experiments with an alloy containing 15.8 at. % Cd confirm this maximum, since the transition occurs at 906°C at 11.2 at. % Cd but does not occur above 890°C in the higher-composition alloy. Henry's law, or independence of the thermodynamic deviation with atomic fraction of cadmium, persists to 15.8 at. % Cd, and it was also found that excess partial molar entropy of the β phase was constant with respect to composition to 15.8 at. % Cd.

IRON-CORE SUPERCONDUCTING MAGNET

J. O. Betterton, Jr. D. S. Easton

Superconducting electromagnets with iron cores and coils of niobium wire were discussed by Autler.[15] A magnet of this type has been made with the superconductor, niobium-clad Nb_3Sn, described by Kunzler *et al.*[16] The magnet will be used in magnetoresistance studies of zirconium alloys and of pure tungsten single crystals at low temperatures. Compared with an air-core solenoid, the iron-core magnet has the advantages in the medium-field-strength region of requiring only short lengths of Nb_3Sn wire for the winding and of having a large volume in which the field is transverse to the specimen.

The magnet was first wound with coils which were lacquer-insulated and wound after annealing, producing a field strength in a preliminary experiment of about 50,000 gauss. Unfortunately, this result was not repeated in later trials with these and other Nb-Nb_3Sn coils, and the maximum field produced was always near 23,000 gauss, the saturation value of the magnet pole tips, in spite of different numbers of turns and different currents.

Two causes are postulated for the above-mentioned nonreproducibility of results. (1) Flux escaping from the saturated pole tip was sufficient to quench the pure niobium cladding. Then the whole coil becomes normal in resistance because of the abrupt transfer of high current from the cladding to the core, quenching the core. (2) It may be that in each length of wire the core was broken at least once by the handling required to insulate and wind the coils.

In an effort to find an insulating material which would permit the coils to be wound while still ductile and then to be heat-treated, Nb-Nb_3Sn wires were heat-treated in silver and in copper jackets. Metallographic examination and current tests showed no deleterious effects of annealing in these metals. A preliminary coil of 14 turns, with a coating of electrodeposited silver, produced a measured field of 840 gauss at 95 amp, in agreement with the mutual coupling[17] of the search coil and the silver-brazed coil, with each turn effectively carrying this current.

Copper is convenient as a drawing lubricant, and, with the next trial, large coils (214 and 524 turns, and 1-$\frac{1}{2}$- by 2-$\frac{5}{8}$-in. inside dimensions) were brazed in copper. No field, however, was detected in the magnet gap with 200 amp flowing into the leads. Further consideration shows, however, that with high inductances and low shunting resistances the time constant of this type of coil would be so long that no field would be expected. Experiments will be continued with

[14] J. O. Betterton, Jr., J. H. Frye, Jr., and D. S. Easton, *Met. Div. Ann. Progr. Rept. July 1, 1960*, ORNL-2988, p 122.

[15] S. H. Autler, *Rev. Sci. Instr.* 31, 369 (1960).

[16] J. E. Kunzler *et al.*, *Phys. Rev. Letters* 6(3), 89–91 (1961).

[17] We are indebted to W. Gauster for this calculation and for the suggestion that $L(di/dt)$ was an important factor in the failure to develop field in the first copper-brazed coil.

additions of alloying elements to the brazing material.

Wire prepared at ORNL (described in Chap. 18, "Metal Forming and Casting," this report) in the manner suggested by Kunzler *et al.*[16] was placed in the air gap transverse to the field, and critical currents were determined to 23,000 gauss as a function of the wire diameter. The results are shown in Fig. 1.3 and indicate that wire from different sources introduces considerable differences. The sharply rising I_c-vs-H curve indicates that the niobium cladding becomes normal between 2000 and 5000 gauss and that the core thereafter carries a considerably smaller current. In view of the approximate proportionality of the critical current to the wire cross section, the larger-diameter wires seem more attractive for solenoids, since the possibility of discontinuity in the Nb_3Sn core should be reduced.

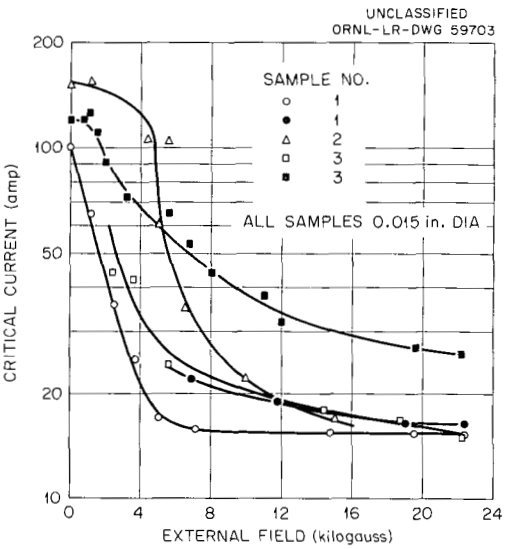

Fig. 1.3. Critical Currents vs External Field Strength in Various Nb-Clad Nb_3Sn Wires at 4.2°K.

HIGH-FIELD STUDIES OF Nb_3Sn SUPERCONDUCTIVITY[18–20]

J. O. Betterton, Jr. G. D. Kneip, Jr.
R. W. Boom[21] C. E. Roos[22]
R. E. Worsham[21]

Samples of niobium-clad Nb_3Sn wire were prepared by the methods suggested by Kunzler *et al.*,[16] and their critical currents as a function of field were measured by a pulsed-field, pulsed-current method at 4.2°K in the Vanderbilt University 200-kilogauss magnet.[18–20] The results are plotted in Fig. 1.4 as a function of field for two samples. Sample 1 was measured both parallel and transverse to the field, while sample 2 was oriented only parallel to the field. Since the start of the present experiments, similar experiments were done by Hart[23] and by Arp *et al.*,[24] and their results have also been plotted on Fig. 1.4 for comparison. Similarly, the ranges of the dc low-field results from eight different samples of wire, as reported above, are also plotted. The curves show that the 0.38-mm-diam samples carry pulsed currents of 210 to 260 amp in zero external field. Sample 1 carries 100 amp at 100 kilogauss with the field parallel to the wire axis. This curve can be joined smoothly with the data of Arp *et al.*,[24] which shows critical fields as high as 167 kilogauss for small measuring currents. Both the current-carrying capacity and the maximum field at which current is carried are lower in sample 2. Even larger differences appear between the results for sample 1 in the transverse field and the results of the other investigators. It may be concluded that (1) the properties of this hard

[18] J. O. Betterton, Jr., *et al.*, *Phys. Rev. Letters* 6(10), 532 (1961).

[19] C. E. Roos *et al.*, "Critical Currents in Nb_3Sn Superconductors," paper presented at American Physical Society Meeting, Washington, D.C., Apr. 24–27, 1961.

[20] C. E. Roos *et al.*, *Bull. Am. Phys. Soc.* 6, 337 (1961).

[21] Electronuclear Research Division.

[22] Vanderbilt University, Nashville, Tenn.

[23] H. Hart, "Superconductivity of Nb_3Sn," paper presented at American Physical Society Meeting, Washington, D.C., Apr. 24–27, 1961.

[24] V. D. Arp *et al.*, *Phys. Rev. Letters* 6(9), 452 (1961).

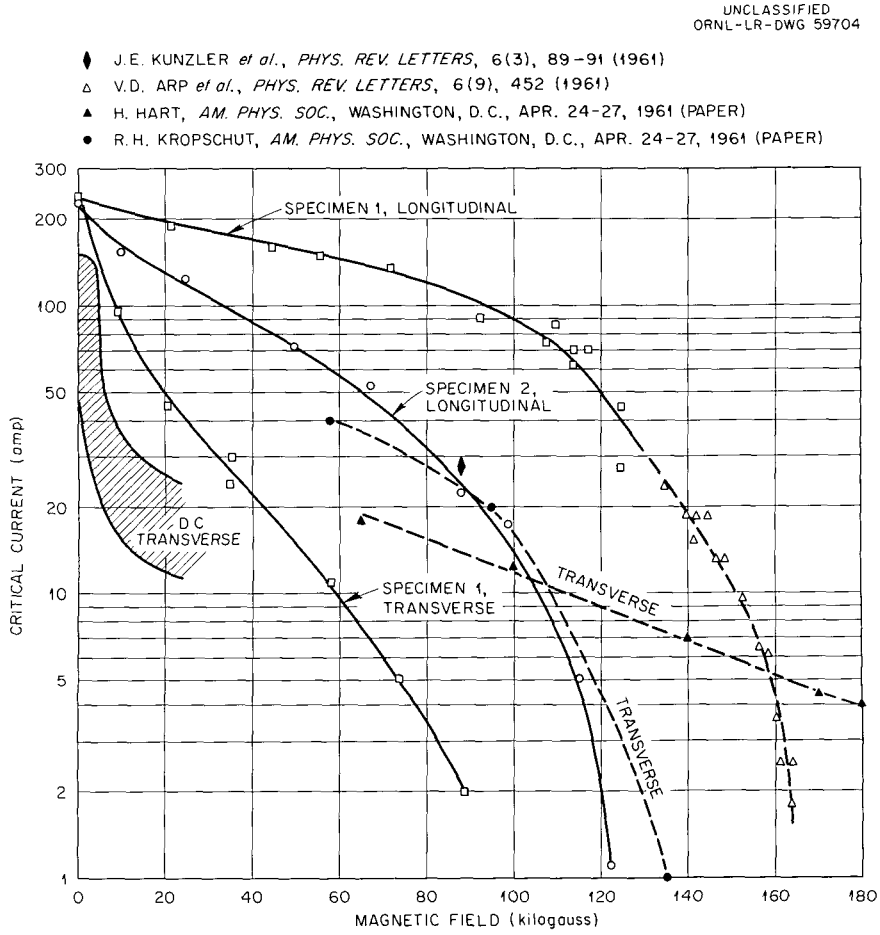

Fig. 1.4. Critical Current vs Applied Magnetic Field for Nb-Clad Nb_3Sn Superconductors.

superconductor are very sensitive to slight differences in strain and defect structure, and (2) the critical currents in the transverse direction are smaller and are widely different between specimens at higher field strengths. In soft or moderately hard superconductors, domain structures[25,26] could explain the differences between transverse and parallel orientations. It is somewhat surprising, however, that such large differences were found in a hard superconductor, such as Nb_3Sn, where the superconducting regions would be expected to depend primarily on the macroscopic physical structure of the wire.

The sensitivity of detection of the transition is 10^{-4} v in the pulse method, compared with sensitivities as high as 10^{-8} v in dc methods. This difference is not so important near zero fields where I_c is large, and, in fact, the pulsed-current method gives higher and possibly more accurate critical currents here than dc methods, since heat is not developed in the joints. At the higher fields where currents are smaller, the measured critical currents may be higher[27] because of the lower sensitivity of the pulsed-field pulsed-current method. A conservative allowance will be required for use of these data in the design of a solenoid.

[25] A. L. Schawlow, *Phys. Rev.* **101**, 373 (1956).

[26] W. D. DeSorbo, p 367 in *Proceedings of the VII International Conference on Low Temperature Physics*, University of Toronto, Canada, 1961.

[27] S. Autler, private communication; I_c (amp) = 11.2, 11.3, 11.7, 12.5, and 13.5 for Nb-Nb_3Sn wire at 60 kilogauss, for voltage sensitivities of 10^{-8}, 10^{-7}, 10^{-6}, 10^{-5}, and 10^{-4} v respectively.

During the pulsed-current experiments, a hysteresis effect was found in the superconducting-to-normal-state transition of niobium-clad Nb_3Sn wires at low fields.[28] If this wire is subjected to one or more current pulses whose peak value is just below the critical current, the value of the current necessary to destroy superconductivity is increased by approx 10%. After this conditioning treatment in a series of current pulses of constant peak value, the first of which is just sufficient to initiate the transition, the critical current becomes progressively smaller and the normal-state resistance becomes larger. Several 30-μsec pulses are required for the critical current to be reduced to a smaller, pulse-independent value and for the wire to reach a maximum normal resistance. The higher critical currents can be restored again by current pulses below the critical value. The phenomenon is not dependent upon the time interval between pulses, but the conditioning can be destroyed by warming the sample, showing that the effect is related to trapped magnetic flux in the specimens. The exact mechanism of flux trapping is complicated by the composite nature of the sample, which has at least two hard, superconducting elements in parallel. Studies of the intermediate state are continuing.

[28] G. D. Kneip, Jr., *et al.*, "Hysteresis Effects in the Nb_3Sn Superconducting Transition," paper presented at American Physical Society Meeting, Washington, D.C., Apr. 24–27, 1961.

2. X-RAY STUDIES OF CRYSTALLINE DEFECTS

SHORT-RANGE STRUCTURE OF THE ALLOY Cu–16 at. % Al

B. S. Borie C. J. Sparks

It has been discovered by Wechsler and Kernohan[1] that the electrical resistivity of the alloy Cu–16 at. % Al decreases upon exposure in a reactor. A possible explanation for this unusual behavior is that the degree of short-range order in the alloy is changed upon exposure. To test this possibility, it was decided to measure the x-ray diffuse scattering before and after exposure in a reactor. The first measurements were carried out by this group two years ago.[2] A very interesting and different diffuse scattering pattern was observed in the h_1h_20 plane of reciprocal space, and it was decided to carry out a detailed interpretation of the short-range order diffuse scattering. To accomplish this, better measurements were necessary. Our first data were obtained at room temperature with a rather imperfect slit system for the diffractometer. Greatly improved measurements result if they are made at liquid-nitrogen temperature in a vacuum. Temperature diffuse scattering, which tends to obscure the short-range order pattern, is greatly minimized; and a correction for air scattering, which is at best crude, is unnecessary.

A low-temperature specimen holder, providing an evacuated path for the incident x-ray beam, has been designed and constructed. In addition, the diffractometer was modified so that it would record the intensity measurements on a paper tape and automatically advance to the next point of measurement and repeat its cycle. The instrument is capable of making high-precision diffuse-intensity measurements at high speed with minimum attention from the operator.

Diffuse-intensity measurements at –190°C in the planes in reciprocal space $h_3 = 0$ and $h_1 + h_2 + h_3 = 0$ have now been completed. A determination of the short-range structure of the alloy from these data is now being carried out.

AN X-RAY DETERMINATION OF THE CHARACTERISTIC TEMPERATURE OF UO_2

B. S. Borie

Because of conflicting reports in the literature and because of the high current interest in the thermal properties of UO_2, the characteristic temperature of this material was measured by diffraction methods. Uranium dioxide is face-centered cubic, $a_0 = 5.46$ A, with the well-known fluorite structure. There are four uranium atoms in the unit cell at 000 (face-centered), four oxygens at ¼¼¼ (face-centered), and four oxygens at ¾¾¾ (face-centered).

A sample supplied by D. L. McElroy had, by chemical analysis, the composition $UO_{2.029}$. The small, black crystals were crushed to a fine powder from which a –325-mesh specimen was prepared. The powder was pressed into a flat sample holder and its diffraction pattern recorded in absolute units.

All measurements were made by using a doubly bent LiF monochromator and CuK_α radiation. Balanced filters were used to eliminate the $\lambda/2$ component in the incident beam, and the region near the sample was evacuated to avoid air scattering. Point counting at appropriate intervals from approx $2\theta = 24°$ to $2\theta = 82°$ was accomplished with a GE-XRD-5 diffractometer. The detector used was a thallium-loaded NaI crystal scintillation counter with pulse-height discrimination. All measurements were converted to absolute units by comparison with the scattering from polystyrene.

We planned to measure the Debye-Waller factor $2M$ by making use of both the integrated intensities of the Bragg maxima and of the diffuse scattering. Such a procedure would require a minimum of theoretically computed quantities and very probably would give the most reliable measure of the characteristic temperature. However, it was found that the integrated intensities did not give an accurate measure of the structure factors because of preferred orientation in the sample. Hence it

[1] M. S. Wechsler and R. H. Kernohan, *Solid State Div. Ann. Progr. Rept. Aug. 31, 1958*, ORNL-2614, p 85.

[2] B. S. Borie and C. J. Sparks, *Met. Div. Ann. Progr. Rept. Oct. 10, 1958*, ORNL-2632, p 38 (classified).

was necessary to determine $2M$ only from the temperature diffuse scattering, which should be very much less sensitive to effects of preferred orientation.

Figure 2.1 compares the experimentally measured diffuse scattering in electron units per primitive unit cell (Compton scattering has been computed and subtracted) with that calculated from theory with $2M = 0.80 \sin^2 \theta/\lambda^2$. The diffuse scattering

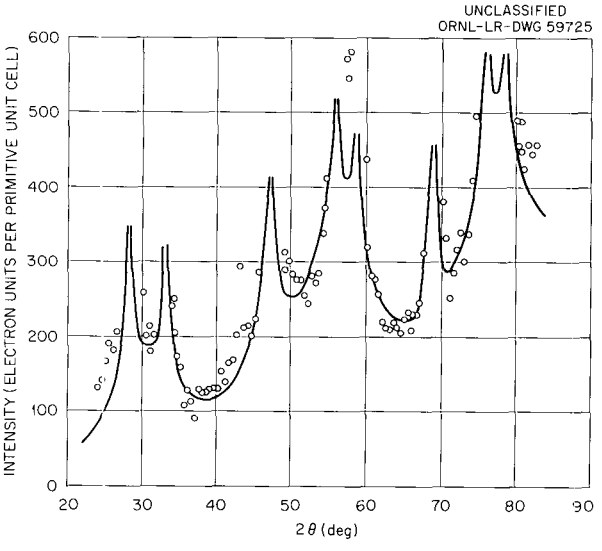

Fig. 2.1. Temperature Diffuse X-Ray Scattering for UO_2 Powder. Curve computed for $2M = 0.80 \sin^2 \theta/\lambda^2$.

was computed by means of Warren's theory,[3] assuming that UO_2 behaves as a face-centered cubic element. This is probably a very good assumption. In effect, it ignores the contribution of the optic modes to the diffuse scattering. The very much greater mass of uranium compared with oxygen justifies this. A further consequence of this assumption is to omit the oxygen contribution to the acoustic modes. In half of the Brillouin zones (those with odd indices) its contribution is zero, in one-fourth (those whose indices sum to a multiple of four) it is positive, and in one-fourth it is negative. Given the kind of averaging over spherical shells about the origin in reciprocal space which occurs for a powder pattern, the general effect of oxygen on the temperature diffuse scattering must be very small.

It has been assumed that all of the diffuse scattering is due to thermal motion. There exists the possibility of some double Bragg scattering contributing to the measurements, but, except in the very low-angle region, this should be negligible.

In general, the fit between experiment and theory shown in the figure is reasonably good. Because of the way in which the sample was prepared, it contained a significant amount of strain; hence the Bragg maxima were broadened. The long tails associated with these broadened peaks account for most of the deviation from theory near the crystalline reflections.

One very weak extra peak in the diffraction pattern was observed at $2\theta = 43°$. There are several other compounds of uranium and oxygen which have strong lines near this position. The degree of contamination of the sample indicated by the presence of this line is extremely small. It surely would not have been detected by the usual less sensitive diffraction techniques.

The Thomas-Fermi atomic scattering factor for uranium given by the *International Tables*[4] was used with a dispersion correction as tabulated by Dauben and Templeton.[5]

With $2M = 0.80 \sin^2 \theta/\lambda^2$, one obtains 188°K for the characteristic temperature of UO_2. The corresponding root-mean-square displacement of uranium atoms from their sites due to thermal motion is 0.12 A.

An assignment of precision to the above quantities is not easy and at best is subjective. A very large dispersion correction in the atomic form factor of uranium was made. This correction is based entirely on theoretical considerations and has never been tested experimentally. The accuracy of the theoretically determined Thomas-Fermi form factor is itself not known. Uranium has a very large and probably not accurately known absorption coefficient that must be used to express our measurements in absolute units. Effects such as double Bragg scattering and surface roughness of the sample, though probably small, may contribute somewhat to the inaccuracy of the

[3] B. E. Warren, *Acta Cryst.* 6, 803 (1953).

[4] W. H. Bragg, M. von Laue, and C. Hermann (ed. committee), *International Tables for the Determination of Crystal Structures*, Gebrüder-Borntraeger, Berlin, 1935.

[5] C. H. Dauben and D. H. Templeton, *Acta Cryst.* 8, 841 (1955).

final result. A conservative guess is that the above quoted characteristic temperature contains an error not greater than 10%.

EPITAXIALLY INDUCED STRAINS IN Cu_2O FILMS. I. X-RAY DIFFRACTION EFFECTS[6]

B. S. Borie C. J. Sparks J. V. Cathcart

X-ray diffraction line broadening measurements of Cu_2O films grown on copper have been interpreted in terms of strains induced in the films as they grow because of the coherence of the films with the substrate. It is expedient to consider the growth of the film to be in two stages. Probable differences in the structure of the films and their influence on the growth rate in the two stages are described and discussed.

TEMPERATURE DIFFUSE SCATTERING FOR CUBIC POWDER PATTERNS[7]

B. S. Borie

General expressions for the various orders of temperature diffuse scattering (TDS) for cubic elements are developed which show that the diffuse peaks at the Bragg maxima are broader for the higher order TDS contributions, and which also show that the average value of lth order TDS (in electron units per atom) is $f^2 e^{-2M}(2M)^l/l!$. The relevance of this result to the Warren theory and the more recent Paskin theory for TDS for cubic powders is discussed, and it is shown that the Warren theory is more accurate.

A DETERMINATION OF THIN OXIDE FILM THICKNESS BY INTEGRATED INTENSITY MEASUREMENTS[7]

B. S. Borie C. J. Sparks

The thicknesses of thin single-crystal oxide films are determined by integrated intensity measurements in absolute units. The method is illustrated with measurements of Cu_2O films grown on copper single crystals. Thicknesses determined from two different Bragg maxima agree well with each other and are reasonably consistent with the thicknesses determined from the line shapes.

THE SEPARATION OF SHORT-RANGE ORDER AND SIZE-EFFECT DIFFUSE SCATTERING[7]

B. S. Borie

In addition to the usual diffuse scattering associated with short-range order in an alloy, there are frequently observed modulations of the diffuse intensity associated with small static displacements of atoms from the sites of the average lattice. These displacements are usually caused by the fact that the two kinds of atoms in a substitutional binary solid solution are of different sizes. A method is described for the separation of the size-effect modulations from the short-range order diffuse scattering. The method is illustrated by its application to the alloy Cu-Au.

---

[6] Abstract of paper submitted to *Acta Metallurgica*.

[7] Abstract of paper to be published in *Acta Crystallographica*.

3. REACTIONS AT METAL SURFACES

J. V. Cathcart
R. E. Pawel G. F. Petersen

The general aim of the present research program is the investigation of factors that determine the degree of protectiveness of oxide films on metals. Previous work[1,2] demonstrated the existence of severe strains in oxide films on several metals and indicated the importance of such strains in destroying the initial protective character of the films. The three projects described below are all related to further efforts to understand the origins of these strains and the precise influence they have on the oxidation process.

OXIDATION OF TANTALUM

Stresses generated in the growing oxide films on tantalum specimens have been shown to cause severe cracking in the oxide films with subsequent loss in the protectiveness of the films. Results of the present research[3] emphasized the unique platelet structure of the oxide and the importance of the resulting geometry of the oxide-metal interface as a factor in stress generation in the films. A stereographic analysis of the surface traces of the oxide platelets showed that the platelets formed parallel to (320) planes in the metal, in contrast with the (100) habit plane reported by other investigators[4,5] for the oxidation of tantalum under somewhat different conditions. Only Ta_4O and TaO were detected in x-ray and electron diffraction studies of the (320) surfaces of lightly oxidized tantalum single crystals, although the primary oxide on more heavily oxidized specimens was Ta_2O_5. The observed habit plane of the oxide platelets was rationalized in terms of the generalized theory of the martensitic cubic-to-orthorhombic phase transformation proposed by Wechsler and Otte.[6] The good agreement obtained between theory and experiment supported the hypothesis that the oxide platelets formed by a precipitation reaction from a tantalum-oxygen solid solution.

SULFURIZATION OF TANTALUM

A study of the sulfurization of tantalum was undertaken in order to investigate the effect of anion size in gas-tantalum reactions. Figure 3.1 shows a sulfurization rate curve for tantalum at 600°C at a pressure of 300 mm Hg. As in the case of the oxidation of tantalum, the sulfide film became nonprotective after a short period of reaction. Electron micrographs showed that the resulting increase in sulfurization rate could be correlated with the appearance of cracks and fissures in the films. In contrast with the oxidation behavior, however, was a tendency for the cracks in the sulfide films to heal themselves, the films thus again becoming protective as sulfurization proceeded. The onset of the second region of protective film formation occurred after approx 12 hr.

The sulfurization differed from the oxidation of tantalum in two additional respects. First, no platelets were observed in the tantalum sulfide films formed either at 425 or 600°C at a sulfur pressure of 300 mm Hg. Second, the disappearance during sulfurization of fine markings present on the original tantalum surface suggested that cation rather than anion diffusion might predominate in the sulfurization process.

Should these preliminary conclusions be borne out by further work, the sulfurization of tantalum will be of special interest since the "break-away" behavior of the sulfide films appears to be governed

---

[1] J. V. Cathcart, R. E. Pawel, and G. F. Petersen, *Met. Div. Ann. Progr. Rept. July 1, 1960*, ORNL-2988, pp 61–84.

[2] J. V. Cathcart, R. E. Pawel, and G. F. Petersen, *Met. Div. Ann. Progr. Rept. Sept. 1, 1959*, ORNL-2839, pp 80–97.

[3] R. E. Pawel, J. V. Cathcart, and J. J. Campbell, "Oxide Platelet Formation in Tantalum Single Crystals," submitted to *Acta Metallurgica*.

[4] R. Bakish, *J. Electrochem. Soc.* 105, 71, 574 (1958).

[5] E. Gebhardt and H. D. Seghezzi, *Z. Metallk.* 50, 248 (1959).

[6] M. S. Wechsler and H. M. Otte, *Acta Met.* 9, 117–24 (1961).

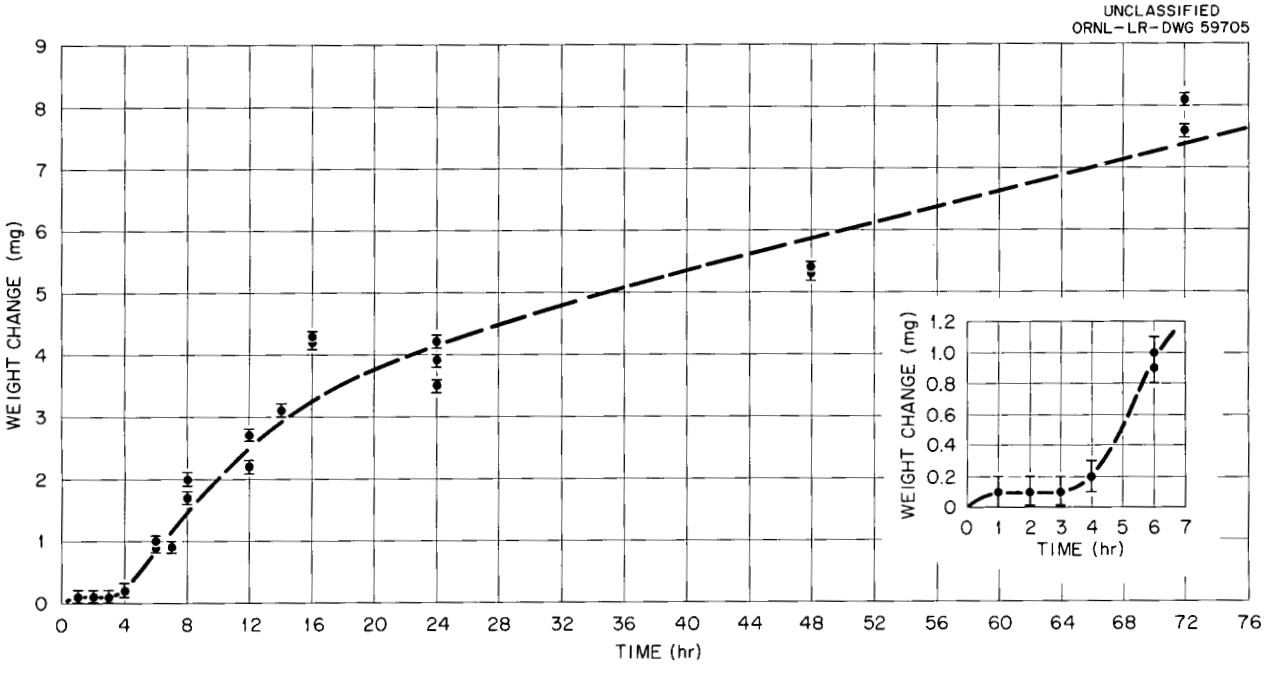

Fig. 3.1. Sulfurization of Tantalum at 600°C.

by a different set of factors than those which are thought to control "break-away" in tantalum oxide films.

OXIDATION OF COPPER

Previous studies demonstrated the existence of severe anisotropic strains of epitaxial origin in thin Cu_2O films on copper single crystals. Despite these strains, the films remain protective. Present work is designed to show in detail how strains are relieved in growing films and how they influence the over-all kinetics of the oxidation process for copper.

The strains are manifested in the optical anisotropy induced in the normally cubic Cu_2O lattice. Efforts are being continued to characterize these optical anomalies by means of polarizing spectrometer measurements. Many raw data have been accumulated; however, on account of the anisotropy of the index of refraction for the films, machine computations are required in order to convert the data to values of film thickness, index of refraction, and absorption coefficient for the oxide. The task of preparing a suitable computer code for processing the data is almost complete.

4. CRYSTAL PHYSICS

G. W. Clark

C. B. Finch O. C. Kopp[1]

Investigations of growth processes of single-crystal high-temperature materials are in progress. A better understanding is desired of growth mechanisms and of the influences of impurities and other system parameters on crystal quality. Select crystals resulting from this effort will be shared with other groups.

Compounds included in this crystal-growth endeavor are BeO, MgO, Cu_2O, ZnO, Al_2O_3, SiO_2, TiO_2, ZrO_2, HfO_2, ThO_2, UO_2, Fe_3O_4, Nb_3Sn, and certain rare-earth nitrides, phosphides, and manganese oxides. The facilities available for these studies include autoclave furnaces, equipment for crystal growth from molten-salt solutions, and several modifications of the Verneuil-type furnace.

A variety of techniques including optical microscopy, x-ray diffraction, infrared spectroscopy, and wet-chemistry methods are used in the evaluation of the perfection and growth habits of single crystals of BeO, Fe_3O_4, ZrO_2, SiO_2, ZnO, and Al_2O_3.

Autoclave experiments at temperatures up to 450°C and pressures up to 20,000 psi have led to the synthesis of (1) the rare mineral kalsilite ($KAlSiO_4$) from muscovite mica,[2] (2) magnetite (Fe_3O_4) crystals up to 3 mm on an edge obtained by the reaction of a low-carbon steel with 0.1 *M* $K_2B_4O_7$ and with 0.5 *M* NaOH, and (3) medium-quality quartz (SiO_2) crystals having a maximum dimension of 2 cm.

Current experiments with supercritical systems include (1) a search for water-based solvents for Cu_2O, ZnO, TiO_2, ZrO_2, HfO_2, ThO_2, and UO_2; (2) an investigation of the use of anhydrous ammonia and its derivatives as solvents for several nitrides and phosphides; (3) improvement of the technique for growing periclase (MgO), bromellite (BeO), magnetite (Fe_3O_4), quartz (SiO_2), and corundum (Al_2O_3); and (4) a study of the chemistry of high-temperature solvents, both as to the particle species in the supercritical vapor and as to the applicability of the electronic theory of acid-base reactions in selecting appropriate solvents.

Crystallization from molten salts has yielded crystals of BeO, MgO, ZrO_2, and ZnO. By hydrolysis of Zr–Li–Na fluoride melts, baddeleyite (monoclinic ZrO_2) crystals greater than 1 mm on an edge were precipitated (a report is being prepared covering this work), and by hydrolysis of $MgCl_2$ melts, imperfect crystals of periclase up to 5 mm on an edge were precipitated. Crystals of ZnO measuring 1.5 mm on an edge were grown out of PbF_2 solvent, confirming the work of Nielsen and Dearborn.[3] Reasonably well-formed BeO crystals about 1 mm on an edge were synthesized during attempts to produce beryl (a beryllium aluminum silicate) by slow cooling of Li_2MoO_4 plus 10 wt % of $6SiO_2$–Al_2O_3–3BeO. Emphasis is now on growing BeO from Li_2MoO_4 or another less complicated system than that mentioned above.[4]

A Verneuil flame-fusion furnace is currently being used to grow MgO crystals; however, only marginal success has been achieved by using an oxyacetylene flame. Efforts are being made to perfect a radio-frequency inductively coupled plasma system and a direct-current arc torch as other high-intensity heat sources for the flame-fusion furnaces.

---

[1] Consultant from the University of Tennessee.

[2] O. C. Kopp, L. A. Harris, and G. W. Clark, "The Hydrothermal Conversion of Muscovite to Kalsilite and an Iron-Rich Mica," *American Mineralogist* (in press).

[3] J. W. Nielsen and E. F. Dearborn, *J. Phys. Chem.* 64, 1762 (1960).

[4] Working independently, S. B. Austerman recently succeeded in growing BeO from Li_2MoO_4, *Am. Ceram. Soc. Bull.* 40, 269 (1961).

5. SPECTROSCOPY OF IONIC MEDIA

G. P. Smith

DILUTE SOLUTIONS OF BISMUTH IN $BiCl_3$ MELTS

C. R. Boston G. P. Smith

Studies of the visible spectra of dilute solutions of bismuth in molten bismuth trichloride, described previously,[1] were considerably extended during the past year and submitted for publication.[2] The more important points from this paper are given here.

There has been much recent debate[3] concerning the molecular constitution of the liquid phases of the bismuth–bismuth trihalide systems. It is usually assumed that bismuth metal dissolves in halide-rich melts to form a single solute species. However, some workers[4,5] assert that there are two or more solute species which are in equilibrium. No specific solute species has been demonstrated to exist in the halide-rich melts. The species which have been postulated include such diverse entities as bismuth atoms,[6] polymers of bismuth atoms,[5] monovalent bismuth ions and their polymers,[5,7] and even "ions plus electrons"[4] with no specified electron traps. The study described below shows that more than one, probably two, species is present and considerably narrows the possible choices of specific species.

Visible absorption spectra were measured for 0.001 to 0.5 M solutions of bismuth metal in molten $BiCl_3$ at path lengths as short as 24 μ and at temperatures of 260, 350, and 433°C. The integrated absorbancy of an intense, broad band with a maximum at about 560 mμ showed large, apparent deviations from Beer's law which were found to be due to a partitioning of solute bismuth into more than one solute species.

The data may be represented to within experimental accuracy by a two-species partitioning equilibrium in which the ratio of activity coefficients in the expression for the equilibrium constant is independent of concentration. The ratio of activity coefficients may be combined with the equilibrium constant in the usual way to give a mass-action constant. In the dilute solution approximation, namely, constant concentration of $BiCl_3$, the expression for a mass-action constant K of any possible two-species partitioning equilibrium may be put in the form

$$\log \frac{1}{\sigma_0}\frac{\bar{A}_s}{b} = \frac{D_n}{D_m}\log M_f - \frac{1}{\sigma_0}\frac{\bar{A}_s}{b} + \left(\log D_n - \frac{D_n}{D_m}\log D_m - \frac{1}{D_m}\log K\right), \quad (1)$$

where M_f is the concentration of solute bismuth in moles per liter of melt, $\bar{A}_s$ is the integrated absorbancy of the 560-mμ band in units of electron volts, b is the optical path length in centimeters, σ_0 is the integrated photon cross section in ev-cm^2/mole taken at the limit as M_f approaches zero (experimentally and theoretically σ_0 is almost independent of temperature), and D_n and D_m are the numbers of moles of bismuth metal which react with $BiCl_3$ to form, respectively, one mole of chromophore and one mole of species m. It may also be shown that $\sigma_0 = \sigma_n/D_n$, where σ_n is the integrated photon cross section of one mole of chromophore, and that $\bar{A}_s/b\sigma_0 = D_n M_n$.

When the data are substituted into Eq. (1), the least-squares values of D_n/D_m are found to be 0.34 at 260°C, 0.32 at 350°C, and 0.40 at 433°C. Since D_n/D_m is expected to be a ratio of small integers, the value $\frac{1}{3}$ is a best estimate at the two lower temperatures, although the neighboring

[1] C. R. Boston and G. P. Smith, *Met. Div. Ann. Progr. Rept. July 1, 1960*, ORNL-2988, pp 9–16.

[2] C. R. Boston and G. P. Smith, "Visible Absorption Spectra of Solutions of Bismuth Metal in Molten Bismuth Trichloride," submitted to the *Journal of Physical Chemistry*.

[3] See reviews in ref 4 and in D. Cubicciotti, *J. Chem. Educ.* 37, 540 (1960).

[4] S. J. Yosim *et al.*, *J. Phys. Chem.* 63, 230 (1959).

[5] M. A. Bredig, *J. Phys. Chem.* 63, 978 (1959).

[6] T. K. Keneshea, Jr., and D. Cubicciotti, *J. Phys. Chem.* 62, 843 (1958); 63, 1112 (1959); 63, 1472 (1959).

[7] J. D. Corbett, *J. Phys. Chem.* 63, 1149 (1959).

values of $\frac{2}{7}$, $\frac{3}{8}$, and $\frac{2}{5}$ cannot be entirely excluded. A best estimate at 433°C is $\frac{2}{5}$, and the data show a slight, systematic nonlinearity. However, the experimental scatter at 433°C is sufficient so that there is reluctance to place any significance either on the nonlinearity or on the difference between $\frac{1}{3}$ and $\frac{2}{5}$ at this temperature. It is concluded that $\frac{2}{7}$, $\frac{1}{3}$, $\frac{3}{8}$, and $\frac{2}{5}$ are possible values of D_n/D_m with $\frac{1}{3}$ being the best single-value estimate.

The present investigation clearly shows that the solute bismuth is partitioned, probably into two primary species. This is the important conclusion to be drawn from the data. However, the measurements provide only ratios of parameters and, hence, do not identify the specific solute species. Despite this fact, experimental bases are at hand for selecting certain species and equilibria in preference to others. These bases are that D_n/D_m must have a value near $\frac{1}{3}$ and that the equilibrium must depend on temperature in such a way that at higher temperatures it shifts to favor species n, the chromophore.

Any two-species partitioning equilibrium, exclusive of chloride ion assignments, may be put in the form

$$(Bi_n)^{n\alpha+} + \left[n\left(\frac{3-\alpha}{3-\beta}\right) - 1 \right] Bi^{3+} = \frac{n}{m}\left(\frac{3-\alpha}{3-\beta}\right)(Bi_m)^{m\beta+}, \qquad (2)$$

where n and m are polymerization numbers, $\alpha+$ and $\beta+$ are oxidation numbers, $(Bi_n)^{n\alpha+}$ is the chromophore, and a negative value for the coefficient of the solute, Bi^{3+}, signifies that this term is to be transposed to the right of the equals sign. In terms of Eq. (6), the stoichiometric coefficients which occur in Eqs. (1) through (5) are given by

$$D_n = \frac{n(3-\alpha)}{3}, \quad D_m = \frac{m(3-\beta)}{3}, \quad \frac{D_n}{D_m} = \frac{n}{m}\left(\frac{3-\alpha}{3-\beta}\right). \qquad (3)$$

Stoichiometrically permissible values of α and β are specified by $n\alpha = 0, 1, 2, \ldots, (3n-1)$ and $m\beta = 0, 1, 2, \ldots, (3m-1)$. The largest polymers which have been proposed for $BiCl_3$-rich solutions contain four bismuth atoms. Thus, if n and m are constrained to have values of four or less, and α and β are allowed to range over all values, a total of 2304 stoichiometrically permissible partitioning equilibria with values of D_n/D_m from $\frac{1}{12}$ to 12 may be obtained from Eq. (2). The experimental data are consistent with only a fraction of these equilibria, namely, those with D_n/D_m values near $\frac{1}{3}$.

Other considerations must be invoked in order to reduce further the remaining equilibria. A plausible restriction is to permit α and β to have the values of only 1 and 3. Then the only equilibria consistent with the data are the following:

$$3Bi^{\circ} = (Bi_3)^{\circ}, \qquad (4)$$

$$3Bi^{+} = (Bi_3)^{3+}, \qquad (5)$$

$$3Bi^{+} = (Bi_2)^{\circ} + Bi^{3+}, \qquad (6)$$

$$3(Bi_2)^{2+} = (Bi_4)^{\circ} + 2Bi^{3+}, \qquad (7)$$

$$4Bi^{3+} + 8Bi^{\circ} = 3(Bi_4)^{4+}. \qquad (8)$$

The only lower valence species of bismuth that has been experimentally identified[8] is the trimer $(Bi_3)^{3+}$. This ion occurs only in Eq. (5), where it is formed by polymerization of the chromophoric monomer Bi^{+}.

It is interesting to calculate some of the parameters which contain D_n and D_m when it is assumed that Eq. (5) represents the partitioning. A value of K was determined for each spectrum by substituting into Eq. (1) the experimental values of $\bar{A}_s/(b\sigma_0)$ and M_f, and values of the stoichiometric constants appropriate to Eq. (5), namely, $\frac{2}{3}$ for D_n and 2 for D_m. The K values at each temperature were averaged to obtain the following estimates and standard deviations: 85 ± 18 at 260°C, 15.2 ± 2.4 at 350°C, and 5.1 ± 2.4 at 433°C. The integrated photon cross section, σ_n of the chromophore Bi^{+}, is 2.2×10^3 ev-cm^2/mole, which is equivalent to an oscillator strength of 0.076, apart from the refractive-index and local-field corrections.

[8] H. A. Levy *et al.*, *J. Phys. Chem.* 64, 1959 (1960).

DILUTE SOLUTIONS OF BISMUTH IN $BiBr_3$ MELTS

C. R. Boston G. P. Smith

Studies of bismuth in $BiBr_3$ melts have been made for determining something of the role of the halide ion in Bi-BiX_3 solutions. Preliminary results are as follows. The visible absorption band of solute bismuth has much the same shape and almost the same limiting integrated cross section, σ_0, in $BiBr_3$ melts as in $BiCl_3$ melts. The band maximum in $BiBr_3$ is shifted by 48 $m\mu$ toward the red, relative to its position in $BiCl_3$. The shift is within 4% of that predicted by Ivey's law[9] for F bands in alkali halide crystals when one uses Ahrens' Bi(III) radius and Pauling's halide radii to compute the interionic distances. The partitioning equilibrium of solute bismuth in $BiBr_3$ melts is shifted in favor of the chromophore, relative to its position in $BiCl_3$ melts.

COLORATION OF $BiCl_3$-KCl MELTS

C. R. Boston

It was recently reported by Topol *et al.*[10] that, whereas molten $BiCl_3$ is yellow, the addition of greater than 20 mole % KCl or KBr to $BiCl_3$ changes the color to violet. This color change was offered as evidence for a corresponding change in the molecular species which contains Bi(III), such as the formation of a new chlorobismuth(III) complex or of bismuth(III) chloride polymers.

A careful spectrophotometric study by us shows that the color of pure $BiCl_3$–30 mole % KCl melts is yellow, that a small contamination of the melt by metallic bismuth produces the characteristic Bi(I) absorption band (see two preceding topics in this chapter) and a consequent violet color, that this bismuth contamination can be formed by reduction of the melt with carbonaceous matter such as cellulose fibers or lint, and that the carbonaceous content of reagent-grade KCl as received can be great enough to produce visible coloration due to the formation of Bi(I).

[9] H. F. Ivey, *Phys. Rev.* **72**, 341 (1947).

[10] L. E. Topol, S. W. Mayer, and L. D. Ransom, *J. Phys. Chem.* **64**, 862 (1960).

SPECTROSCOPY OF IONIC NITRATE MELTS

G. P. Smith C. R. Boston

In a recent paper[11] systematic changes were reported in the spectroscopic parameters of the nitrate $n \rightarrow \pi^*$ transition over the series of molten alkali nitrates. The most striking of these systematic changes was the almost linear correlation between the mean transition energy (E_{max}, measured at the band maximum) and the reciprocal of the cationic radius, r. A qualitative theory was proposed for the effect of noble-gas configuration cations on internal charge-transfer transitions of neighbor anions. According to this theory E_{max} for nitrate $n \rightarrow \pi^*$ in melts should increase with increasing cationic charge to radius ratio, Z/r. In order to test this assertion, spectra were measured for the following systems: $Ba(NO_3)_2$-$LiNO_3$ up to $\bar{N}_{Ba} = 0.24$,[12] $Ba(NO_3)_2$-KNO_3 up to $\bar{N}_{Ba} = 0.50$, $Sr(NO_3)_2$-KNO_3 up to $\bar{N}_{Sr} = 0.40$, $Ca(NO_3)_2$-KNO_3 up to $\bar{N}_{Ca} = 0.56$, $Ca(NO_3)_2$-$NaNO_3$ up to $\bar{N}_{Ca} = 0.57$, $Ca(NO_3)_2$-$(Li_{0.43}, K_{0.57})NO_3$ up to $\bar{N}_{Ca} = 0.60$, $Mg(NO_3)_2$-KNO_3 up to $\bar{N}_{Mg} = 0.50$, $Mg(NO_3)_2$-$(Li_{0.43}, K_{0.57})NO_3$ up to $\bar{N}_{Mg} = 0.60$, $La(NO_3)_3$-$(Li_{0.43}, K_{0.57})NO_3$ up to $\bar{N}_{La} = 0.45$, $Y(NO_3)_3$-$(Li_{0.43}, K_{0.57})NO_3$ up to $\bar{N}_{Y} = 0.16$, $LiNO_3$-KNO_3 over entire range, $LiNO_3$-$CsNO_3$ over entire range, KNO_3-$RbNO_3$ over entire range, and $LiNO_3$-$NaNO_3$ over entire range.

Although a study of the data is by no means complete, the following result of general importance has been found to hold. The energy of the $n \rightarrow \pi^*$ transition, E_{max}, approximates the same linear function of $\Sigma_j (Z_j/r_j)\bar{N}_j$ for every composition of every system except for the systems containing the very high Z/r ions, Mg^{2+} and Y^{3+}. Details of this phenomenon will be published.[13]

[11] G. P. Smith and C. R. Boston, *J. Chem. Phys.* **34**, 1396 (1961).

[12] $\bar{N}_{Ba}$ = electrical equivalent fraction of Ba^{2+}.

[13] G. P. Smith and C. R. Boston, *Discussions Faraday Soc.* No. 32 (to be published).

VOLUMETRIC PROPERTIES OF IONIC MELTS

G. P. Smith

In order to convert absorption data to units of optical cross section, it is necessary to know the volume density of light absorbers. For much molten-salt work, this is best calculated from the density or molar volume of the salt. Frequently, volumetric data are unavailable for the molten-salt mixtures under investigation, and on such occasions volumetric properties are measured by this group. During the past year, two papers covering 34 density equations were submitted for publication.[14,15] In one of these papers, a logical ambiguity was pointed out in the usual treatment of additive molar volumes for reciprocal salt mixtures, and an alternative treatment was proposed and shown to be in accord with the extant molar volume data for molten reciprocal salt systems. The proposal is outlined here.

Consider a reciprocal salt system containing cations, M_1^+ and M_2^+, and anions, X_1^- and X_2^-. The three thermodynamic components may be chosen equally well from among the equivalent constituent salts M_1X_1, M_1X_2, M_2X_1, and M_2X_2. Thus, for every ternary composition it is possible to compute the additive volume V^A in four ways and in general get four different values. Two of these ways are

$$V_1^A = V_{11}^0 + N_2^- (V_{22}^0 - V_{21}^0) + N_2^+ (V_{21}^0 - V_{11}^0) , \quad (9)$$

$$V_2^A = V_{12}^0 + (1 - N_2^-) (V_{11}^0 - V_{12}^0) + N_2^+ (V_{21}^0 - V_{11}^0) , \quad (10)$$

where N_i^+ is the cationic fraction of M_i^+, N_i^- is the anionic fraction of X_i^-, and V_{ij}^0 is the real molar volume of M_iX_j. A real system will obey these equations only if

$$V_{12}^0 + V_{21}^0 = V_{11}^0 + V_{22}^0 . \quad (11)$$

As an alternative to additive volumes, V_i^A, we propose a single function which, for mnemonic purposes, may be written as

$$V^Q = N_1^+ N_1^- V_{11}^0 + N_1^+ N_2^- V_{12}^0 + N_2^+ N_1^- V_{21}^0 + N_2^+ N_2^- V_{22}^0 . \quad (12)$$

This function has the following useful properties, none of which are possessed by the volumetric additivity relations [Eqs. (9), (10), etc.]. First, V^Q defines a single-valued deviation parameter. Second, for binary compositions V^Q transforms into the equations for binary additivity. Third, at the composition of each of the four pure salts, it yields the empirical value for the molar volume. Fourth, V^Q reduces to a linear isotherm when either the anionic fractions alone or the cationic fractions alone are held constant.

It is interesting to note that along the two pseudo-binaries the V_i^A give two straight lines which do not intersect at their common composition (a physical absurdity), while V^Q gives two parabolas which do intersect.

GROWTH OF SINGLE CRYSTALS OF INORGANIC SALTS

J. J. McBride

Single-crystal specimens of controlled purity are required for important phases of the spectroscopic research. A controlled-atmosphere apparatus for pulling crystals from a melt was built. This apparatus consistently produces large single crystals (about 1 in. in diameter by 2 to 3 in. long) of KCl and has produced some smaller crystals of $NaNO_3$. Modifications in the apparatus are in progress with a view toward reducing crystalline imperfections. It is anticipated that in the near future several kinds of crystals of spectroscopic interest will be grown.

---

[14] G. P. Smith and G. F. Petersen, "Volumetric Properties of the Molten System (Li,K)–(Cl,NO_3)," submitted to the *Journal of Chemical and Engineering Data*.

[15] G. F. Petersen, W. M. Ewing, and G. P. Smith, "Densities of Some Molten Salt Mixtures. The Systems $LiNO_3$-$LiClO_4$, KNO_3-$Ca(NO_3)_2$, KNO_3-$Sr(NO_3)_2$, and KNO_3-$Ba(NO_3)_2$," submitted to the *Journal of Chemical and Engineering Data*.

6. DEFORMATION OF CRYSTALLINE SOLIDS

R. O. Williams J. A. Wheeler, Jr.

The changes that take place within solids as a result of extended deformation are complex. While much is known about such changes, much remains to be learned. The primary purpose of this group is to provide information and understanding in this field, particularly with respect to metals and alloys. For the present the investigation is limited to making measurements of the fraction of the deformation energy that remains within the metal after deformation. It is evident that this energy is directly associable with the changes that have taken place within the metal, although such changes are so complex that extended energy measurements and/or supplementary measurements will be required for a reasonably complete picture.

The method currently being used depends upon measuring the mechanical energy put into the sample and the heat liberated within the sample, the stored energy being the difference. As previously reported,[1] this is accomplished by pulling a tensile sample inside a calorimeter as illustrated in Fig. 6.1. This calorimeter is analogous to the ice calorimeter, except that instead of utilizing the energy in melting ice, it is used to vaporize a liquid. The same liquid is used externally to maintain thermal isolation. The advantages of using vaporization are sensitivity, speed of response, and range of operating temperatures. In this design the volume of the vaporization chamber also increases. This would not be permissible in an ice calorimeter. As shown in the diagram, an Instron tensile machine is used. This machine has a very constant rate of crosshead movement

[1] R. O. Williams, *Met. Div. Ann. Progr. Rept. July 1, 1960*, ORNL-2988, p 6.

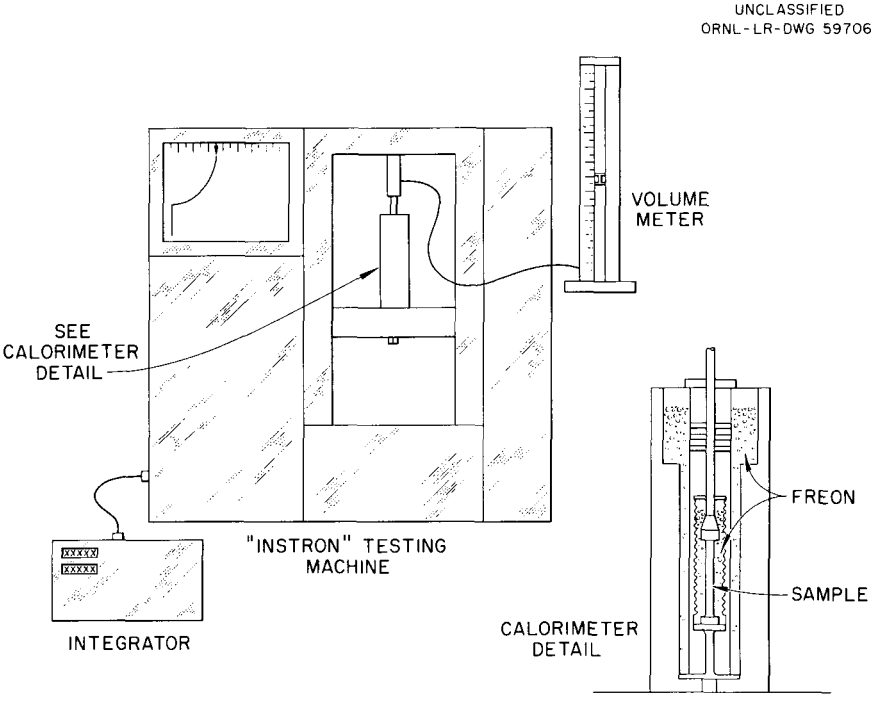

Fig. 6.1. Apparatus for Making Stored-Energy Measurements.

which greatly facilitates the measurement of energy input. Additionally, an integrator is used which gives the energy directly during the test and greatly facilitates the measurements with respect to speed and accuracy. The volume of gas liberated is measured by a volumeter which consists of a mercury-sealed float in a precision-bore tube. By using industrial refrigerants, the heats of vaporization are accurately known.

There are certain corrections and problems, but these need not be discussed here. The techniques that are required have been worked out fairly well, although some improvement is anticipated. It is true, however, that the present calorimeter is not considered an optimum design, and some changes will be made. It seems safe to state that at the present time, measurements on alloys that store appreciable energy can be satisfactorily run, and this may be true for some pure metals.

The capabilities at present are illustrated in Fig. 6.2 for a commercial 70-30 brass pulled at −30°C in CCl_2F_2 (Freon-12). It will be noticed that for these two runs the reproducibility was very good, about 1 part in 300 for the primary measurements. The features shown here are similar to those previously found by another method for the same alloy, using a higher strain rate at room temperature.[2] No detailed analysis of these data is in order from this isolated run, since the behavior is unquestionably complex. It is to be noted, however, that the samples initially stored between 50 and 60% of the energy. Because the rate of storage was changing rapidly, coupled with a rapid increase of load, a detailed picture at very low strains is not possible. At higher strains the fractional rate of storage slowly drops from 40% to about 25% at the end. It is expected that when these results can be extended over the complete temperature and composition range, some of the components of the storage process will become evident.

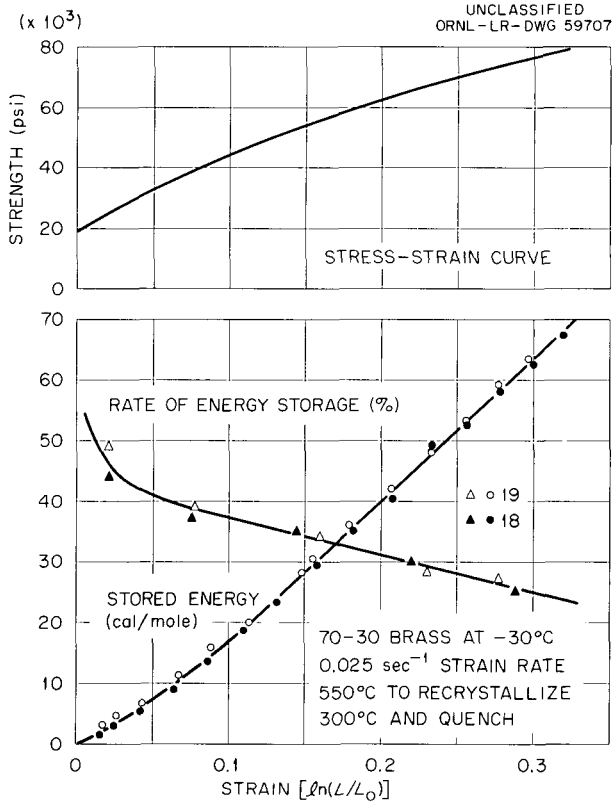

Fig. 6.2. Stored Energy and Strength of Brass.

[2] R. O. Williams, "The Stored Energy of Cold-Worked Alloys of Cu-Al, Cu-Zn, Al-Ag, and Ni-Al," submitted to *Acta Metallurgica*.

7. STRUCTURE OF METALS

C. J. McHargue

PHASE TRANSFORMATIONS IN CERIUM[1]

C. J. McHargue H. L. Yakel, Jr.

The room-temperature crystal structure of cerium that has not been cooled to lower temperatures is face-centered cubic. The face-centered cubic structure transforms upon cooling to a hexagonal close-packed structure (c/a = 3.239) with an $ABAC$ stacking sequence of close-packed planes. This transformation has many of the typical martensitic characteristics. The transformation starts at 263 ± 10°K. At 100°K that portion of the face-centered cubic phase that has not transformed to hexagonal close packed begins to transform to a second face-centered cubic phase with a volume decrease of 16.5%. The kinetics of this transformation also resemble that of the martensite reaction. Below a temperature between 77 and 43°K, the hexagonal structure appears to also transform to the collapsed cubic form. Plastic deformation at any temperature suppresses the transformation to the hexagonal form and may even cause it to revert to the normal cubic form. Deformation below 100°K favors the collapsed cubic form. Thermal cycling produces more of the hexagonal phase than can be obtained on one cooling. After a large number of cycles, neither the hexagonal nor normal cubic phase will transform to the collapsed cubic phase upon cooling. Plastic deformation at 4.2°K removes the thermal-cycling effects.

NEUTRON DIFFRACTION INVESTIGATIONS OF METALLIC CERIUM AT LOW TEMPERATURES[2]

M. K. Wilkinson[3] C. J. McHargue
H. R. Child[3] W. C. Koehler[3]
E. O. Wollan[3]

Neutron diffraction experiments have been performed on metallic cerium at a series of temperatures between room temperature and 4.2°K in an attempt to clarify the anomalous behavior which has been observed in previous specific heat and magnetic susceptibility measurements. Results on three specially prepared samples show that the interesting magnetic behavior can be correlated with the three crystallographic phases present in the samples. There is a change in the electronic configuration of the cerium atoms when the collapsed face-centered cubic phase is formed, and antiferromagnetic ordering occurs in the hexagonal close-packed phase at about 12.5°K.

ON A COMPLEX RECRYSTALLIZATION TEXTURE IN 3% Si–Fe[4]

C. G. Dunn[5] C. J. McHargue

Components in a complex primary recrystallization texture, which is a matrix texture for secondary recrystallization to the Goss texture in 3% Si–Fe strip, have been determined by the axis-chart method of Jetter, McHargue, and Williams. The results obtained are compared with former pole-figure results and found to include components not previously resolved or noted. It is found also that the components of the texture explain reasonably well the observed magnetic torque curve of the material.

THE EFFECT OF INITIAL ORIENTATION ON THE FIBER TEXTURE OF ALUMINUM RODS[6]

C. J. McHargue

Rods of 99.99+% Al which had initial orientations of <001>, <118>, <115>, <111>, and random were swaged at room temperature. Changes in orientation as a function of deformation were studied on axis distribution charts. The <001> orientation appeared to be relatively stable due to the inhomogeneity of the deformation process.

[1] Abstract of published paper: *Acta Met.* 8, 637 (1960).

[2] Abstract of paper to be published in the *Physical Review.*

[3] Physics Division.

[4] Abstract of published paper: *J. Appl. Phys.* 31, 1767 (1960).

[5] General Electric Research Laboratory, Schenectady, New York.

[6] Abstract of paper to be published in *Transactions of the Metallurgical Society of AIME.*

Orientations near the <100> zone were quickly reoriented towards <001>. Orientations on the <1$\bar{1}$0> zone between <118> and <115> appeared to be stable to reductions of about 50%, then were reoriented toward <001>. At very high reductions, movement away from the <111> orientation was observed.

TWINNING IN VANADIUM[7]

C. J. McHargue

Deformation twins were observed in electron-beam-melted vanadium single crystals slowly compressed at 77°K. The interstitial impurity content of 0.039% was at least an order of magnitude lower than in vanadium previously studied. The results indicated that further reduction in interstitials would result in deformation twin formation at room temperature.

TWINNING IN NIOBIUM[8]

C. J. McHargue

Deformation twins were observed in the temperature range of 77 to 293°K in single crystals of niobium containing 80 ppm interstitial impurities. It was established that the twin plane was {112} and the twin direction was <11$\bar{1}$>. Certain morphological features could be explained by assuming that the twins nucleate as thin disks which grow both lengthwise and laterally. Indications were found that the saw-toothed appearance may be associated with pile ups of dislocations due to slip-on intersecting {110} planes in the matrix. This view also was supported by observations that prestrain of about 6% at room temperature inhibited twinning at 77°K.

FURTHER STUDIES ON TWINNING IN NIOBIUM

C. J. McHargue

Effect of Interstitial Impurities

In the course of the work reported above, it became apparent that niobium and vanadium deformed by mechanical twinning with a much higher frequency than would be expected from published accounts of the low-temperature deformation of these metals.[9,10] One obvious difference between this work and other studies is the purity of the material – that used here having at least an order of magnitude lower interstitial impurity content. However, it is commonly believed that less-pure body-centered cubic metals deform by twinning with greater ease than high-purity metals.[11] Since the usual contaminants of the refractory body-centered cubic metals include the interstitials oxygen, nitrogen, hydrogen, and carbon, it is important that any relationship between purity and deformation process be clarified.

Single-crystal prisms approx $\frac{1}{4}$ to $\frac{1}{2}$ in. on a side were cut from an ingot of double electron-beam-melted niobium. In several instances, multiple specimens were cut from the same crystal, so that the only variable in a series of tests will be composition. These specimens will be contaminated with the interstitial elements to several levels of concentration ranging from that present in the ingot (10 ppm C, 40 ppm N, 32 ppm O) to the solubility limit. The crystals are deformed at liquid-nitrogen temperature by slow compression or by impact. The effects of the impurities are noted from the frequency of twins and the relative number of twin bands and slip lines. These deformation markings are analyzed to find any effect of composition on the choice of slip or twin plane.

The tests are complete only for crystals containing 2000 and 3000 ppm O. There was a very marked reduction in the occurrence of twins at both oxygen levels. Metallographic examinations of all the surfaces and several cross-section planes revealed only five to ten twin bands per specimen. This compares with several hundred twin bands in the high-purity samples deformed in the same manner but for much less total deformation. There was evidence of large amounts of slip in the oxygen-bearing specimens, and, in general, the slip was localized into several broad bands. In contrast, only a few widely spaced slip lines were observed in the pure specimens except for slip lines associated with the tips of adjacent twins.

[7] Abstract of published paper: *Acta Met.* 8, 900 (1960).

[8] Abstract of paper submitted to *Transactions of the Metallurgical Society of AIME.*

[9] W. R. Clough and A. S. Pavlovic, *Trans. Am. Soc. Metals* 52, 948 (1960).

[10] M. A. Adams, A. C. Roberts, and R. E. Smallman, *Acta Met.* 8, 328 (1960).

[11] E. O. Hall, *Twinning and Diffusionless Transformations in Metals*, pp 56–68, Butterworthe, London, 1954.

Other tests are in progress at lower oxygen levels and for the other interstitials.

Surface Effects on Twinning

In connection with the study of the effects of interstitial impurities on twinning, it was observed that the presence of a thin oxide film on the crystal faces completely prevented twinning in crystals containing 200 to 2000 ppm O. After removal of the oxide by etching, the crystals did twin upon being reloaded.

Several experiments are in progress to study the effects of surface films and the absence of free surfaces on the twinning frequency. In one set of tests, a thin nickel film was plated onto three surfaces of a crystal and the other three faces were left clean. This specimen will be deformed at 77°K and examined for surface twins after removal of the nickel layer. Another crystal will be contaminated with oxygen but will not be homogenized. This should give a specimen having a high concentration of oxygen in solution at the surface but having the original composition near the center. Since oxygen appears to inhibit twin formation, this specimen should show whether or not twins can nucleate in the center of the crystal.

The surface effects will be analyzed in terms of the crystallographic relationship to the twinning process, for example, with the shear direction parallel and perpendicular to the surface.

AN X-RAY STUDY OF DEFORMATION STACKING FAULTS AT LOW TEMPERATURES IN LEAD, SOME LEAD ALLOYS, AND ALUMINUM[12]

G. F. Bolling[13] T. B. Massalski[14]
C. J. McHargue

The deformation stacking fault probability, α, has been determined by the deformation of bulk specimens of zone-refined lead at 4.2 and 77°K. Aluminum (99.996%), α-brass (70:30), Pb–0.1 at. % Ag, and Pb–20.0 at. % In were also examined at 4.2°K. It is shown that a major difference exists between aluminum and lead, the latter being copper-like in its value of α. The influence of increased deformation in increasing the value of α is demonstrated. Addition of indium to lead suppresses a measurable value of α which correlated with observations made on twinning in this alloy.

[12]Abstract of paper presented at the Fall Meeting of the Metallurgical Society of AIME, Oct. 19, 1960, Philadelphia, Pa.; to be published in the *Philosophical Magazine*.

[13]Westinghouse Research Laboratory, Pittsburgh, Pa.

[14]Mellon Institute, Pittsburgh, Pa.

DEFORMATION STACKING FAULTS IN FACE-CENTERED CUBIC THORIUM AND CERIUM[15]

C. J. McHargue

The deformation stacking fault probabilities were calculated from the peak shifts of x-ray diffraction lines for thorium and cerium deformed at room temperature. The values of 0.018 to 0.031 for cerium and 0.019 for thorium are considered to be high, indicating that these metals have low stacking fault energies.

ANNEALING OF DEFORMED METALS

R. A. Vandermeer C. J. McHargue

Impurity-Controlled Grain-Boundary Migration During Recrystallization[16]

It is well established that minute quantities of foreign atoms dissolved in pure metals can greatly reduce the rate of recrystallization of these metals. Lücke and Detert[17] have attempted to explain this phenomenon in terms of a quantitative theory of impurity-controlled grain-boundary migration. There exist, however, only a few quantitative measurements for comparison with the theoretical predictions.

Essentially no agreement between the theory and the observed boundary motion was reported by Aust and Rutter[18] in dilute alloys of zone-refined lead. On the other hand, the studies of Vandermeer and Gordon[19] have shown an apparent agreement between theory and experiment in the case of small

[15]Abstract of paper to be published in *Acta Metallurgica*.

[16]This work was initiated at the Illinois Institute of Technology under the direction of P. Gordon, and part of the data of Fig. 7.1 will appear in a thesis submitted by R. A. Vandermeer to that school.

[17]K. Lücke and K. Detert, *Acta Met.* 5, 628 (1957).

[18]K. T. Aust and J. W. Rutter, *Trans. Met. Soc. AIME* 215, 820 (1959).

[19]R. A. Vandermeer and P. Gordon, *The Recrystallization of Zone-Refined Aluminum as Influenced by Recovery and Impurities*, Technical Report No. 2, U.S. Army Office of Ordnance Research, Contract AD-11-022-ORD-1984 (October 1960).

amounts of copper dissolved in zone-refined aluminum. The current program is concerned with extending these observations to include both a wider range of copper compositions, especially at the higher impurity levels, and other solutes in zone-refined aluminum.

In the theory proposed by Lücke and Detert, it is assumed that interaction forces exist between a grain boundary and the foreign atoms in solid solution such that at thermal equilibrium the concentration of foreign atoms in the boundary is higher than in the bulk material. At high concentrations of foreign atoms in the boundary or at low temperatures, a moving grain boundary is held back by this interaction, so that the speed of the boundary is controlled by the speed at which the atmosphere of foreign atoms can diffuse behind the moving boundary. At low concentrations or high temperatures, the interaction is insufficient to allow the impurity atmosphere to maintain its hold on the moving boundary, so that the boundary breaks away from the foreign atoms and moves at a much faster velocity. Lücke and Detert derived the following equation for the rate of grain-boundary migration when the impurities exert their drag on the boundary:

$$G = \frac{a^2}{4\sqrt{2}} \frac{D_0}{kT} \frac{P}{C} \exp\left(-\frac{Q_D + V}{kT}\right), \qquad (1)$$

where

G = velocity of boundary migration,

a = lattice parameter of solvent,

D_0 = bulk diffusion constant of solute atoms,

k = Boltzmann's constant,

T = absolute temperature,

P = driving force for migration in units of energy per unit volume,

C = atomic fraction of solute in bulk material,

Q_D = activation energy for bulk diffusion of solute atoms,

V = gain in energy as a result of putting a foreign atom in a grain boundary.

If we take

$$G_0 = \frac{a^2}{4\sqrt{2}} \frac{D_0}{kT} \frac{P}{C} \qquad (2)$$

and

$$Q = Q_D + V, \qquad (3)$$

then Eq. (1) is identical in form to the usual Arrhenius type of equation that expresses the temperature dependence of the rate of grain-boundary migration during recrystallization.

The theory also predicts that for a given temperature there will be a critical value of the bulk concentration at which the grain boundary will break away from the atmosphere of foreign atoms. This concentration is given by Lücke and Detert as

$$C^* = \frac{a^3}{8} \frac{P}{V} \exp\left(-\frac{V}{kT}\right). \qquad (4)$$

Aluminum-copper alloys, containing 0.00047, 0.0286, and 0.060 wt % Cu, have been melted and cast under vacuum. These were fabricated into strip by cold rolling with intermediate recrystallization anneals. A final reduction of 40% was carried out by rolling at 0°C. Isothermal recrystallization studies were conducted on specimens cut from the strip containing 0.060 wt % Cu at temperatures in the range 139 to 200°C. Grain-boundary migration rates were obtained at four different temperatures for this alloy. These are tabulated in Table 7.1.

Table 7.1. Grain-Boundary Migration Rates in an Aluminum Alloy Containing 0.060 wt % Cu

T (°C)	G (cm/sec)
200	2.5×10^{-5}
187	7.8×10^{-6}
169	2.6×10^{-6}
139	1.7×10^{-7}

One of the predictions of the Lücke-Detert theory is that the activation energy for impurity-controlled grain-boundary migration is equal to $Q_D + V$, and that at concentrations exceeding C^* this value should be essentially constant. Figure 7.1 shows the experimental activation energies (determined from plots of log G vs $1/T$) as a function of the logarithm of concentration. It should be noted that at concentrations above 5×10^{-5} atomic fraction of copper the experimental activation energy for boundary motion is constant with a value of about

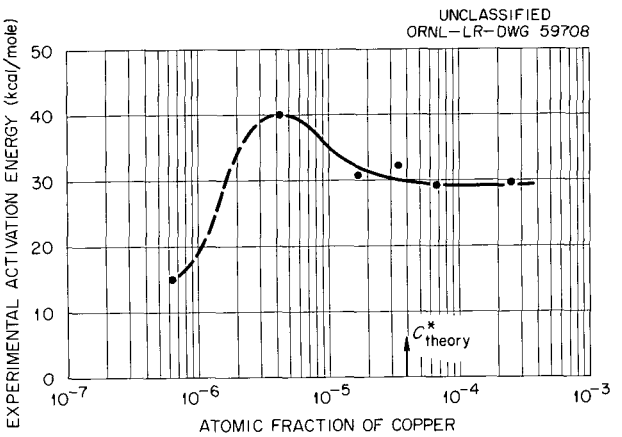

Fig. 7.1. Relationship Between Experimental Activation Energy for Grain-Boundary Migration and Concentration of Copper in Aluminum.

29.5 kcal/mole. This may be compared with the theoretical value $(Q_D + V)$ of 33.7 kcal/mole.

In addition, the critical concentration at which breakaway should occur according to the Lücke-Detert theory can be calculated from Eq. (4) for copper in aluminum. Taking $a = 4.04 \times 10^{-8}$ cm, $P \cong 12 \times 10^{-6}$ erg/cm^3, $V = 1.6 \times 10^{-13}$ erg/atom, $T = 423°K$, and $k = 1.38 \times 10^{-16}$ erg/°C, the critical concentration C^* is approx 4×10^{-5}. This compares very favorably with the C^* value of 5×10^{-5} estimated from Fig. 7.1 as the point beyond which the activation energies are constant.

A theoretical estimate of G_0 for the impurity-controlled grain-boundary migration predicted by the Lücke-Detert theory can be made by using Eq. (2). Table 7.2 is a listing of such theoretical values and the experimental values of G_0 for three alloys. The copper contents of two of the alloys are greater than the critical breakaway concentration of C^*, that is, they are in the impurity-controlled region, while the other alloy contains less than C^* and is in the breakaway region. For the alloys in the impurity-controlled region $(C > C^*)$ the disagreement is about a factor of 20. Usually, discrepancies of many orders of magnitude are found for G_0, as in the case of the 0.001 wt % Cu alloy here.

Experimental evidence has been presented which agrees semiquantitatively with the theoretical predictions of the Lücke-Detert theory of impurity-controlled grain-boundary migration for the case of copper impurities in aluminum. However, studies of a wider range of copper concentration and of other solutes will be carried out in order to provide a rigorous test of the theory.

Table 7.2. Comparison of Theoretical and Experimental Values of G_0

Alloy (wt % Cu)	Experimental G_0 (cm^2/sec)	Theoretical G_0 (cm^2/sec)
0.001	3.1×10^{17}	1.2×10^{9}
0.016	4.3×10^{9}	2.2×10^{8}
0.060	1.2×10^{9}	0.6×10^{8}

Preferred Orientation in Annealed Aluminum Rods

The earlier results of McHargue *et al.*[20] on the preferred orientation of aluminum extruded at temperatures between 20 and 350°C showed the recrystallization texture to be entirely <001> when the primary recrystallization occurred during the fabrication process. Some additional annealing experiments have been conducted on specimens taken from an aluminum rod extruded at liquid-nitrogen temperature, where no recrystallization could occur during fabrication. It was observed that annealing in the range 139 to 270°C produced a duplex primary recrystallization texture containing approximately equal amounts of <001> and <111> orientations. Furthermore, it appears that the <001> recrystallized component resulted from the growth of the pre-existing nuclei. These nuclei are fragments of <001> grains which were carried over from the cast structure during the extrusion process.

It was proposed previously[21] that a stress applied while recrystallization is taking place might affect the recrystallization process. There are two factors which might be influenced by such a stress – the nucleation and the relative growth rates in various crystallographic directions.

[20] C. J. McHargue, L. K. Jetter, and J. C. Ogle, *Trans. Met. Soc. AIME* 215, 831 (1959).

[21] C. J. McHargue and L. K. Jetter, *Met. Div. Ann. Progr. Rept. Oct. 10, 1957*, ORNL-2422, pp 212–13 (classified).

Work has been started to test this hypothesis and to learn the origin of any effect. Preliminary results have been obtained by annealing portions of the low-temperature (77°K) extrusion in a salt bath at 231°C and in a press under a compressive stress at 240°C. The data are summarized in Table 7.3 and indicate that the rate of recrystallization is greatly reduced by the applied stress and that the <001> component is favored by the stress.

This work will be continued and will include studies of the effect of prior recovery on recrystallization rate and texture and of the nature and origin of recrystallization nuclei.

Table 7.3. Effect of Stress on Recrystallization of Aluminum

Time (hr)	Fraction Recrystallized	Fraction of <001>
	Anneal in Salt Bath at 231°C	
2	0.428	0.144
20	0.819	0.381
	Anneal Under Stress at 240°C	
20	0.528	0.342

8. X-RAY DIFFRACTION

H. L. Yakel

ROUTINE ANALYSES

H. L. Yakel R. M. Steele
O. B. Cavin L. A. Harris

The Metallurgy and Ceramics X-Ray Diffraction Laboratories have examined over 650 samples submitted for routine analyses during the period of of this report. Lattice-parameter measurements, phase identifications, single-crystal orientation measurements, estimations of preferred orientation, and stress-level determinations are representative of these analyses.

X-RAY SCATTERING FROM IRRADIATED BeO

R. M. Steele

Polycrystalline specimens of BeO, irradiated to 10^{21} *nvt* (fast neutrons) in the ETR, have been examined by means of a Debye-Scherrer diffraction technique. Measurements of the photographs from samples irradiated at approx 110°C show several heretofore unreported diffraction effects. Notable among these is the selective symmetric or asymmetric broadening of reflections $(hk \cdot l)$, with l even or odd (but not zero). Attempts are being made to correlate these diffraction effects with a model of a damaged BeO lattice. Lattice-parameter data from the specimens are summarized in Table 8.1. Published results of other investigations are included for comparison.

CRYSTAL STRUCTURE OF $LuMnO_3$

H. L. Yakel

A refinement of the structure of $LuMnO_3$, based on the space group $P6_3cm$, has been completed.[1] Although a satisfactory agreement factor of 13% (based on F^2) has been achieved, the structure is in doubt because of the anomalous β_{22} temperature-factor components of two of the oxygen atoms. These, together with the other atom parameters resulting from the refinement, are given in Table 8.2.

[1] H. L. Yakel, *Met. Div. Ann. Progr. Rept. July 1, 1960*, ORNL-2988, p 136.

Table 8.1. Lattice Parameters of Unirradiated and Irradiated BeO

Sample Condition	Number	a_0 (A)	c_0 (A)	c/a
Unirradiated, sintered	X41 4-C	2.6978 ± 0.0001	4.3778 ± 0.0003	1.6227
Unirradiated*		2.6981 ± 0.0002	4.3774 ± 0.0004	1.622
Irradiated to 10^{21} *nvt* (fast) at ~110°C	X41 5-7a(C)	2.7006 ± 0.0003	4.410 ± 0.005	1.633
	X41 5-7b(P)	2.7007 ± 0.0003	4.408 ± 0.005	1.632
Irradiated to 10^{21} *nvt* (fast) at > 110°C	X41 4-19	2.6997 ± 0.0003	4.398 ± 0.005	1.629
Irradiated to 10^{21} *nvt* (thermal), 5×10^{19} *nvt* (fast)*		2.6989 ± 0.0002	4.3909 ± 0.0004	1.627
Irradiated to 10^{21} *nvt* (fast) at ~110°C + DTA to 1200°C		2.6977 ± 0.0003	4.384 ± 0.003	1.625
Irradiated to 10^{21} *nvt* (thermal) + 4 hr at 1000°C*		2.6982 ± 0.0002	4.3845 ± 0.0004	1.625

*J. Elston and R. Caillat, *Proc. Intern. Conf. Peaceful Uses Atomic Energy, 2nd, Geneva, 1958* 5, 345 (1959).

Table 8.2. Atomic Parameters for $LuMnO_3$ Given by Least-Squares Refinement Based on the Space Group $P6_3cm$

$a_0 = 6.0420 \pm 0.0017$ A $\quad c_0 = 11.371 \pm 0.006$ A

Atom	Position	X	Y	Z	β_{11}	β_{22}	β_{33}	β_{12}	β_{13}	β_{23}
Lu(I)	2*a*	0.0000*	0.0000*	0.2705	0.0032	0.0032	0.0018	0.0016	0.0000	0.0000
Lu(II)	4*b*	0.3333*	0.6667*	0.2266	0.0030	0.0030	0.0017	0.0015	0.0000	0.0000
Mn	6*c*	0.3212	0.0000*	0.0000**	0.0031	0.0041	0.0017	0.0020	−0.0005	0.0000
O(I)	6*c*	0.3071	0.0000*	0.1699	0.0036	Neg	0.0010	Neg	−0.0001	0.0000
O(II)	6*c*	0.6328	0.0000*	0.3397	0.0147	0.0233	0.0014	0.0117	−0.0006	0.0000
O(III)	2*a*	0.0000*	0.0000*	0.4836	0.0061	0.0061	0.0019	0.0032	0.0000	0.0000
O(IV)	4*b*	0.3333*	0.6667*	0.0189	0.0019	0.0019	0.0035	0.0010	0.0000	0.0000

*Parameter fixed by space group.

**Arbitrarily fixed Z parameter.

It is possible that the anomalous oxygen-atom temperature factors are a result of an incorrect assignment of space group. Thus, if the atoms in question were not constrained by the mirror plane of $P6_3cm$ (i.e., if the space group were actually $P3cl$), a more acceptable result might be obtained. The problem will be re-examined from this point of view.

A preliminary description of this class of structures was presented at the Fifth Congress of the International Union of Crystallography.[2]

STRUCTURES OF PHASES IN BINARY OXIDE SYSTEMS CONTAINING BeO

L. A. Harris

CaO-BeO

Satisfactory single crystals of $Ca_2Be_3O_5$ have been secured from a supercooled eutectic melt (60 mole % BeO). A cubic unit cell with a_0 = 14.008 A is observed. Space groups $Fm3m$ or $Fm3$ are possible on the basis of observed extinctions. A test for pyroelectricity in these crystals was negative, suggesting that a structure based on $Fm3m$ could be assumed. Collection of CuK_α three-dimensional intensity data is in progress, preparatory to structure analysis.

[2]H. L. Yakel *et al.*, "Erbium Manganite – A New ABO_3 Structure," paper presented at the Fifth International Congress and Symposia of the International Union of Crystallography, Cambridge, England, Aug. 15–24, 1960.

Y_2O_3-BeO

Crystals of a previously reported phase[3,4] in this system have been grown and analyzed. A formula $Y_2Be_2O_5$ is proposed. Diffraction data indicate an orthorhombic unit cell with the dimensions a_0 = 3.51 A, b_0 = 10.36 A, and c_0 = 13.04 A.

A PRESSURE-INDUCED PHASE TRANSFORMATION IN A UO_3 MONOHYDRATE[5]

L. A. Harris

An orthorhombic dipyramidal form and an orthorhombic lath-shaped form of UO_3 monohydrate have been grown hydrothermally. Optical constants and unit cell parameters for the two crystalline modifications are given in Table 8.3.

A previously unreported phase transformation was observed to take place in the orthorhombic dipyramidal phase upon the application of pressure. Optical and x-ray examinations of the new phase showed it to be identical to the orthorhombic lath phase. The transformation appears to fit Buerger's[6] "displacive transformation" classification.

[3]C. E. Weir and A. VanValkenburg, *J. Research Natl. Bur. Standards* 64A(1), 103 (1960).

[4]R. A. Potter, *Met. Div. Ann. Progr. Rept. July 1, 1960*, ORNL-2988, p 190.

[5]Abstract of paper presented at the American Ceramic Society Meeting, Toronto, Canada, Apr. 23–27, 1961.

[6]M. J. Buerger, *Am. Mineralogist* 33, 101–21 (1948).

Table 8.3. X-Ray and Optical Data for Two Forms of $UO_3 \cdot H_2O$

	Orthorhombic Dipyramid	Orthorhombic Lath
X-Ray Data		
Space group	*Pbca*	Face centered
a	5.63 ± 0.03 A	4.27 ± 0.02 A
b	6.30 ± 0.03 A	6.93 ± 0.02 A
c	9.94 ± 0.03 A	10.19 ± 0.02 A
Z	4	4
Optical Data		
Sign	(+)	(+)
α	1.740 ± 0.005	1.850 ± 0.005
β	1.750 ± 0.005	1.855 ± 0.005
γ	1.780 ± 0.005	1.880 ± 0.005
2 *V* (estimated)	15°	8°
Orientation	$Z = c$	$Z = a$

Optical observations made on partially transformed dipyramidal crystals lying on their (001) faces showed the two phases joined along a (11·*l*) dipyramid plane. The displacive movement appears to have taken place in a <110> dipyramid direction.

ORDERING OF COPPER-GOLD ALLOYS

H. L. Yakel

A prolonged high-temperature diffraction experiment, in which a polycrystalline Cu–31.6% Au sample is being slowly cooled from 440°C through the ordering transition to room temperature, is in progress. Within the transition region the sample is being held at a given temperature for at least two weeks in an attempt to approach true equilibrium.

The results to date have shown the following:

1. A normal thermal contraction of the disordered face-centered cubic lattice from 440 to 350°C ($\alpha = 17.82 \times 10^{-6}$/°C).

2. A pretransition lattice contraction between 350 and 337°C. No development of superstructure reflections can be observed in this interval, nor are the high-angle reflections broadened or split.

3. A probable two-phase region between 337 and 330°C. Only one temperature (333°C) was maintained within this region, and its exact limits are therefore uncertain. Satellited superstructure reflections are first observed in this interval, indicating that the transition to the antiphased structure has begun.[7,8] Broadening of high-angle fundamental reflections is interpreted as evidence for a classical two-phase region separating the disordered and the antiphased phase fields. Note that this transition region is 10 to 15°C lower in temperature than that observed by Scott in an alloy of the same composition.[8]

4. Complete transition to the antiphased structure below 330°C. The structural properties of this phase are good in agreement with those cited in an earlier report.[7] The stability region of the antiphased structure extends at least down to 310°C, the lowest temperature attained thus far. Figure 8.1 summarizes the data to this point.

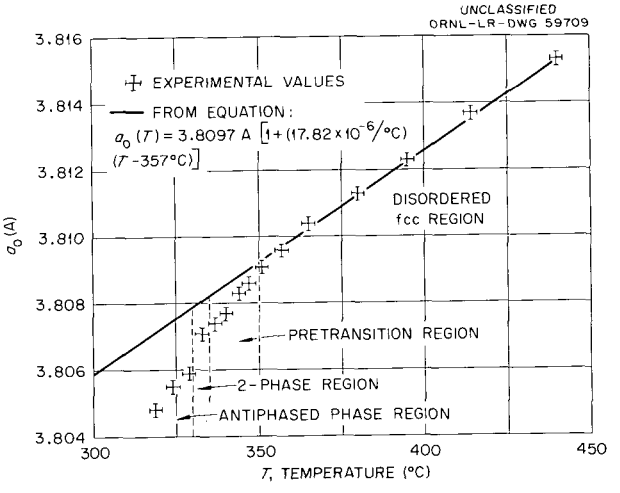

Fig. 8.1. Lattice Parameter of Cu–31.6 at. % Au Alloy vs Temperature on Cooling Polycrystalline Sample from 440 to 319°C.

AGING TRANSFORMATIONS IN METASTABLE ALLOYS

O. B. Cavin

Zirconium-Niobium

Two Zr–15 at. % Nb single crystals have been irradiated in the ORR for periods of one week at

[7] B. S. Borie, C. J. Sparks, and H. L. Yakel, *Met. Div. Ann. Progr. Rept. Sept. 1, 1959*, ORNL-2839, p 58.

[8] R. E. Scott, Ph.D. thesis, Physics Department, Massachusetts Institute of Technology (1958).

250 and 425°C respectively. The estimated integrated thermal neutron dose received by these crystals was 10^{19} *nvt*. X-ray diffraction studies of these crystals should give further data on the effect of reactor radiation on the formation of the metastable Ω phase in this alloy system.[9]

Zirconium-Chromium, Zirconium-Vanadium

Attempts to retain the high-temperature body-centered cubic β phase in zirconium alloys containing 1 and 2 wt % Cr have not been successful. Similar experiments with Zr-V alloys have awaited the development of satisfactory homogenization procedures, since the cast structures show significant mass segregation. Further work in both alloy systems is planned.

Uranium-Niobium

Diffraction experiments with alloys containing 5, 7.5, and 10 wt % Nb quenched from 1000°C (in the γ-phase field) have shown that only the 7.5 wt % Nb samples undergo a quenching transformation to a metastable tetragonal phase. Low-temperature equilibrium phases were found in the γ-quenched 5 wt % Nb alloys, while the γ phase was retained in the 10 wt % Nb alloys. Further experiments at the 7.5 wt % composition are in progress.

[9] H. L. Yakel, *Met. Div. Ann. Progr. Rept. Sept. 1, 1959*, ORNL-2839, p 51.

Part II

LONG-RANGE APPLIED METALLURGY

9. PHYSICAL PROPERTIES STUDIES

D. L. McElroy T. G. Kollie

A limitation to the development of nuclear technology is the lack of knowledge of the magnitude and mechanisms of heat-transport phenomena at high temperatures in refractory materials of interest for reactor fuels, moderators, and claddings. Applied and basic interests are encompassed in the goals of this study and include:

1. measurement of thermal conductivity k between −100 and 2200°C;
2. determination of the effects of physical and chemical variations in a material on its k value;
3. obtaining accurate k data and auxiliary information for the evaluation of methods of measuring k, and the treatment of the mechanisms of heat transport.

Accomplishments during the past year include: (1) operation of a thermal comparator apparatus to 400°C, (2) operation of a radial heat flow apparatus to 800°C, (3) initiation of construction of a quenching apparatus to measure thermal diffusivity to 1400°C, (4) design of a direct heating apparatus to measure k from 800 to 2200°C, and (5) measurement of the characteristic temperature of UO_2.

THERMAL COMPARATOR APPARATUS[1-3]

This apparatus, given schematically in Fig. 9.1, shows promise of yielding comparison k data reproducible to within ±3%, between 50 and 600°C. The upper furnace contains two instrumented spheres mounted at slightly different heights and maintained at a temperature different from that of the lower furnace. The lower furnace contains the thermally shielded specimen disk, $\frac{1}{4}$ in. thick and 1 in. in diameter. The equipment may be operated in an inert atmosphere or in vacuum. At zero time, the specimen is raised to contact the lower sphere. The noncontacting sphere corrects for heat transfer other than specimen conduction. The differential temperature-time response of the two spheres is measured for 30 sec and is proportional to the k of the specimen. A calibration curve, using materials of known k, is being determined.

A typical response curve for Pyrex at 175°C in helium is shown in Fig. 9.2*a*. Also shown is the normalized response $\overline{R}$ as a function of time. Tests on a particular material have shown $\overline{R}$ to be constant at a given time for initial specimen-sphere temperature differences between −25 and +25°C. Handbook values of k for Pyrex, INOR-8, and iron are plotted in Fig. 9.2*b* as a function of $\overline{R}$. A variation of ±3% from a smooth curve was indicated by these data. Additional calibration materials and their corresponding range of k values are listed in Fig. 9.2. The effects of grain size, porosity, stoichiometry, and impurities on k for UO_2 will be studied as soon as the calibration curve is definitely established.

RADIAL HEAT FLOW APPARATUS

An effort was spent in perfecting the radial heat flow apparatus patterned after the design of Hedge and Fieldhouse.[4,5] This work led to major changes and improvements resulting in (1) easier assembly of the apparatus – by slight specimen changes and improved thermocouple installation; (2) achievement of reproducible and meaningful temperature control – by use of commercial temperature controllers; and (3) power uniformity and stability for the core heater – by redesign of the heater and by use of a transistorized solid-state power supply. These changes, coupled with an improved switching and monitoring arrangement for the measurement of direct and differential thermocouple emf's, have made this equipment operational

[1] A. I. Dahl and D. W. Jones, "Thermal-Conductivity Studies with the Powell Method," ASME paper 60-HT-30, ASME-AIChE Heat Transfer Conference, Buffalo, New York, Aug. 15–17, 1960.

[2] R. W. Powell, *J. Sci. Instr.* 34, 485 (1957).

[3] Battelle Memorial Institute has similar equipment under study; H. W. Deem, private communication, Mar. 30, 1961.

[4] J. P. Hedge and I. B. Fieldhouse, *Measurement of Thermal Conductivity of Uranium Oxide*, AECU-3381 (Sept. 20, 1956).

[5] S. D. Fulkerson, *Met. Div. Ann. Progr. Rept. July 1, 1960*, ORNL-2988, p 195.

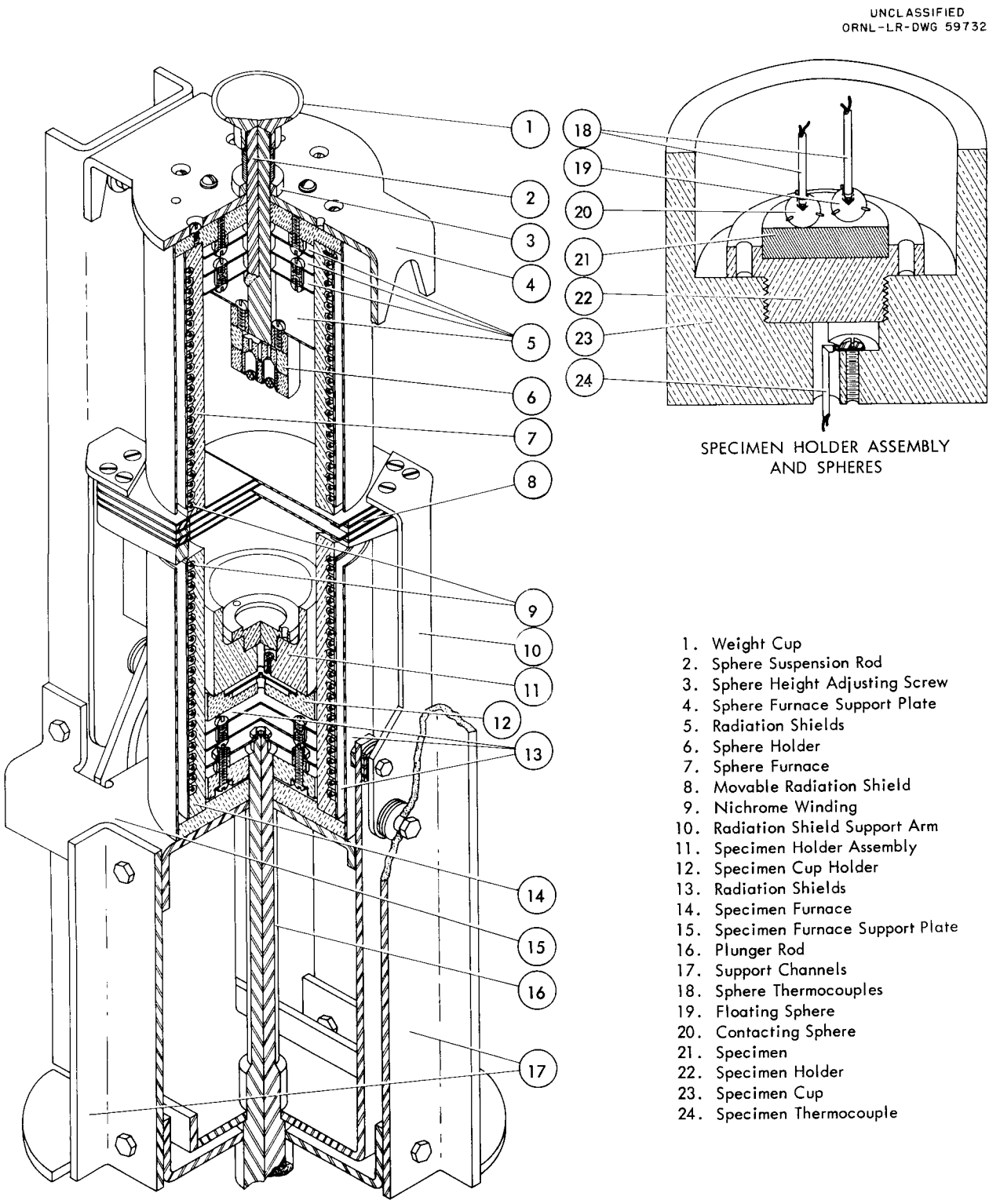

Fig. 9.1. Schematic Drawing of Thermal Comparator Apparatus.

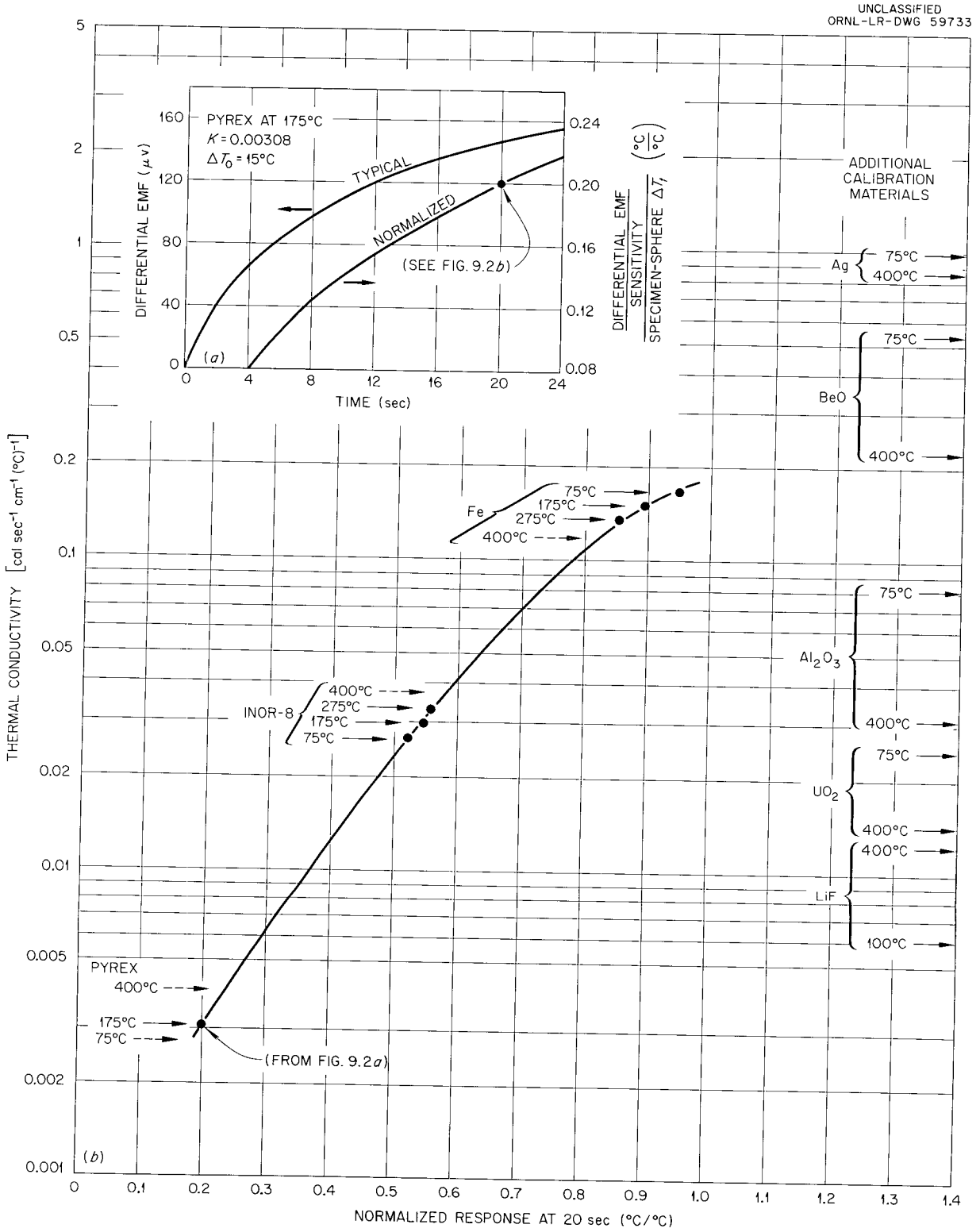

Fig. 9.2. Preliminary Calibration of Thermal Comparator Apparatus. (*a*) Typical response vs time for Pyrex in helium at 175°C, and normalized response vs time. (*b*) Handbook k values vs normalized response at 20 sec.

in the sense of yielding reproducible (±2%) and accurate (±5%) k data to 800°C. Results obtained with these and other modifications are reported elsewhere.[6] Efforts are being continued to reduce the specimen size and to extend the temperature limit to 1600°C.

RELATED PROJECTS

A quenching apparatus for measuring thermal diffusivity ($\alpha = k/\rho \cdot C_p$) to at least 1400°C has been designed and is currently under construction. Components of this apparatus include: (1) two cylindrical furnaces having $MoSi_2$ heating elements (1700°C, in air); (2) two 48-in.-long impervious Al_2O_3 tubes, 3 and 6½ in. in internal diameter; (3) equipment for maintaining an inert atmosphere in the tubes; and (4) a fluidized bed, 5 in. in outside diameter and 15 in. high. The smaller furnace is mounted directly above the large furnace and initially will contain the specimen, a cylinder 1 in. in outside diameter and 10 in. long. After the specimen attains thermal equilibrium, it is quenched into the fluidized bed, which is approx 50°C hotter or colder than the specimen. The time-temperature response of the geometrical center of the specimen is recorded, and from this the thermal diffusivity is determined.[7,8] Specimen shapes other than cylinders can be tested. The specimen response data also will yield specific heat values if the heat transfer of the fluidized bed can be defined.

Design of a direct heating apparatus for measuring the thermal conductivity between 800 and 2200°C has been initiated. Design features include vacuum operation, an auxiliary isothermal furnace to achieve temperatures needed for initiation of direct resistance heating of the specimen, temperature measurements by optical and thermoelectric means, and a stable specimen power source. Specimens will be heavy-wall tubes or solid rectangular columns.

CHARACTERISTIC TEMPERATURE OF UO_2

Crystals of $UO_{2.029}$ for the measurement of the characteristic temperature, Θ, were grown by passing water-saturated argon over an LiF-NaF-UF_4 melt at 850°C. A diffuse x-ray scattering method, using CuK_α radiation and a doubly bent LiF monochromator, was employed to measure Θ.[9] Treatment of point counting data to obtain absolute intensities did not give an accurate measure of the structure factors because of a preferred orientation in the sample. The factor $2M$ was therefore determined from temperature diffuse scattering, which is less sensitive to preferred orientation. A value of 188°K for Θ was obtained for UO_2, with a corresponding 0.12-A rms displacement of uranium atoms from their sites due to thermal motion. A conservative estimate is an error not greater than 10% in Θ. Low-temperature specific heat data on UO_2 contain a large maximum of uncertain origin at 29°K and yield a Θ of 160°K.[10] From a consideration of the above and the $1/T$ dependence of k at high temperatures for UO_2, one would expect a maximum of k to occur at 0.28Θ, or 53°K, and to have a value of approx 0.67 w cm^{-1} $(°C)^{-1}$.

[6] T. G. Godfrey and D. L. McElroy, "Thermal Conductivity Studies," chap. 13, this report.

[7] E. S. Fitzsimmons, *J. Am. Ceram. Soc.* 33, 327 (1950).

[8] F. C. W. Olson and O. T. Schultz, *Ind. Eng. Chem.* 34, 874 (1942).

[9] B. S. Borie performed all the x-ray measurements and calculations; private communication, Feb. 27, 1961.

[10] W. M. Jones, J. Gordon, and E. A. Long, *J. Chem. Phys.* 20, 695 (1952).

10. SINTERING STUDIES

C. S. Morgan

SINTERABILITY OF ThO_2 POWDERS[1]

C. S. Morgan

The sinterability of similarly pressed compacts prepared from thoria powders with different properties was determined as a function of particle size, crystallite size, surface area, immersion density, and particle size after treatment for 20 min in a Waring Blendor. The sinterability, as indicated by density after firing at 1800°C for 2 hr, decreased gradually with increasing particle size, but the scatter of points far exceeded experimental error. For surface area, crystallite size, and immersion density, there was a rough correlation with sinterability for powders that varied according to the method of precipitation. However, for the sinterability of thoria powders with properties changed by higher calcination temperature, there was an abrupt departure from the correlation. The best correlation of sinterability with powder properties was with particle size after Waring Blendor treatment, which represents a measure of particle integrity. The larger the resultant particle size after comminution of the particles in the Blendor, the lower the sinterability of the powder from which the sample was taken.

The failure of sinterability to consistently follow surface area, immersion density, crystallite size, or particle size suggests that no one of these properties is sufficient to characterize a powder. Other properties or a combination of properties must control the sinterability of ThO_2. The particle integrity under strong agitation reflects particle topology, mechanical property, and lattice defects, all of which could influence sinterability.

MODEL STUDIES

C. S. Morgan C. S. Yust

Model studies involving weld growth between two spheres, between a sphere and a flat surface, or between other geometric shapes that are touching have been used extensively to investigate sintering mechanisms. Results usually have been interpreted as indicating that a volume-diffusion process predominated.[2] Weld-neck growth was measured between ThO_2 spheres at temperatures close to 1800°C, in air. The spheres were approx 80 μ in diameter and were produced by the Houdry Process Corporation by spraying a thorium hydroxide gel into oil, with careful control of drying. Electron diffraction indicated that the spheres used were composed of 400- to 500-A crystallites. Metallographic examination indicated porosity and cracks in some spheres. Total impurities amounted to a few hundred parts per million.

Spheres were placed in a groove in a Pt-Rh wire or put on the surface of a thin sheet of sapphire. The neck between two spheres was determined with a movable-hairline measuring microscope. Spheres became attached to the metal or sapphire support, and little change occurred in end-to-end measurements of two spheres in contact.

Weld-neck growth was measured for a number of sphere pairs, and the logarithm of neck width was plotted as a function of the logarithm of time at temperature in order to determine the exponent n in the equation

$$x^n = A(T)t \ ,$$

where

x is the neck width,

$A(T)$ is the function of temperature and is related to flow properties of the material,

t is the time.

Kuczynski[3] and Frenkel[4] deduced that the value of n should be related to the method of material transport during sintering. The present results had some irregularities, but the majority of cases

[1] Abstract of paper to be submitted to the *Journal of the American Ceramic Society.*

[2] R. G. Bernard, *Powder Met.* No. 3 (1959).

[3] G. C. Kuczynski, *Trans. Met. Soc., AIME* 185, 169 (1949).

[4] J. Frenkel, *J. Physics (USSR)* 9, 385 (1945).

had a value close to 2 for n. Such a value indicates that a plastic-flow mechanism is operative for material transport. This agrees with results for TiO_2 spheres.[5]

SINTERING-RATE STUDIES

C. S. Morgan C. S. Yust

The sintering-rate behavior of thorium oxide compacts is being investigated as part of an effort to evaluate the mechanism of material transport in sintering. The oxide used in these studies was prepared from thorium oxalate by thermal decomposition, followed by calcination at 650°C for 2 hr. The calcined powder was formed by cold pressing into compacts having a green density of approx 4.75 g/cc.

The densification of thorium oxide compacts has been measured for heating rates of 1.6 to 8.0°C/sec, and the data are presented in Fig. 10.1. Within this range of heating rates, the densification of compacts heated to a particular temperature and then air quenched was found to be independent of the time required to come to temperature. The densification is also independent of the heating cycle. A compact heated to 1000°C at a rate of 4°C/sec, held at 1000°C for 1 min, and then heated to 1500°C at a rate of 2.67°C/sec was found to have experienced the same densification as a compact heated directly to 1500°C. Limited investigation of prolonged heating cycles indicates that for heating periods as long as 1 hr, independence of heating rate persists. At very slow heating rates, the influence of isothermal densification should begin to have a more significant effect, and the temperature dependence of densification would be less specific.

The densification data of Fig. 10.1 can be replotted as densification rate vs temperature or time, as shown in Fig. 10.2. The densification rate curves exhibit an initial peak and a minimum at approx 1000 and 1200°C respectively. The significance of the minimum in the curve is not clear at present, although it may be indicative of the operation of two or more sintering mechanisms.

To further test the existence of the minimum in the densification rate curve, compacts of thoria calcined at 1000°C for 2 hr were prepared for rate study. The variation of rate with temperature for these compacts is also shown in Fig. 10.2. The rate of densification is seen to exhibit the same minimum.

[5] G. Parravano, H. M. O'Bryan, Jr., and V. J. Lee, "Sintering Mechanism of Titania," paper presented at the International Powder Metallurgy Conference, New York, June 13–17, 1960.

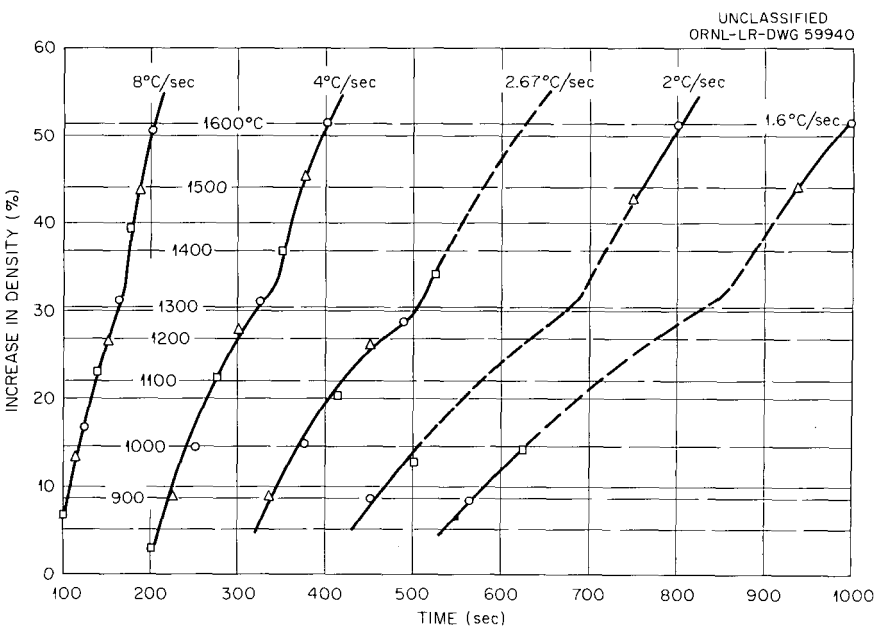

Fig. 10.1. Densification of Thoria Compacts as a Function of Heating Rate and Temperature.

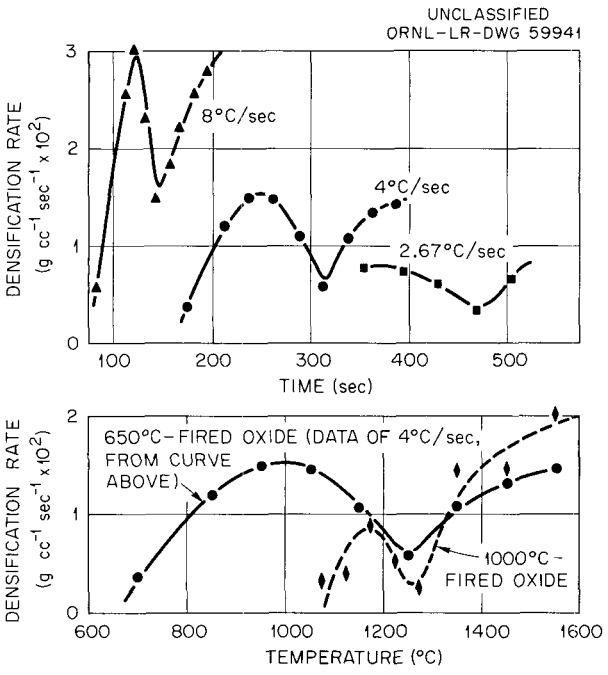

Fig. 10.2. Densification of Thoria Compacts as a Function of Time and Temperature.

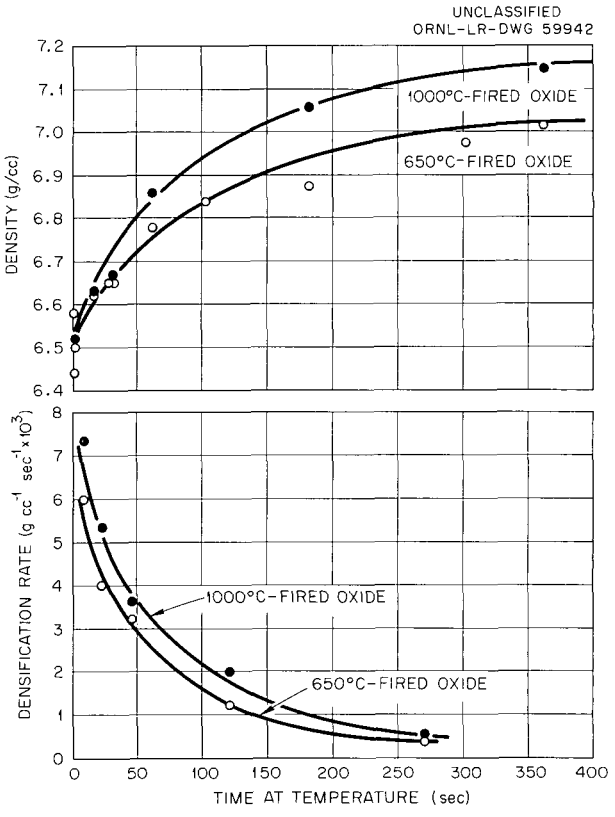

Fig. 10.3. Densification of Thoria Compacts at 1400°C.

Isothermal densification data also have been accumulated for compacts prepared from thoria calcined at 650 and 1000°C. Since significant densification takes place during heating, the isothermal component starts at some density which differs from the cold-pressed density. As shown in Fig. 10.3, a compact prepared from 650°C-fired oxide pressed to a density of 4.75 g/cc had already increased in density 37% when the isothermal densification at 1400°C started. As the compact was held at temperature, the density increased with time, while the rate at which the density increase occurred diminished rapidly. The data for compacts prepared from 1000°C-fired oxide are also presented in Fig. 10.3. In this case the compact had densified 13.5%, over its green density of 5.75 g/cc, before isothermal densification. The densification rates were about the same in both cases, although the degree of prior compact densification differed by a factor of 3, and the absolute density of both oxide compacts upon reaching 1400°C was also the same, approx 6.5 g/cc. The relative behavior of the two oxides indicates that a significant portion of the initial densification is intraparticle rather than interparticle, and that the particles do not distinguish between the initial densification experienced as a single particle, as opposed to the initial densification experienced as a particle in a compact.

DIFFUSION OF OXYGEN IN THORIA

C. S. Morgan C. S. Yust

A knowledge of the diffusion coefficient of the constituent ions is desirable when the mechanism of sintering in a material is considered. In principle, these data and the rate of densification allow one to determine the role of bulk diffusion in the process. The diffusion coefficient for oxygen in thoria microspheres has been determined by O^{18} ion exchange with CO_2 gas at temperatures from 600 to 1400°C, by the method described by Belle.[6] The experiment involves the measurement of the rate of exchange of oxygen atoms in a gas of normal isotopic composition with O^{18}-enriched

[6] J. Belle, "Properties of Uranium Dioxide," *Proc. U.N. Intern. Conf. Peaceful Uses Atomic Energy, 2nd, Geneva, 1958* 6, 569–89 (1959).

oxygen ions in the solid. The rate of exchange is governed by the rate of diffusion of the oxygen ions in the solid. The results are plotted in Fig. 10.4. The energy of activation was 14.7 kcal/mole.

The accuracy of values of the diffusion coefficient determined by this method depends upon the value used for the diameter of the sphere. The value of 10 μ used in these experiments was based on a combination of particle size, which was determined by sedimentation, and surface area, which was determined by nitrogen adsorption. Diffusion of oxygen was also measured in an active thoria powder that contained irregularly shaped particles 0.2 to 3 μ in diameter. The uncertainty of the value of an equivalent spherical particle diameter makes the absolute magnitude of the results uncertain. The energy of activation for diffusion, however, was lower than with the larger spheres.

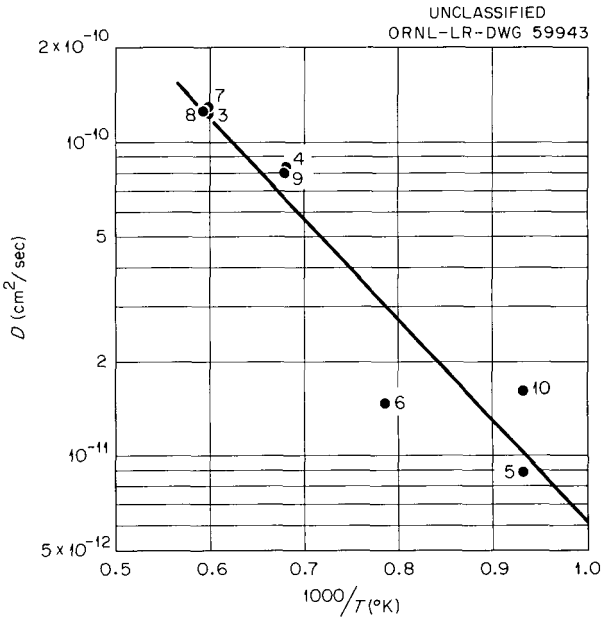

Fig. 10.4. Diffusion Coefficient of Oxygen Ions in ThO_2 Microspheres.

11. SOLID REACTION STUDIES

T. S. Lundy

DIFFUSION OF SOLID FISSION PRODUCTS IN FUEL AND CLADDING MATERIALS

J. I. Federer

The purpose of this study is to assist in defining conditions that might contribute to the diffusion release of fission products from nuclear reactor fuel and cladding materials. The scope of the current program has been a study of the diffusion of zirconium, niobium, and strontium in zirconium and in uranium dioxide. The main efforts to date have been on the self-diffusion of zirconium, the development and evaluation of isotope deposition techniques, and the procurement of special equipment for the study of diffusion in UO_2.

In the experiments thin layers of radioactive isotopes of the diffusing elements are deposited on the flat faces of nonradioactive, cylindrical specimens. Isothermal diffusion heat treatments are then performed under suitable environmental conditions. The concentration C of the radioactive species is determined as a function of the perpendicular distance x from the originally deposited layer and of the time t of the heat treatment. Theoretically, this concentration obeys the following solution to Fick's second law:

$$C(x,t) = \frac{M}{\sqrt{\pi Dt}} e^{-x^2/4Dt} ,$$

where

M is the amount of radioactive isotope deposited on the specimen,

D is the diffusion coefficient.

The plot of ln $C(x,t)$ vs x^2 yields a straight line having a slope which may be readily related to the diffusion coefficient.

Preliminary data have been obtained on the diffusion of Zr^{95}, Nb^{95}, and Sr^{95} in the body-centered cubic β phase of zirconium. The studies involving the diffusion of Zr^{95} have been hampered by the presence of the daughter Nb^{95}, due to the difficulty of discriminating between the isotopes. However, chemically pure solutions of Nb^{95} and Sr^{95} have been obtained, and experiments using these isotopes are being performed.

The study of the diffusion of strontium and niobium in UO_2 was initiated with high-purity, high-density, fused single crystals of UO_2. The requirement that each specimen have a flat surface and a constant cross section necessitated shaping the crystals by grinding and polishing. All crystals examined contained numerous cracks, and an uncracked region of sufficiently large size could not be found in most crystals. A few apparently uncracked specimens were prepared; however, these were unsuitable because stresses resulting from the crystal manufacturing method induced thermal cracking and disintegration. The studies are now being performed with high-purity polycrystalline specimens fabricated to 97% of theoretical density by compacting and sintering UO_2 powder. The surface of each specimen is lapped to a flatness of about two helium light bands (23 μin.) prior to deposition of the isotope to be studied. The isotope is deposited in a thin layer on the flat surface by evaporation from a filament under vacuum or by direct placement of drops of solution. In the latter case, compounds are selected which can be decomposed to a stable oxide by heating. For example, Sr^{85} was obtained as $Sr(NO_3)_2$ in weak nitric acid solution. Strontium nitrate decomposes[1] at 600 to 750°C in the following manner:

$$2Sr(NO_3)_2 \longrightarrow 2SrO + 4NO_2 + O_2 .$$

Niobium oxalate in oxalic acid solution appears to behave in a similar manner. Following the diffusion anneal, successive thin sections are removed parallel to the flat face by means of a precision lapping machine. The cumulative gamma activity collected on the lapping surface is

[1] P. F. Campbell, M. H. Ortner, and C. J. Anderson, *Anal. Chem.* 33(1), 58 (1961).

counted, and the thickness removed is measured by using an electronic comparator. The activity profile is then related to the diffusion coefficient, as previously discussed. Presently, UO_2 specimens having Sr^{85} and Nb^{95} isotopes deposited from solutions are being annealed in the temperature range 1500 to 1800°C.

SELF-DIFFUSION OF ALUMINUM

T. S. Lundy J. F. Murdock

The previously reported[2] method of obtaining Al^{26} for use in these experiments was abandoned because of the large quantities of Co^{56} produced as a by-product. The gamma spectrum of the Co^{56} overlaps that of the Al^{26} and for short decay times makes detection and quantitative counting of the Al^{26} impossible. However, proton-irradiated septum tubes having long decay times relative to the Co^{56} half-life of 77 days were obtained from J. J. Pinajian of the Electronuclear Research Division. These tubes, originally type 1100 aluminum, contained adequate amounts of Al^{26} to perform the self-diffusion experiments and also contained enough Mn^{54} to simultaneously determine its diffusion rate in aluminum.

Cylindrical diffusion couples of the thick-layer type were prepared. Disks about 0.015 cm thick containing the radioactivity were placed in contact with the polished, flat faces of "infinitely thick," inactive, cylindrical specimens of large-grained high-purity aluminum. The assemblies were held together at heat-treating temperatures in capsules, making use of the large thermal expansion of aluminum. Isothermal annealing, precision lathe sectioning, and activity counting of the sections were performed by standard techniques.

The applicable solution to Fick's law for these boundary conditions is:

$$\frac{A(x)}{A_0} = \frac{1}{2}\left(\operatorname{erf}\frac{h-x}{2\sqrt{Dt}} + \operatorname{erf}\frac{h+x}{2\sqrt{Dt}}\right), \qquad (1)$$

where

$A(x)$ is the activity at a normal distance x from the specimen surface,
A_0 is the original foil activity,
h is the foil thickness,
D is the diffusion coefficient,
t is the time of the heat treatment.

An approximate equation for the conditions of this experiment is obtained by assuming that h is very small. Then

$$A(x) \approx \frac{M}{\sqrt{\pi Dt}}\, e^{-x^2/4Dt}, \qquad (2)$$

where M is the amount of radioactivity at $t = 0$ and $x = 0$. The customary method of treating data from diffusion couples of this type is to plot $\ln A(x)$ as a function of x^2 and examine the linearity. If a straight line results, it usually is assumed that Eq. (2) applies, and the slope is set equal to $-1/(4Dt)$. However, such an assumption is not always valid, and, in fact, in the case of data from this experiment would lead to erroneous results. Plots of $\ln A(x)$ vs x^2 yield straight lines, but the actual diffusion coefficients are as much as 11% less than those calculated by making the assumption that Eq. (2) is applicable.

When the logarithm of $A(x)$, as given by Eq. (1), is differentiated with respect to x^2, the following is obtained:

$$\frac{d \ln A(x)}{dx^2} = \frac{e^{-(h+x)^2/4Dt} - e^{-(h-x)^2/4Dt}}{2x\sqrt{\pi Dt}\left[\operatorname{erf}(h-x)/2\sqrt{Dt} + \operatorname{erf}(h+x)/2\sqrt{Dt}\right]}. \qquad (3)$$

Examination of Eq. (3) by substituting approximate values of Dt and h revealed that for this experiment the slope does not change significantly over the maximum range of x. Thus the slope may be represented by its actual value at $x = h$, or

$$\frac{d \ln A(x)}{dx^2} = \frac{e^{-h^2/Dt} - 1}{2h\sqrt{\pi Dt}\,\operatorname{erf} h/\sqrt{Dt}}. \qquad (4)$$

[2] T. S. Lundy *et al.*, *Met. Div. Ann. Progr. Rept. July 1, 1960*, ORNL-2988, p 156.

The experimental data were plotted as ln $A(x)$ vs x^2 and the slopes set equal to that given by Eq. (4). The diffusion coefficients were then readily calculated by a simple iterative process. Typical penetration curves for Al^{26} and Mn^{54} are given in Fig. 11.1. It is noted that the large

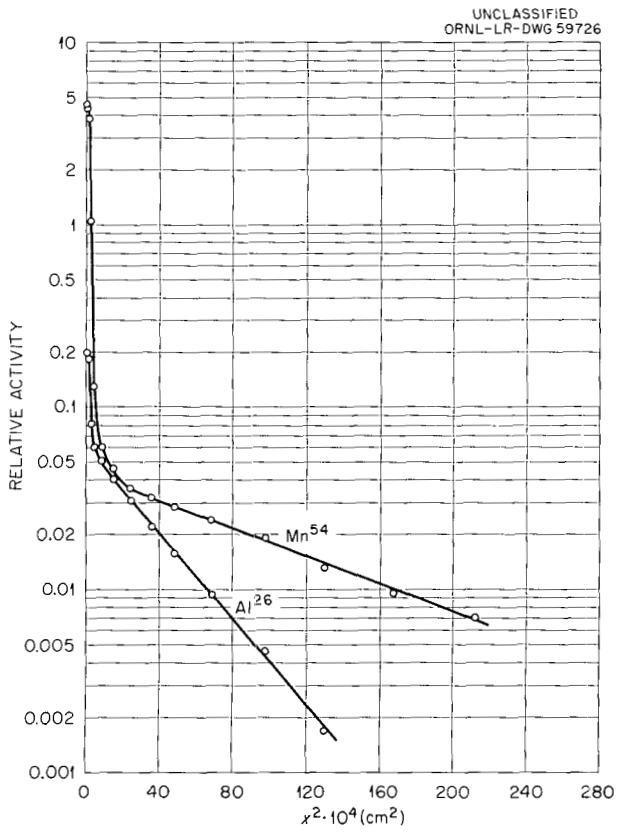

Fig. 11.1. Typical Penetration Plots for Al^{26} and Mn^{54} in Aluminum (95.5 hr at 571°C).

values of $A(x)$ near $x = 0$ may be explained by the presence of a diffusion barrier of Al_2O_3 at the foil interface. Also noted is the fact that Al_2O_3 is a much larger barrier for the movement of Mn^{54} than for that of Al^{26}.

Figure 11.2 contains plots of the diffusion coefficients of both Al^{26} and Mn^{54} in aluminum as functions of the inverse absolute temperature. The data fitted the following equations:

$$D_{Al^{26}}(T) = 1.3e^{-33,600/RT}, \qquad (5)$$

$$D_{Mn^{54}}(T) = 3.2e^{-33,500/RT}. \qquad (6)$$

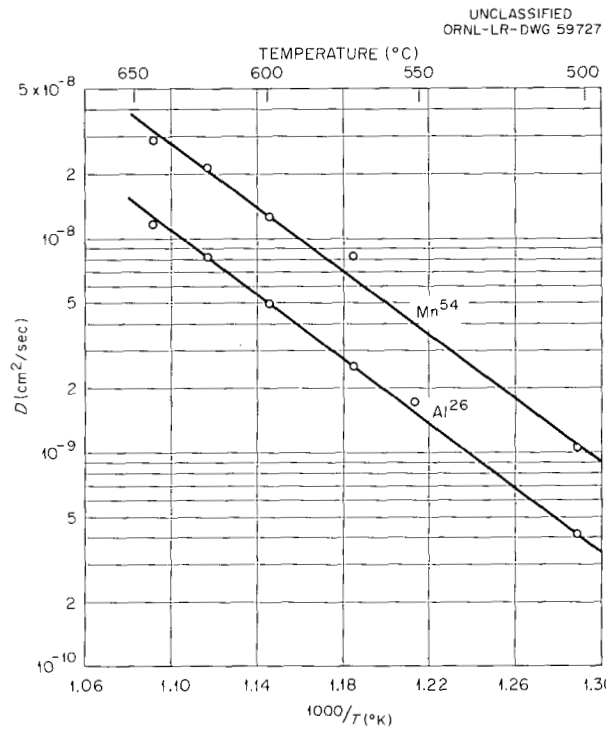

Fig. 11.2. Arrhenius Plots for Al^{26} and Mn^{54} in Aluminum.

URANIUM MONOCARBIDE–BERYLLIUM REACTION

J. F. Murdock

The extent of reaction between arc-cast uranium monocarbide and hot-pressed beryllium has been determined at temperatures from 700 to 1000°C. Diffusion couples of these materials were assembled into Inconel capsules and were described previously.[3] Intimate contact between the uranium monocarbide and the beryllium was ensured by the high thermal expansion of the type 347 stainless steel plug relative to that of the Inconel. The assemblies were welded closed in an argon-filled dry box. They were then isothermally heat-treated for various lengths of time.

After completion of the heat treatments, the diffusion couples were mounted in Hysol epoxy resin and sectioned and polished normal to the uranium monocarbide and the beryllium interface. The polished surface was chemically anodized

[3] J. F. Murdock, *GCR Quart. Progr. Rept. Mar. 31, 1961*, ORNL-3102, p 108.

to facilitate measuring of the reaction-zone thickness. An ultrasonic-microchiseled sample of the reaction product from the 1000°C sample was identified by x-ray diffraction as UBe_{13}.

Figure 11.3 illustrates the reaction zone resulting from heat treatment at 1000°C and is typical for all specimens examined. Figure 11.4 shows the finely dispersed precipitate, probably free carbon, observed within the reaction zone of all the specimens.

Thicknesses of the UBe_{13} layers, measured with a precision measuring microscope, are given in Table 11.1. These data indicate that in the range 750 to 800°C there is a marked increase in the reaction rate with increasing temperature.

Table 11.1. Summary of Reaction Data for Uranium Monocarbide–Beryllium Diffusion Couples

Temperature (°C)	Time (hr)	Average UBe_{13} Thickness (μ)
700	185	7
750	187	27
800	162	115
850	144	106
900	121	150
950	103	131
1000	90	176

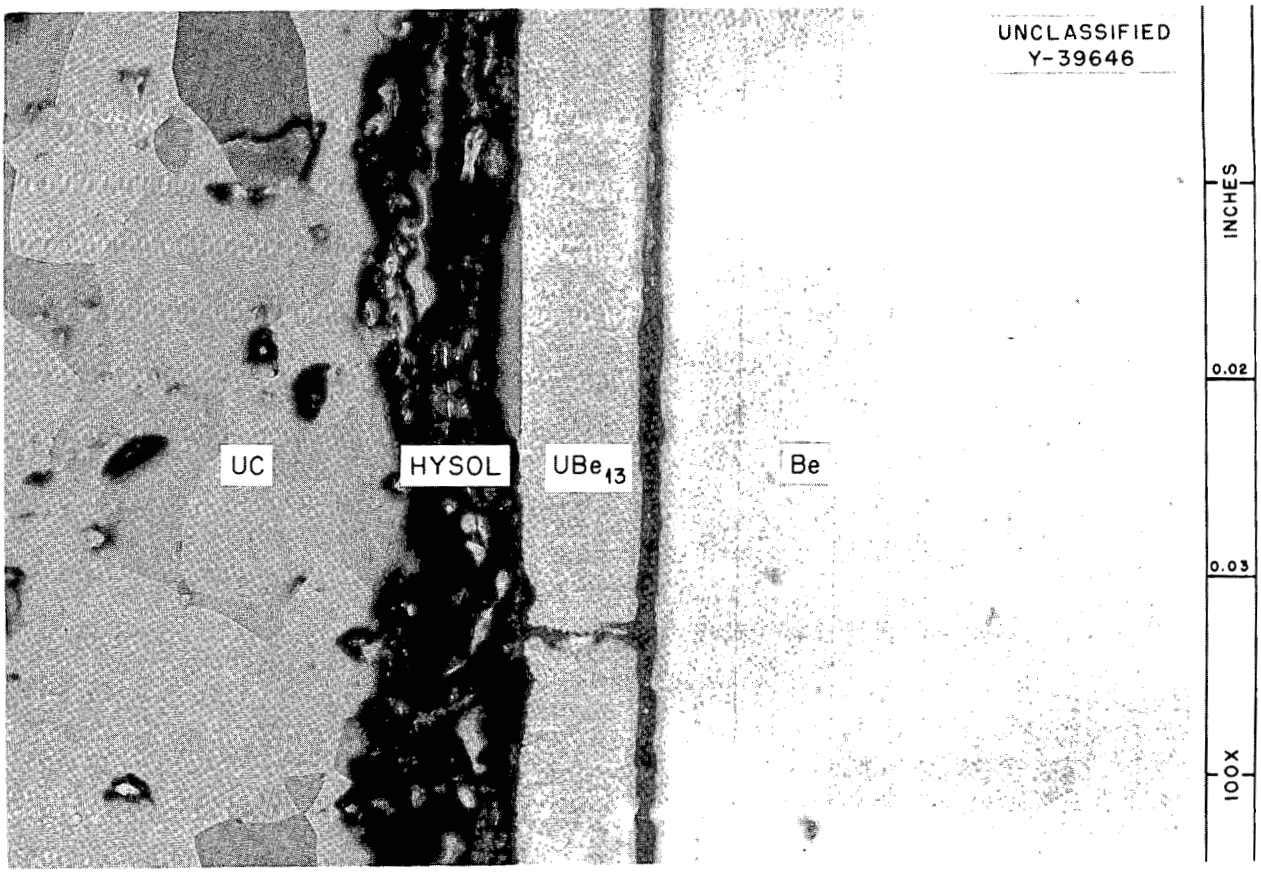

Fig. 11.3. Uranium Monocarbide–Beryllium Diffusion Couple Heat Treated at 1000°C for 90 hr. The UC was etched with 1:1:1 H_2O, CH_3COOH, HNO_3.

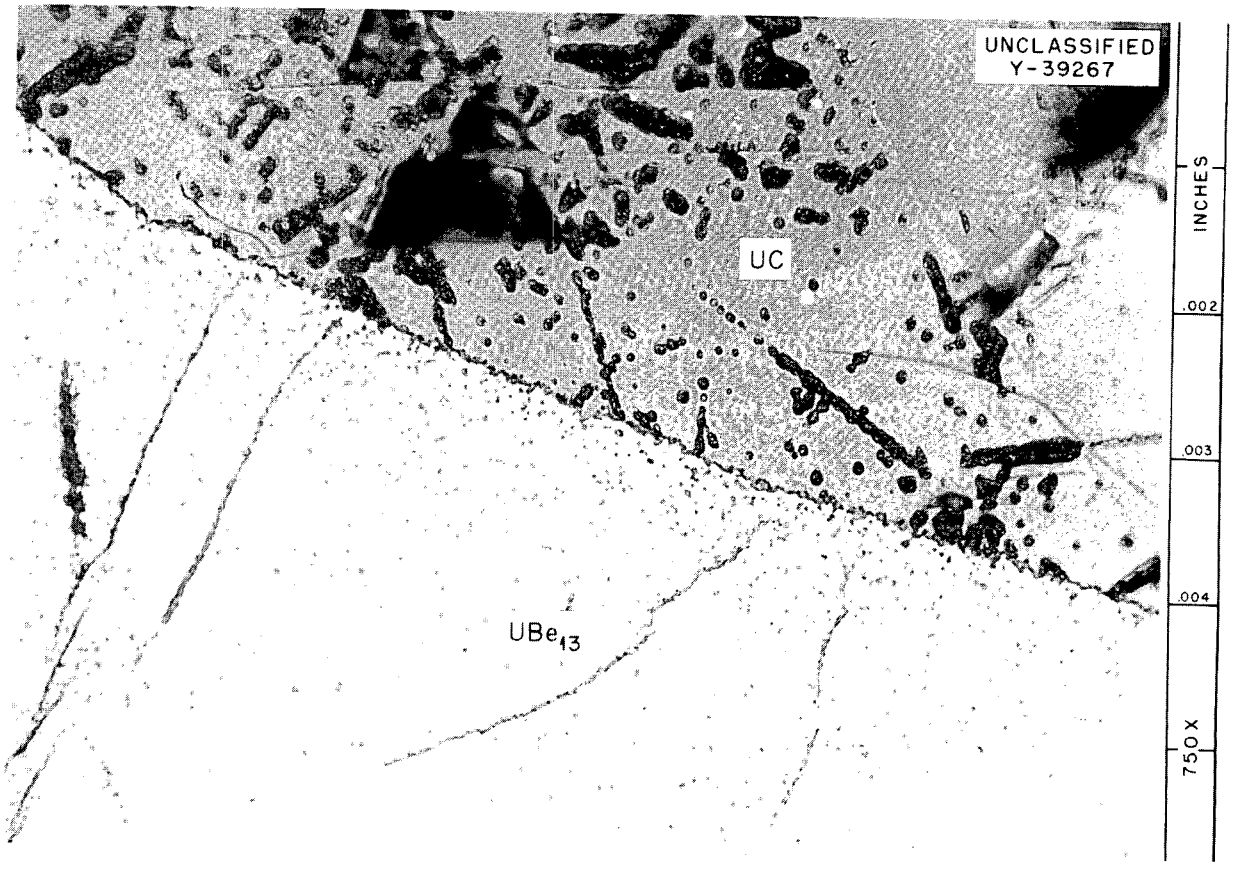

Fig. 11.4. Uranium Monocarbide–Beryllium Diffusion Couple Heat Treated at 1000°C for 90 hr. The UC was etched with 1:1:1 H_2O, CH_3COOH, HNO_3.

12. ZIRCONIUM ALLOY RESEARCH

M. L. Picklesimer

ZIRCONIUM ALLOY DEVELOPMENT

M. L. Picklesimer P. L. Rittenhouse

Zirconium-base alloys are of interest for use as potential structural materials in several water-cooled and/or -moderated reactor systems, since their use in reactors using low-enrichment fuels can result in considerable economy of neutrons. A development study of such alloys has been under way for several years. The prior work has been reported in HRP quarterly progress reports and in several previous Metallurgy Division annual progress reports.

The alloy systems presently being studied are Zr-Nb, Zr-Mo, Zr-Pd, and Zr-Cu, of hypo-, hyper-, and eutectoid compositions; Zr–15% Nb–X; and Zircaloy-2. Data on the transformation kinetics as determined by hardness and microstructure have been reported on most of the alloys previously.[1,2] The work of the past year has been principally confined to a study of the transformation kinetics by use of resistivity measurements during heating and cooling cycles and during transformation at constant temperature. The equipment used for the study consists of a resistivity bridge which automatically and continuously plots resistivity vs temperature. In the studies conducted at constant temperature the bridge plots resistance vs time. Modifications are in progress to permit automatic plotting of resistivity vs time or the logarithm of time. The present useful temperature range of the equipment is from 100 to 1200°C.

Iodide Zirconium

Resistivity curves for zone-purified iodide zirconium during heating and cooling cycles showed the transformation range to be from 864 to 880°C on heating and from 876 to 858°C on cooling. Normal reactor-grade iodide zirconium has a slightly larger transformation range because of higher iron and oxygen content. The relative effect of oxygen on the upper and lower temperatures of the $\alpha + \beta$ region on heating was shown by the increase of the transformation range from 864–880°C to 870–916°C after the specimen was held for 10 to 15 hr at temperatures above 800°C in a vacuum of 1×10^{-5} mm Hg or better.

Zircaloy-2

Resistivity curves for Zircaloy-2 containing less than 20 ppm H_2 showed the temperature range of the $\alpha + \beta$ phase region to be 832 to 970°C on heating at a rate of 16°C/min. Suppression of the $\alpha/\alpha + \beta$ temperature to 775°C was found for a cooling rate of 16°C/min and to 760°C for a rate of 200°C/min. The suppression of the $\beta/\alpha + \beta$ temperature is only about half as great at any given cooling rate. A hump was observed in the cooling curve in the temperature range of about 850 to 780°C and is thought to be due to the presence of at least three phases in the material under this condition.

Zr–15% Nb–X

The transformation kinetics of a Zr–15 Nb and a Zr–15 Nb–2 Mo (wt %) alloy have been studied by using heating and cooling cycles, transformation at constant temperature, and combinations of these. Heating and cooling curves for the Zr–15% Nb alloy in the β-quenched condition, presented in Fig. 12.1, show a peak at 390°C on heating, which is believed to be due to a maximum in the rate of formation of ω phase; a continuing decrease in resistivity on further heating to 540°C, which is apparently due to a reversion of the ω phase to the β phase; and a resistivity minimum at 317°C on cooling, which is thought to be due to the formation of the Widmanstätten precipitate in a retained β matrix. Faster heating and cooling rates decrease the

[1] M. L. Picklesimer *et al.*, *Met. Div. Ann. Progr. Rept. Oct. 10, 1957*, ORNL-2422, p 117; *Oct. 10, 1958*, ORNL-2632, pp 67–70 (classified).

[2] G. M. Adamson *et al.*, *HRP Quart. Progr. Rept. Oct. 31, 1956*, ORNL-2222, pp 114–16; *Jan. 31, 1957*, ORNL-2272, pp 119–23; *Apr. 31, 1957*, ORNL-2331, pp 124–28; *July 31, 1957*, ORNL-2379, pp 122–26; *Oct. 31, 1957*, ORNL-2432, pp 131–33; *Jan. 31, 1958*, ORNL-2493, pp 141–43; *Apr. 30 and July 31, 1958*, ORNL-2561, p 245; *Oct. 31, 1958*, ORNL-2654, p 188.

height of the ω peak on heating and smear out the resistivity minimum on cooling.

Heating curves for the Zr–15% Nb alloy after aging at 400 and 500°C for 19½ and 24½ hr and cooling to 100°C are shown in Fig. 12.2. The monotectoid temperature appears to be 610°C, and the formation of the β phase is completed at 675°C, in approximate agreement with the phase diagram for the alloy system.

The behavior of the Zr–15% Nb–2% Mo alloy was found to be quite similar to that of the Zr–15% Nb binary alloy, although considerably more

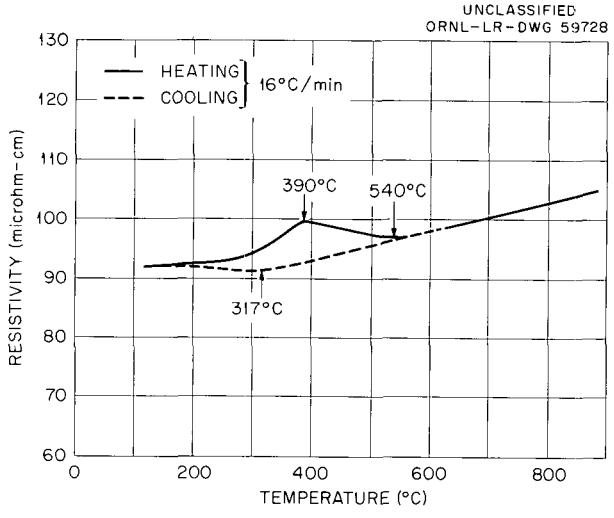

Fig. 12.1. Resistivity-Temperature Curve for Zr–15% Nb Alloy.

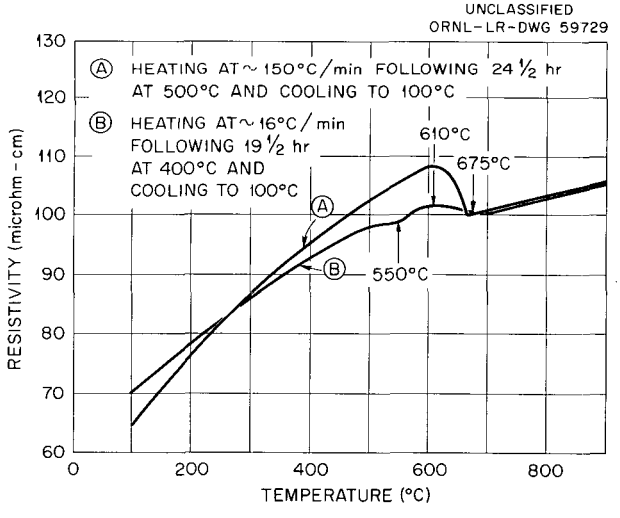

Fig. 12.2. Resistivity-Temperature Curve for Zr–15% Nb Alloy After Two Aging Treatments.

sluggish. At a heating rate of 16°C/min, the resistivity peak associated with ω-phase formation was found to be at 478°C, with the reversion being completed at 516°C. After aging for 21 hr at 522°C and reheating, the monotectoid temperature was found to be 608°C, and the $\alpha + \beta$ reaction was found to be completed at 678°C.

Zirconium-Molybdenum Alloys

A Zr–7.5 Mo (wt %) alloy, of eutectoid composition, showed the same type of behavior as the Zr–15% Nb alloy. The resistivity data plus metallographic examination and hardness measurements made on specimens isothermally transformed at 400, 500, 600, and 700°C for times ranging from 6 sec to 16 hr allow the following generalizations to be made on the transformation behavior of retained β phase in the eutectoid alloy:

1. The Widmanstätten (W) phase which forms on quenching of β phase in the Zr-Nb alloy system also occurs in the retained β alloys of the Zr-Mo system.
2. At 400°C, the transformation sequence is $\beta_r \rightarrow \beta_e + \omega$ after an incubation period of approx 1 hr.
3. At 500 to 700°C, the reaction sequence is $\beta_r \rightarrow \beta_e + \alpha \rightarrow \beta_e + \alpha + ZrMo_2$, with the transformation to $\alpha + ZrMo_2$ being 95% complete in 16 hr at 500°C. The amount of transformation occurring in 16 hr at 600 and 700°C is less.
4. If ω phase is formed at 500°C and higher, its presence has not been definitely detected. It is known to be absent after aging for 1 hr.

The notations are defined below:

β_r = retained beta phase

β_e = beta phase enriched in the alloying element

α = alpha zirconium containing the solubility limit of the alloying element

ω = omega phase, a metastable transition phase, lean in the alloying element and having a hexagonal crystal structure

W = Widmanstätten precipitate formed during quenching of retained β alloys from temperatures in the β field, having a body-centered-tetragonal crystal structure with axes aligned along the <100> axes of the body-centered-cubic matrix

For a Zr–4% Mo alloy (hypoeutectoid), the transformation sequence is the same, although more rapid. The β-quench and reheat transformation

sequence for both alloy compositions is the same as the isothermal sequence but more rapid.

Zirconium-Copper Alloys

Two binary Zr-Cu alloys, 1 and 1.6 wt % Cu, have been investigated by using hardness measurements, metallography, and resistivity measurements. No resistivity changes were observed to occur during either isothermal or β-quench and reheat transformation.

The eutectoid temperatures and the $\alpha + \beta/\beta$ temperatures for the two alloys are presented in Table 12.1. Little superheating occurred at any heating rate, but some supercooling did occur at the faster cooling rates.

Table 12.1. Transformation Temperatures for Zr-Cu Alloys

1% Cu: temperatures extrapolated to 0°C/min: eutectoid, 809.5°C; $\alpha + \beta/\beta$, 851.0°C
1.6% Cu: temperatures extrapolated to 0°C/min: eutectoid, 810.0°C; $\alpha + \beta/\beta$, 836.5°C

Alloy	Heating or Cooling Rate (°C/min)	Eutectoid Temperature (°C)	$\alpha + \beta/\beta$ Temperature (°C)
1% Cu	2	810	852
	4	812	
	8	814	854
1.6% Cu	2	811	
	4	812	841
	8	814	843
	16	817	852

The transformation from β phase to a martensitic α phase occurred between 600 and 650°C for the 1% Cu alloy and between 550 and 600°C for the 1.6% Cu alloy. The transformation sequence observed at temperatures above the M_s temperature was $\beta_r \rightarrow \alpha + Zr_2Cu$ in a cellular structure. At temperatures below the M_s, the sequence was found to be $\beta_r \rightarrow$ martensitic structure $\rightarrow$ tempered martensitic structure of acicular $\alpha + Zr_2Cu \rightarrow \alpha + Zr_2Cu$ in a cellular structure. The end product for both isothermal and β-quench and reheat transformations above and below the M_s temperature was always the same cellular structure. The kinetics of the transformation were much faster in the 1.6 wt % Cu alloy. The data also indicate that the eutectoid composition is considerably higher than that of 1.6 wt % Cu as has been reported.

Zirconium-Palladium Alloys

Binary Zr-Pd alloys containing 5, 7.5, 10, and 15 wt % Pd have been prepared and have been heat treated at temperatures ranging from 600 to 1000°C. Little information on the microstructures and phase boundaries has been obtained because of difficulties in metallographic preparation. No chemical polish or etchant has been found which will reveal the microstructure through an ever-present black stain. Electrolytic polishing and etching has not been successful.

Table 12.2. Transformation Temperatures for Zr–10% Pd Alloy

T_1 extrapolated to zero ΔT: 760°C
T_2 extrapolated to zero ΔT: 790°C

Heating or Cooling Rate (°C/min)	Number of Determinations	T_1		T_2		T_3	
		Heating (°C)	Cooling (°C)	Heating (°C)	Cooling (°C)	Heating (°C)	Cooling (°C)
2	1	764	738	799	772	931	864
4	3	765	735	801	766	900 ± 16	820
8	2	766	732	806	757	923 ± 13	826
16	1	766	727	810	749	935	Not observed
75	1	767	724	807	750	913	Not observed
270	2		703		729		Not observed

The Zr–10% Pd alloy has been run in the resistivity apparatus. The transformation temperatures observed are presented in Table 12.2 for heating rates from 2 to 75°C/min. Cooling curves have shown that the β phase can be supercooled approx 30°C at a cooling rate of 4°C/min and 43°C at 75°C/min. It is known that the Zr–10% Pd alloy is two phase at 700°C, two phase but of a different morphology at 900°C, and single phase at 1000°C. The temperatures given as T_1 and T_2 in Table 12.2 are thought to be the limits of the temperature range over which the reaction α + compound → β + compound occurs at these heating and cooling rates, and T_3 is probably the temperature of the reaction β + compound → β. More information will have to be obtained before the Zr-Pd phase diagram can be roughly approximated.

OXIDATION-RATE MEASUREMENTS

S. Peterson

The apparatus being used for the determination of oxidation rates of zirconium alloys consists of two regions: a storage region kept at essentially constant pressure and a reaction region separated from the storage region by a solenoid valve which is normally closed. As oxygen is consumed by the reaction with the metal specimen, the pressure in the reaction region drops, producing a differential pressure between the two regions. When the differential pressure reaches a preset value, as sensed by a photocell located on one leg of the differential oil manometer between the two regions, the solenoid valve is opened, and the pressure in the two regions again equalizes. The time interval between valve openings is measured and recorded. Since the system is sensitive to pressure differential, not absolute pressure, a constant weight of oxygen is consumed in the reaction region for each valve operation. The raw data are then the reciprocals of the differential of the normal rate curve. An early model of this system has been previously described.[3]

The work of the past year has been primarily concerned with development of the technique and elimination of equipment errors. Data have been collected on iodide zirconium and Zircaloy-2 specimens, which have served as standards for evaluation of the equipment and the technique. The temperatures of oxidation have been 600 and 700°C, at oxygen pressures of 10 and 20 mm Hg. The rate curves for Zircaloy-2 show the typical behavior of an oxide film which is protective in the early stages of oxidation but nonprotective in the later stages. The data for the iodide zirconium indicate that no transition occurs from the "protective" type of oxidation behavior under the conditions of test. The data as actually determined by the differential technique for the Zircaloy-2 run at 700°C are presented in Fig. 12.3. Expanded portions of the curve presented in Fig. 12.4 indicate that, on a fine scale, the oxidation process is not smooth. Several equipment errors could contribute to the irregularity of the data, among these being the limited precision and fluctuating response of the manometric sensing system, temperature variations and fluctuations in the gas in the apparatus, and incomplete pressure equilibration during valve operation. The effects of these equipment errors have been examined by replacing the specimen tube with a similar tube containing a side arm to which a vacuum leak valve was attached, permitting a constant leak rate from the reaction region to a vacuum system. Several check runs were made at different leak rates, with the specimen furnace at temperature under normal control. The data indicate that a portion of the "scatter" observed during an oxidation run can be ascribed to equipment errors. The conclusion that the oxidation process is not smooth is consistent with observations of irregular changes in the apparent film thickness of Cu_2O on Cu as a function of time, as measured by optical methods during oxidation.[4]

The present equipment is limited in sensitivity to about 100 to 150 A of oxide formation per valve opening and is too sensitive to fluctuations in room temperature. Thermostating of the entire oxidation apparatus and replacement of the oil manometer with an electronic differential manometer sensitive to a pressure difference of 0.1 μ Hg are in progress. The modifications should permit a sensitivity of about 10 to 15 A of oxide thickness per valve opening for a specimen having a surface area of about 5 cm^2.

[3] J. C. Banter and S. Peterson, *Met. Div. Ann. Progr. Rept. July 1, 1960*, ORNL-2988, pp 180–81.

[4] E. C. Williams and P. C. S. Hayfield, *Vacancies and Other Point Defects in Metals and Alloys, Inst. Metals (London), Monograph and Rep. Ser. No. 23*, pp 131–57 (1958).

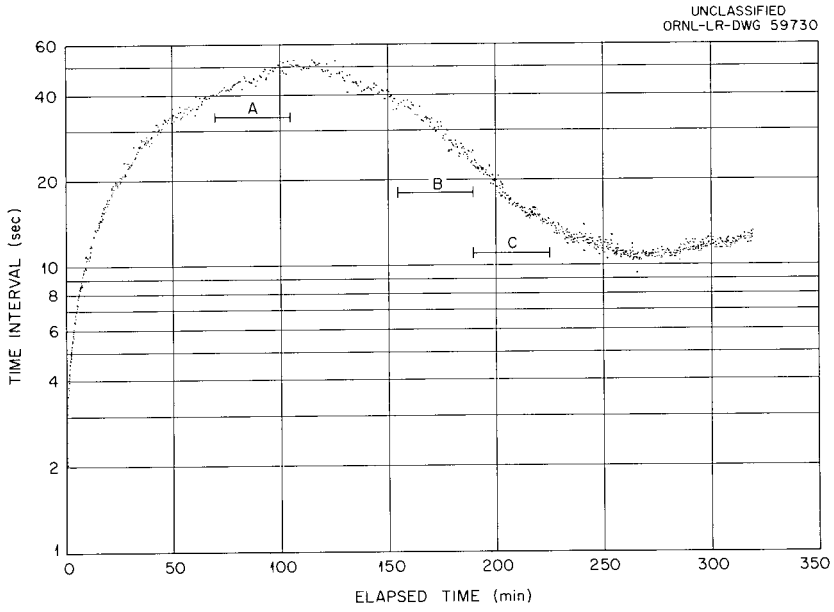

Fig. 12.3. Typical Oxidation Curve for Zircaloy-2 at 700°C by Differential Technique (Reciprocal Rate Plot).

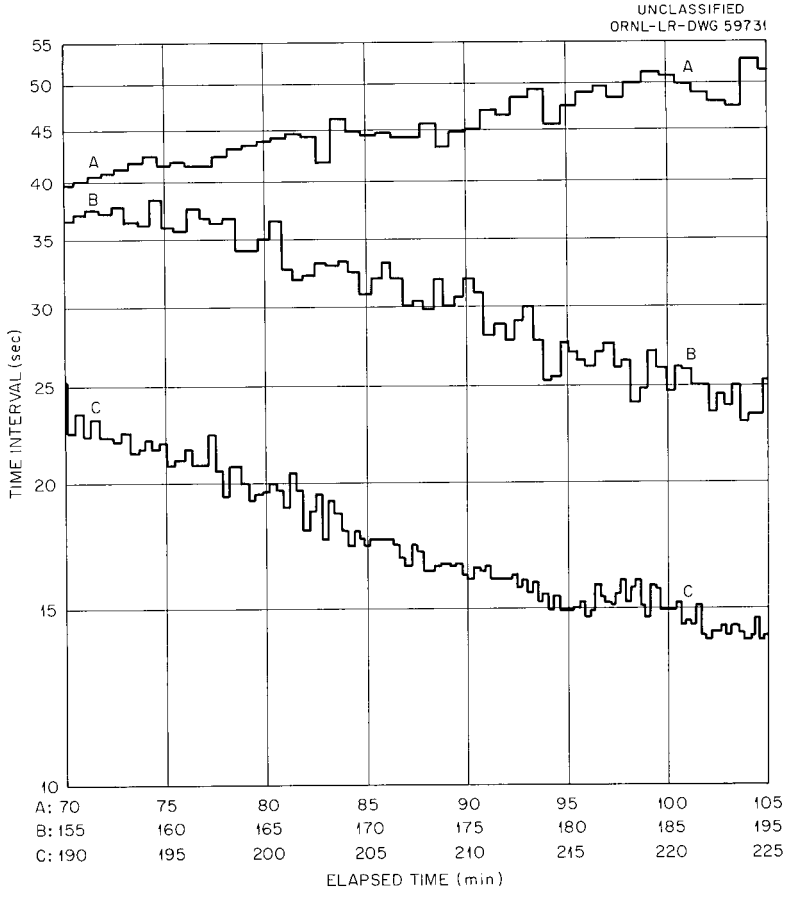

Fig. 12.4. Selected Portions of Reciprocal Rate Plot for Zircaloy-2 (Fig. 12.3) on Expanded Scale.

OXIDE-FILM STUDIES

J. C. Banter

Consideration of the physical condition of a thin oxide film formed on a metal leads to the conclusions that (1) the index of refraction of the thin-film oxide *in situ* may be different from that of the bulk oxide; (2) if the film is nonstoichiometric, a defect structure will exist that might change with film thickness, environment, composition of both oxide and metal, and strain in the film; and (3) optical measurements may yield information that might characterize the state of the film thickness.

To this end, two spectrophotometers have been obtained to measure the spectral reflectance from unoxidized and oxidized zirconium-alloy specimens over the region of the spectrum from 0.2 to 16 μ wavelength. Several reflectance accessories for the spectrophotometers have been or are being built which will permit the desired measurements to be made.

A treatment relating film thickness, refractive index of the oxide, phase shift during reflection, wavelength, and angle of refraction of the incident light for conditions of maximum interference and reinforcement has been developed for a homogeneous isotropic oxide film on a metal. These relationships were shown to give reasonable values for the thickness of the oxide on Zircaloy-2 specimens which had been chemically polished and anodized. Previous experience indicated that films produced under the experimental conditions are insensitive to grain orientation and anodization time. In these tests, the phase shift was neglected, and the value of the refractive index for bulk oxide was used.

The next phase of this work will be a modified Brewster angle experiment[5] for measurement of the refractive index and phase shift as functions of wavelength. Modifications will then be made in the treatment for consideration of inhomogeneous oxide films. It is hoped that the nature of the inhomogeneities in the oxides *in situ* can be determined from x-ray diffraction studies and from the absorption spectra.

[5] O. S. Heavens and J. C. Kelly, *Optica Acta* 6, 339 (1959).

Part III

REACTOR METALLURGY

13. CERAMICS TECHNOLOGY

W. O. Harms

GRAPHITE AND FUELED-GRAPHITE STUDIES

Experimental Gas-Cooled Reactor Graphite Support Sleeves

F. L. Carlsen, Jr. S. D. Fulkerson

The purpose of this study is to evaluate graphite and coated graphite materials for use as support sleeves in the Experimental Gas-Cooled Reactor (EGCR). The EGCR fuel assemblies will consist of fuel rods mounted inside a graphite support sleeve which is nominally 3 in. in inside diameter, 5 in. in outside diameter, and 30 in. long. The surfaces of the sleeve will be coated with an oxidation-resistant material.

The primary functions of the sleeve are to position the elements within the coolant channel, to transmit the collective load of the fuel elements, and to provide a simple shape that can be readily handled by the charge machine. The function of the coating on the sleeve is to prevent sustained burning of the graphite in the event that air is admitted to the core as a result of a rupture in the coolant system.[1] Because the graphite in the sleeves amounts to approx 10% of the total moderator in the EGCR core, the thermal-neutron absorption cross section of the sleeve must not be too large.

Oxidation Studies. – The oxidation resistance of coated graphite specimens was determined by comparative oxidation tests on both coated and uncoated specimens. To be suitable for this application, the coating should reduce the oxidation rate of the graphite in air by a factor of 20 at 600°C.

Tests were performed on coatings of SiC, Si-SiC, and pyrolytic graphite applied to three representative nuclear graphite grades, as well as to nine special graphite grades. The oxidation tests were performed by heating the specimens in an oxidation-test assembly which allowed for close control of the temperature, length of exposure, and air flow.[2] It was shown that only SiC or Si-SiC coatings when applied to the special isotropic grades of graphite are sufficiently protective at 600°C.[2-4]

Mechanical Property Tests. – Eddy-current inspections of uncoated graphite sleeves supplied by three vendors resulted in the rejection of 34, 88, and 92% of three lots of 50 sleeves.[5] The sleeves contained defects in the form of cracks and low-density inclusions. The effects of defective areas of this type on rupture strength were studied, since stresses of 1200 psi may develop in service.[6]

Defects were marked in three sleeves containing low-density areas and cracks, and test specimens were machined to include the defective areas. Defect-free specimens and specimens containing artificial defects were also prepared.

The rupture strength was measured by fracturing the specimens in a manner which caused fracture in the defective area. The results of this study[7] indicated that, while the defects lowered the rupture strength, the value of this property for all specimens was greater than 1200 psi.

Fueled-Graphite Fabrication

A. W. Seifert

A study was undertaken to exploit the high bulk densities which can be achieved by using natural graphite for graphite-based fuel components.[8,9]

---

[1] *GCR Quart. Progr. Rept. Dec. 31, 1960*, ORNL-3049, pp 127–33.

[2] *GCR Quart. Progr. Rept. Mar. 31, 1961*, ORNL-3102, pp 112–15.

[3] *GCR Quart. Progr. Rept. Dec. 31, 1960*, ORNL-3049, p 208.

[4] *GCR Quart. Progr. Rept. June 30, 1961*, ORNL-3166 (in press).

[5] *GCR Quart. Progr. Rept. June 30, 1960*, ORNL-2964, pp 121–22.

[6] *Ibid.*, p 41.

[7] *GCR Quart. Progr. Rept. Sept. 30, 1960*, ORNL-3015, pp 78–80.

[8] *GCR Quart. Progr. Rept. Sept. 30, 1960*, ORNL-3015, pp 74–75.

[9] *GCR Quart. Progr. Rept. Dec. 31, 1960*, ORNL-3049, pp 202–4.

Preliminary fabrication studies on unfueled components showed that phenol-formaldehyde-type binders were most satisfactory and that specimens with bulk densities as high as 2.09 g/cm^3 could be produced.

Development work was then carried out for the production of fueled specimens containing particles of UC, UO_2, UC_2, and pyrolytic-carbon-coated UC_2-UC. The general fabrication scheme in all cases was to dry mix the natural graphite with binder and fuel, cold press at 90,000 psi, and fire at a rate of 20°C/hr to 1000°C in argon. The results of this study are as follows:

1. Pellets containing uniform dispersions of UO_2 in graphite were prepared satisfactorily, using fuel particles in the size ranges −60 +100 mesh and −200 mesh.
2. Laminations and surface protrusions were observed on fueled pellets made with uncoated UC and UC_2-UC. These effects were due at least partially to the oxidation of the carbides by the gases given off by the binders. Reaction products around the particles were identified as UO_2, and the reaction-product layers were greater near the surface of the specimen than near the center.
3. Sound pellets were prepared by using the coated UC_2-UC particles. Several particles protruded at the surface, however, due to the shrinkage of the graphite around surface particles during baking.

Coated-Particle Fuel-Element Development

T. Hikido J. M. Kerr F. L. Carlsen, Jr.

A program has been initiated to develop fuel elements based on the coated-particle concept. The over-all effort involves the Metallurgy, Reactor, Reactor Chemistry, Chemical Technology, and Solid State Divisions and comprises studies on irradiation, fabrication, physical and mechanical properties, compatibility, and chemical reprocessing.

The initial interest in this program is in uranium carbide and uranium carbide–thorium carbide spheroidal particles coated with pyrolytic carbon. The emphasis is on determining the behavior of these particles and the fuel elements containing them under irradiation at high temperatures. The ability of the particle coatings to retain fission products as a function of temperature and burnup is of particular interest. The role of the Ceramics Laboratory is to specify and procure the fuel particles and fuel bodies, perform the necessary preirradiation examinations, specify the conditions for and assist in the design of the irradiation tests, and assist in the postirradiation examinations.

Three types of irradiation facilities are to be used in this program: (1) the LITR static capsules, (2) the ORR C-1 instantaneous fission-gas release facility, and (3) the ORR poolside sweep capsules. The Ceramics Group has assisted the other divisions in the design of cans for each of the facilities. The first test is now being irradiated in the LITR at temperatures of 2000 and 2330°F.[10]

URANIUM OXIDE AND THORIA FABRICATION DEVELOPMENT

Fabrication of UO_2 Pellets

A. J. Taylor J. M. Robbins

A variety of UO_2 shapes have been fabricated for studies related to the EGCR fuel. These pellets have all been sintered to within specified dimensional and density tolerances. One group of pellets which required a very high bulk density was made to 97.5% of theoretical density. Two groups of pellets, one for LITR experiments and the other for experiments in the ORR C-1 facility, required that grain size be controlled in addition to density and size. These pellets were sintered to meet their specified dimensional, density, and widely separated grain-size requirements. Control of grain size was achieved by varying the time of the standard sintering technique (1750°C in a hydrogen atmosphere). Experiments using inert-gas sintering atmospheres showed that argon had a strong depressing effect on the grain growth of UO_2. The average grain diameter in these specimens ranged from 30 to 50 μ.

One set of pellets for Be-UO_2 compatibility studies required a high oxygen-to-uranium ratio in addition to a controlled size and density. Fabrication studies on these pellets have yielded interesting information on the effect of inert-atmosphere sintering on the O/U ratio. An oxide with an initial O/U of 2.18 was sintered at 1750°C in argon, with a resulting O/U of 2.012. In order

[10] *GCR Quart. Progr. Rept. Mar. 31, 1961*, ORNL-3102, pp 104–7.

to determine whether or not the reduction in O/U ratio was caused by hydrogen contaminant in the argon, a hot U_3O_8 trap was incorporated into the gas purification system. Pellets sintered at 1450°C in argon purified in this way also had a final O/U of 2.012. These results indicate a higher-than-expected degree of O/U-ratio reduction by thermal decomposition. Studies are planned with various partial pressures of oxygen in the atmosphere in order to gain a better understanding of the U-O system with relation to sintering.

Characterization of UO_2 Microspheres

A. J. Taylor M. P. Haydon
J. M. Robbins

The fuel elements for core B of the Fast Breeder (Fermi) Reactor will contain UO_2 microspheres dispersed in a stainless steel matrix. It is desirable that the fuel be present as uniformly dispersed spheroidal particles in the finished fuel elements. A study is being made to correlate the initial properties of UO_2 microspheres with their behavior during fabrication of the fuel plates. This work is intended to provide a basis for characterizing the fuel particles and for preparing material specifications.

Examination of many of the rolled fuel plates led to the conclusion that the type of particle which fails by fragmenting and stringering is almost invariably a very porous low-bulk-density particle or one which has a gross flaw, such as a large void, crack, or re-entrant.

The standard mercury-pycnometer technique for determining bulk density yielded inaccurate values due to the very large number and the very small volume of the individual particles. A technique was developed, therefore, in which the sample is embedded in an epoxy resin. In this method an accurate measurement is made of the volume of the embedment specimen, the volume of the epoxy resin is calculated from its weight and density, and the bulk volume of the UO_2 sample is obtained by difference. This technique gives results which are reproducible to within ± 0.01 g/cm^3, but accuracy is limited to those samples having open pores not greater than approx $\frac{1}{2}\ \mu$ in diameter. The plastic in the fluid stage enters openings greater than this diameter, causing the measured bulk density to be too high.

In order to determine the extent of the penetration of porous particles by the plastic, a "grind-etch" technique has been developed. A cross section of the embedded particles is exposed by grinding; then the sample is etched deeply with 20% nitric acid. Part or all of the UO_2 is removed, leaving a white, filamentous, plastic skeleton, which delineates the surface-connected porosity which has been penetrated by the plastic. Any particle or portion of a particle which has been heavily penetrated by the plastic represents a particle which is almost certain to fail and stringer when rolled into a dispersion-type plate element. The plastic skeleton is easily seen under a low-power microscope, and the amount and the type of plastic penetration, in combination with the apparent bulk density determined by the embedment technique, offer promise of becoming a reliable index to the quality of the sample being studied.

Storage Specifications for EGCR Fuel Pellets

J. M. Robbins A. J. Taylor

Vaporization and expansion of water adsorbed by the UO_2 pellets of the EGCR fuel elements can lead to significant internal pressures at the high operating temperatures anticipated. Therefore, the specifications for these fuel elements limit the UO_2 moisture content to 10 ppm. A series of experiments was performed to study the outgassing procedure and storage conditions necessary to ensure meeting this specification.

The pellets used in these experiments were taken from two batches which had been ultrasonically cleaned, outgassed, and then stored for five and eight months in nonairtight glass jars, that is to say, essentially exposed to laboratory atmosphere. A group of pellets from each of these batches was outgassed at 250°C and 10^{-4} to 10^{-5} mm Hg for 4 hr. The initial moisture content was calculated from the weight loss; then readsorption of moisture was determined by continuous weighing until the pellets had reached equilibrium with room-atmospheric conditions.

Since it is anticipated that the EGCR fuel pellets will be machined to the final dimensions, using water as a coolant, the second experiment was designed to determine the length of time required for thoroughly wetted pellets to reach equilibrium with their environment. Two groups of pellets were wetted – one by simple immersion

and the other by vacuum impregnation. The weight change was followed to equilibrium as these pellets dried in room-temperature air. Then the vacuum outgassing and the readsorption test described above were performed on these pellets.

A third experiment was performed in such a manner as to simulate the evacuation step immediately preceding the helium backfill and end closure of the stainless steel fuel-element cans.

The results of these experiments indicate that the pellets reach equilibrium with room-atmospheric conditions at an average moisture content of 27 ± 3 ppm by weight. Equilibrium was attained rapidly, the specified limit of 10 ppm being reached in all cases in less than 30 min. It can reasonably be concluded, therefore, that in order to attain the specified limit of 10 ppm some form of outgassing and environmental protection will be required for the UO_2 pellets. It was indicated that the necessary outgassing may be accomplished during the evacuation step preceding end closure. If, however, it becomes necessary to accomplish outgassing in a separate operation, the pellets will have to be stored in either an evacuated or a desiccated environment in order to prevent the very rapid readsorption of moisture.

Vibratory Compaction Studies

W. S. Ernst, Jr. A. W. Seifert

Vibratory compaction is a relatively simple process for packing granular-oxide fuel rods. Because of its simplicity, this method is economically attractive for first-cycle UO_2 fuels and lends itself to remote operation in the recycling of Th-U^{233} oxide fuels. The objective of the studies described here is a definition of the conditions which affect the bulk density of fuel rods of the type which pertain to these fuel cycles. Details of these studies, which have been limited to ThO_2-UO_2 materials and to pneumatic vibrators, have been reported elsewhere.[11]

The primary factor which controls the bulk density of vibrated material is particle-size distribution, particularly where densities approaching 90% of theoretical are sought. Using three particle-size fractions, 25 different distributions were vibrated. Only nine of these distributions yielded densities in excess of 8.8 g/cm^3, and only two yielded 8.9 g/cm^3 or higher. However, a density of 8.68 g/cm^3 could be obtained when only the coarse and fine fractions were used. Mixtures of this type are of particular interest from the standpoint of economical fabrication because they eliminate the need for the expensive medium fraction. It also was observed that bulk densities ranging from 8.54 to 8.74 g/cm^3 could be obtained by using continuous particle-size distributions. These distributions utilized all the starting material and were prepared by selective grinding only.

The compaction process as carried out in these studies is practically completed in 10 min. Vibration for an additional 5 hr did not effect a significant increase in bulk density.

Evaluation of dense, granular ThO_2–5 wt % UO_2 prepared by the sol-gel process[12] was initiated to determine the suitability of this material for vibratory compaction. Bulk densities of 8.0 to 8.3 g/cm^3 were obtained for the initial batches supplied. Microscopic studies revealed re-entrant surfaces which in effect acted as closed pores. The sol-gel process was modified accordingly, with the result that enriched oxide prepared for irradiation in the NRX Reactor showed considerable improvement.[12] Compacted bulk densities of approx 8.7 g/cm^3 were then obtained easily (see Table 13.1, set F).

The rod-to-rod reproducibility of bulk densities obtained by vibratory compaction is considered to be good. Table 13.1 shows the results for six sets of experiments. Although there were variations from set to set, each run of a set was compacted under identical conditions. Among the sets, the maximum deviation varied from ±0.4 to ±1.4% of the average density, while the average deviation varied only from ±0.2 to ±0.6% of the average. X-ray absorption techniques are under development for use in determining the axial variation of bulk density.

A new vibratory compaction facility is expected to be completed about July 1, 1961. The installation of electrodynamic equipment as well as larger pneumatic vibrators will provide for a substantial broadening of the scope of this study. Equipment

[11] S. D. Clinton, W. S. Ernst, Jr., and J. W. Snider, *A Study of Vibratory Compaction for Loading Fissile and Fertile Oxide Materials into Nuclear Fuel Assemblies*, ORNL-3007 (in press).

[12] *Fuel Cycle Development Semiann. Progr. Rept. Mar. 31, 1961*, ORNL-3142 (in press).

Table 13.1. Reproducibility of Bulk Density of Vibratorily Compacted ThO_2-UO_2

Tube material was type 304 stainless steel except for set B, for which aluminum alloy 1100 H14 was used; fuel material was fused ThO_2–3.4 wt % UO_2 except for set F, in which ThO_2–5 wt % UO_2 prepared by the sol-gel process was used

Set	Nominal Tube Dimensions			Runs per Set	Bulk Density (Arithmetic Average) (g/cm^3)	Average Deviation (Arithmetic) (g/cm^3)	Maximum Deviation (g/cm^3)
	Length (ft)	Outside Diameter (in.)	Wall Thickness (in.)				
A	8	3/8	0.035	10	8.61	±0.02	±0.03
B	8	3/8	0.035	9	8.49	±0.05	±0.12
C	4	1/2	0.035	11	8.57	±0.03	±0.09
D	4	1/2	0.020	6	8.57	±0.03	±0.05
E	2	3/8	0.035	5	8.86	±0.05	±0.10
F	1	5/16	0.025	8	8.69	±0.03	±0.04

for sizing granular oxides in large quantities will provide for a substantial expansion of studies of continuous as well as the gap-graded distributions.

Thoria-Pellet Development

R. A. McNees A. J. Taylor

Thoria pellets to be used in the blanket system of aqueous reactors must not only be resistant to chemical and neutron damage but must also be mechanically strong. In addition, they must be shaped so that they can be efficiently cooled by circulating water and easily pumped into and out of the reactor. The ideal shape for this use is a sphere about 1/8 in. in diameter; an acceptable substitute is a cylinder with domed ends. During the past year, the problems associated with forming large quantities of both these shapes were investigated. With both shapes, the problem has been the elimination of imperfections resulting from nonuniform stresses introduced during the forming of rounded bodies. During the sintering operation, the strains set up as a result of these stresses produce laminations and nonuniform physical properties.

The results of concerted efforts to modify the available slurry-type thoria powders in order to eliminate this effect in domed-end pellets were unsatisfactory. A typical slurry-type oxide is prepared by calcining carefully precipitated thorium oxalate to 800°C and is characterized by having a surface area of approx 25 m^2/g, an average particle size of 1 to 3 μ, and a crystallite size of 250 to 300 A. The studies involved varying the calcination temperature, drying times and temperatures following ball-milling, amounts and types of binders and lubricants, and granulation procedures. Cold pressing was done by use of an automatic single-action press.

An indirect method of forming spherical thoria pellets was then developed. Slurry-type oxide was modified by calcining to 1000°C and adding 2 wt % Carbowax 4000, and this material was then pressed into cubes. The cubes were tumbled dry in the green state to essentially spherical shapes. After being "soft-sintered" at 1300°C, the spheres were polished by wet tumbling and then sintered at 1650 to 1850°C. This modification of the fabrication technique produced sound green bodies free of both large internal voids and laminations, and gave final densities ranging up to 98% of theoretical after sintering at 1850°C.

In addition to work with slurry-type oxides, limited studies have been made with oxides prepared from thorium formate and from a thorium oxide–thorium nitrate sol. The oxide from the

formate responded satisfactorily to cold pressing without modification other than adding Carbowax, and it sintered readily to produce a density of 9.2 g/cm^3 at 1650°C. Sufficient quantities of this material have not been available for large-scale tests, however. An oxide prepared by the Chemical Technology Division, using a sol-gel technique and thermal dehydration at 415°C, was nonsinterable at 1650°C. Other powders dehydrated at lower temperatures and by chemical means are being tested.

BeO AND FUELED-BeO STUDIES

Phase Relationships in BeO–Metal Oxide Systems

A. T. Chapman R. A. Potter
R. E. Meadows

Investigations of phase relationships in BeO–metal oxide systems were continued.[13] In consideration of BeO as a nuclear reactor material, this information is of interest concerning reactions with the oxides which are (1) added to enhance sinterability, (2) present as coatings for corrosion resistance and fission product retention, and (3) added to improve fuel retention.

BeO-CaO. – The effects of heat treatment and cooling rates in dry argon on the formation and decomposition of the intermediate phase $Ca_2Be_3O_5$ in the BeO-CaO system were investigated.[14]

It was shown that the types of products which result on cooling BeO-CaO mixtures (including the eutectic composition of 60 mole % BeO) from supersolidus temperatures are dependent on the cooling rate. At cooling rates of less than 20°C/min over the range 1500 to 1300°C, decomposition of the eutectic liquid yielded two-phase structures containing BeO and CaO. However, at rates of approx 160°C/sec over the range 1500 to 850°C, the reaction product was the intermediate phase, $Ca_2Be_3O_4$. Single crystals of this compound were grown successfully from supercooled melts of the eutectic composition.

The intermediate phase was not detected in oxide mixtures heated at subsolidus temperatures for 100 hr, nor was the reaction

$$\text{eutectic liquid} \longrightarrow CaO + BeO \longrightarrow Ca_2Be_3O_5$$

demonstrated experimentally by slowly cooling melts at less than 20°C/min and subjecting them to heat treatment at various temperatures.

BeO-Y_2O_3. – An intermediate compound in the BeO-Y_2O_3 system[13,15] was produced by quenching melted mixtures of the oxides. The composition of this phase was tentatively established as $2BeO \cdot Y_2O_3$. Single crystals of the compound were grown successfully.

BeO-Eu_2O_3. – Mixtures of BeO-Eu_2O_3 containing 5 to 75 wt % BeO were heated to approx 1600°C on a platinum strip and then air-quenched. No evidence of an intermediate phase in the system was detected. Liquid formation was visually observed in the Eu_2O_3-rich mixtures in the composition range 5 to 20 wt % BeO.

Cooling curves obtained from mixtures of 5, 12, and 20 wt % BeO cooled from 1550°C in a muffle furnace showed a thermal arrest at approx 1425°C in each of the compositions. The longest thermal arrest occurred in the specimen containing 12 wt % BeO.

BeO-SrO. – Single crystals of an intermediate compound[14] in the BeO-SrO system were grown successfully from melted oxide mixtures consisting of 60 mole % BeO.

BeO-MgO, BeO-CeO_2, BeO-ZrO_2. – A technique was developed to determine the eutectic temperature and composition for binary systems which require temperatures above 1800°C to produce melting. The success of this technique, which is applicable for simple eutectic configurations as found in many BeO systems, depends upon the very fluid nature of BeO-rich melts. Experimentation showed that small quantities of BeO-rich melts could "drain" out of a thin wafer-shaped specimen and be absorbed in a porous BeO body. The porous BeO acts as a collector for the liquid and also draws the liquid away from the wafer-collector interface, effectively preventing these pieces from bonding together. By proper temperature control and analysis, both the eutectic temperature and the composition may be determined. The reason for the BeO pellet collector

[13] *Met. Div. Ann. Progr. Rept. July 1, 1960*, ORNL-2988, pp 190–91.

[14] *ANP Semiann. Progr. Rept. Apr. 30, 1961*, ORNL-3144 (in press) (classified).

[15] C. E. Weir and A. Van Valkenburg, *J. Research Natl. Bur. Standards* **64A**(1), 105 (1960).

remaining porous during heating in air was discussed by Aitken of GE-ANP in a recent paper.[16]

The results of studies employing this technique for the BeO-MgO, BeO-CeO_2, and BeO-ZrO_2 systems are tabulated below:

System	Eutectic Temperature (°C)	Eutectic Composition (mole % BeO)
BeO-MgO	1860 ± 10	69 ± 2
BeO-CeO_2	1900 ± 20	63 ± 3
BeO-ZrO_2	2045 ± 10	58.7 ± 2

Uranium-Oxygen System. – The effects of temperature and pressure on phase relationships in the U-O system are of interest in connection with fuel migration and loss in BeO-UO_2 fuel components. Accordingly, a study of this type has been initiated. For this purpose a thermogravimetric apparatus has been designed and fabricated for use at temperatures as high as 1800 to 2000°C in a vacuum of 2×10^{-6} mm Hg, or in various gases to 1600–1800°C.

Preliminary results show that above 1200 to 1300°C in vacuum, UO_{2+x} ($0 < x < 0.2$) loses weight, and the magnitude of this loss indicates that a uranium oxide, presumably UO_3, is the volatile species. Experimentation at 1500 to 1700°C showed that this process stopped when the O/U ratio reached 2.02 to 2.04.

Related quenching studies of U_3O_{8-y} heated in air revealed that the orthorhombic U_3O_{8-y} phase reverts to the fluorite structure of UO_{2+x} at approx 1550°C.

Fabrication Development of BeO

R. L. Hamner

Fabrication development was initiated on high-purity BeO bodies to be used in irradiation experiments designed to evaluate BeO specimens with regard to density, grain size, and temperature at high fast-neutron doses.

Shrinkage characteristics and fired densities were studied as a function of green densities to obtain the information required to fabricate specimens to specifications without machining.

Bodies having 95% of theoretical density were obtained by cold pressing without binder and then sintering in hydrogen for 1 hr at 1750°C. Bodies having 85 to 88% of theoretical density, sintered under the same conditions, were obtained by adding fugitive organic materials.

Efforts were made to promote grain growth in high-density and low-density specimens by heat treatment after the initial sintering rather than by the use of additives which would introduce additional variables in irradiation experiments. It was observed that grain size was not increased after heating at 1500°C for 120 hr in air. Growth of grains by a factor of 2 to 3 in high-density specimens was promoted by heating at 1750°C for 10 hr in hydrogen. No significant change in grain size was noted in low-density specimens under the same conditions.

Fabrication Development of Fueled BeO

R. L. Hamner

Fueled-BeO studies were continued[17] as a part of a long-range research and development program for advanced gas-cooled power reactor concepts. Initial fabrication development was undertaken on BeO bodies containing large volumes of fuel as fine-particle dispersions.[18] Advanced development work in progress is concerned with large-fuel-particle dispersions.[18,19]

Fine-Particle Fuel Dispersions in BeO. – Beryllium oxide bodies containing 30 vol % fuel as UO_2 and as a UO_2-ThO_2 mixture, uniformly dispersed as submicron particles, were fabricated to 95% of theoretical density by cold pressing, without binder, and sintering at 1750°C. Representative specimens enriched in U^{235} were fabricated to dimensional specifications for irradiation testing at 1100 to 1370°C.

In the fabrication of BeO containing enriched UO_2, gross cracking occurred during sintering in hydrogen; this had not been encountered with depleted fuel mixtures. The cracking was attributed to a difference between the shrinkage behaviors of the enriched UO_2 and the depleted

[16] E. A. Aitken, *J. Am. Ceram. Soc.* 43, 627–33 (1960).

[17] *Met. Div. Ann. Progr. Rept. July 1, 1960*, ORNL-2988, pp 189–90.

[18] *GCR Quart. Progr. Rept. Dec. 31, 1960*, ORNL-3049, pp 196–202.

[19] *GCR Quart. Progr. Rept. Mar. 31, 1961*, ORNL-3102, p 97.

UO_2, resulting from different processes used in preparing the UO_2 powders.

The shrinkage of the enriched powders was adjusted and cracking was eliminated by using an argon atmosphere to maintain a high O/U ratio during sintering.

Large-Fuel-Particle Dispersions in BeO. – In the use of UO_2 as a fuel dispersed in a BeO matrix, it is desirable from the standpoint of fission-gas retention and radiation damage that the fuel particles be in the size range 100 to 500 μ. The fabrication of such a composite without the formation of cracks or large voids around fuel grains requires a knowledge of the shrinkage relationships of both components during sintering.

Coarse fuel particles were prepared by granulating pressed compacts of fine-grained UO_2 powder. Shrinkage "profiles," showing the shrinkage characteristics of fuel and matrix components as a function of green density, were obtained by room-temperature shrinkage measurements of UO_2 and BeO pellets sintered to successively higher temperatures. Based on these shrinkage profiles, it was undertaken to fabricate BeO bodies containing large particles of UO_2 which had been preshrunk a calculated amount by low-temperature firing before incorporation so that the residual shrinkage should approximate that of the BeO. Studies were made with 20, 25, and 30 vol % UO_2 as 100 to 150 μ and 150 to 250 μ particles.

In the first attempts to fabricate composite bodies, voids were observed around fuel particles. It was concluded that the fueled BeO did not shrink to the same extent, based on green density, as unfueled BeO. Bulk densities were then increased to 95% of theoretical by increasing the preshrinkage of the fuel particles before incorporation.

It was found that the polyvinyl alcohol binder used in the fabrication process tended to inhibit densification and to cause cracking during removal. Studies were made of the thermal dissociation characteristics of the binder, and the heating cycle was programmed accordingly so that cracking during binder removal was eliminated.

The cause for microscopic cracking of specimens during sintering has not yet been determined. It was observed that specimens were more prone to crack when the size range of the fuel particles was increased from 100–150 μ to 150–250 μ. No significant difference was noted as a function of fuel quantities ranging from 20 to 30 vol %. This cracking was reduced, but not consistently eliminated, by adjusting the heating rate during sintering.

THERMAL CONDUCTIVITY STUDIES

T. G. Godfrey D. L. McElroy[20]

Development work on the radial heat flow apparatus, using Armco ingot iron[21] and INOR-8[22,23] specimens, has shown that the apparatus functions satisfactorily to at least 800°C. The data for INOR-8 indicate that a precision of ±2% and an accuracy of at least ±5% were obtained. The small magnitude of these values is the result of extensive modification of the apparatus suggested in part by an error analysis[24] and by critical analysis of the data obtained.

The present apparatus is described in detail elsewhere.[23] The specimen consists of a 9-in.-tall stack of bushings, 3 in. in outside diameter and $\frac{5}{8}$ in. in inside diameter. Three of these are machined to receive the 12 measuring thermocouples, four in each bushing at two radial positions. These instrumented bushings are located in the central 3-in. portion of the specimen stack. The temperature gradient is produced by a double-spiral-wound, dc-powered Pt–10% Rh core heater, with voltage taps across the 3-in. central section for power measurement. Uniform axial specimen temperature is achieved by flat circular guard heaters on the ends of the stack, which respond to differential thermocouples within the specimen. The mean temperature of the specimen is controlled by a cylindrical muffle heater. The apparatus is normally operated in an inert atmosphere, but provisions are made for use in a vacuum.

Thermal Conductivity of INOR-8[23,24]

As part of the development of the apparatus, the thermal conductivity of a specimen of INOR-8 was measured in the temperature range 166 to

[20] Physical Properties Group.

[21] *GCR Quart. Progr. Rept. June 30, 1960*, ORNL-2964, p 82.

[22] *GCR Quart. Progr. Rept. Mar. 31, 1961*, ORNL-3102, p 92.

[23] *GCR Quart. Progr. Rept. June 30, 1961*, ORNL-3166 (in press).

[24] *Private communication*, T. G. Kollie, Physical Properties Group, May 1960.

816°C. The INOR-8 specimens were machined from a plate which had been hot-forged at about 2150°F. The specimens were given no heat treatment prior to incorporation in the apparatus, but during developmental work they received several very slow heating and cooling cycles from room temperature to 850°C.

The thermal conductivity of the INOR-8 was found to increase linearly with temperature to about 450°C, where a slight rise of approx 4% was observed. This rise was followed by another linear portion with a slightly greater slope. At about 680°C, a second, larger increase of approx 10% was seen, followed by what appeared to be another linear region. No unequivocal explanation for this behavior can be given; however, similar inflections in specific heat[25] and thermal expansion coefficients[26] have been observed in Ni-Mo alloys of slightly different composition.

Thermal Conductivity of UO_2[23,24]

The apparatus was recently assembled, incorporating UO_2 specimens whose physical and chemical characteristics have been described previously.[23] Final preparations have been made in order to determine the thermal conductivity of UO_2 to 1500°C.

RARE-EARTH OXIDE STUDIES

R. A. Potter R. A. McNees

In connection with the APPR Program, investigations were initiated to determine the effects of variations in environmental conditions on the sintering behavior and aqueous corrosion resistance of europium oxide. These studies were concerned with phase transformations, composition changes, and impurity effects which may be encountered during the process of preparation and incorporation of europium oxide in SM-1-type absorber plates.

Data obtained by differential thermal analysis on heating cubic europia to 1500°C failed to show the cubic-to-monoclinic phase transformation reported to occur at 1050 to 1100°C.[27] However, the transformation must have proceeded, although slowly, since x-ray diffraction patterns indicated that both monoclinic and cubic structures were present in the heated sample. Once the monoclinic phase is formed, the inversion from monoclinic to cubic apparently does not take place readily, as evidenced by the absence of cubic oxide after heating monoclinic material for 100 hr at 950°C. In addition, the monoclinic phase was observed to persist when heated to 900°C in a thermal gravimetric apparatus when the pressure was 1×10^{-5} to 1.8×10^{-5} mm Hg; the total weight loss was 0.2%.

Sintering of Rare-Earth Oxides

C. E. Curtis

Oxides of the rare-earth series of elements (except promethium) in the form of dry-pressed ($\frac{1}{4}$ in.) cylinders were fired in both oxygen and hydrogen atmospheres for 2-hr periods at 1300, 1500, and 1600°C. A constant cold-pressing pressure of 15,000 psi was used. The major phases concerned in densification, determined from the 1600°C specimens fired in oxygen, were: CeO_2 and Pr_6O_{11} (fcc); hexagonal Nd_2O_3; monoclinic Sm_2O_3, Eu_2O_3, and Gd_2O_3; Tb_4O_7 (fcc); and cubic sesquioxides of the remainder of the series. Indeterminate phases were present also in some cases.

Relatively low bulk densities were attained after 1600°C sintering in oxygen for Gd_2O_3, CeO_2, Nd_2O_3, Tb_4O_7, Dy_2O_3, Ho_2O_3, and Er_2O_3. On the other hand, after sintering at 1300°C the densities of specimens of Pr_6O_{11} and Sm_2O_3 were nearly those corresponding to theoretical. Europium oxide and Yb_2O_3 were about average, with 93% of theoretical density attained at 1600°C, while Tm_2O_3 and Lu_2O_3 apparently attained theoretical density at that temperature. There seemed to be no relationship between the crystal structure and sinterability.

Bulk densities attained after sintering in hydrogen were similar to those attained in oxygen except for Dy_2O_3 and Lu_2O_3, which were much less dense after firing in hydrogen.

The sintering characteristics of Sc_2O_3, which have not been determined previously due to its scarcity, were studied also. After cold pressing at 15,000 psi and sintering at 1600°C in air, a bulk density corresponding to 96% of theoretical was achieved.

---

[25]Private communication, E. E. Stansbury, Dept. of Chemical and Metallurgical Engineering, University of Tennessee.

[26]Private communication, J. R. Riddle, Metallography Group.

[27]C. E. Curtis and A. G. Tharp, *J. Am. Ceram. Soc.* 42, 154 (1959).

COMPATIBILITY STUDIES ON REFRACTORY MATERIALS

J. M. Kerr

Knowledge of the compatibility of refractory metals and compounds is valuable in designing apparatus for use at high temperature. Short-time, high-temperature tests have been extended to include tests on Fansteel 82 alloy (32½% Ta, ¾% Zr, 66¾% Nb) in contact with Al_2O_3, Be, BeO, C, MgO, ThO_2, TiO_2, UC, UO_2, and ZrO_2.

The Fansteel 82 was used as the resistance strip in a small, inert-atmosphere strip-heater resistance furnace. The test materials were placed on the strip and heated until reaction was observed or to approx 2100°C. Metallographic examination indicated no reaction between Fansteel 82 and Al_2O_3, BeO, or ZrO_2 at temperatures up to the 2000 to 2100°C range. Severe reaction was observed between Fansteel 82 and beryllium at 1465°C, UC at 1355°C, TiO_2 at 1775°C, graphite and MgO between 1800 and 1900°C, and ThO_2 and UO_2 between 2000 and 2100°C.

Comparison of these results with data previously obtained in similar tests on unalloyed niobium indicates that the Fansteel 82 is more compatible with the compounds tested.

14. CORROSION ENGINEERING

J. H. DeVan

Large-scale corrosion loops are being operated in support of the Experimental Gas-Cooled Reactor (EGCR) and the Molten-Salt Reactor (MSR). These loop experiments simulate the service environments and conditions of the respective reactor systems and provide a systematic evaluation of the corrosion behavior of reactor components as a function of operating parameters. Tests in support of the EGCR deal with the corrosion processes arising from impurities in high-temperature helium, namely, CO, CO_2, H_2, H_2O, and CH_4, as they affect ferrous alloys. MSR studies have been concerned with the long-term corrosion rates of high-temperature nickel-base alloys in molten fluoride salts that are employed both as the fuel and the secondary coolant in this reactor concept.

GAS-COOLED REACTOR MATERIALS COMPATIBILITY TESTS

J. H. DeVan B. Fleischer

The outgassing of graphite, together with in-leakage of air and steam, constitutes a serious impurity source in helium-cooled graphite moderated reactor systems. Accordingly, studies are in progress in support of the EGCR to establish the concentrations of such impurities in helium that can be tolerated by both high- and low-alloy structural steels. The results of these studies, which are reviewed below, indicate that austenitic stainless steels will be oxidized by the EGCR gas atmosphere and that carburization may also occur at temperatures above 1500°F. Lower alloy materials exposed at 1100°F have been found to undergo appreciable oxidation even at extremely low impurity concentrations.[1-4]

[1] J. H. DeVan, "Reactions of Reactor Materials with Contaminants Outgassed from Graphite," pp 698–732 in *Proceedings of the US/UK Meeting on the Compatibility Problems of Gas-Cooled Reactors, Held at Oak Ridge National Laboratory, Feb. 24–26, 1960*, TID-7597, Book 2 (Mar. 3, 1961).

[2] *GCR Quart. Progr. Rept. Sept. 30, 1960*, ORNL-3015, pp 123–25.

[3] *GCR Quart. Progr. Rept. Dec. 31, 1960*, ORNL-3049, pp 273–76.

Compatibility of Graphite and Structural Metals in Helium Contaminated by CO and CO_2

J. H. DeVan

Additional compatibility experiments have been operated under dynamic flow conditions to investigate gas-metal reactions occurring between various structural steels and CO-CO_2 impurities in helium. The experiments utilized a type 316 stainless steel thermal-convection loop in which impure helium at 45 psia was circulated through a heated test section at 1100°F and a cold-leg section at 500°F.[5] The test section contained various steel specimens and graphite maintained at 1100°F, together with a type 304 stainless steel element maintained at 1500°F. Gaseous impurity levels were continuously controlled and were established within the specifications tentatively proposed for the EGCR.

The concentrations, which are shown in Table 14.1, ranged from a minimum level of 0.01 vol % of each gas to a maximum level of 1.0 vol % CO_2 and 0.25 vol % CO.

Steels containing 7% or more chromium in all tests exhibited relatively light, adherent oxide films and correspondingly low weight gains, which showed little dependence on impurity concentrations or ratios. The type 304 stainless steel heated elements exposed at 1500°F exhibited heavier oxide films than companion specimens at 1100°F, but the oxide remained protective at the higher temperature. In contrast, steels containing less than 7% Cr underwent heavy oxidation at even the lowest impurity concentrations. Table 14.1 compares weight-gain data for the latter steels with data from air tests. The oxidation resistance derived from chromium additions up to 5% is seen

[4] *GCR Quart. Progr. Rept. Mar. 31, 1961*, ORNL-3102, pp 212–13

[5] D. B. Trauger, pp 165–84 in "Materials Compatibility and Fuel Element Test Program," *Information Meeting on Gas-Cooled Power Reactors, Oak Ridge National Laboratory, Oct. 21–22, 1958*, TID-7564 (December 1958).

Table 14.1. Oxidation of Low-Alloy Steels in Air and in Helium Contaminated by CO and CO_2

Helium pressure, 45 psia
Test temperature, 1100°F
Test duration, 900 hr

Loop No.	Impurity Concentration (vol %)	$\frac{p_{CO_2}}{p_{CO}}$	Nominal Steel Composition (wt %)					
			Plain Carbon (0.15 C)		$2\frac{1}{4}$ Cr–1 Mo		5 Cr–$\frac{1}{2}$ Mo	
			Weight of Oxide Film (mg/cm^2)	Weight of Metal Reacted (mg/cm^2)	Weight of Oxide Film (mg/cm^2)	Weight of Metal Reacted (mg/cm^2)	Weight of Oxide Film (mg/cm^2)	Weight of Metal Reacted (mg/cm^2)
10	0.13 CO_2 + 0.18 CO	0.72	14.1	10.2	7.9	5.7		
12	0.15 CO_2 + 0.18 CO	0.83	7.3	5.3	5.5	4.0	5.7	4.1
13	0.05 CO_2 + 0.045 CO	1.1	12.8	9.3	10.5	7.6	5.9	4.3
14	0.01 CO_2 + 0.01 CO	1.0	10.5	8.3			6.6	4.8
15	1.0 CO_2 + 0.25 CO	4.0	21.3	15.0	20.2	14.6	14.4	9.2
	Air[a,b]		98	71	54	39	18	13

[a] H. H. Uhlig, *The Corrosion Handbook*, pp 644–47, Wiley, New York, 1948.
[b] *Steels for Elevated Temperature Service*, pp 21–25, United States Steel Co., 1949.

to be considerably less in the impure helium environments than in air.

Graphite-Metal Contact Studies

B. Fleischer

Compatibility studies were recently extended to evaluate the rate of carburization of type 304L stainless steel in direct contact with graphite as a function of contact pressure, temperature, and surface treatment. A preliminary test at 1300°F has indicated that a serious self-welding problem in graphite–stainless steel couples exists at contact pressures as low as 500 psi in the absence of oxidizing impurities. However, pretreatment of stainless steel surfaces by either oxidation or copper plating prevented interaction at 1300°F at contact pressures up to 2000 psi.

MOLTEN-SALT REACTOR PROGRAM

J. H. DeVan R. C. Schulze

Forced-Convection Loops

The corrosion behavior of Inconel and INOR-8 during prolonged exposures to fluoride salt mixtures has been investigated in forced-convection loops operating from one to two years.[6,7] A total of 24 loop experiments were completed prior to concluding this final phase of corrosion testing in support of the MSR Program. Salt systems used in these investigations have been of the types LiF-BeF_2-(ThF_4, UF_4) and NaF-BeF_2-(ThF_4, UF_4). Maximum operating temperatures have ranged from 1200 to 1300°F.

Results of five loop experiments which were recently examined are summarized in Table 14.2. Two Inconel loops included in this table sustained relatively heavy attack in the form of subsurface voids after exposures of 13,000 and 15,000 hr respectively. A trend apparent in these results and generally true in the case of previous loop tests is the indication that large ThF_4 additions effect lower corrosion rates than do much smaller UF_4 additions.

The results of three INOR-8 loops included in Table 14.2 provide further confirmation of the

[6] *MSR Quart. Progr. Rept. July 31, 1960*, ORNL-3014, pp 56–58.
[7] *MSR Progr. Rept. for Period from Aug. 1, 1960 to Feb. 28, 1961*, ORNL-3122.

Table 14.2. Results of Metallographic Examinations of Forced-Convection Loops Operated with Fused Fluoride Mixtures

Flow rate, approx 2 gpm
Reynolds No., 3000–4000

Loop Material	Time (hr)	Maximum Salt-Metal Interface (°F)	Loop ΔT (°F)	Salt Mixture (mole %)	Results of Metallographic Examination
Inconel	15,038	1300	200	62.0 LiF–36.5 BeF_2–1.0 ThF_4–0.5 UF_4	Intergranular voids to 24 mils
Inconel	13,155	1300	200	71 LiF–16 BeF_2–13 ThF_4	Intergranular voids to 13 mils
INOR-8	8,110	1300	200	70 LiF–10 BeF_2–20 UF_4	Heavy surface roughening and pitting to $1\frac{1}{2}$ mils
INOR-8	14,498	1300	200	62 LiF–36.5 BeF_2–0.5 UF_4–1 ThF_4	Surface film to approx $\frac{1}{3}$ mil; no pitting or void formation
INOR-8	19,943	1200	100	27 NaF–35 LiF–38 BeF_2	No attack

excellent corrosion resistance of this alloy to fluoride salt mixtures. With the exception of one experiment which incorporated 20 mole % UF_4, attack of loop surfaces was limited to the formation of a thin ($\frac{1}{3}$ to $\frac{1}{2}$ mil) intermetallic surface layer. The loop containing 20 mole % UF_4 underwent somewhat greater attack, although the corrosion rate would not preclude the use of such a salt, even for relatively long exposures. Salt samplers located at the pumps of two of the INOR-8 loops permitted continuous monitoring of corrosion-product concentrations in the circulating salt mixtures. Of the components comprising INOR-8, only chromium was found to enter the salt in detectable amounts. The chromium concentration of salt mixtures containing up to 1 mole % UF_4 increased less than 100 ppm over a 15,000-hr period, while in the case of the salt containing 20 mole % UF_4, the chromium concentration increased about 1500 ppm.

The nature of the thin corrosion films formed in most of the long-term INOR-8 loop tests is being studied by means of an electron-beam microprobe analyzer.[8] The compositions of these films were determined by use of both spot and scan techniques. In general, the spot analyses of the surface of the films indicated a slight decrease in the nickel content and virtually complete depletion of chromium and iron. The scan analysis, obtained along the cross section of one specimen, showed that the depth to which the concentrations of chromium, iron, and nickel were affected was approx $\frac{1}{2}$ mil. These analyses support the assumption, based on hardness and qualitative analyses, that the film represents an intermetallic phase of the composition Ni_4Mo.[9]

[8] *MSR Quart. Progr. Rept. July 31, 1960*, ORNL-3014, p 56.

[9] *Met. Div. Ann. Progr. Rept. July 1, 1960*, ORNL-2988, pp 206–8.

15. FUELS EVALUATION

J. L. Scott

D. F. Toner R. E. Adams

The work of the Fuels Evaluation Group during the past year was directed toward evaluating the fission-gas-retention properties of selected ceramic fuels and analyzing the basic phenomena governing the irradiation behavior of dispersion fuels. The ceramic fuels studied included UO_2, dispersions of UO_2 in BeO, UC_2 particles coated with pyrolytic carbon, and a solid solution of 5 wt % UO_2 in ThO_2. All of these have application in the Experimental Gas-Cooled Reactor (EGCR) or in advanced gas-cooled reactors. The approach used in evaluating dispersion fuels was the design of experiments to clarify basic failure mechanisms.

The neutron activation technique was used to determine the fission-gas-retention properties of the ceramic fuels. It involves low-temperature irradiations followed by heat treatments ex-pile, during which the rates of release of Xe^{133} are measured. The apparatus and procedural details have been described previously.[1]

BULK UO_2

Studies on UO_2 were a continuation of the work reported last year.[1] Recent accomplishments included a study of the correlation between BET (nitrogen) surface area and D' and a study of the release of fission gases at 1000°C and below in vacuum.

Results of the study[2] of the correlation between BET surface areas and D' showed that D' values were proportional to the square of the BET surface area, as predicted by diffusion theory. The value of the diffusion coefficient of xenon in UO_2 at 1400°C was computed from the data to be 7.5×10^{-6} cm^2/sec. The correlation explained the four orders of magnitude of variation of D' values for pilot batches of EGCR UO_2 from various vendors. The variation was the result of two orders of magnitude variation of BET surface areas for the batches of UO_2. It was also concluded that an upper limit of BET surface area should be included in UO_2 specifications.

Measurements of the rates of release of Xe^{133} from UO_2 at 1000°C and below at a pressure of approx 1 μ Hg showed that the mechanism of release in the temperature range 600 to 1600°C was diffusion with an activation energy of about 70 kcal/mole.[3] At 400°C a linear rate of release was observed after an incubation period of about 30 hr. The linear rate of release was attributed to a linear rate of oxidation of the UO_2 to form a second phase which spalled off, making new surfaces available for further oxidation.

SAMPLES OF BeO CONTAINING 30 vol % UO_2

The samples were fabricated by Hamner[4] by sintering cold-pressed ADU-type UO_2 and UOX-grade BeO for 1 hr at 1750°C in hydrogen. The grains sizes of both the UO_2 and BeO phases were 3 to 4 μ, and the final densities were over 95% of theoretical.

The rates of release of Xe^{133} from neutron-activated samples were determined at 1200, 1400, 1600, and 1800°C.[5] Duplicate runs at each temperature gave excellent agreement. At 1200 and 1400°C a small burst of xenon was observed during heatup, and subsequent release was by a diffusion mechanism. At 1600°C the initial release was much higher than at the lower temperatures, but apparently was diffusion-controlled. Finally, at 1800°C the rate of release was approximately

---

[1] J. L. Scott, D. F. Toner, and R. E. Adams, *Met. Div. Ann. Progr. Rept. July 1, 1960*, ORNL-2988, pp 213–20.

[2] D. F. Toner and J. L. Scott, "Study of the Factors Controlling the Release of Xe^{133} from Bulk UO_2," paper to be presented at the ASTM Symposium on Radiation Effects in Refractory Fuel Compounds, Atlantic City, N.J., June 26–30, 1961 (to be published).

[3] J. L. Scott and D. F. Toner, *GCR Quar. Progr. Rept. Mar. 31, 1961*, ORNL-3102, pp 93–97.

[4] R. L. Hamner, *Met. Div. Ann. Progr. Rept. July 1, 1960*, ORNL-2988, p 189.

[5] D. F. Toner, *GCR Quart. Progr. Rept. Dec. 31, 1960*, ORNL-3049, p 204.

linear and was sufficiently high that all the Xe^{133} was released in 30 hr.

In order to account for the high rates of release at 1600 and 1800°C, unirradiated samples of the BeO-UO_2 were heat-treated in the same way as the neutron-activated samples and then examined metallographically. Grain growth of both the UO_2 and BeO phases was observed at 1600 and 1800°C, with good qualitative agreement between the amount of grain growth and the amount of Xe^{133} released. Sublimation of the UO_2 was also a contributing factor at 1800°C.

COATED-PARTICLE STUDIES

Preliminary studies have been made of the fission-gas-retention properties of UC_2 particles coated with pyrolytic carbon. These samples were manufactured by the Minnesota Mining and Manufacturing Company and contained 200-μ-diam UC_2 spheres coated with 80 μ of pyrolytic carbon. The conditions of application of the coatings were such that the carbon structure was amorphous. Individual samples consisting of approx 100 of these coated particles were irradiated for 160 hr at a neutron flux of approx 8×10^{11}, in the ORNL Graphite Reactor.

Two samples have been heat-treated to date. The first sample was held at 1825°C for 90 hr, during which time no measurable gas release occurred. The temperature of the sample was then cycled between room temperature and 2500°C, and some of the coatings ruptured. Particles continued to rupture at room temperature after the last thermal cycle. The second sample was held at a constant temperature of 2050°C for 118 hr. Then the particles began to rupture, with a resulting burst of fission gas. In 100 hr, approx 50 particles had ruptured. No additional ruptures were observed at room temperature.

It was concluded that the 3M coatings are very retentive unless subjected to rather severe thermal treatments.

SPECIMENS OF ThO_2 CONTAINING 5 wt % UO_2

Several specimens of ThO_2–5 wt % UO_2 made by the sol-gel process[6] were tested for fission-gas-retention properties in the temperature range 1440 to 2200°C by the neutron-activation technique. Results[7] showed that the release curves were parabolic in the temperature range 1440 to 2015°C and indicated that the mechanism of release was diffusion. The activation energy for the diffusion of Xe^{133} in ThO_2–5 wt % UO_2 was found to be 75.6 kcal/mole. At 2200°C a linear rate of release was observed similar to that in bulk UO_2 at 1800°C. In both instances, sublimation of the oxide was the rate-controlling step in the release process. The increased stability of the ThO_2-UO_2 was expected as a result of the higher melting point of ThO_2 (3300°C), compared with that of UO_2 (2750°C).

FAILURE ANALYSIS OF DISPERSION FUELS

A theoretical analysis of dispersion-fuel systems indicates that considerable additional information is required before their behavior can be defined in terms of the variables of design, irradiation environment, materials properties, and burnup. The accumulation of such information is a long-range effort because of the many complex factors involved. A program to obtain such information is suggested as follows: (1) assimilate information currently being obtained on fission-gas release and swelling of dispersant materials in order to define the mechanisms that control generation of gas pressure in dispersion fuel systems; (2) study experimentally the mechanism of swelling and failure of dispersion fuels as a function of pressure generation and materials properties; and (3) study experimentally the geometry factors by irradiation tests on idealized and conventional dispersions. The irradiation experiments will be simplified by using dispersions of boron carbide in copper instead of enriched uranium. Helium gas pressure will be generated from the B^{10} isotope by an (n,α) reaction to simulate the fission-gas pressure. This technique will minimize the problem of heat generation during irradiation, generate gas much more rapidly than by uranium fission, and simplify postirradiation examination because the reaction products are not radioactive.

---

[6] O. C. Dean and K. H. McCorkle, *Fuel Cycle Development — Semiann. Progr. Rept. Sept. 30, 1960*, ORNL CF-60-11-56, p 5.

[7] D. F. Toner and J. L. Scott, *Fuel Cycle Development — Semiann. Progr. Rept. Mar. 31, 1961*, ORNL-3142 (in press).

16. MATERIALS COMPATIBILITY

E. E. Hoffman

POTASSIUM-OXYGEN STUDIES

A. P. Litman E. E. Hoffman

The advantages of using potassium as the working fluid in Rankine-cycle turbogenerator systems for space power applications have been reported.[1,2] In this regard, a more detailed approach to certain problems beyond comparative studies on potential container materials for flowing potassium is necessary. It has been established that oxygen contamination of alkali metals has a deleterious effect on the corrosiveness of these media.[3] The studies discussed below deal with the various aspects of the potassium-oxygen system that must be investigated in order to obtain a basic understanding of the role of oxygen in potassium–container-metal compatibility studies.

Solubility Studies of Oxygen in Liquid Potassium

Only a limited amount of work has been done on the solubility of oxygen in potassium.[3] Indications are that the solubility in potassium is considerably higher than in lithium or sodium. Initial solubility studies on potassium will utilize techniques developed for lithium.[4]

The monoxide of potassium is the one most likely to be present normally in potassium because of the deficiency of oxygen and the thermodynamic stability of K_2O. Methods of preparation of high-purity K_2O for the solubility studies are being investigated. Several runs attempting to prepare K_2O by reacting oxygen with potassium and subsequently distilling off the excess potassium were not successful. Initial attempts to make the monoxide by the dissociation of KOH were also unsuccessful. Other possible methods of preparation that are being investigated include the reaction of KNO_3 or KNO_2 with potassium and the reacting of HgO with excess potassium.

Evaluation of Analytical Methods for Determining Oxygen in Potassium

Although reasonable data have been obtained on the analysis of oxygen in potassium by the *n*-butyl bromide technique, the reproducibility and accuracy of the method have never been investigated. The *n*-butyl bromide procedure was originally developed for the determination of oxygen in sodium.[5] Recent studies indicate that several improvements can be made in the original bromide method. The cooperation of the Analytical Chemistry Division has been enlisted to study all facets of this analytical problem. This will include investigation of the mercury amalgamation method and, possibly, neutron activation techniques for determining oxygen in potassium.

Both *n*-butyl bromide and mercury-amalgamation systems have been assembled and made operational by the Analytical Chemistry personnel. To date, duplicate oxygen-content determinations on potassium show poor correlation between the two methods.

Purification of Potassium: Methods of Reducing the Oxygen Content

The relatively high free energy of formation of K_2O (ref 6) indicates that hot gettering should be successful as a purification method and that a number of metals can be used as getters. These include several readily available and easily handled materials such as titanium and zirconium.

---

[1] A. P. Fraas, P. G. Lafyatis, and J. R. Simmons, *A Comparative Study of Fission Reactor-Turbine-Generator Power Sources for Space Vehicles*, ORNL-2768 (to be published).

[2] H. M. Dieckamp, R. Balent, and J. R. Wetch, *Nucleonics* 19(4), 76 (1961).

[3] C. B. Jackson (ed.), *Liquid-Metals Handbook, Sodium-NaK Supplement*, p 175, Atomic Energy Commission, Department of Navy, Washington, D.C., 1955.

[4] E. E. Hoffman, *Corrosion of Materials by Lithium at Elevated Temperatures*, ORNL-2924, pp 141–44 (Oct. 3, 1960).

[5] J. C. White, W. J. Ross, and R. Rowan, Jr., *The Determination of Oxygen in Sodium*, ORNL-1286 (Apr. 30, 1952).

[6] A. Glassner, *The Thermochemical Properties of the Oxides, Fluorides, and Chlorides to 2500°K*, ANL-5750 (1957).

Cold trapping, low-temperature filtration, and vacuum distillation are being studied as possible purification techniques.

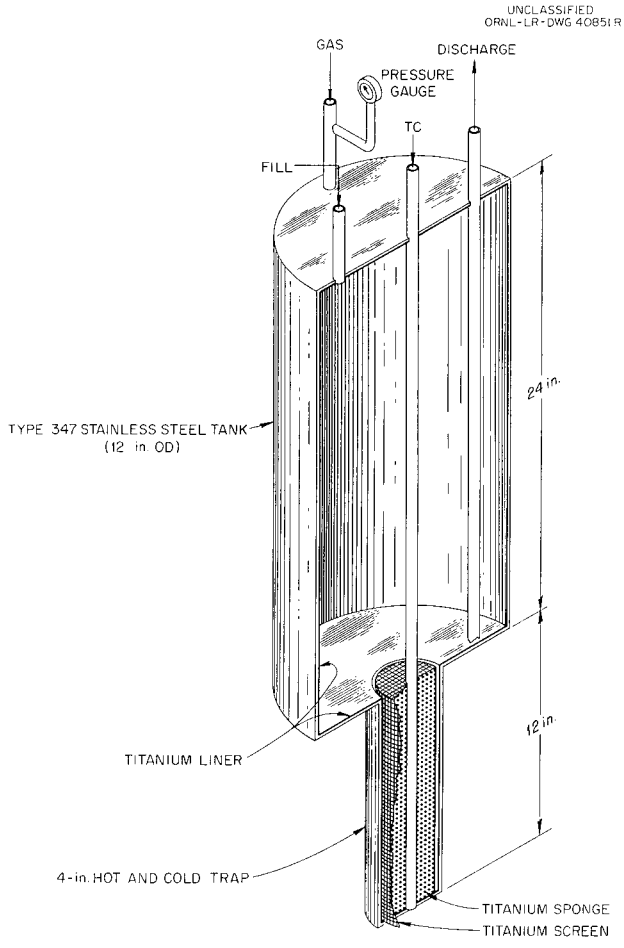

Process Description	Temperatures (°C)	Time (hr)	Oxygen Content** (ppm) Individual Analyses	Average
As Received			246, 268, 293	269
Hot Gettered at 650°C	650	50	26, 36, 38	33
Using 8.4-kg Ti Sponge		150	18, 50	36
	650	250	20, 20, 20	20
		100	33, 40, 65	46
		250	32, 38, 40	37
Cold Trapped*	250	400	49, 51	50
Using 8.4-kg Ti Sponge		550	20, 25, 50	32
	80 45	700	19, 27, 28, 47, 57	36
		100	18, 27, 35	27
Cold Trapped*	100	200	16, 42	29
Using 8.4-kg Ti Sponge		300	14, 19, 20	18
	35 30	400	18, 33	28

*Melting Point K – 64°C
**Analytical Method: n-butyl bromide (Ref. ORNL-1286)

Fig. 16.1. Potassium Purification Experiment (90-kg Batch).

Two batches (10 and 90 kg) of commercial potassium containing 270 ppm oxygen were purified by hot gettering with titanium at 650°C and subsequent cold trapping. The results of the two experiments were quite similar, and the results on the 90-kg batch are summarized in Fig. 16.1.

Approximately 40 oxygen determinations (*n*-butyl bromide method) made on triplicate samples of potassium taken at 12 intervals during the 1350-hr purification experiment indicated that most of the oxygen was removed during the first 50 hr of gettering treatment. Future research will include study of the important variables in gettering procedures so as to optimize the purification method.

BOILING-POTASSIUM STUDIES

D. H. Jansen E. E. Hoffman

Compatibility tests are being conducted in refluxing-potassium-capsule systems and in natural-circulation boiling-potassium loop systems to provide screening information regarding the comparative corrosion resistance of iron-, nickel-, cobalt-, and niobium-base alloys. The status of these studies was presented in detail in a recent report.[7]

Refluxing-potassium tests have been conducted for 500 and 1000 hr at 1500 and 1600°F on Inconel, Haynes alloy No. 25, and types 310 and 316 stainless steel. Sleeve-type insert specimens lined the test capsules. Small weight losses were observed in the condensing region and weight gains in the boiler (liquid) region of each of the test systems. Type 316 stainless steel has shown the best resistance of any of the alloys studied in refluxing systems to date.

A boiling-potassium, type 316 stainless steel loop has been operated at a boiler temperature of 1600°F for 3000 hr. The test system is shown in Fig. 16.2. A mass flow of 170 g/min and a vapor velocity of 46 fps were maintained for the entire test period.

Results indicated that, in general, weight losses occurred on the sheet tensile specimens from the hot liquid and vapor regions of the loop, while weight gains and mass-transfer deposits were observed on the specimens that were in contact with liquid potassium in the cold leg of the loop.

[7] E. E. Hoffman, *NASA-AEC Liquid-Metals Corrosion Meeting, Dec. 7–8, 1960, Washington, D.C.*, NASA TN D-769, pp 15–24, (February 1961).

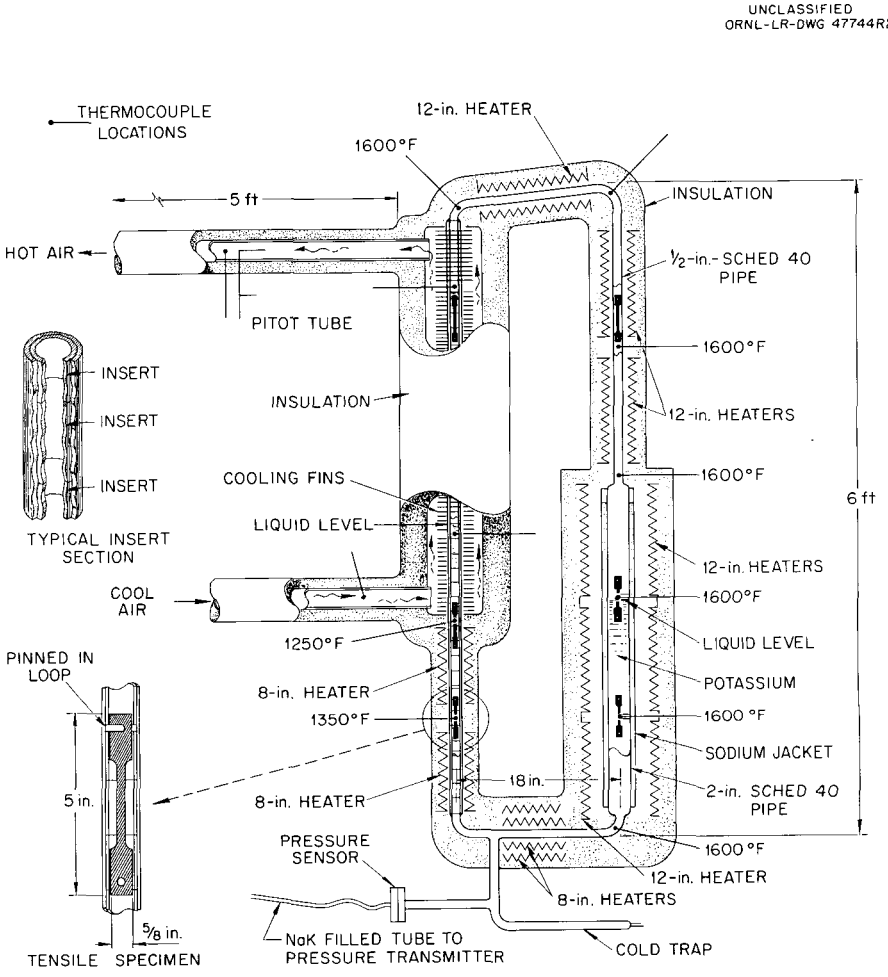

Fig. 16.2. Type 316 Stainless Steel–Boiling-Potassium Loop.

Metallographic examination of many sections cut from the loop revealed that the maximum attack (2 mils) occurred near the liquid-vapor interface in the boiler. Room-temperature tension tests on specimens from the various regions of the loop and on control specimens heat treated in vacuum indicated no significant effect of the potassium environment on the alloy. Normal tensile strength levels (78–91 $\times$ 10^3 psi) and elongation values (43 to 61%) were obtained on these specimens.

Chemical analyses of turnings machined from the inside pipe wall in the condenser region and cool-liquid region indicate substantial mass transfer of carbon from the hot to the cooler regions. Chromium carbide ($Cr_{23}C_6$) was detected on the pipe and specimen surfaces in the cool-liquid regions of the loop.

Boiling-potassium-loop tests are currently being conducted on Inconel and Haynes alloy No. 25. These tests also will be operated for 3000 hr at a boiler temperature of 1600°F. Analysis of the corrosion data from the three loop-test systems (type 316 stainless steel, Inconel, and Haynes alloy No. 25) should indicate which of these alloy systems is most compatible with boiling potassium.

OXIDATION TESTS ON POTENTIAL POTASSIUM CONTAINER MATERIALS

D. H. Jansen

In order to evaluate the compatibility of various conventional alloys with boiling potassium, it is necessary that these alloys possess adequate oxidation resistance in the temperature range 1800 to 2000°F. Several of the candidate alloys have been screened to determine their relative oxidation resistances. The results of these short-time tests are given in Table 16.1.

Table 16.1. Results of 100-hr Oxidation Tests in Static Air

Material	Nominal Composition (wt %)	Thickness of Surface Layer Affected by Test (mils)[a]	
		1800°F	2000°F
Inconel	(78 Ni–14 Cr–7 Fe)	0.5	1.0
Haynes alloy No. 25	(50 Co–20 Cr–15 W–10 Ni–3 Fe)	0.5	2.5
Haynes alloy No. 56	(46 Fe–21 Cr–13 Ni–11 Co–5 Mo–2 Fe)	2.0	3.0
Type 310 stainless steel	(52 Fe–25 Cr–20 Ni–2 Si)	2.0	4.0
Type 316 stainless steel	(69 Fe–17 Cr–12 Ni–2 Mo)	4.5	11.0
Type 446 stainless steel	(75 Fe–25 Cr)	0.5	7.0

[a]Includes metal converted to oxide and areas in which subsurface oxidation occurred.

MASS-TRANSFER EFFECTS IN NIOBIUM-SODIUM-TYPE 316 STAINLESS STEEL SYSTEM

J. R. DiStefano E. E. Hoffman

Tests have been conducted on the niobium-sodium-stainless steel system at temperatures from 1500 to 1800°F and for times up to 1000 hr. The tests were conducted in nonflowing isothermal systems. The ratio of stainless steel to niobium surface area was varied from 0.1 to 20. Mass transfer of iron, nickel, and chromium from the stainless steel to the niobium was negligible in these tests. It was found, however, that carbon and nitrogen from the stainless steel were transferred to the niobium. Metallographic examination of the niobium specimens after exposure showed two brittle surface layers. These layers were identified by x ray as NbC and Nb_2N. From chemical analyses of the niobium before and after these layers were removed, it was determined that the increase in carbon concentration was confined to the surface layer, but the nitrogen penetrated the entire 0.040-in. specimens.

A systematic investigation of the various test variables led to the conclusion that mass transfer of carbon and nitrogen increases with time, temperature, and the stainless steel–to–niobium surface ratio. In the test at 1700°F, with a surface area ratio of 0.1, no transfer of carbon or nitrogen occurred. Transfer of niobium to the surface of the stainless steel did occur. The 0.040-in.-thick stainless steel specimen contained 0.5% Nb following test. The niobium was present as an NbC surface layer.

An evaluation of the effect of the pickup of carbon and nitrogen was made on the basis of changes in tensile properties. A large increase in the ultimate tensile strength and a decrease in the per cent elongation were observed both at room temperature and at 1700°F. These same results were observed even after the surface layers were removed. It is concluded that the changes in properties are due to the penetration of the niobium alloy specimens by nitrogen.

VAPOR PRESSURE OF NaK

J. R. DiStefano

The vapor pressure of NaK (43.7 wt % K) has been determined from 1520 to 1832°F. Vapor pressures of NaK as measured in this experiment are given in Table 16.2. For purposes of comparison the vapor pressure was also calculated from Raoult's law and empirical equations for the vapor pressure of pure sodium and potassium as a function of temperature.

Table 16.2. Vapor Pressure of NaK (43.7 wt % K)

Temperature		Pressure (mm Hg)	
°K	°C	Calculated	Measured
1100	827	758	977
1123	850	924	1163
1173	900	1388	1587
1223	950	2014	2016
1273	1000	2850	2420

The calculated values do not correct for molecular species which might be present in the vapor, and this might explain some of the observed difference.

GRAPHITE–MOLTEN-FLUORIDE-SALT STUDIES

W. H. Cook

It is desirable that the graphite moderator in the Molten-Salt Reactor be unclad in order to minimize the volume of the high-cross-section material in the core and thus improve the neutron economy. This would require that portions of the structural alloys of the reactor be exposed to the molten salt in contact with the graphite at the reactor operating temperature of approx 1200°F.[8] The compatibility and permeation of the unclad graphite with the molten salt plus the effects of carburization, if any, on the structural alloys at the operating conditions must be known before these components can be incorporated into the design of the reactor.

Permeation of Various Grades of Graphite by Molten Salts

Distribution of Fluoride Salt Permeated into Various Grades of Graphite. – Radiography was used to determine the distribution and depth of penetration of a LiF-BeF_2-ThF_4-UF_4 mixture into specimens of graphite. Nine different grades of graphite were exposed for 100 hr to fused salt under 150 psig at 1300°F. The details are described in a recent progress report.[9]

The most significant thing shown by the radiographic examination was that certain grades of graphite can be fabricated in which salt permeation is limited to less than 50 mils below the external surfaces of the graphite.

Oxidation and Permeation. – Brazing of graphite-to-graphite and graphite-to-metal joints in oxidizing atmospheres would be desirable from a fabrication standpoint. Such an operation would probably increase the pore sizes of a graphite because of the low oxidation resistance of graphite. "Oxidized" specimens were prepared by exposing graphite to air for 20 sec at approx 2372°F, a typical brazing cycle. The percentages of the bulk volume of graphite permeated by molten salt were 0.3 and 0.5, respectively, for the control ("unoxidized") and the "oxidized" specimens. The higher permeation value for the "oxidized" specimens indicated that their voids had been enlarged. Therefore, it does not appear practical to braze graphite in air if one cannot tolerate an increase in its porosity.

Effect of Original Fabrication Size and Shape. – The alteration in the resistance of a grade of graphite to impregnation by fluoride salts was shown to be a function of size, shape, density, and configuration in standard screening permeation tests. Specimens from four different shapes and sizes of the base stock[10] for grade B-1 graphite were investigated.

The results indicated that as the size of a shape is increased, the bulk density and the resistance to permeation of the fabricated grade of graphite decrease. The results also suggest that for solid cylinders and pipe that have similar external diameters, the pipe shape tends to have the lower resistance to salt permeation.

Precipitation from Molten Salts in Contact with Graphite

Precipitation of UO_2 from Fluoride Salts. – Studies that revealed the problem of the precipitation of UO_2 from the fused salts were conducted initially on fuels that contained neither zirconium fluoride nor thorium fluoride.[11] Tests had indicated and it was suggested that these salts would act as inhibitors to the UO_2 formation, and experiments were conducted on several salts containing them. It was found that 5 mole % ZrF_4 eliminated any precipitation of UO_2.[12] The addition of 4 mole % ThF_4 to the salt did not prevent precipitation, but the addition of 14 mole % was effective.[13]

---

[8] H. G. MacPherson *et al.*, ORNL CF-57-4-27 (Apr. 29, 1957) (classified).

[9] *MSR Quart. Progr. Rept. Jan. 31, 1961*, ORNL-3122 (in press).

[10] Base stock denotes fully graphitized material that has not been given special impregnation treatments with carbonaceous materials to reduce and seal off void spaces to produce a low-permeability graphite.

[11] W. H. Cook, *Met. Div. Ann. Progr. Rept. Oct. 10, 1958*, ORNL-2632, p 105.

[12] *MSR Quart. Progr. Rept. Jan. 31, 1961*, ORNL-3122 (in press).

[13] W. H. Cook, *Met. Div. Ann. Progr. Rept. July 1, 1960*, ORNL-2988, p 227.

A series of 100-hr precipitation tests have been made with AGOT graphite and a $LiF-BeF_2-UF_4$ mixture at 1300°F to determine the effect of graphite volume on the amount of UO_2 precipitated.[14] Approximately 9 wt % of the uranium in the salt precipitated as UO_2 when the volume ratio of graphite to fuel was 9:1. This corresponds to the ratio proposed for the Molten-Salt Reactor Experiment (MSRE). These data are limited to the experimental conditions described and the particular graphite used. However, they do indicate what might be expected with a reactor-grade graphite and this particular fuel salt.

Standard compatibility tests were run with the MSRE fuel ($LiF-BeF_2-ZrF_4-ThF_4-UF_4$). The molten salt was exposed for 500 hr to AGOT graphite at 1300°F. A similar charge of salt was used as a control in a capsule containing no graphite. The tests were monitored by radiography after 100 and 500 hr. Precipitates were noted in the control capsule after 100 hr. Approximately five times as much precipitation was seen in the test capsule containing graphite. No additional precipitation was noted after 500 hr. X-ray analyses indicated that the precipitate was entirely monoclinic ZrO_2. Thus, zirconium fluoride appears to prevent the formation of UO_2 under these conditions.

Removal of Oxygen Contamination from Graphite

Purging with Molten Fluorides. – Work has continued on the evaluation of various molten-fluoride salts as purging agents to remove the normal oxygen contamination from graphite. As reported previously[15] and discussed above, uranium fluoride or zirconium fluoride may precipitate as oxides from the molten salts when oxygen is present in the system. The principal source of oxygen in the MSRE is the graphite moderator.

One method suggested for the removal of the majority of the oxygen from the graphite is to purge the system with a fused salt. The usual method is to purge a standard crucible of AGOT graphite with the purging salt of interest at 1300°F in a vacuum for various time periods. To evaluate the effectiveness of this procedure, the purging salt is replaced with $LiF-BeF_2-UF_4$ and the test is repeated with exposure time as a variable. If oxygen is present, a UO_2 precipitate readily forms and can be detected by radiography.

As a result of the tests, it appears that some benefit can be derived from the purging of graphite with molten salts, but it does not seem to be 100% effective. To date, fused $NaF-ZrF_4-UF_4$ has been the most effective purging salt tested, and precursory tests indicate that its effectiveness may be time dependent. The time and expense of such a treatment are obvious disadvantages. It should be emphasized, however, that the metal surfaces must be cleaned in any case, and the operation of the "plumbing" system must be checked after the construction of the reactor is completed. A barren salt could be used for these purposes and could also purge the graphite of much of its oxygen contamination.

Purging with Ammonium Bifluoride. – It has been reported that in less than 20 hr the thermal decomposition products of $NH_4F \cdot HF$ in the presence of graphite apparently removed the normal oxygen contamination in graphite to such an extent that no UO_2 precipitation occurred when the graphite was exposed to an $LiF-BeF_2-UF_4$ mixture at 1300°F.[16]

The effectiveness of the $NH_4F \cdot HF$ treatment has been demonstrated for a relatively long test period. A treated AGOT graphite crucible subsequently contained an $LiF-BeF_2-UF_4$ mixture for 2000 hr at 1300°F without a UO_2 precipitate forming.[17] Tests also indicate that it is not necessary for the $NH_4F \cdot HF$ to be in intimate contact with the graphite during the pretreatment. Therefore, it might be possible to pump the decomposition products of $NH_4F \cdot HF$ to heated graphite and remove the oxygen.

The pretreatment of graphite as described above also would require that INOR-8, the structural material of the MSRE, be exposed to the thermal decomposition products of $NH_4F \cdot HF$. Precursory tests at 1300°F have indicated that there is a slight reaction between INOR-8 and the decomposition products. A 0.0005-in.-thick nonporous reaction layer developed on the INOR-8.[17]

---

[14] *MSR Quart. Progr. Rept. July 31, 1960*, ORNL-3014, p 69.

[15] *MSR Quart. Progr. Rept. Jan. 31, 1961*, ORNL-3122 (in press).

[16] W. H. Cook, *Met. Div. Ann. Progr. Rept. July 1, 1960*, ORNL-2988, p 227.

[17] *MSR Quart. Progr. Rept. Jan. 31, 1961*, ORNL-3122 (in press).

Inconel and INOR-8 in the Salt-Graphite Test Systems

D. H. Jansen W. H. Cook

The use of unclad graphite as moderator in the Molten-Salt Reactor will make it necessary for the graphite to be in direct contact with the fuel and the INOR-8 or Inconel.[18] Therefore, to determine whether INOR-8 and Inconel would be carburized, they were tested in static LiF-BeF_2-UF_4 which was in contact with bare graphite.

Tests at 1300°F in multiples of 2000-hr duration from 2000 through 12,000 hr indicated that no carburization occurred and that the tensile properties of the INOR-8 were not altered.[18–20] The last of this series, a 14,000-hr test, has been completed. Metallography revealed a slight roughening to a maximum depth of less than 0.5 mil on the INOR-8 specimens.

As in the shorter-duration tests, the room temperature and 1250°F tensile strength and elongation values of INOR-8 specimens subjected to the fuel-graphite exposure in this 14,000-hr test were not significantly different from those of control specimens subjected to argon at the same temperature.

Inconel which had been exposed to the salt in the presence of graphite for only 4000 hr was attacked to such an extent that any minor effect of carburization on the tensile properties could not be determined. Consequently, tensile tests on Inconel specimens were omitted from the tests of longer duration.

CORROSION OF CONTAINER MATERIALS USED IN THE REPROCESSING OF REACTOR FUELS

A. P. Litman

Continued assistance was given the Chemical Technology Division on corrosion problems, selection of materials of construction, fabrication, failure analysis, welding, and brazing in connection with their work on recovering uranium and fission products from spent reactor fuels. The majority of this support was in regard to pilot-plant-scale studies on the ORNL Fluoride Volatility Process, although some aid was given to groups studying aqueous fuel reprocessing by use of the Sulfex, Zirflex, Purex, and Darex processes.

Hydrofluorination Corrosion

Installation of a 17-ft INOR-8 hydrofluorinator-dissolver in the Volatility Pilot Plant (VPP) now permits the plant to reprocess zirconium-uranium heterogeneous fuels. After 204 hr of exposure to anhydrous HF and equimolar NaF-LiF containing 22 to 52 mole % ZrF_4 at 495 to 655°C, wall-thickness changes on the dissolver were determined by ultrasonic techniques. The following conditions were encountered during dissolution of seven unirradiated Zircaloy-2 simulated fuel element subassemblies: (1) Maximum wall thickness losses for the hydrofluorinator were noted in the vapor region. (2) A maximum loss of 11 mils was found, which corresponds to 0.05 mil/hr, based on HF exposure time, and 17 mils/month, based on molten-salt residence time.[21]

Fluorination Corrosion

Another L nickel fluorinator vessel, MK III, using a new dumbbell configuration to reduce entrainment problems, was fabricated and installed in the VPP. Experimental nickel-rich binary alloys containing Al, Co, Fe, and Mn which have been exposed to the fluorination environment show improved corrosion resistance when compared with L nickel. Corrosion of these alloys was found to be directly proportional to fluorine exposure time, temperature, and the presence of uranium in the system.

Based on the corrosion results observed on L nickel control specimens during nonirradiated, uranium-bearing runs at temperatures of 450 to 670°C, the MK III fluorinator should experience maximum corrosion losses of 0.6 mil/hr, based on fluorine sparge time, or 18 mils/month, based on molten-salt residence time.

---

[18] *Molten-Salt Reactor Program Status Report*, ORNL CF-58-5-3, p 6 (May 1, 1958).

[19] *MSR Quart. Progr. Rept. June 30, 1958*, ORNL-2551, p 59.

[20] *Met. Div. Ann. Progr. Rept. July 1, 1960*, ORNL-2988, pp 228–29.

[21] E. C. Moncrief and A. P. Litman, *Corrosion of the Volatility Pilot Plant INOR-8 Dissolver After Seven Cold Dissolution Runs*, ORNL CF-60-11-80 (Nov. 30, 1960).

Brief fluorine passivation treatments on L nickel specimens did not modify the L nickel corrosion resistance on subsequent exposure to the fluorination environment. Similar passivation treatments on INCO-61 weld metal used in fabricating the fluorinator had a detrimental effect on the corrosion resistance of this alloy to the fluorination environment.

Arrangements have been made for Battelle Memorial Institute to extend contemporary fluorination corrosion data on experimental ORNL alloys and other materials of interest. This work will be done on Chemical Technology Division Subcontract No. 988 and be monitored by the Metallurgy Division.

17. MECHANICAL PROPERTIES

J. R. Weir

DIMENSIONAL BEHAVIOR OF THE EXPERIMENTAL GAS-COOLED REACTOR FUEL ELEMENT AT ELEVATED TEMPERATURE

W. R. Martin

The dimensional behavior of a simulated EGCR fuel element has been studied at the pressure and thermal conditions[1] predicted for reactor operation. Particular emphasis was placed on determining (1) the relationship between the fuel temperature and axial expansion characteristics of the fuel, (2) the effect of cladding and fuel interaction on heating and subsequent cooling, (3) the effect of rapid temperature excursions on the degradation of the fuel, and (4) accumulative effects in the fuel capsule due to the thermal cycling.

The element that contains a radial gap between the cladding and the fuel pellet responded to thermal cycling as the individual components would respond under the same thermal conditions if tested separately. Both the axial expansion and the radial expansion of the fuel element are very nearly a function of the maximum central temperature.[2] The axial expansion of the fuel-pellet column can be reduced appreciably at elevated temperature by "dishing" the ends of the pellet. The pellets fracture radially and circumferentially upon heating, but redistribution of the fuel does not occur.

If there is no radial gap between the fuel and the cladding, the expansion characteristics of the capsule during thermal cycling are a function of the fuel temperature, cladding temperature, and the external pressure exerted on the capsule by the coolant stream. Thermal cycling may introduce plastic axial strains[3] into the cladding, depending upon the details of the temperature cycle and the pressure conditions. The appearance of the cladding after cycling is shown in Fig. 17.1. This clearly shows the location of radial and circumferential ridges similar to those observed from in-pile fuel element irradiations. Thus it is concluded that this experimental apparatus will provide an accurate picture of the behavior of fuel capsules in service.

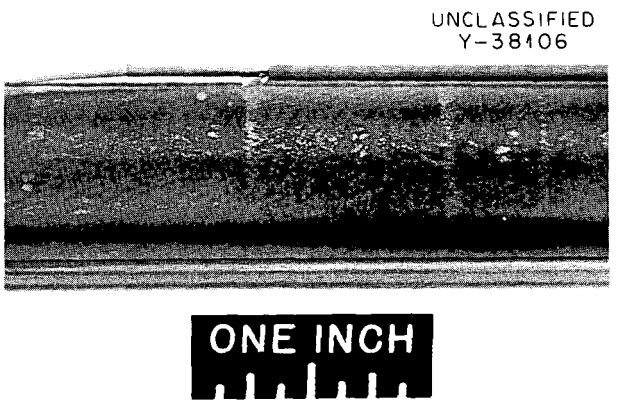

Fig. 17.1. Appearance of Cycling Capsule. Note circumferential and axial ridges formed in clad.

RADIATION EFFECTS ON TYPE 304 STAINLESS STEEL

J. T. Venard J. W. Woods

In order to examine the effects of neutron irradiation on type 304 stainless steel, tube-burst tests have been run by the Solid State Division in the poolside facility of the ORR. A stress-rupture plot of these results along with those of control tests on specimens taken from the same heat of material is shown in Fig. 17.2.

[1] W. R. Martin and J. R. Weir, *A Device to Simulate the Service Thermal Conditions in EGCR-Type Fuel Elements*, ORNL-3032 (Dec. 28, 1960).

[2] W. R. Martin, "Dimensional Studies of Simulated EGCR Fuel Element at Elevated Temperatures," paper presented at the American Nuclear Society Meeting at Pittsburgh, Pa., June 4–8, 1961.

[3] W. R. Martin and J. R. Weir, *Dimensional Behavior of the Experimental Gas-Cooled Reactor Fuel Element at Elevated Temperatures*, ORNL-3103 (in press).

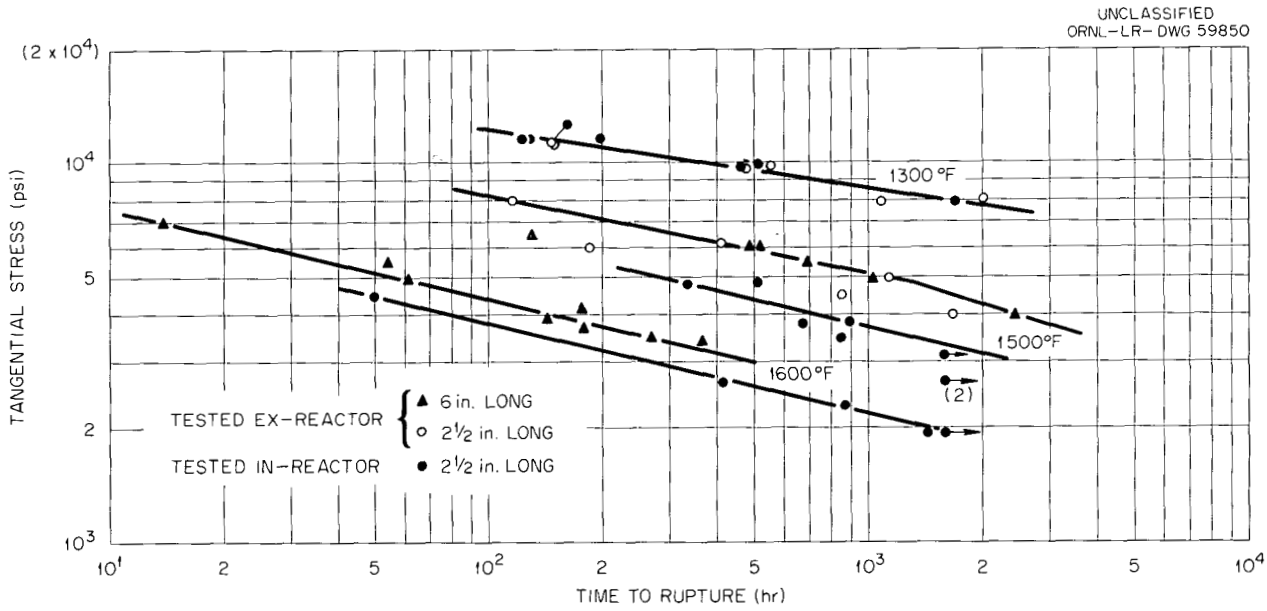

Fig. 17.2. Tube-Burst Tests in Air. Type 304 stainless steel; Superior heat 23999X; 0.750-in. OD, 0.020-in. wall.

At 1500°F the stress for rupture in 100 hr in-pile is approx 75% of the ex-pile stress. At 1600°F the in-pile stress is approx 85% of the ex-pile stress for rupture in 100 hr. No difference is seen in the 1300°F tests so far as stress-rupture life is concerned.

In examining the data obtained on the maximum tangential strain at failure in the above tests, it is interesting to note:

1. Both in-pile and control specimens show an increase in maximum tangential strain to failure with increasing temperature.

2. The ratio of out-of-pile to in-pile maximum tangential strain to failure also increases with increasing temperature.

These data indicate a relative loss of ductility under irradiation with increasing temperature. It should be pointed out that this trend is based on only a few tests and may not be a true indication of the behavior of the material.

MECHANICAL PROPERTIES OF INCONEL

C. R. Kennedy J. W. Woods

The effects of irradiation on the mechanical properties of Inconel are of interest because it is a solid-solution high-temperature alloy typical of many that may be used in various structural components in high-temperature reactors. Since it was the first material in which a significant reduction in rupture life attributable to irradiation was observed, efforts have continued to understand the mechanism responsible for this behavior.

Tube-burst tests have been performed on two heats of Inconel, both in- and out-of-reactor at 1500°F. The results of the tube-burst testing are shown in Fig. 17.3. One possible cause for the reduction in life might be a result of the boron (n, α) reaction forming helium gas under thermal-neutron bombardment. This possibility is being investigated with tube-burst-test specimens of six laboratory heats, each heat containing different amounts of natural and isotopic boron. Preliminary results, given in Table 17.1, do not

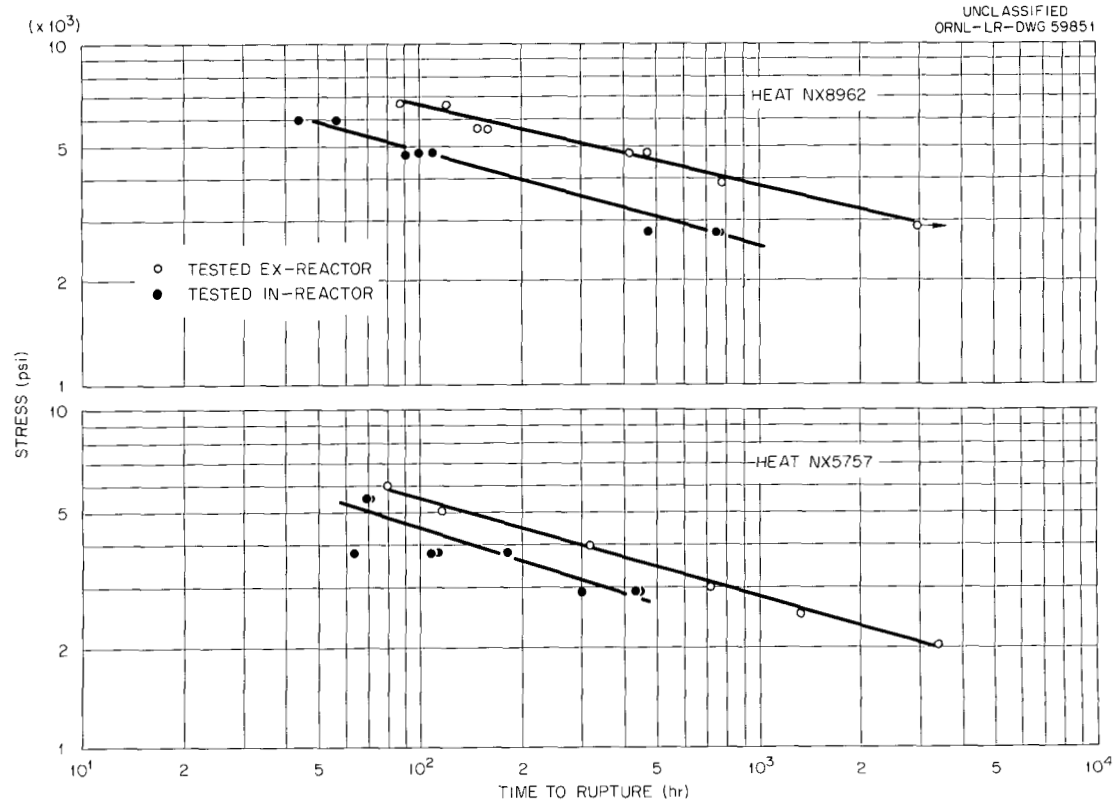

Fig. 17.3. Inconel Tube-Burst Test Results. In air, at 1500° F.

Table 17.1. Preliminary Results Obtained from Tube-Burst Testing of Controlled-Boron-Content Heats of Inconel, In-Reactor

Specimen Number	Isotopic Proportions of Boron (ppm)		$\frac{\Delta\sigma}{\sigma}$ [a]
	B^{10}	B^{11}	
4B-11	0.6	40	0
6B-11	0.9	59	0.28
OB	<2	<10	0.12
NX8992	5.6	25.4	0.26
NX5757	7.6	34.4	0.18
10B	19	81	0.19
6B-10	57	3	0.32

[a] $\frac{\Delta\sigma}{\sigma} = \frac{\sigma_x - \sigma_i}{\sigma_x}$, where σ_x = 100 hr life tested ex-reactor, and σ_i = 100 hr life tested in-reactor.

indicate conclusively that boron is responsible for the reduction in rupture life. Additional tests are programmed to verify the data.

BRAZING MIDPLANE SPACER ON EGCR FUEL ELEMENTS

J. T. Venard

One of the problems associated with the attachment of fuel element spacers to the type 304 stainless steel cladding of EGCR fuel elements is the effect of the brazing-temperature cycle on the grain size and properties of the tube. The use of GE-81 brazing alloy for attaching the spacers requires heating the entire fuel element cladding to 2150° F. As has been previously reported,[4,5] such a treatment results in excessive grain growth, an inhomogeneous structure, and a loss of stress-

[4] *GCR Quart. Progr. Rept. Mar. 31, 1960*, ORNL-2929, pp 115–16.

[5] *Met. Div. Ann. Progr. Rept. July 1, 1960*, ORNL-2988, pp 256–57.

rupture strength in the type 304 stainless steel cladding.

It was suggested that a 2020°F copper braze be substituted for the GE-81 braze. Preliminary burst tests performed on type 304 stainless steel tubing subjected to a copper-brazing thermal cycle indicate a more satisfactory stress-rupture behavior than was observed with the GE-81 braze.

Figure 17.4 shows photomicrographs of as-received tubing, a copper-brazed tube, and a GE-81 brazed tube. Note that some grain growth does occur with the copper braze, but not to the degree that is observed in the GE-81 braze.

UNCLASSIFIED
PHOTO 54523

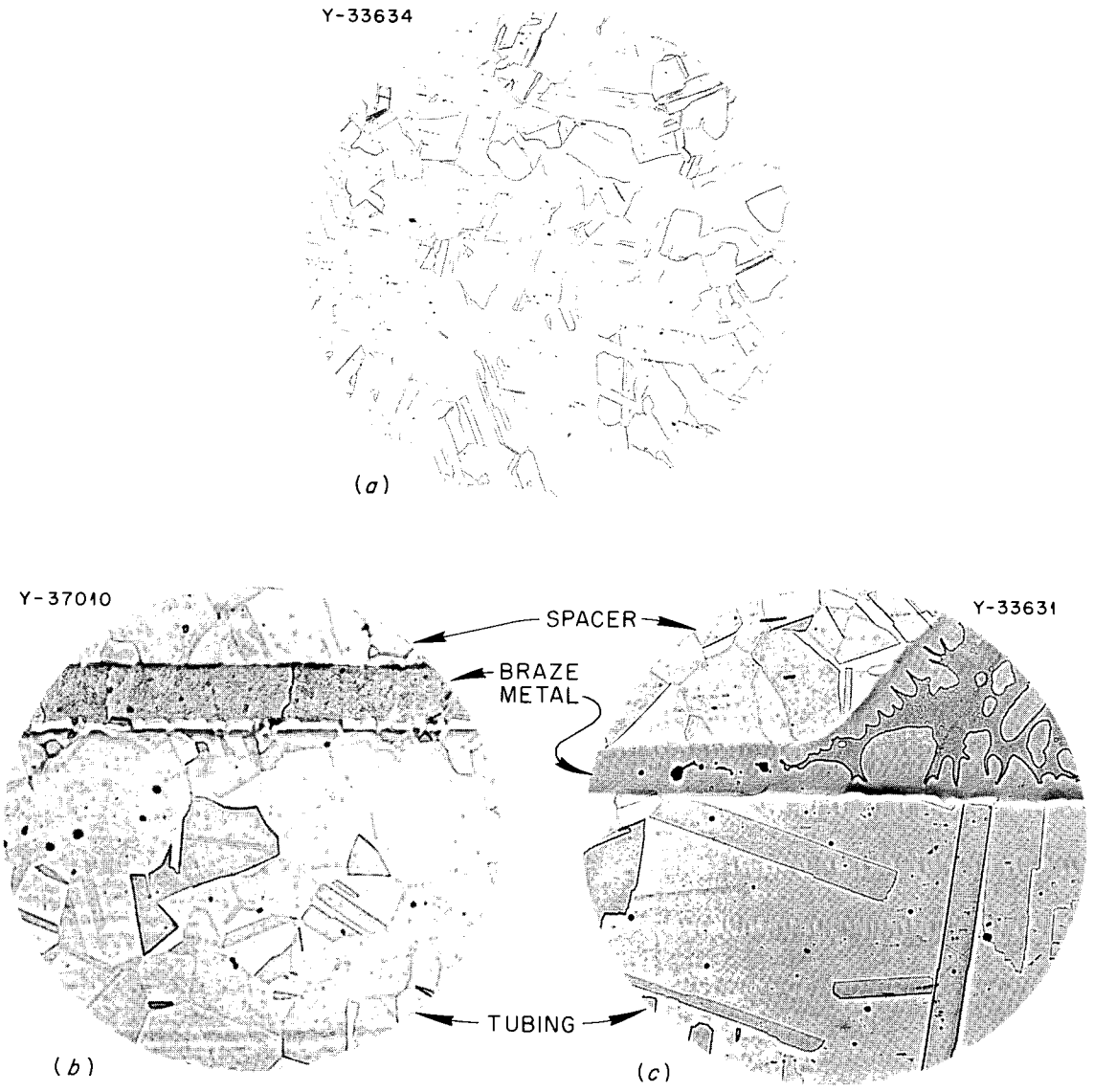

Fig. 17.4. Photomicrographs Showing Grain-Growth Behavior of Type 304 Stainless Steel Tubing Subjected to Copper and GE-81 Alloy Brazes. (*a*) As-received tubing, etched with modified aqua regia; (*b*) Copper braze on as-received tubing, etched with glyceria regia; (*c*) GE-81 alloy braze on as-received tubing, etched with modified aqua regia.

COLLAPSING AND CREEP-BUCKLING EXPERIMENTS

J. T. Venard

The proposed loops in the EGCR that will be used to test fuel elements in coolant streams separate from the main reactor coolant will operate at elevated temperatures under various conditions of mechanical loading. Failure of the in-pile portion of these loops could result from a collapsing of the tubes due to the main coolant pressure acting on the outside of the tubes.

Tests on model tubes have therefore been performed to determine the relationship between the instantaneous collapse pressure P_c and the ratio of the mean tube radius r to the wall thickness t. Also being investigated are the effects of the "ovality" ratio k, defined as the ratio of minimum tube diameter to maximum tube diameter, and the wall-thickness variation V, defined by $V = 100\,(t_{av} - t_{min})/t_{av}$.

A number of experiments have been performed to find a relationship between collapsing pressure and time to collapse. All tests to date have been conducted at 1200°F in air on specimens machined from type 304 stainless steel seamless tubing. The tubes were of essentially infinite length (length-to-diameter ratio > 10) and had diameters of 0.75 and 1.00 in. Curves showing the relationship of P_c vs r/t and the effects of ovality ratio k and wall-thickness variation V have been published.[6]

Work is continuing in all the above phases of the tube-collapse study, with future emphasis to be placed on time to collapse.

MECHANICAL PROPERTIES OF AGOT GRAPHITE

C. R. Kennedy

The mechanical properties of AGOT graphite have been studied to provide a basis for predicting its behavior in the EGCR. Graphite columns in the reactor will initially be under compressive loading, but after the reactor goes critical, the columns will undergo radiation-induced shrinkage. Because of the neutron-flux gradient from point to point in the reactor, bending strains will be forced into the graphite columns. Therefore, to establish a failure criterion, the mechanical properties, time and temperature dependence of these values, and the creep behavior of AGOT graphite were investigated.

Specimens of AGOT graphite taken from three blocks have been examined, using incrementally loaded short-time tensile, short-time bending, and creep tests under compressive, tensile, and bending loads. Incremental-loading tests are essentially very long-time tensile tests for demonstrating the time dependency in the tensile behavior of graphite.

The majority of the results have been summarized previously[7] except for those shown in Figs. 17.5 and 17.6. These results were obtained from testing longitudinal bend and tensile specimens from an actual block of EGCR graphite.

The following conclusions can be made from the results of the test program.

1. The mechanical properties of graphite are not thermally activated in the temperature range from 75 to 1100°F; thus the fracture stresses and strains are not time or temperature dependent.
2. There exist in graphite wide variations in mechanical properties, and the mechanical anisotropy is very difficult to predict.
3. The fracture stresses calculated on the basis of elasticity theory for bending are greater than the fracture stresses under tensile loads; however, the fracture strains are very similar.
4. Graphite exhibits a small initial stage of creep; however, the creep rate decreases to less than 5×10^{-9} in. in.$^{-1}$ hr^{-1} in a very short time.
5. It is apparent that, as the section size of the graphite block increases, the strength variation is also greater across the block.
6. It is apparent that the graphite moderator blocks will be weakest in the areas from which material will be removed in machining the fuel-element channels.
7. It is apparent, in view of the very low ductility of graphite, that it will not sustain the tensile strains produced by the variable radiation dose without fracturing. However, fracturing may not occur if the radiation-induced shrinkage is either inhibited or stopped by the occurrence of stress, or if radiation will allow graphite to sustain greater tensile strains before fracturing.

[6] *GCR Quart. Progr. Rept. Dec. 31, 1960*, ORNL-3049, pp 146–47.

[7] *GCR Quart. Progr. Rept. Mar. 31, 1961*, ORNL-3102, pp 116–24.

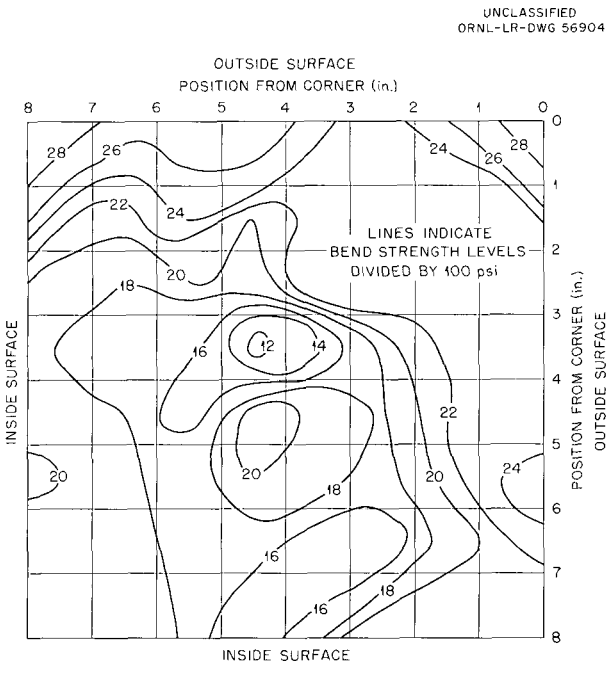

Fig. 17.5. Variation in Bend Strength Across One Quarter of an 18 × 18 in. Block of AGOT Graphite.

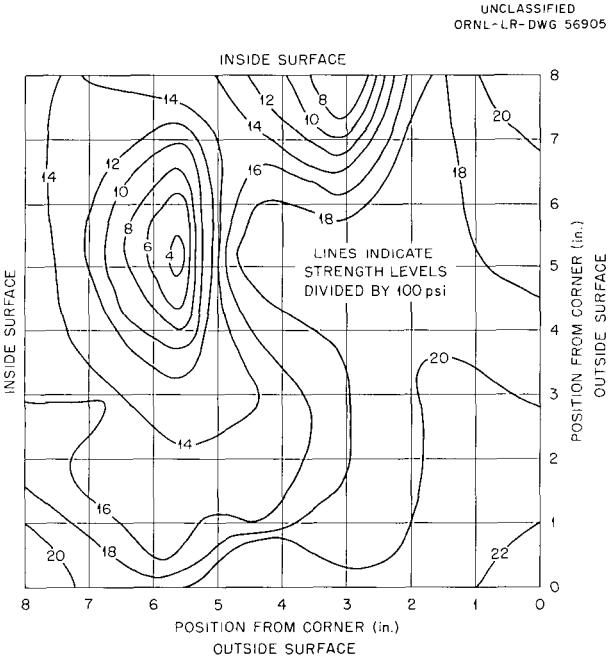

Fig. 17.6. Variation of Axial Tensile Strength Across One Quarter of an 18 × 18 in. Block of AGOT Graphite.

EFFECTS OF ENVIRONMENT ON METALS

H. E. McCoy W. R. Martin
R. L. Stephenson

The effects of service variables, such as temperature and stress, on the high-temperature mechanical behavior of metals are recognized to be of practical importance. In recent years, the service environment of the metal also has been shown to be a significant factor. The importance of the chemical reactivity of the material with the service environment, the effect of environment on surface and grain-boundary energies, and the ratio of surface area to volume of the component has been discussed by McCoy *et al.*[8] Work is continuing in an effort both to point out metal-environment combinations that alter the service performance of the metal and to determine the operative mechanisms whereby the mechanical behavior is affected.

Carburization and Oxidation of Type 304 Stainless Steel in Flowing Carbon Dioxide

The results of studies to determine the effects of environments, such as CO, CO_2, O_2, N_2, air, H_2, and Ar, on the high-temperature creep characteristics of type 304 stainless steel have been summarized previously.[9] Additional heats of material have been tested during the past year. The results of these tests confirm those reported previously.

The observation of carburization of type 304 stainless steel specimens tested in flowing CO_2 at 1500°F has led to further studies to determine the mechanisms involved. Several specimens 0.005 in. thick have been exposed to flowing CO_2 in a system that facilitates continuous measurement of the specimen weight. Reaction rate curves coupled with metallographic and chemical studies have pointed out the following pertinent factors:

1. The weight-change-vs-time curves are characterized by several breaks. The number of breaks and the time at which they occur depend on the temperature.

---

[8]H. E. McCoy, W. R. Martin, and J. R. Weir, "Effect of Environment on the Mechanical Properties of Metals," *1961 Proceedings of the Institute of Environmental Sciences National Meeting, Apr. 5–7, 1961, Washington, D.C.*, pp 163–76, Institute of Environmental Sciences, Mt. Prospect, Illinois.

[9]H. E. McCoy, *Met. Div. Ann. Progr. Rept. July 1, 1960*, ORNL-2988, p 280.

2. The oxides which form on the surface are multilayered. Efforts to identify these layers are in progress.

3. The amount of carbon picked up over the temperature range 1200 to 1700°F increases with increasing temperature as well as with time at a given temperature.

4. The oxidation and carburization rates increase as the pressure of CO_2 is increased, up to relatively high pressures. The oxidation rate seems to be insensitive to pressure above approx 100 mm Hg, and the carburization rate is not affected by pressures in excess of about 200 mm Hg.

Radiotracer techniques have been developed to determine the distribution of carbon in type 304 stainless steel specimens carburized in flowing $C^{14}O_2$. Typical as-polished photomicrographs and autoradiographs are compared for a cross-sectioned specimen in Figs. 17.7 and 17.8. These studies indicate the following significant facts.

1. The carbon gradient from the austenite grain to the grain boundary is very small.

2. There is a small carbon concentration in the oxide film.

3. The carbon gradient in a 0.020-in.-thick sample carburized at 1500°F in flowing CO_2 is very small. These experimental facts suggest that the limiting factor in carburizing type 304 stainless steel at 1500°F in flowing CO_2 is the supply of carbon to the oxide-metal interface.

Effects of Interstitials on Niobium-Base Alloys

The effects of additions of oxygen, nitrogen, and hydrogen on the room- and elevated-temperature mechanical properties of niobium have been summarized.[10] Studies during the past year have further substantiated these results. Contamination experiments conducted with an Nb–1% Zr alloy show similar trends. Examination of the niobium and the Nb–1% Zr specimens after deformation indicates that the presence of interstitial elements alters the tendency for twinning to occur in these metals. A joint program is in progress with the Structure of Metals Group to evaluate this effect in niobium for various interstitial elements.

The role of interstitials in the mechanical behavior of niobium-base alloys has been further demonstrated by the observations of an aging reaction in the Nb–1% Zr alloy[11] which is currently thought to be associated with oxygen.[12] Because of the established usefulness of internal-friction measurements for studying the precipitation of interstitial solutes from supersaturated solid solutions in body-centered cubic metals,[13–15] this technique is being used in an effort to determine the element responsible for the observed aging. A torsional pendulum has been constructed, and a device for automatically sensing and recording vibrational amplitude as a function of time has been developed. Figure 17.9 shows the internal-friction spectrum δ of an Nb–0.66% Zr alloy containing three levels of oxygen. Figure 17.10 shows the spectrum of a specimen contaminated with nitrogen. Work is now in progress to identify the damping peaks present and to determine their heights as a function of interstitial content.

Influence of Hydrogen on Nickel-Base Alloys

The relatively low-temperature phenomenon of hydrogen embrittlement has been documented for several metals.[16] However, hydrogen has also been shown to influence the mechanical behavior of some metals at elevated temperatures. This effect is characterized by a loss in creep strength in hydrogen, as compared with the strength in other environments, and does not involve any embrittlement. Besides the fundamental interests in this problem, the influence of hydrogen on the high-temperature mechanical behavior of materials is of practical importance to the nuclear industry. Many structural materials absorb hydrogen from aqueous solutions, and the use of metal hydrides

[10] H. E. McCoy, *Met. Div. Ann. Progr. Rept. July 1, 1960*, ORNL-2988, pp 279–80.

[11] D. O. Hobson, *A Preliminary Study of the Aging Behavior of Wrought Columbium–1% Zirconium Alloys*, ORNL-2995 (Jan. 6, 1961).

[12] D. O. Hobson, "Aging Phenomenon in Columbium-Base Alloys," paper presented at the AIME High-Temperature Materials Conference, Cleveland, Ohio, Apr. 26–27, 1961 (to be published in the proceedings).

[13] C. Wert, *Thermodynamics in Physical Metallurgy*, ASM, Cleveland, Ohio, 1950.

[14] P. M. Robinson and R. Rawlings, *Iron and Steel* 31, 65 (1958).

[15] A. S. Nowick, *Progr. in Metal Phys.* 4, 37 (1953).

[16] A. R. Troiano, *Trans. Am. Soc. Metals* 52, 54–80 (1960).

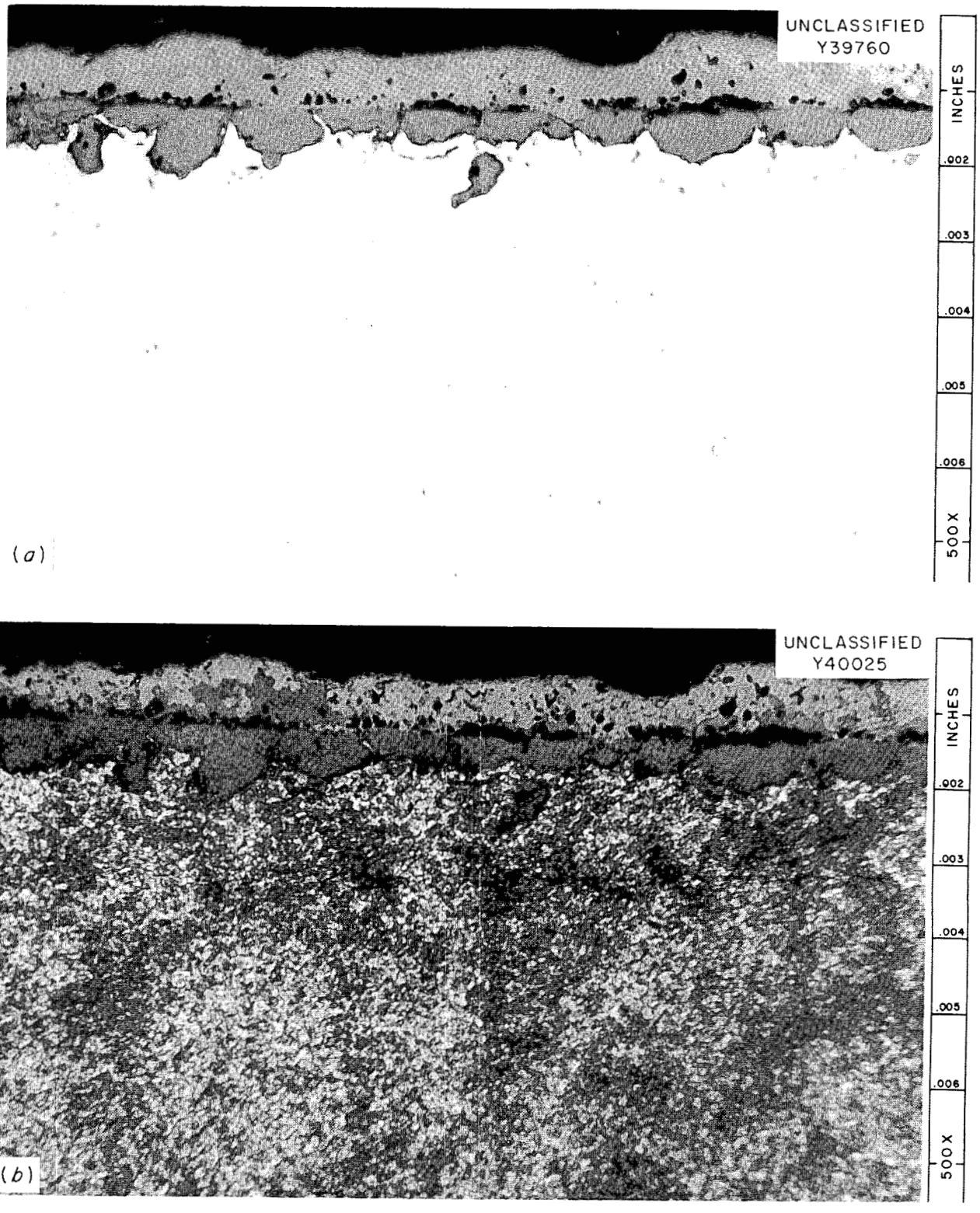

Fig. 17.7. Representative Structure 0.0021 in. from Original Metal Surface of Type 304 Stainless Steel Specimen (0.020 × ½ × 1 in.) Exposed 37.8 hr at 1500°F in Flowing $C^{14}O_2$ Environment. (*a*) As polished; (*b*) autoradiograph, 20-hr exposure with NBT film.

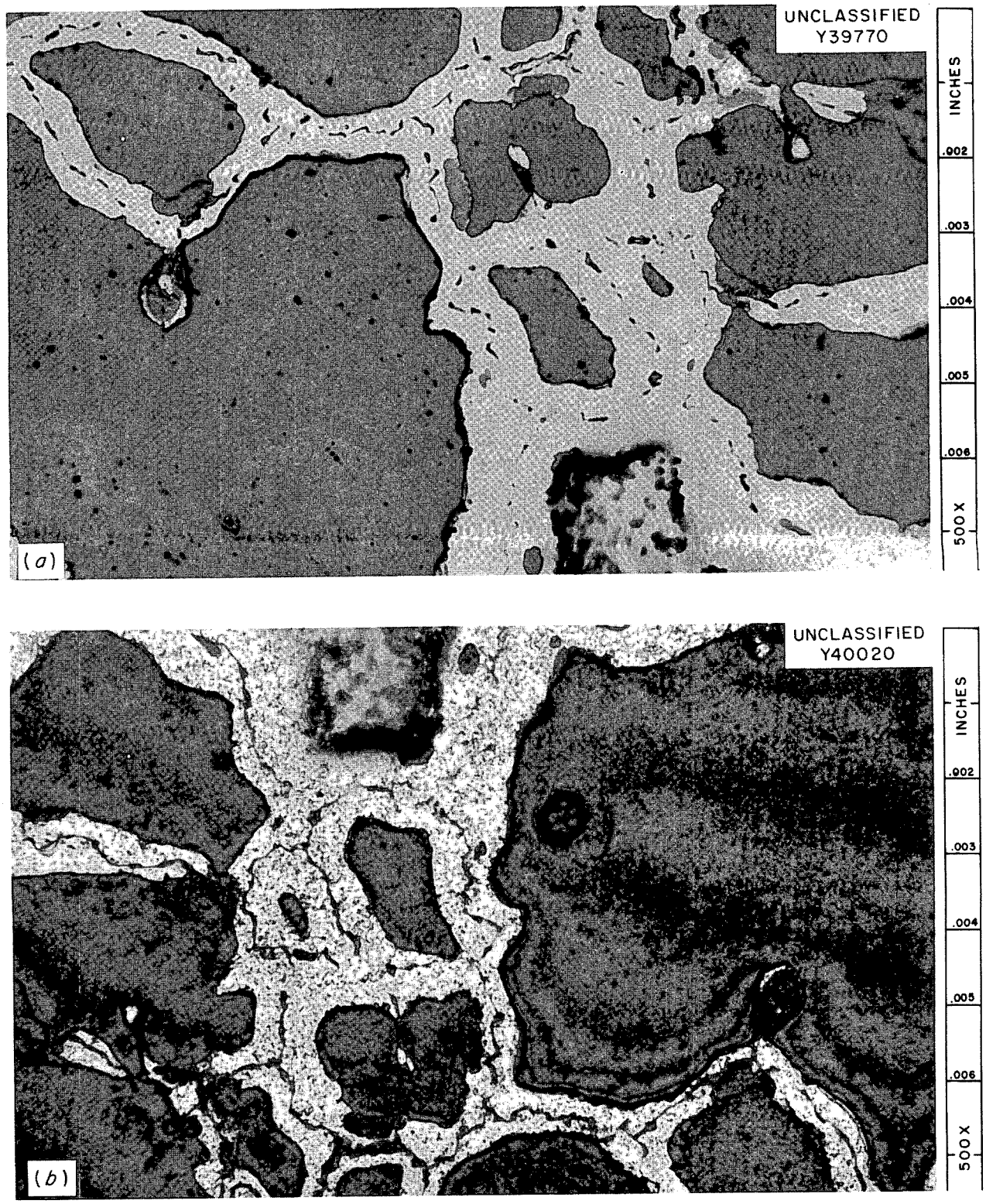

Fig. 17.8. Representative Structure 0.001 in. from Metal Surface of Type 304 Stainless Steel Specimen (0.020 × ½ × 1 in.). Exposed 37.8 hr at 1500°F in flowing $C^{14}O_2$ environment. Total surface beta count of specimen, 6226 counts/min. (*a*) As-polished; (*b*) autoradiograph, 24-hr exposure with NBT film.

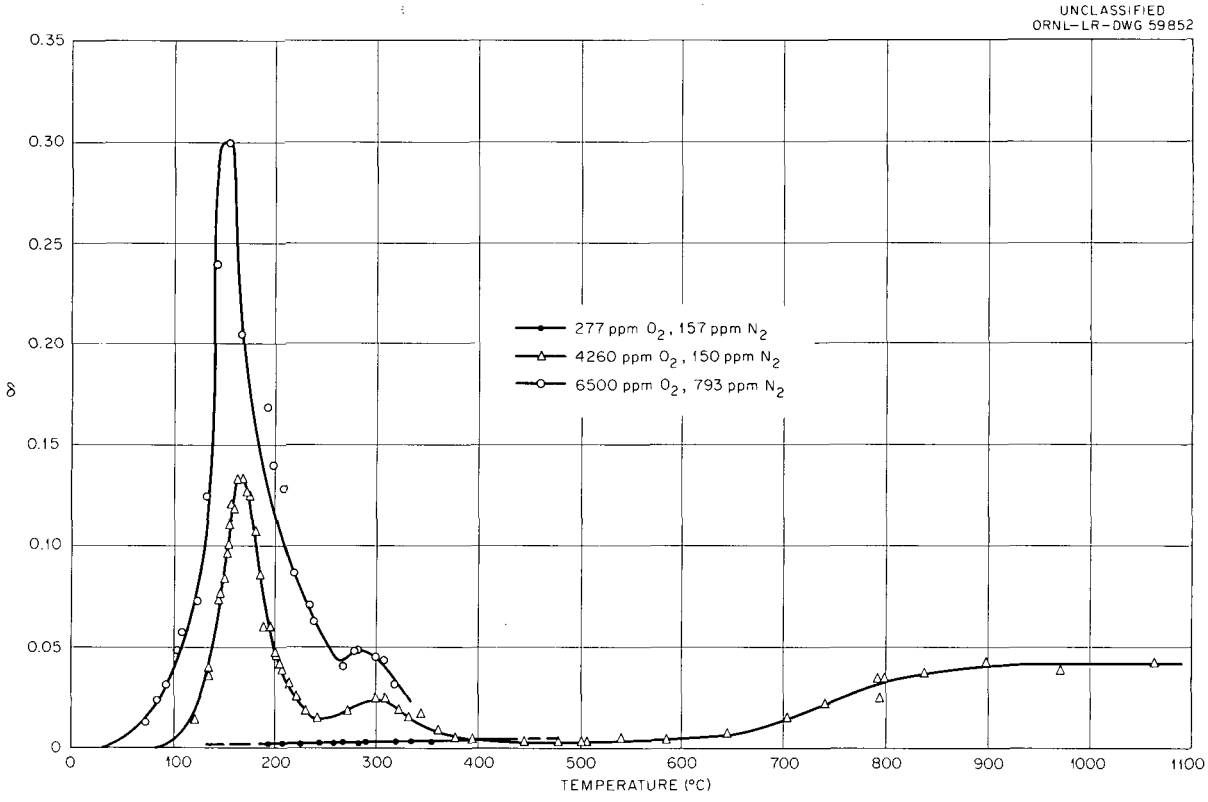

Fig. 17.9. Effect of Oxygen on Internal Friction Spectrum of Nb–0.66% Zr Alloy.

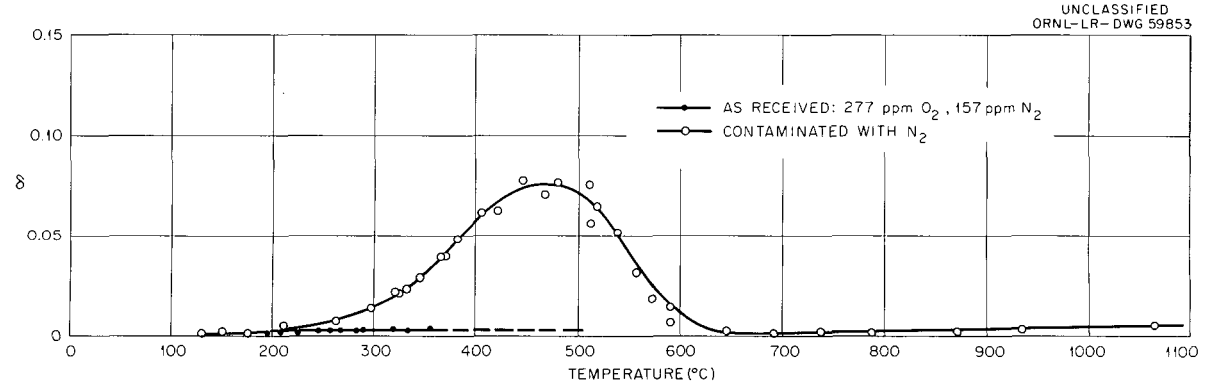

Fig. 17.10. Effect of Nitrogen on Internal Friction Spectrum of Nb–0.66% Zr Alloy.

presents another source of hydrogen in a reactor system. The use of hydrogen as a reactor coolant offers many advantages, and such an application may occur in the future.

Previous work at ORNL[17] has shown that hydrogen has a large effect on the creep behavior of Inconel. Work during the past year has been directed toward studying the effects of alloy composition and strain rate on the magnitude of the hydrogen effect.

Nickel-base alloys containing various amounts of chromium and iron were prepared, and their creep properties were evaluated at 1500°F in argon and in hydrogen environments. The creep strengths of all alloys were observed to be less

[17] D. A. Douglas, *High-Temperature Materials* (ed. by R. H. Hehemann and G. M. Ault) p 433, Wiley, New York, 1959.

in hydrogen than in argon. Several of these alloys, as well as commercial Inconel, were used to evaluate the effect of strain rate. The results of a series of tests of Inconel are shown in Fig. 17.11 and illustrate the fact that the magnitude of the hydrogen effect is inversely proportional to the strain rate. A tentative explanation of the observed results has been made, based on the influence of hydrogen on fracture by a vacancy mechanism. Deformation by vacancy diffusion has been shown[18] to be important only at low strain rates. Fracture occurs as a result of the coalescence of small holes formed by vacancy diffusion. At high strain rates, deformation occurs primarily by slip, and the formation of cracks at points of very large stress concentrations leads to fracture. The latter process is not significantly affected by the presence of hydrogen, and hence the properties of metals at high strain rates are equivalent in hydrogen and in inert environments.

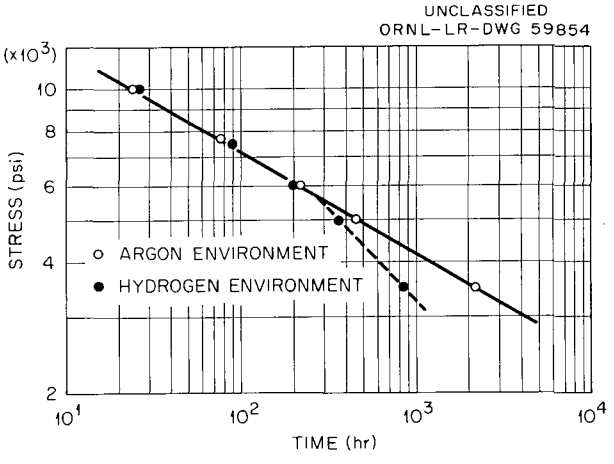

Fig. 17.11. Stress-Rupture Properties of Inconel at 1500° F. Heat 892, tested as received.

FRACTURE OF METALS UNDER DYNAMIC LOADS

R. W. Swindeman C. R. Kennedy

During the last year, the interrelation of cyclic and monotonic creep rupture of Inconel has been studied. This program consists of a series of tests in which the ratio of maximum to minimum stress R was varied from 1, corresponding to the monotonic creep test, to −1, corresponding to the pure fatigue test. Tests were performed at a frequency of 1 cycle/hr at 1500°F. The mean creep rate, cycle strain, rupture life, and rupture ductility were measured. The stress-rupture curves corresponding to the various stress ratios were compared on the basis of the following equation:[19]

$$\frac{1}{t} = A^{-n}\sigma^{n} \qquad (1)$$

where t is the rupture life, σ is the amplitude of the maximum stress, and A and n are constants. Values of A^{-n} and n for four stress ratios are given below:

Stress Ratio, R	1	∞	−2	−1
A^{-n}	25,500	31,000	32,000	33,000
n	4.16	4.15	4.16	4.16

It is apparent that the value of n is practically the same for all tests and that A is nearly the same for all tests except for the monotonic creep test ($R = 1$). If it is assumed that the time under the maximum stress controls failures, then the cyclic tests in which R is negative should be expected to last twice as long as the monotonic creep test, since the maximum stress is applied for only half the cycle. Doubling the rupture time for the monotonic stress-rupture curve increases the value of A^{-n} from 25,500 to 30,000 psi. This value is in fair agreement with A for the cyclic tests.

A Goodman-type diagram for 1000-hr life can be drawn to describe the failure under cyclic and mean stresses. For Inconel the equation which approximates the diagram is:

$$\sigma_a = \sigma_c - \sigma_m , \qquad (2)$$

where

σ_a = alternating stress amplitude,

σ_m = mean stress,

σ_c = stress required to produce rupture in monotonic creep in a specified time.

[18] A. H. Cottrell, *Fracture* (ed. by B. L. Averback *et al.*) pp 38–40, Technology Press of MIT and Wiley, New York, 1959.

[19] R. W. Swindeman, *Met. Div. Ann. Progr. Rept. July 1, 1960*, ORNL-2988, p 261.

The equation is conservative for all negative values of R by the amount shown below:

Stress Ratio, R	−1	−1.2	−1.5	−2	−3	−∞
Percentage deviation	6	6	13	9	−1	1

The cyclic creep tests in pure fatigue ($R = -1$) can also be described by a strain-fatigue curve, the equation of which is:

$$\epsilon_p N^{0.77} = 0.41 ,$$

where

ϵ_p = cyclic plastic strain range,

N = number of cycles to failure.

The stress state imposed by thermal or strain cycles is rarely a simple uniaxial state. Thus, in order to apply the uniaxial data, the effect of the stress state must be known. A torsional-strain-cycle test series has been performed on Inconel at 1500°F to determine this relationship. Previous static testing[20] under complex stresses indicated that failure may result from either of two fairly similar criteria:

1. accumulated time under the maximum principal stresses, or
2. fracture strain ratios based upon the deviation stresses.

The results of this test series agreed well with the second, as shown in Fig. 17.12, and does not disagree very markedly with the principal stress criterion. This agreement fortunately does not complicate the adaptability of isothermal tests to thermal-cycling behavior, since the analysis can be based on strains. It does point out, however, that for the most common case, which is balanced tensile or compressive stress states, the strain per cycle will be twice as effective in causing failure than it is in the uniaxial case.

[20] C. R. Kennedy, W. O. Harms, and D. A. Douglas, *J. Basic Engr.* 81, 599–609 (1959).

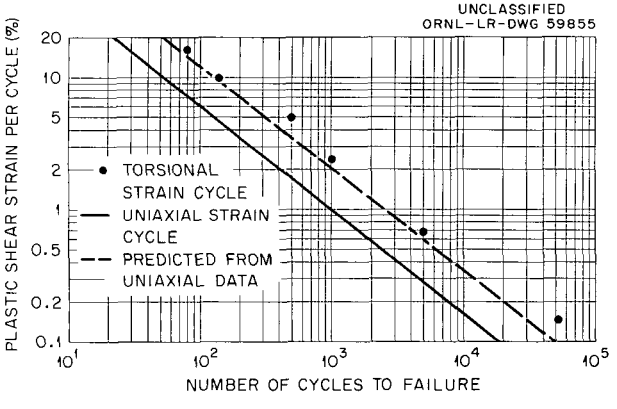

Fig. 17.12. Results of Inconel Torsional Strain-Cycle Test at 1500° F.

BERYLLIUM IRRADIATION EFFECTS

J. R. Weir

Changes in the mechanical and physical properties of beryllium that result from neutron irradiation may be attributed to the displacements produced by energetic neutrons or the products from the $(n, 2n)$ and (n, α) reactions with beryllium and to the effects produced by agglomeration of the helium produced by these transmutations.

A program of irradiations[21] was conducted wherein beryllium specimens of various purities and fabrication histories were taken to neutron exposures between 1×10^{20} *nvt* and 6×10^{20} *nvt* (>1 Mev) at temperatures between 50 and 780°C. Postirradiation bend tests and hardness measurements were made, and the density decrease during the irradiations was determined. Stress-rupture experiments on beryllium tubes were conducted at 600 and 700°C in neutron fluxes of approx 3×10^{20} *nvt* and 9×10^{20} *nvt* (>1 Mev). Some specimens were stressed immediately when the test reactor attained full power level, and others were held at the testing temperature until significant neutron exposure was attained, at which time the specimens were stressed to produce rupture.

The conditions under which beryllium was found not to swell appreciably (greater than a few tenths of a per cent) were the following:

1. irradiation at 600°C to 3.6×10^{20} *nvt* (>1 Mev), and
2. irradiation at 700°C to 1.3×10^{20} *nvt* (>1 Mev).

Irradiation at temperatures greater than 700°C to exposures larger than approx 1.7×10^{20} *nvt* (>1 Mev) caused swelling.

[21] J. R. Weir, "The Effect of High-Temperature Reactor Irradiation on Some Physical and Mechanical Properties of Beryllium," (submitted to the *Journal of the Institute of Metals*).

The mechanism for gas agglomerating into the large bubbles that cause swelling appears to be the migration of small gas-filled cavities (possibly cylindrical) to inclusions or other suitable nuclei where surface-tension restraining forces are small. Thus the swelling is probably controlled by the creep properties of the matrix and the rate of movement of the gas-filled cavities to the large bubbles.

Appreciable hardening of beryllium occurs on irradiation to 6×10^{20} *nvt* (>1 Mev) at approx 60°C, and further hardening occurs on annealing at temperatures below 600°C for 1 hr. The hardening associated with the annealing does not affect the ductility at room temperature. In addition, there is a hardness increase as a result of irradiation at <600°C to 3.6×10^{20} *nvt*.

The stress-rupture strength at 600 and 700°C is reduced as a function of integrated flux, as shown in Fig. 17.13. The percentage decrease in 100-hr rupture stress is plotted vs the integrated flux. It is interesting to note that the irradiation effect for this manner of presentation appears to be independent of temperature between 600 and 700°C. The same mechanism that results in the transport of helium to the bubbles that cause swelling should allow the gas to collect in grain-boundary voids or cracks that are produced during creep and thereby bring about the deleterious effect on the stress-rupture strength.

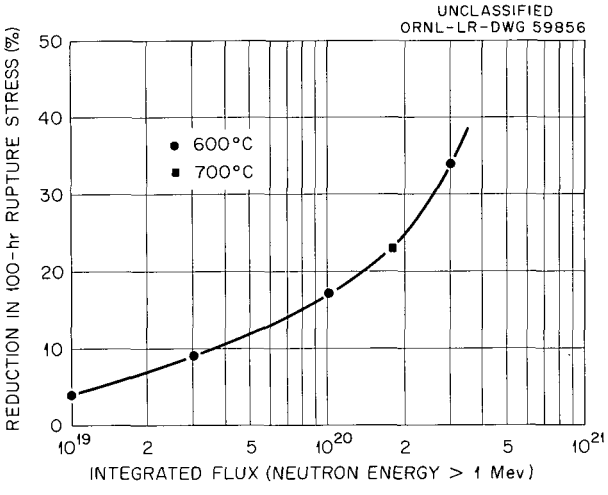

Fig. 17.13. Effect of Integrated Flux on Stress-Rupture Properties of Beryllium Tubes Tested In-Reactor.

CORRELATION OF NONDESTRUCTIVE-TEST RESULTS WITH MECHANICAL PROPERTIES OF BERYLLIUM TUBING

J. J. Cademartori[22] J. R. Weir

A program has been initiated to find a correlation between the results of nondestructive tests on tubing and the variations in mechanical properties that might result from defects observed nondestructively. The types of nondestructive examination used have been radiographic, eddy current, ultrasonic, and visual.

Correlations have been made between the radiographic results and the stress-rupture properties at 600 and 700°C. The results indicate that premature failure of the beryllium tubes in stress-rupture tests in most cases may be associated with defect indications observed during radiographic examination. Thus the evidence is that correlations of this type will be successful, and further work involving the other nondestructive testing techniques is contemplated.

MECHANICAL PROPERTIES OF ZIRCALOY-2

C. R. Kennedy

Zircaloy-2 tubing has been tested to determine an analytical model to describe the mechanical anisotropy and to determine the effect of radiation upon the creep-rupture life. It has been shown previously[23] that the fracture characteristics can be described fairly well by the relationship:

$$F(S_t - S_r)^2 + G(S_u - S_r)^2 + H(S_u - S_t)^2 = 1 , \quad (3)$$

where

S_t = tangential stress,

S_r = radial stress,

S_u = axial stress,

F, H, and G = anisotropy constants.

Performing the analysis on tubing tested at room temperature, the yield strength, fracture stresses, and the deformation ratios are described very well by the following constants: $H/F = 1$, and $G/H = 3.7$.

[22] On loan from AEPSC.

[23] C. R. Kennedy, discussion of the paper, "Effect of Combined Stress on Yield and Fracture of Zircaloy-2," by R. L. Mehan, presented at the ASME Annual Meeting, New York, December 1960.

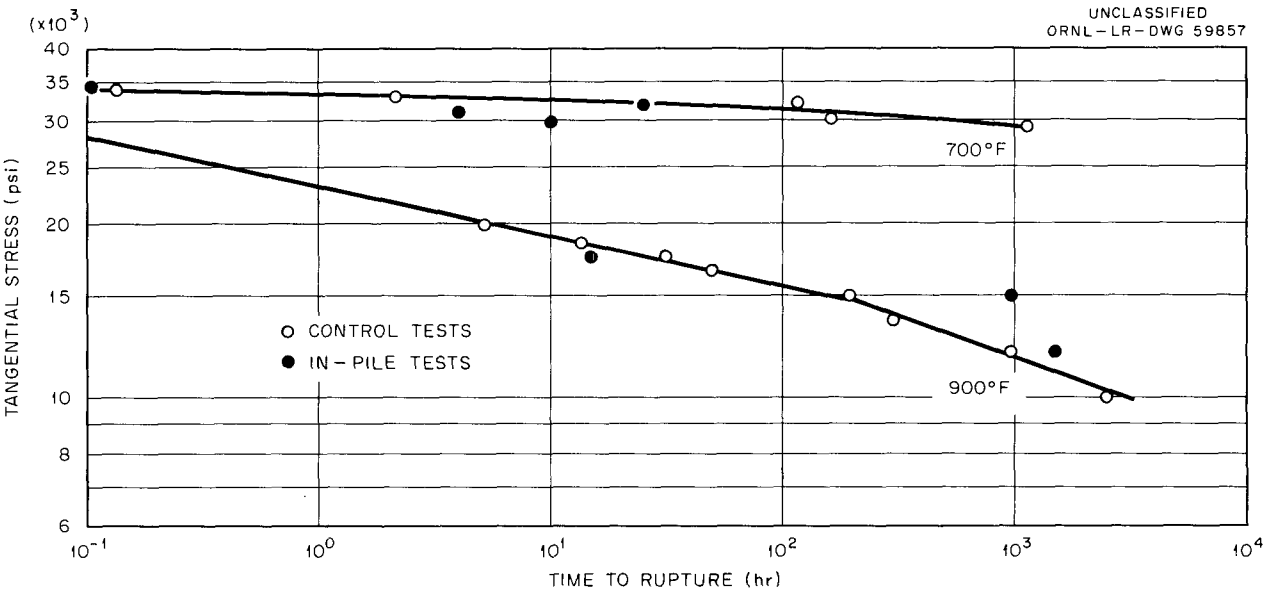

Fig. 17.14. Results of Zircaloy-2 Tube-Burst Test at 700 and 900° F in Helium.

Preliminary creep-rupture results under varying stress ratios indicate that these same constants are applicable in describing creep-rupture properties at 700 and 900°F under tension-tension stress states.

Tube-burst specimens have been tested in the ORR at 700 and 900°F (neutron flux = 10^{13}, >1 Mev). The results to date, shown in Fig. 17.14, are fairly preliminary; however, they do indicate an interesting trend. All the in-pile specimens were given an approximate neutron dosage of 4×10^{18} *nvt* (>1 Mev) before stressing. The results shown in Fig. 17.14 indicate that the effect is to reduce initially and then increase the rupture life. This trend will be confirmed by programming long-time tests in the next year.

AIR-GAGE EXTENSOMETER

J. T. Venard

As was reported earlier,[24] a system utilizing air-gage techniques is being investigated in the development of an accurate and reliable in-pile extensometer.

A prototype air motor and reset mechanism were placed in an experiment inserted in the B-8 position of the ORR in March 1960. Although the mechanism did not operate successfully, sufficient information was obtained to allow redesign to what is believed will be a reliable system. The major problem, gamma heating, should be solved by a change of materials and further miniaturization.

Preliminary bench tests on air-gage calibration, using helium, have indicated that large quantities of gas are required. A proposed system for helium conservation and recycling is now under study. The proposed system requires considerable development before it will be fully satisfactory, and work is progressing toward this end both in-pile and out-of-pile.

MECHANICAL PROPERTIES OF INOR-8

R. W. Swindeman

INOR-8 is a nickel-base structural alloy developed for use in the Molten-Salt Reactor. Since this is a new alloy, a mechanical testing program has been required to establish the allowable design stresses. This program has consisted of tensile, creep, relaxation, and fatigue studies. Many of the data generated on this alloy have been reported.[25] In the past year, emphasis was placed on an investigation of the creep and tensile

[24] *Met. Div. Ann. Progr. Rept. July 1, 1960*, ORNL-2988, p 246.

[25] R. W. Swindeman, *The Mechanical Properties of INOR-8*, ORNL-2780 (Jan. 10, 1961).

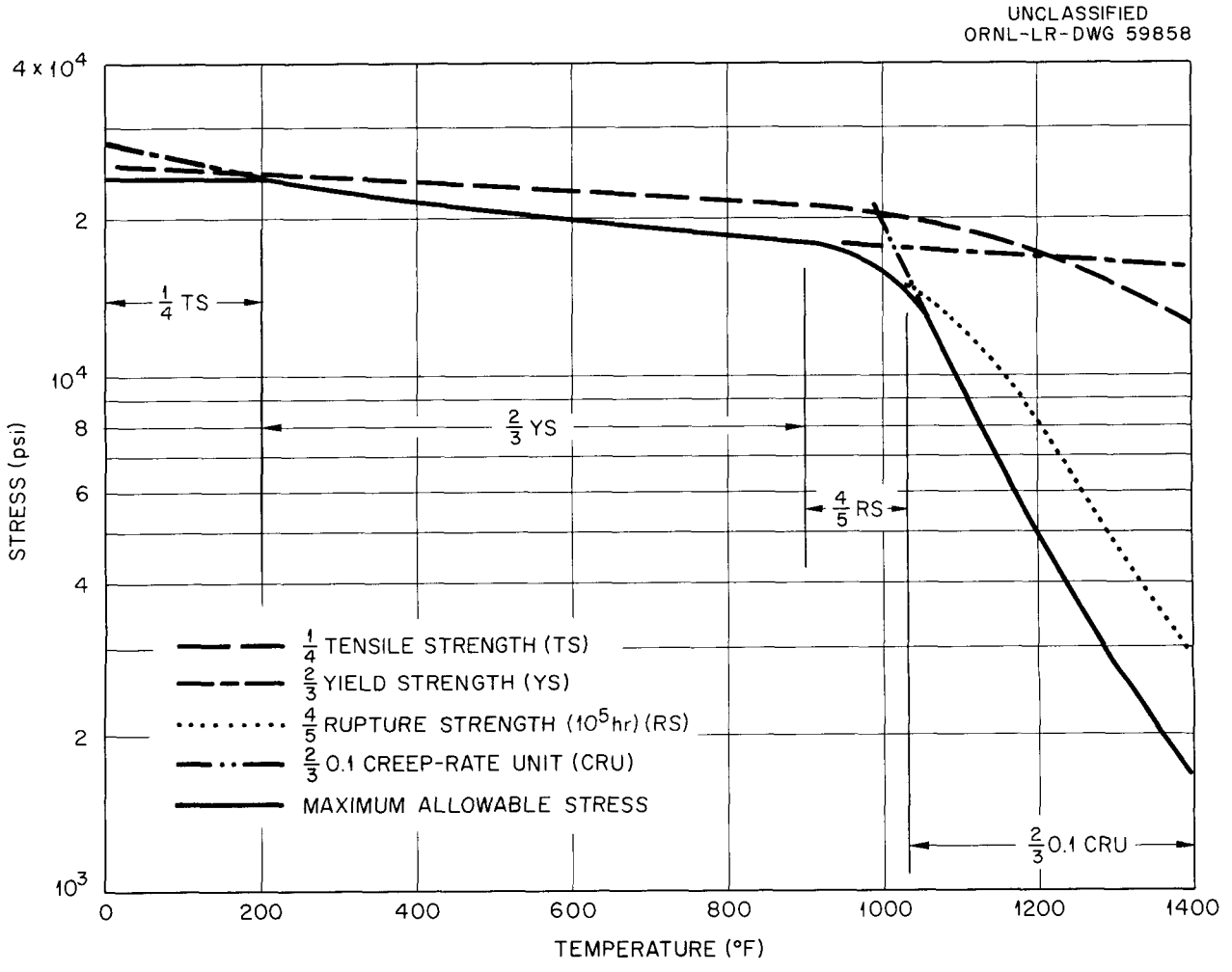

Fig. 17.15. Criteria for Establishing Static Design Stresses for INOR-8.

properties of new heats of alloy. This information, in addition to earlier data, has been carefully evaluated and used to establish safe-working stresses. Approximately 50 tensile tests at intermediate and elevated temperatures were conducted on seven heats of material. These data are backed up by data from several hundred tests obtained from material vendors and from aging studies. Well over 100 creep and stress-rupture tests were performed in the temperature range 1100 to 1400°F. Over 400,000 hr of creep testing have been completed on seven heats of alloy. These data were employed to construct the curves shown in Fig. 17.15, which presents various criteria for establishing static design stresses. As indicated in the figure, the selected criteria are (1) a quarter of the tensile strength up to 200°F, (2) two-thirds of the yield strength up to 900°F, (3) four-fifths of the 100,000-hr rupture strength up to 1050°F, and (4) two-thirds of the 0.1 CRU (creep-rate unit) stress (which corresponds to a minimum creep rate of 10^{-5}%/hr) up to 1400°F.

18. METAL FORMING AND CASTING

R. J. Beaver

IRRADIATION TESTING OF ALUMINUM-BASE FUEL DISPERSIONS OF UAl_3, U_3O_8, AND UC_2 IN ALUMINUM PLATES

R. J. Beaver A. E. Richt[1]

Studies have been made to evaluate irradiation effects in aluminum-base fuel-containing dispersions of U_3O_8, UC_2, and UAl_3 in aluminum for low-temperature research reactors. The U_3O_8 and UC_2 dispersions were prepared by powder-metallurgy techniques; the UAl_3 dispersoid occurred as a phase in a 48 wt % U–Al alloy which was modified with 3 wt % Si. This program is associated with the application of uranium 20% enriched in U^{235} for foreign research reactors. Compositions of the material irradiated were 64 wt % UAl_3–36 wt % Al, 62 wt % U_3O_8–38 wt % Al, and 60 wt % UC_2–40 wt % Al.

Specimens consisted of miniature Alclad plates which were bonded by roll cladding.[2–4] Irradiation was conducted in the MTR, and the center-line fuel temperature was estimated to be 175°F. Irradiation exposure varied from 1.6×10^{20} to 6.5×10^{20} fissions/cc (15 to 60% burnup of the U^{235} atoms). Density changes as a function of burnup are illustrated in Fig. 18.1 and reveal that dispersions of UAl_3 (the U-Si-Al alloy) and UC_2 exhibited decreases in density, whereas dispersions of U_3O_8 showed density increases. The density of dispersions of U_3O_8 increased rapidly during the early stages of irradiation and then appeared to stabilize and remain unchanged even after rather extensive burnup of the U^{235} atoms. The density data are supported by dimensional measurements.

As illustrated in Fig. 18.2, a phase presently not identifiable appears at the periphery of the UAl_4. A comparison of unirradiated and irradiated UC_2 dispersions is shown in Fig. 18.3. The microstructure of the unirradiated material shows the presence of a significant quantity of an unaccounted-for phase throughout the matrix as well as around several of the UC_2 particles. The deterioration of the UC_2 dispersions under irradiation is believed to be associated with these phases. A comparison of the microstructures of dispersions of U_3O_8 in aluminum, illustrated in Fig. 18.4, shows that a reaction occurs predominantly between the finer U_3O_8 particles and aluminum during irradiation. Previous studies revealed that at 600°C, U_3O_8 dispersions in aluminum react in a short time, with the appearance of UO_2; then after long exposures at this temperature, intermetallics of UAl form.[5] The phase shown in the irradiated material is probably a mixture of the intermetallic compound and Al_2O_3.

The magnitudes of the changes in density and dimensions in the specimens containing dispersions of UAl_3 and U_3O_8 are not considered sufficient to cause deleterious effects in the performance of research reactor fuel elements in applications that require the use of uranium limited to 20% in enrichment of the U^{235} isotope. Dispersions of UC_2 in aluminum, on the other hand, do not appear attractive.

---

[1] Metallography Group.

[2] C. F. Leitten, Jr. and W. C. Thurber, *Phase I – Foreign Reactor Fuel Sample Irradiation of a U-Si-Al Alloy. Irradiation Request ORNL-MTR-35*, ORNL CF-58-2-109 (Oct. 13, 1958).

[3] C. F. Leitten, Jr. and W. C. Thurber, *Phase II – Foreign Reactor Fuel Sample Irradiation of UC_2-Al Dispersions. Irradiation Request ORNL-MTR-35*, ORNL CF-58-10-20 (Oct. 13, 1958).

[4] C. F. Leitten, Jr. and W. C. Thurber, *Phase III – Foreign Reactor Fuel Sample Irradiation of U_3O_8-Al Dispersions. Irradiation Request ORNL-MTR-35*, ORNL CF-58-10-30 (Oct. 18, 1958).

[5] *Met. Div. Ann. Progr. Rept. Oct. 10, 1958*, ORNL-2632, p 155 (classified).

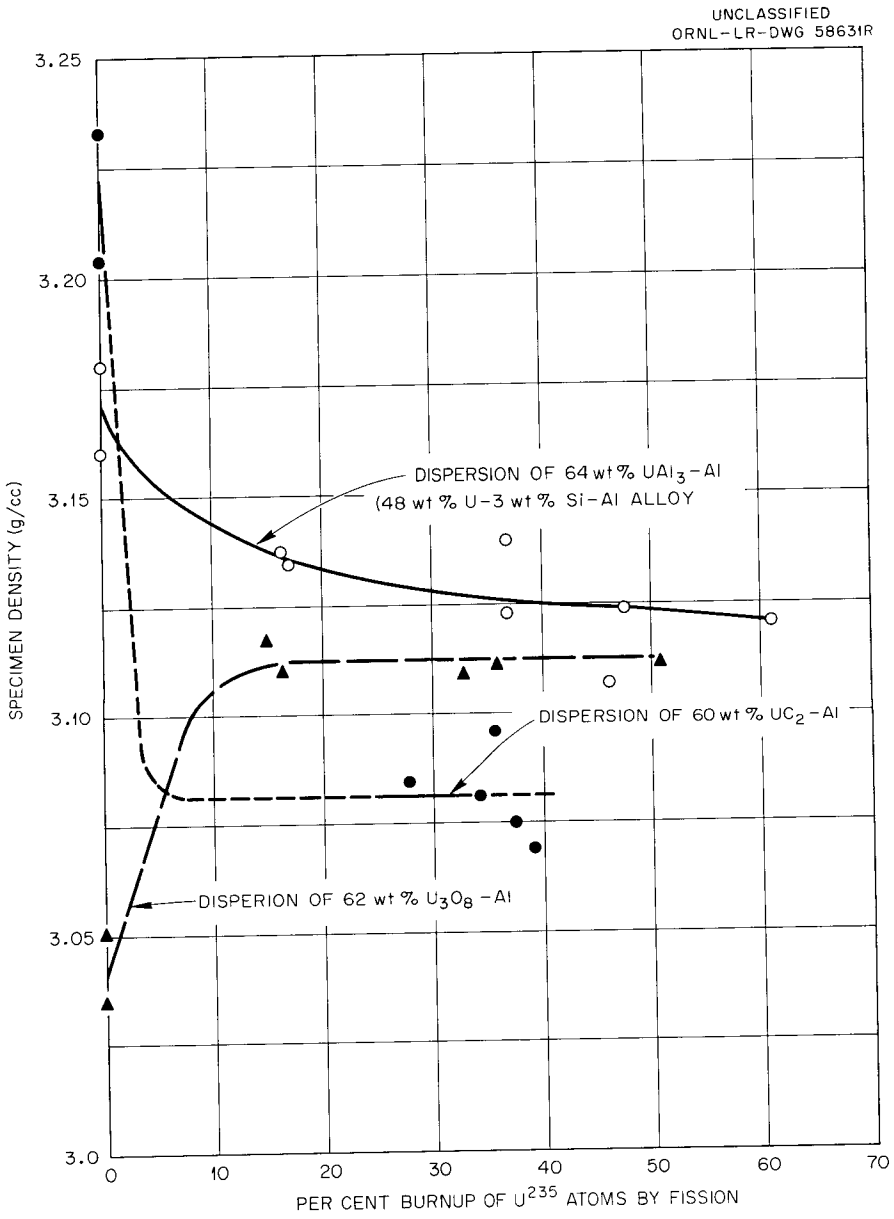

Fig. 18.1. Effect of Irradiation on the Densities of Miniature Composite Aluminum-Clad Plates Containing Dispersions of UAl_3, UC_2, and U_3O_8. Specimen size: $1 \times 6 \times 0.050$ in.

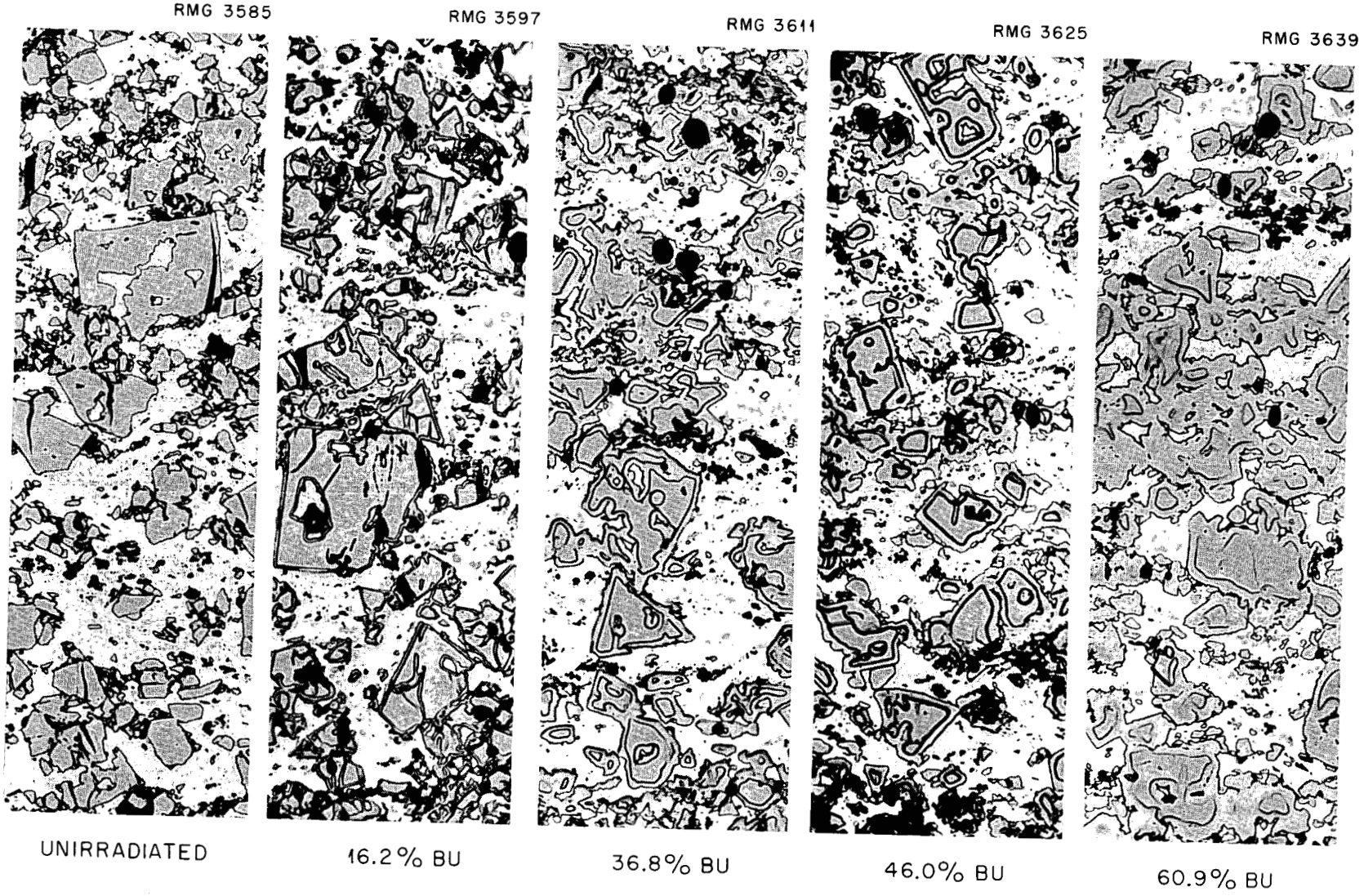

Fig. 18.2. Reaction Between UAl_3 and Aluminum Matrix of Composite-Plate Specimens as a Function of U^{235} Burnup (BU) in 64 wt % UAl_3–Al Dispersions. Etchant: 1% HF, 10% HNO_3. 250X.

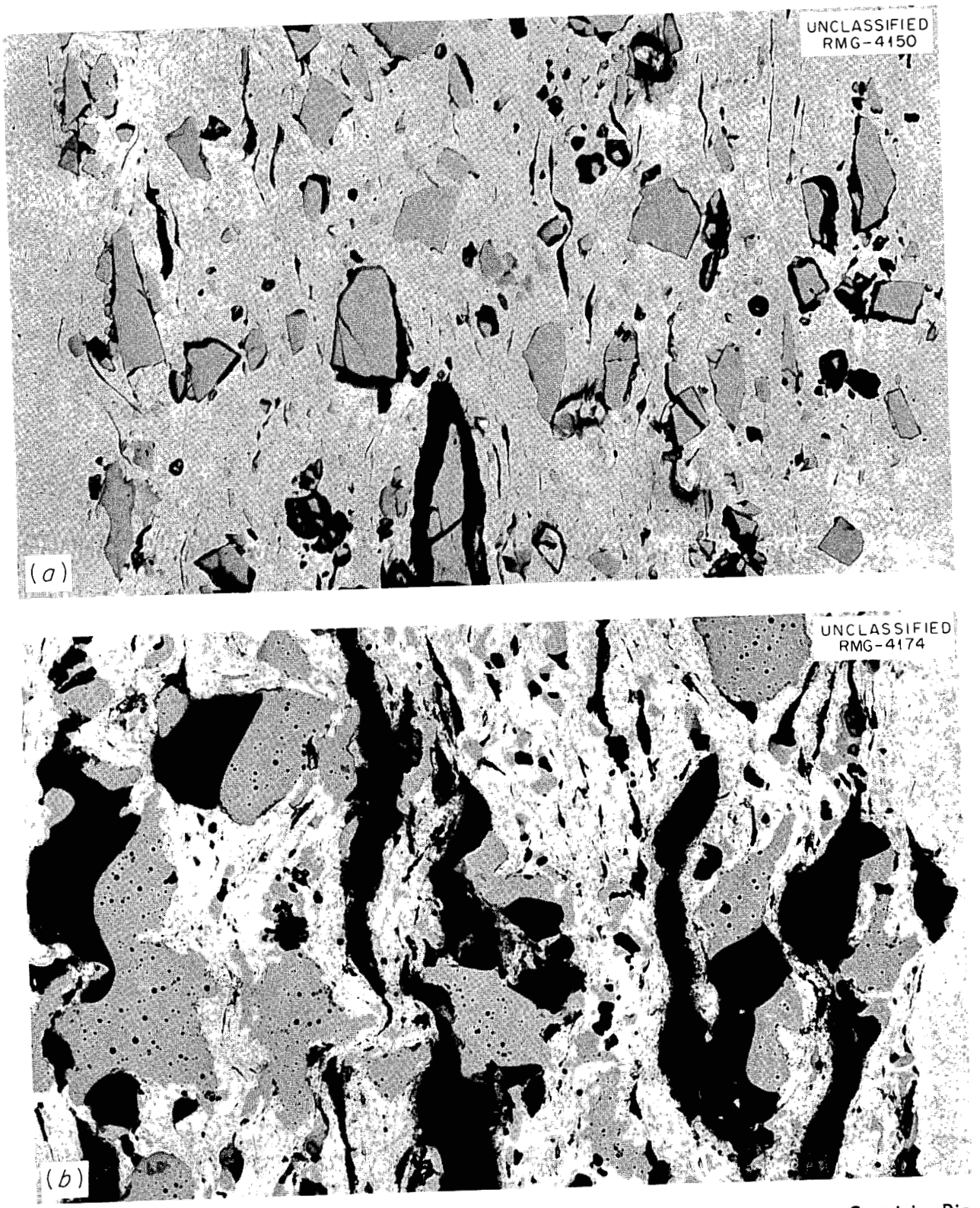

Fig. 18.3. Void Formation as a Function of U^{235} Burnup (BU) in Composite-Plate Specimens Containing Dispersions of 60 wt % UC_2–Al. (*a*) Unirradiated; (*b*) 34% BU. As polished. 250X.

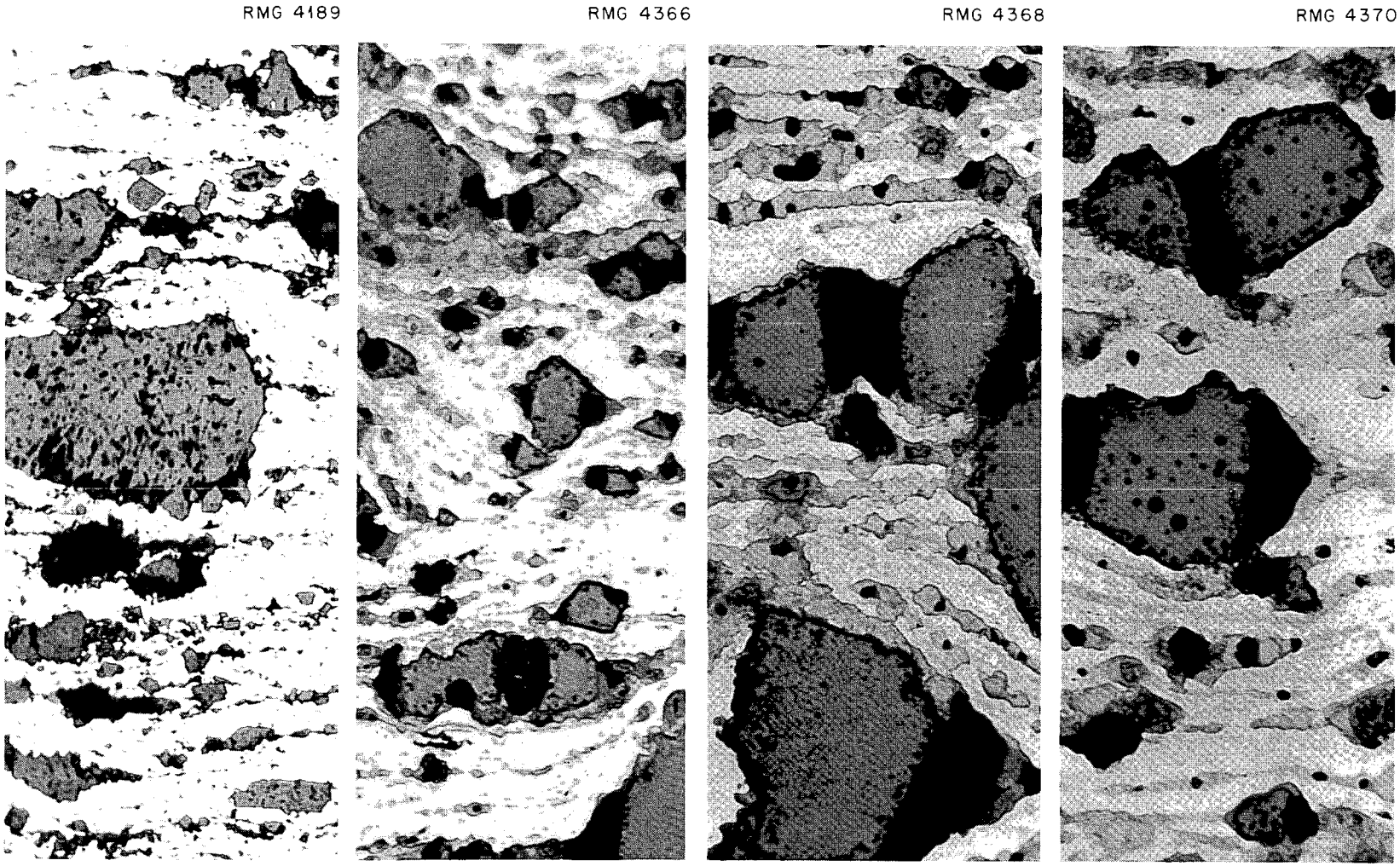

Fig. 18.4. Reaction Between U_3O_8 and Aluminum Matrix in Composite-Plate Specimens as a Function of Burnup (BU) in 62 wt % U_3O_8–Al Dispersions. As polished. 500X.

ALUMINUM-BASE FUEL ELEMENT FABRICATION

Development work has been directed primarily at improvements in aluminum-base fuel element technology aimed at high-flux, high-performance reactors which can operate at elevated central fuel temperatures (400 to 475°F), high neutron fluxes (2×10^{15} neutrons cm^{-2} sec^{-1}), and heat fluxes well above a million Btu ft^{-2} hr^{-1}. A typical example is the metallurgical investigation being made for the High Flux Isotope Reactor (HFIR).[6] The development of a fuel element for this reactor is a joint effort of the Reactor Projects, Powder Metallurgy and Fuel Cycle, Welding and Brazing, and Metal Forming and Casting Groups. Other phases of this program are discussed in Chaps. 23 and 24.

The complexity of the HFIR element is illustrated by the photograph in Fig. 18.5, which is a top view of the element fabricated for critical testing. The fuel plates must be formed into the involute curvature shown and assembled into units while maintaining plate spacings of 0.050 ± 0.003 in. averaged for any cross section with no individual measurement varying by more than ±0.010 in. In all units assembled to date, the inside plate edges have been mechanically joined to a tubular side plate, while the outer edges have been secured by both mechanical and welding techniques. Design specifications are given in Table 18.1.

[6] T. E. Cole, *High Flux Isotope Reactor — A General Description*, ORNL CF-60-3-33 (March 1960).

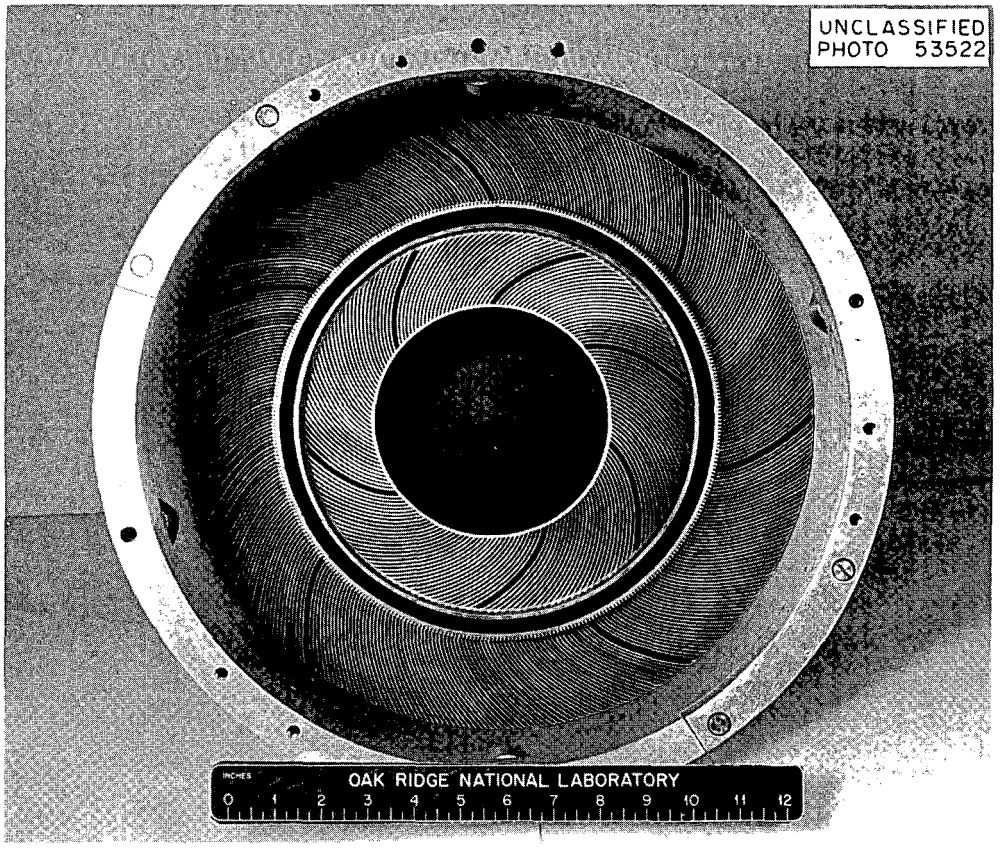

Fig. 18.5. Completed HFIR Critical Assembly.

Table 18.1. Tentative Design Specifications of Inner-Annulus and Outer-Annulus Plates for High-Flux Isotope Reactor

	Inner-Annulus Plates	Outer-Annulus Plates
Over-all size (in.)		
Length	24.000 ± 0.005	24.000 ± 0.005
Width	3.581 ± 0.002	3.195 ± 0.002
Thickness	0.050	0.050
Number of plates	171	369
Fuel-section size (in.)		
Length	20.0 ± ½	20.0 ± ½
Width	3.095 ± 0.032	2.782 ± 0.032
Thickness, max	0.028	0.028
Materials		
Cladding	Type 6061 aluminum	Type 6061 aluminum
Frame	Type 6061 aluminum	Type 6061 aluminum
Fuel section	26 wt % U_3O_8–0.07 wt % B_4C–Al	24 wt % U–Al alloy
Filler piece	0.065 wt % B_4C–Al	Type 1100 aluminum

Fuel Plate Fabrication

D. T. Bourgette W. J. Kucera
J. H. Erwin T. D. Watts[7]

To minimize radial flux peaking, each fuel plate in the HFIR will contain a fuel core that varies in thickness (or in uranium content) in a nonlinear manner. To provide a rectangular shape more suited for roll cladding and, also, a means of achieving a uniform boron content across the plate, additional complementary filler pieces are added. Transverse sections of plates for both annuli are shown in Fig. 18.6.

The general procedure used to fabricate the plates for the critical experiment and the one now considered most likely to yield acceptable plates consisted of either casting and extruding 24 wt % U–Al alloy to ⅞-in.-diam rod or cold-pressing aluminum-base rectangular compacts containing 26 wt % U_3O_8 and 0.07 wt % B_4C. The two methods for preparing core blanks resulted from the fact that the cores for the inner-annulus plates contain B_4C and are produced from powders, while the outer-annulus plates do not contain boron and permit the use of the U-Al alloy. In both cases, the fuel-bearing part was hot-forged to a curved core, encased with the matching inserts in type 6061 aluminum, and roll-clad to specified size.

The main problems encountered in the fabrication of the shaped cores have been associated with segregation. For the inner plates a powder core was substituted for the originally planned alloy to simplify a boron segregation problem. It has been possible to vacuum melt, cast, and extrude binary 0.07 wt % B–Al alloys, and to achieve recoveries of 85% and indices of homogeneity of 96%. However, large and erratic losses of boron occurred when 20 to 30% U along with 2% Si was added to the melts. Another segregation problem was a variation in uranium content in the extruded U-Al alloys. For the critical experiment, with density used as a measure of uranium content, adjustments were made in the volume of each cylindrical forging blank. Such control resulted in meeting the required loading of 5590 g of U^{235} within 1 g with a 99% certainty. It is expected that this segregation may be minimized by casting into slab molds. Excellent control of homogeneity was achieved with the powder cores. In the hot-forged shaped cores, the variation in bulk density

[7] Powder Metallurgy and Fuel Cycle Group.

either within sections of single cores or between entire cores was ±1.5%, and the variations of uranium and boron from the nominal were both ±3%.

In converting the forged cores into clad plates, the problems encountered included (1) achieving tight dimensional tolerances for both the plates and the fuel cores, (2) obtaining sound bonds between the core, inserts, and cladding, and (3) avoidance of blisters. The first two items are now under control, but the third remains a serious problem. Blisters of varying sizes and location were found on almost all fabricated and annealed plates. The causes of these blisters have not been resolved but are being intensively investigated.

In the fabrication of both alloy and powder core plates for the critical experiment, the desired fuel-section thickness was obtained within ±0.001 in. The core configurations obtained are compared with those specified in Fig. 18.7. The solid curves indicate the desired configuration, with the

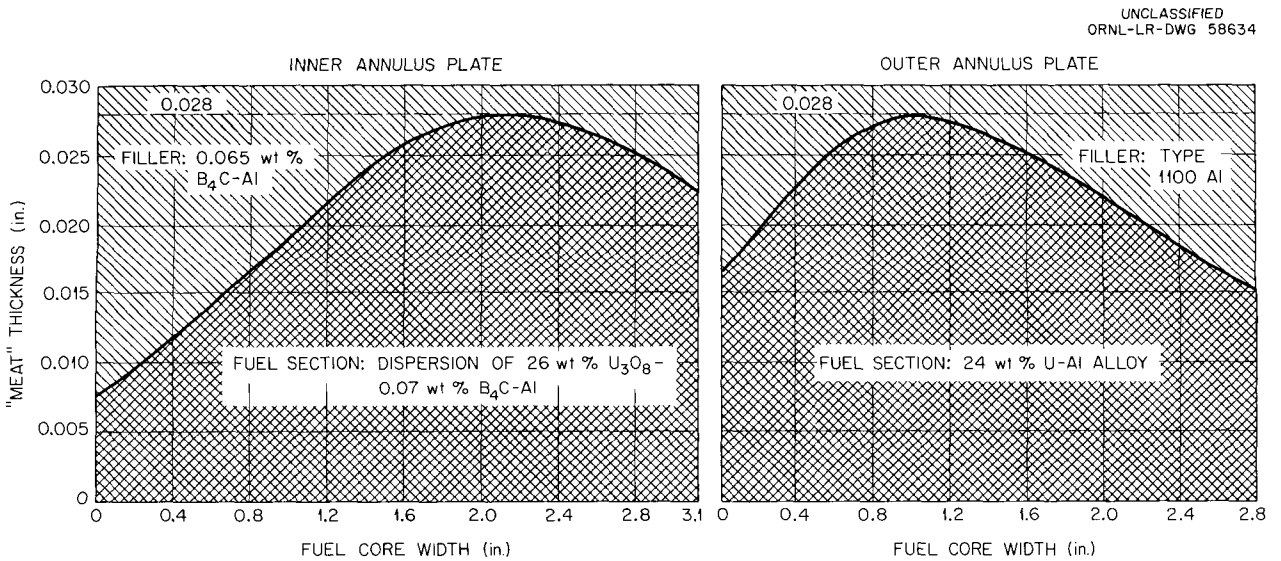

Fig. 18.6. "Meat" Section Design of HFIR Composite Fuel Plates, Representing Method for Obtaining a Transverse Fuel Gradient.

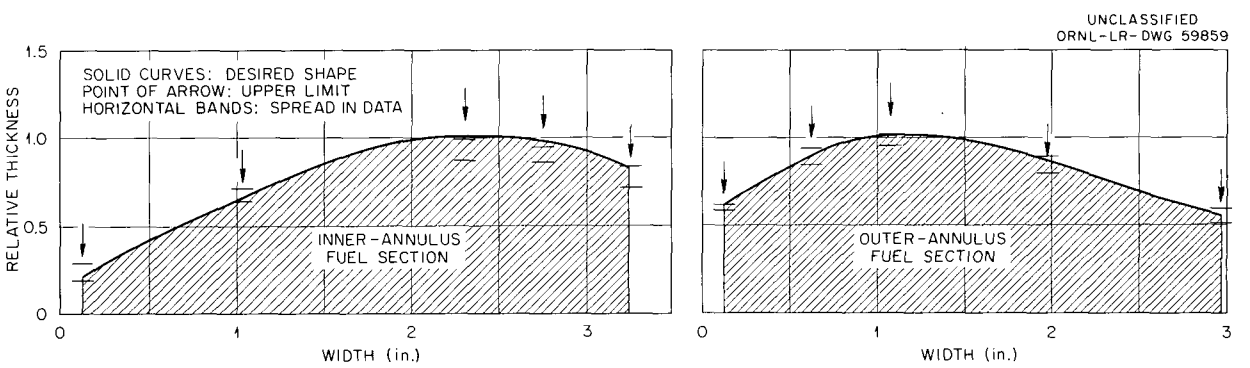

Fig. 18.7. Comparison of Theoretical and Actual Fuel Shapes Produced in Roll Cladding HFIR Composite Plate.

points of the arrows indicating the permissible upper variation (no lower limit has been established). The bands indicate the spread found in the metallographic examination of randomly selected plates. It is obvious that, even at this early stage in the development, good control over the core shape has been achieved.

Plate Forming and Assembly

J. H. Erwin

Before the roll-clad composite plates may be assembled into an element, they must be formed into the necessary shape. To obtain the required final tolerances, such forming must be capable of yielding a closely controlled uniform plate. The desired shape is given to the plates by a "marforming" technique. As shown in Fig. 18.8, the plate required for these partially welded elements must be shaped into an involute and must have the outer edge formed into a second involute. The success achieved with the first two groups of plates which contained cores may be seen by the data in Table 18.2. The data were obtained by averaging values of the radii measured at specific points on randomly selected plates. The agreement, especially on the inner annulus, between the measured and the theoretical values and the reproducibility down each radial position indicate excellent control and uniformity. Plates for the inner annulus are slightly superior to those for the outer annulus.

Both segments of the critical element were assembled by using the arrangement shown in Fig. 18.8. Assembly of both units proceeded with only minor difficulties. The diameter of the outer element was slightly oversize, and some deformation of the plates occurred when it was reduced to the correct diameter. After assembly, both units were turned over to the Welding and Brazing Group for welding and measuring.

An alternative type of inner element was assembled from solid aluminum plates by use of an all-mechanical assembly sequence. For this unit, the plates were formed as a single involute (no broken edge), and control of spacing was obtained by strips spot-welded to the plate. Each plate and

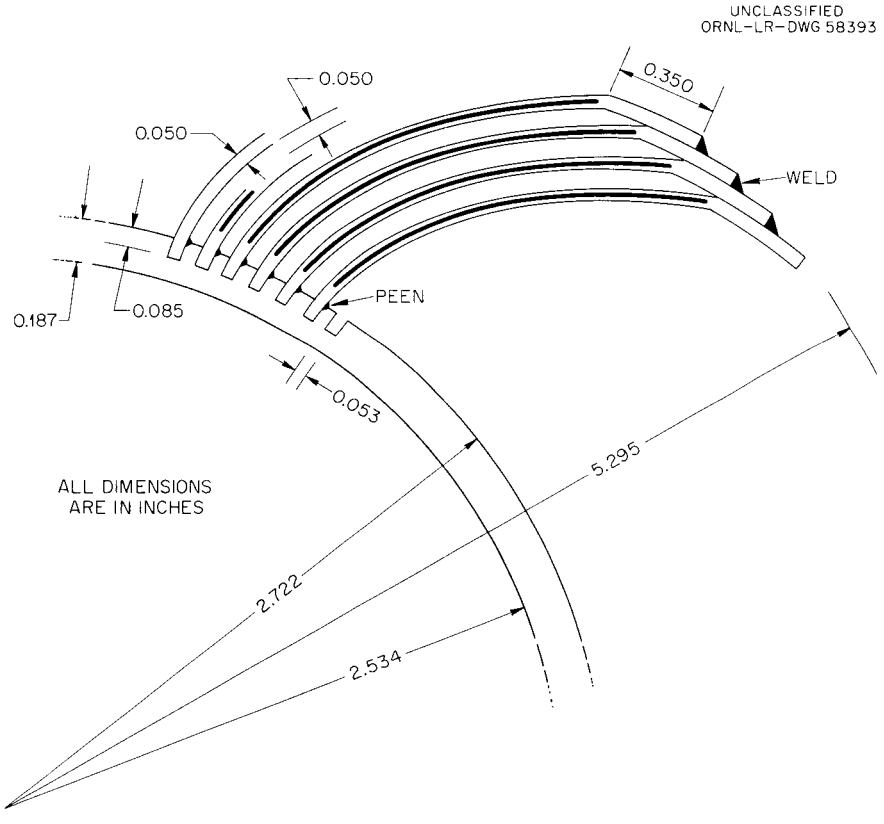

Fig. 18.8. Segment of Inner-Annulus HFIR Assembly.

Table 18.2. Tabulation of Averaged Radii Obtained at Specific Positions on Formed HFIR Plates

Vertical Position	Inner-Annulus Plate[a]				Outer-Annulus Plate[b]			
	R_1	R_2	R_3	R_4	R_1	R_2	R_3	R_4
Theoretical[c]	1.425	2.731	3.563	4.917	2.460	4.305	5.484	7.816
1	1.421	2.736	3.561	4.916	2.456	4.303	5.485	7.814
2	1.431	2.736	3.560	4.915	2.463	4.312	5.494	7.817
3	1.431	2.735	3.560	4.914	2.464	4.315	5.499	7.819
4	1.431	2.736	3.560	4.913	2.462	4.315	5.499	7.818
5	1.431	2.736	3.560	4.912	2.463	4.315	5.497	7.817
6	1.431	2.736	3.560	4.914	2.462	4.310	5.493	7.814
7	1.431	2.737	3.563	4.918	2.457	4.301	5.484	7.816

[a]Average of 18 fuel plates measured.
[b]Average of 35 fuel plates measured.
[c]Calculated radius of involute of locations measured.

Table 18.3. Plate Spacing for HFIR Inner-Annulus Pinned Element

	Entire Element	52 Spaces
Channels		
Number measured	182	52
% within 0.005-in. tolerance	94	100
% within 0.003-in. tolerance	70	98
Cross sections		
Number measured	1280	364
% within 0.005-in. tolerance	98	100
% within 0.003-in. tolerance	88	98
% of individual measurements outside ±0.010 in.	1	0

its strip were mechanically pinned to the lower plates. Dimensional control achieved on this element is shown by the data in Table 18.3. This table is divided into two columns, the first for the entire element and the second for a group of plates assembled in order near the completion of the unit. This column should be indicative of what might be achieved on a second unit.

The tolerance data obtained on these elements present an optimistic picture, with such close control being achieved on the first attempt to assemble such configurations. However, they also point out potential difficulties, with large total deviations resulting from accumulation of variations of only minutes in angles and of only mils in linear dimensions.

STAINLESS-STEEL-BASE FUEL ELEMENT FABRICATION

Development of Swaged UO_2–Stainless Steel Fuel Rods

J. T. Lamartine

Primary efforts in the development of swaged UO_2–stainless steel fuel rods have been directed toward (1) achieving greater fuel densities through elevated-temperature swaging and postswaging fuel sintering treatments and (2) defining the source of gases which may be responsible for swelling of fuel tubes when brazed into fuel elements.

In studies of UO_2 density vs swaging temperature by use of oxides from various sources, fused-and-ground UO_2 yielded a density of 94%.[8]

For the first time, a postswaging heat treatment shows promise of yielding increases in density of swaged UO_2. Use is made of the findings of increased low-temperature sinterability of UO_2 with

[8]*Maritime Reactor Project Ann. Progr. Rept. Nov. 30, 1960*, ORNL-3046, pp 50–51.

a high O/U ratio.[9-10] Tubes filled with oxides normally considered not swagable but which had had their O/U ratio increased to 2.2 were swaged to theoretical densities of 55.4 and 71.4%; after being heat treated in hydrogen at 1300°C, the densities had increased to 90.2 and 87.8%, and the O/U ratios were both 2.002. Difficulties with this process would be the long times and control of dimensions with the large shrinkage encountered.

During the preparation of swaged fuel-rod clusters for the Maritime Irradiation Test Program, it was observed that several of the rods had swelled during the brazing operation, which was performed at 1010°C in hydrogen. This was a surprising result, since four similar fuel-rod clusters had previously been fabricated without difficulty.[11] As a consequence, an investigation was initiated to determine the source and nature of gas within the fuel rods that could produce sufficient pressure to cause deformation of the thin-wall stainless steel cladding at the brazing temperature. Two gas-evolution experiments were conducted. The first was designed to identify and measure the quantity of gas released on heating fused-and-ground fuel to 1010°C. The objective of the second experiment was to collect and identify the gases contained within a swollen rod.

In the first experiment, fused-and-ground UO_2 from each of four batches was heated *in vacuo*, and the evolved gases were collected in the temperature ranges 0 to 300, 300 to 500, 500 to 750, and 750 to 1010°C and were spectrographically analyzed.

The volume of gases released from each of these oxides is presented in Table 18.4. In each instance, the predominant gas species (greater than 90% of the total volume) was spectrographically identified as nitrogen. The data also show that the volume of gases released to 1010°C *in vacuo* correlates with the nitrogen in the UO_2 based on Kjeldahl analyses. Of the total gas accumulated, less than 15% was released at temperatures below 500°C.

Dispersions of Spherical UO_2 in Stainless Steel

J. H. Cherubini

Within the past year, rather thick (0.112 in.), flat stainless-steel-clad plates containing dispersions of 36 wt % spherical UO_2 were successfully developed.[12] The investigations revealed that the quality of spherical UO_2 procured from industrial sources varied from batch to batch, and the microscopic distribution in the fabricated plate in some cases showed extensive fragmentation of the spherical UO_2. It was also found that spherical UO_2 in this concentration could not be

[9] R. Scott and J. Williams, *Trans. Brit. Ceram. Soc.* 57, 199 (1958).

[10] Olin Mathieson Co., *Fuel Cycle Development Program, First Quarter Report, Sept. 30, 1959*, NYO-2684.

[11] *Met. Div. Ann. Progr. Rept. July 1, 1960*, ORNL-2988, p 300.

[12] J. H. Cherubini *et al.*, *Fabrication Development of UO_2–Stainless Steel Composite Fuel Plates for Core B of the Enrico Fermi Fast Breeder Reactor*, ORNL-3077 (Apr. 4, 1961).

Table 18.4. Results of UO_2 Gas-Evolution Experiments on Fused-and-Ground Uranium Dioxide

Oxide Batch Number	Volume of Gas Released *in Vacuo* to 1010°C (cc per g of UO_2 at STP)	Major Gas Species	Kjeldahl Analysis of N_2 Content in UO_2 (ppm)
1	0.380 0.390	N_2	455
2	0.175 0.260	N_2	310
3	0.135	N_2	150
4	0.041	N_2	105

dry-blended to obtain acceptable homogeneity. It was therefore necessary to resort to a paste-blending technique by use of a mixture of 5% paraffin in carbon tetrachloride. A large number of plates was produced, and the reliability of the fabrication procedures to meet the proposed specifications was demonstrated. The data generated have enabled Atomic Power Development Associates to prepare specifications for the core B loading of the Enrico Fermi Fast Breeder Reactor.

Boron Losses in Boron-Bearing Stainless Steel Compacts

J. H. Cherubini

Studies of boron losses in stainless steel compacts were completed, and a report was issued.[13] The results of these comprehensive investigations on boron reactions with the elementals and oxides of the elements present in sintered stainless steel compacts revealed that boron losses are always likely to occur when the sintering is done in hydrogen. It was further emphasized that if sintering had to be done in hydrogen, the hydrogen should be dry (less than 1 ppm H_2O) to minimize such losses. It was also concluded that losses can be eliminated by sintering in vacuum.

NEUTRON ABSORBER DEVELOPMENT

R. J. Beaver A. E. Richt[14]
T. D. Watts[15]

During the course of developing plate-type stainless-steel-clad neutron absorber sections for the SM-1 reactor at Fort Belvoir, Virginia, three types of absorber materials were studied: (1) a dispersion of 3 wt % B^{10} in iron, (2) dispersions of 20 to 36 wt % Eu_2O_3 in stainless steel, and (3) dispersions of 1.0 to 3.0 wt % B^{10} in stainless steel. Work on dispersions of 3 wt % B^{10} in iron was completed with the post-irradiation examination of all miniature plate specimens irradiated in the MTR at a maximum temperature of 170°F. A summary of the results is illustrated in Fig. 18.9, which shows swelling as a function of burnup.

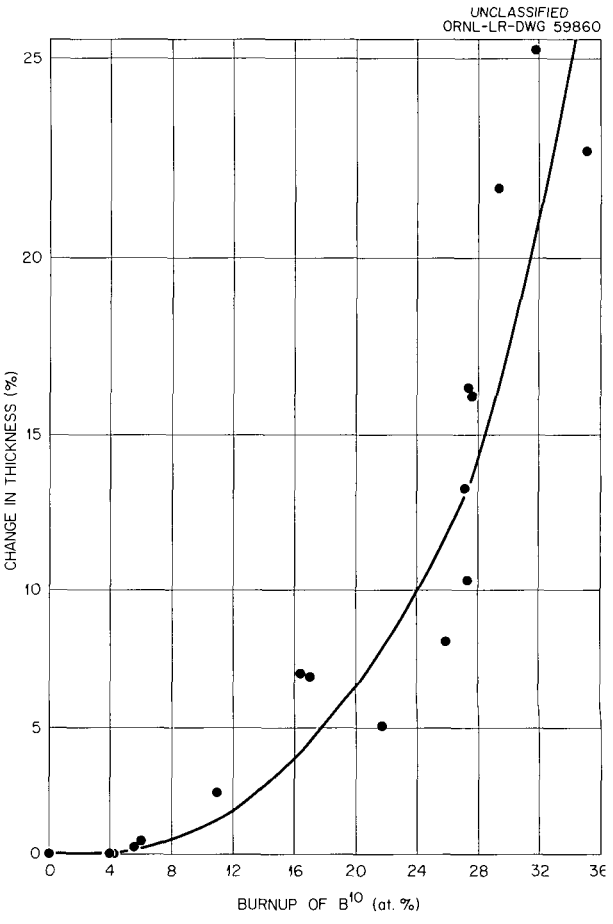

Fig. 18.9. Effect of Burnup on Swelling in Stainless Steel Composite-Plate Specimens Containing 3 wt % B^{10} in Iron. Specimen size: 0.156 × 1 × 6.5 in.

Changes in thickness were the only dimensional changes observed and were principally due to separation of the stainless steel cladding as a result of damage at the surface of the boron-bearing material and accumulation of helium. This effect can be observed in Fig. 18.10, which shows the severity of the damage in the proximity of the bonded interface. It can be concluded that 3 wt % B^{10} in iron is limited to a maximum B^{10} burnup of 5 at. %.

Dispersions of 36 wt % Eu_2O_3 in stainless steel, the current neutron absorber in the SM-1, offer better resistance to radiation damage, since the europium is a gamma emitter and therefore should not deteriorate because of the boron (n,α)

[13] J. H. Cherubini, *Determinations of the Mechanisms and Kinetics of Deboronization at 1135°C*, ORNL-3141 (in press).

[14] Metallography Group.

[15] Powder Metallurgy and Fuel Cycle Group.

UNCLASSIFIED
RMG-4304

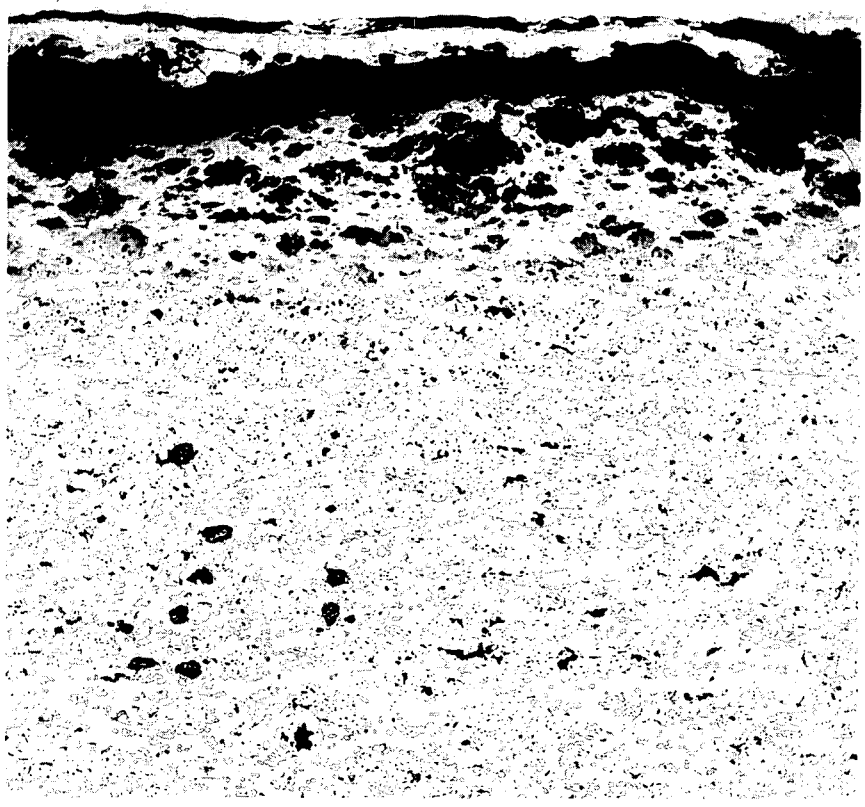

Fig. 18.10. Irradiation Damage to 3 wt % B^{10}–Fe, Showing Deterioration at Surface of Material and at Bonded Core-Clad Interface After a B^{10} Burnup of 16.5 at. %. Etchant: 2% Picral. 100X.

reaction.[16] Postirradiation results on miniature composite plates irradiated in the MTR at 170°F have been extremely encouraging. Dimensional measurements have shown no geometrical changes at exposures estimated to be as high as 9×10^{20} *nvt*, and, as shown in Fig. 18.11, no microstructural effects can be observed.

Although dispersions of Eu_2O_3 in stainless steel appear to be very reliable under irradiation, the high cost of Eu_2O_3 is a detraction. Studies therefore continue on highly enriched boron, by using a concept of a boron gradient throughout the thickness of the plate which takes into account the self-shielding of boron. The gradient is designed to permit uniform burnup rather than concentrating it at the surface layers. In a four-step gradient the boron concentration is varied from 1.0 wt % B^{10} to 3.0 wt % B^{10} (ref 17). In this manner it is believed that the life of such an absorber can be increased fivefold. The elemental boron (90% enriched in the B^{10} isotope) was dispersed in type 200 stainless steel by using powder-metallurgy procedures, and was rolled with type 304L stainless steel. After determining that no boron losses occurred during fabrication, composite plates were fabricated and joined in accordance with specifications published previously for neutron absorbers presently operating in the SM-1 reactor.[16] Testing of this section in Alco Products Critical Facility revealed it to have a nuclear worth of five cents

[16] C. F. Leitten, Jr. *et al.*, *Specifications and Fabrication Procedures on Europium-Bearing Absorber Sections for Reactivity Control in Core II of SM-1*, ORNL-2733 (July 29, 1959).

[17] *Met. Div. Ann. Progr. Rept. July 1, 1960*, ORNL-2988, pp 318–21.

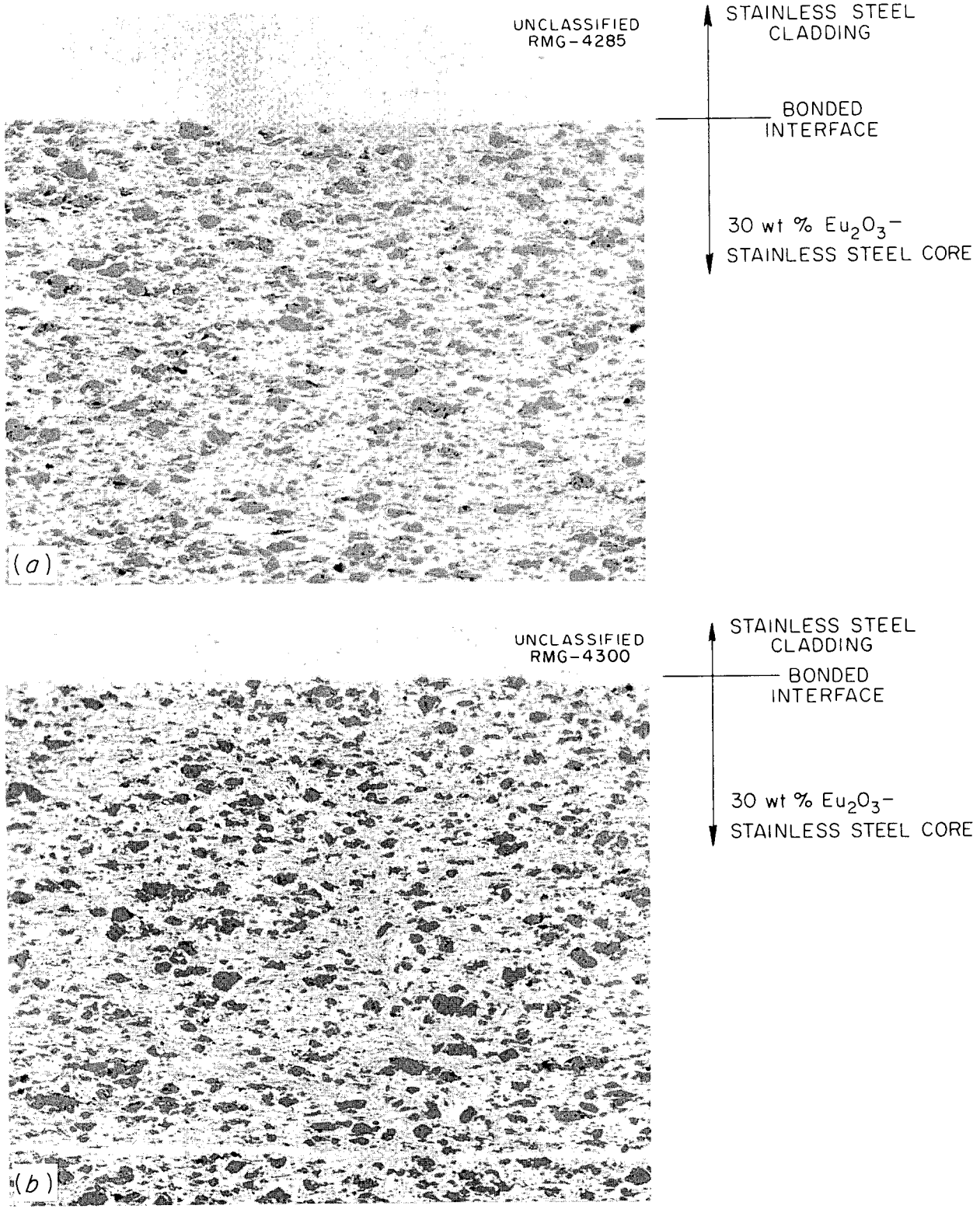

Fig. 18.11. Comparison of Microstructures of Unirradiated and Irradiated Dispersion of 30 wt % Eu_2O_3 in Stainless Steel After an Estimated Exposure of 9×10^{20} *nvt*. (*a*) Unirradiated, (*b*) irradiated. As polished. 100X.

more than the Eu_2O_3-bearing neutron absorbers[18] presently operating in the SM-1. The boron-gradient absorber is scheduled for operation in the SM-1 in the near future.

MELTING AND CASTING OF REFRACTORY METALS AND ALLOYS

D. T. Bourgette T. Hikido

The electron-beam furnace continued to be very effective for producing high-purity refractory-metal samples. Niobium, in approx 300-g heats, was purified consistently to less than 100 ppm total oxygen, nitrogen, and carbon content.[19] Purification was not obtained by melting with a nonconsumable inert-atmosphere arc. It was possible, however, to arc-remelt the electron-beam-purified material and maintain the purity. Tungsten, tantalum, molybdenum, and refractory-metal-base alloys were melted also. However, the composition of alloys in which the minor constituent had a higher vapor pressure than the base metal, such as niobium-zirconium, was difficult to control.[19] The electron gun, which was originally designed for klystrons, proved to be somewhat inadequate for use in a melting furnace. Design of a new gun with replaceable filament and cathode was initiated. Instrumentation to control electron emission and a sight-glass-shield assembly were installed. These improvements should make extended furnace operation feasible so that ingots may be melted more readily.

A series of niobium alloys with various nitrogen contents was prepared by remelting the electron-beam-purified material in atmospheres with various nitrogen partial pressures.[20] After being analyzed, the ingots were cold rolled until cracking occurred. A slight decrease in ductility, from 98% reduction to 96%, was found in the alloys containing from 64 to 590 ppm nitrogen. A very marked decrease in this property, reduction of only 21%, was found with the next alloy which contained 730 ppm nitrogen.

SHAPE CASTING OF STOICHIOMETRIC URANIUM MONOCARBIDE

D. T. Bourgette

Investigations have been conducted in alloying uranium with carbon to produce stoichiometric uranium monocarbide (4.80 wt % C) by arc melting, remelting, and casting into small-diameter cylindrical shapes. These shapes are to be irradiated for evaluation as advanced fuel material for the Experimental Gas-Cooled Reactor.[21] This program differs from others[22] in this field in that efforts are directed at casting uranium carbide with a closely controlled stoichiometric composition. By selection of high-purity uranium with less than 50 ppm C, spectrographic carbon, and a tungsten-tipped electrode, it was demonstrated that stoichiometric uranium monocarbide could be arc-melted on a water-cooled copper hearth. A knowledge of the charged constituents, particularly the carbon in the uranium, the weights of the material before and after arc melting, and the metallographic examination were the criteria for stoichiometry.

For remelting, a copper mold was designed which contained a graphite insert but did not permit molten carbide to be in contact with graphite for any appreciable period. The microstructure of material melted and cast under these conditions is shown in Fig. 18.12. The very clear single-phase structure has none of the usual dicarbide needles present within the grains. Four 100-g, crack-free castings of this quality have been made.

FABRICATION OF SUPERCONDUCTIVE Nb-CLAD Nb_3Sn WIRE

J. T. Lamartine

In light of the remarkable properties of Nb_3Sn (see Chap. 8), a program has been generated with the possibility of fabricating this material into superconducting solenoid magnets having fields potentially as high as 100,000 gauss. The fabrication portion of this program involves the production of wire of this material.

---

[18] J. Coombe *et al.*, *Hazards Report for the SM-1 Core II with Special Components*, APAE No. 84 (Mar. 30, 1961).

[19] *ANP Semiann. Progr. Rept. Apr. 30, 1961*, ORNL-3144 (in press).

[20] *Met. Div. Ann. Progr. Rept. July 1, 1960*, ORNL-2988, pp 332–40.

[21] *GCR Quart. Progr. Rept. Dec. 31, 1960*, ORNL-3049, pp 244–46.

[22] A. C. Secrest, Jr., E. L. Foster, and R. F. Dickerson, *Preparation and Properties of Uranium Monocarbide Castings*, BMI-1309 (Jan. 2, 1959).

At present, more than 1500 ft of copper-clad wire exhibiting a smooth surface and good apparent ductility has been successfully fabricated in approx 500-ft lengths by tamp-packing a powder mixture of 60 wt % Nb–40 wt % Sn in a $\frac{1}{4}$-in.-OD, $\frac{1}{8}$-in.-ID electron-beam-melted niobium tube, swaging at room temperature to a 0.168-in. diameter, encasing in copper, and finally drawing to a 0.015-in. diameter by using a 20% reduction per pass.

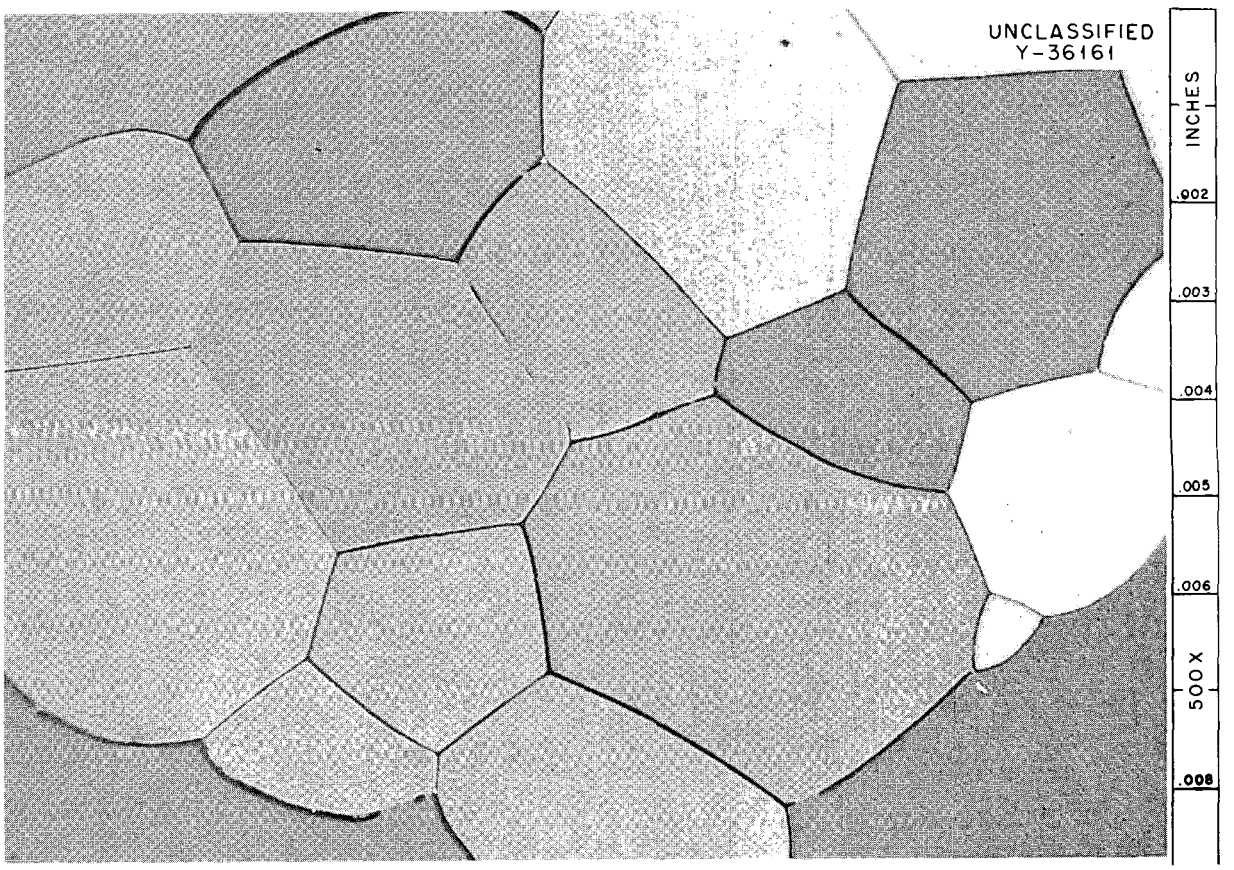

Fig. 18.12. Typical Microstructure of Uranium Monocarbide Arc Cast into a Graphite Sleeve Mold Contained in Copper Insert Molds. Etchant: H_2O-HNO_3-acetic acid.

19. METALLOGRAPHY

R. J. Gray

During the past year, effort in the metallographic group was distributed among three major activities: (1) development of new techniques and equipment, (2) specialized metallographic studies, and (3) reactor-project support work. Accomplishments in each of these three areas are summarized.

DEVELOPMENT OF NEW TECHNIQUES AND EQUIPMENT

Polishing and Etching of Uranium-Molybdenum Alloys

G. Hallerman

The physical and chemical natures of U-Mo alloys present a problem in producing suitable surfaces for optical examinations. Conventional etching methods for specimens containing the retained γ phase in U–10-to-16.75 wt % Mo are not satisfactory due to excessive pitting and/or formation of oxide films during etching. Furthermore, there is no single etching technique suitable for specimens with various compositions or thermal histories.

During investigation of several etching methods, two techniques, described below, were found to give improved results for uranium alloys containing 10 to 16.75 wt % Mo.

1. Cathodic vacuum etching reveals sharp grain boundaries of the retained γ phase with a minimum amount of pitting. This method works well in the entire composition range. Specimens in the as-cast condition, however, do not show a cored structure typical of this condition.

2. Electrolytic polishing and etching affords a rapid means of processing specimens, and this method is recommended for routine examination of the γ phase in U-Mo alloys. Of all the electrolytes tested, chromic and acetic acids produced the best metallographic surface.

Figure 19.1 shows the results of the two techniques as applied to the same specimen. Both techniques are suitable for grain-size determinations. The cathodic vacuum method, however, is better where the amount of microporosity is to be studied.

Metallographic Preparation of Zirconium-Base Alloys Containing Copper

D. M. Hewette II

The microstructure of heat-treated samples of Zr-Cu alloys is difficult to reveal by the usual mechanical polishing techniques. Chemical polishing produces flat surfaces that are suitable for examination with polarized-light illumination but not for bright-field studies. Electrolytic polishing applied to ground or mechanically polished specimens produces surfaces that, although well etched, are not flat and are often heavily pitted. Through a combination of the two techniques, chemical polishing followed by a short electropolish, excellent microstructures can be obtained in Zr–1% Cu and Zr–1.6% Cu.[1] These microstructures are suitable for examination with either bright-field or polarized-light illumination and at high or low magnification.

Etching ThO_2 Particles in the Range 1 to 5 μ

C. K. H. DuBose

Thorium oxide samples as small as $\frac{1}{8}$ in.[3] can be examined metallographically. The etching requires removal of the specimen from the mount, as standard mounting materials do not withstand boiling HNO_3 and HF.[2] It is obvious that such a technique of specimen removal cannot be followed in the handling of powders in the size range 1 to 5 μ.

In preliminary experiments ThO_2 particles were embedded in a glass, thereby eliminating the necessity for removing the particles from the mount before etching. A lead peroxide–boric acid glass was used as mounting material for particles 1 to 5 μ in size. The particles were embedded in the glass at 450°C, far below the sintering temperature of ThO_2.

---

[1] J. E. Spruiell and D. M. Hewette II, *Metallographic Preparation of Zirconium-Base Alloys Containing Copper*, ORNL-3139 (to be published).

[2] *Met. Div. Ann. Progr. Rept. July 1, 1960*, ORNL-2988, p 361.

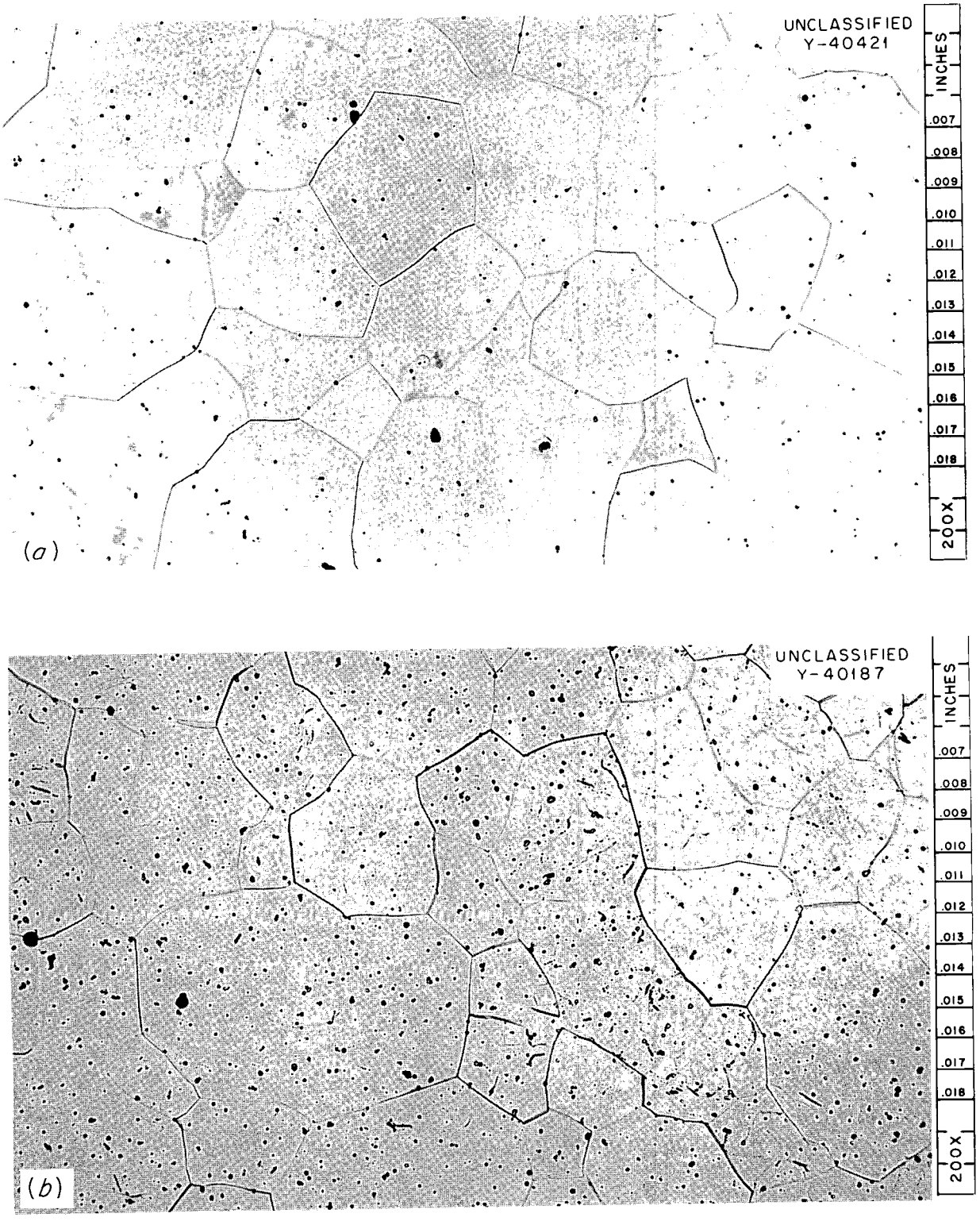

Fig. 19.1. Uranium–15 wt % Molybdenum, Vacuum-Induction Melted, Heat Treated for 19½ hr at 950°C, then Water Quenched. (*a*) Cathodic vacuum etched (15 min at 3.2 kv); (*b*) electrolytically polished and etched (CrO_3, acetic acid, H_2O).

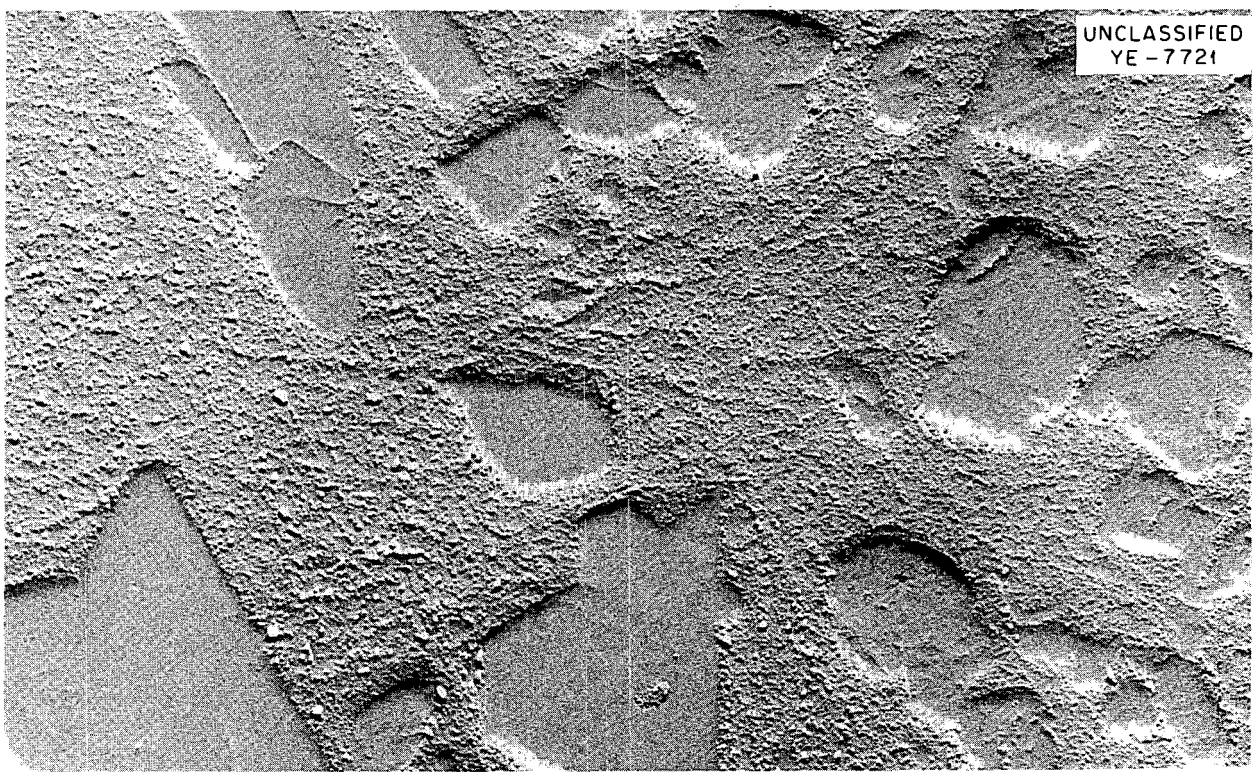

Fig. 19.2. Electron Photomicrograph of As-Polished 1–5-μ ThO_2 Powder Particles Mounted in Glass. 13,600X.

For as-polished examination, the results were far superior to those from any other process investigated to date. Particles in this size range normally agglomerate, due to an electrostatic charge. The glass mounting material, however, wets each particle and separates them (see Fig. 19.2). The lead peroxide–boric acid glass withstands the ThO_2 etchant to the extent that it etches as a platelet-like structure. This etched glass structure makes finding and interpretation of the etched ThO_2 particles somewhat difficult. Further research will be carried on in an effort to find an even better mounting material to withstand the ThO_2 etchant.

Microradioautography

W. H. Bridges

During a study of the fate of carbon in type 304 stainless steel by exposing it to an atmosphere containing C^{14} and subsequently using microradioautography to trace the active radionuclides, a portion of the emulsion was stripped from the sample. As it was quite thin, it was mounted in the electron microscope and examined. A typical electron photomicrograph is shown in Fig. 19.3. From the initial observations it appears that some of the active carbon is displaced from its original position and distributed about the surface during the polishing. It is then caught by scratches and other microroughness. Note in particular the inclusion at the left of picture. There is a buildup of C^{14} at one end and a tailing off at the other.

A cursory scan of the literature has not revealed any instances of the application of combined electron microscopy and radioautography to metallurgy, although it has been used in a few cases in biological studies – first by Liquier-Milward[3] and most recently by Van Tubergen.[4] Further efforts are being made to develop the techniques and determine the areas of usefulness of ultramicroradioautography.

---

[3] J. Liquier-Milward, *Nature* **177**, 619 (1956).

[4] R. P. Van Tubergen, *J. Biophys. Biochem. Cytol.* **7**, 219 (1961).

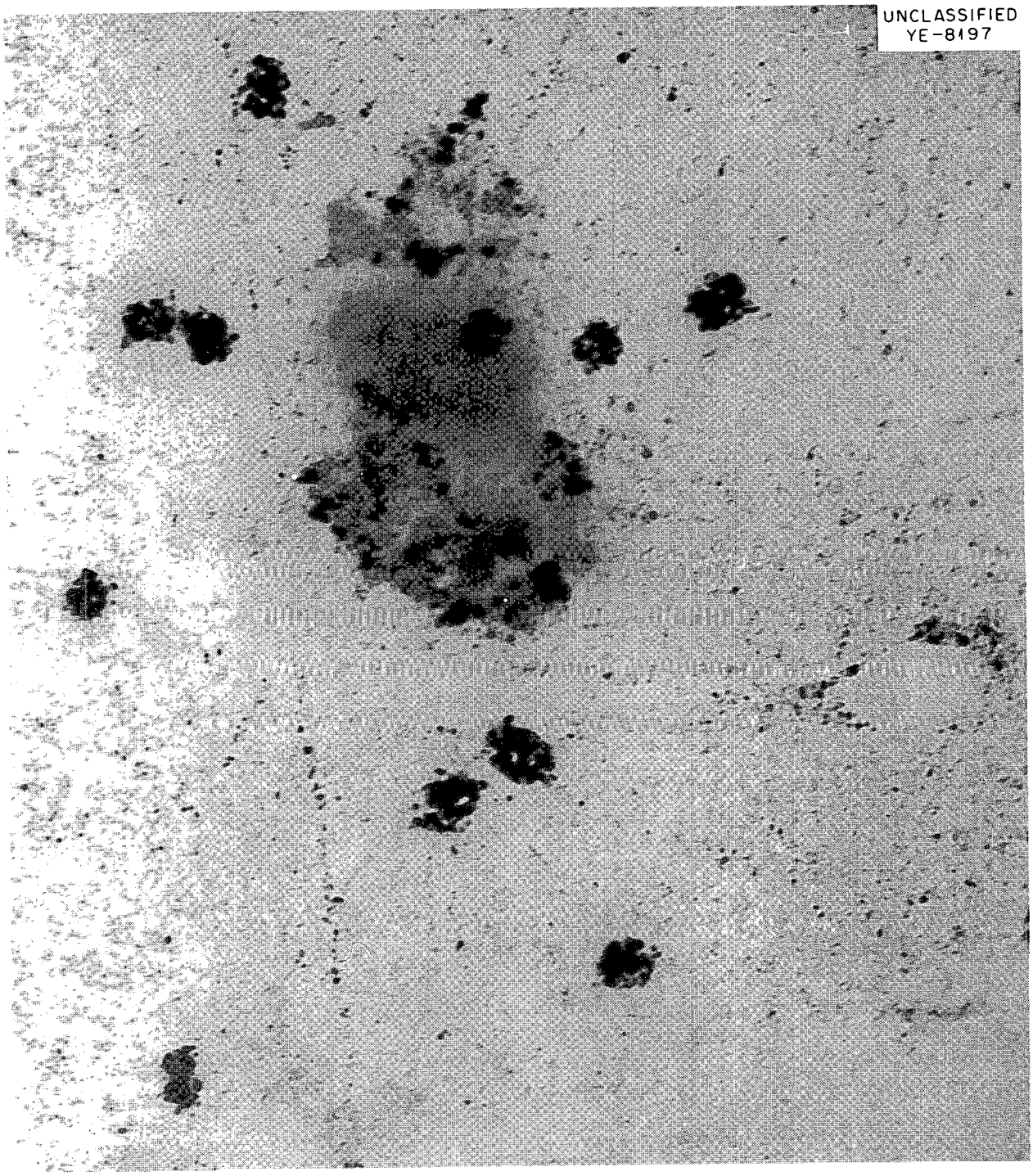

Fig. 19.3. Kodak NTE Liquid-Emulsion Film After Exposure and Development; Stripped from Type 304 Stainless Steel Carburized in a C^{14}-Containing Atmosphere. The metallographic specimen was as polished. 18,400X.

Evaluation of a New Polishing Cloth

R. S. Crouse

The polishing characteristics and wearing qualities of a new type of polishing cloth[5] were evaluated. The cloth was tested both in vibratory and hand-polishing operations with several different metals and alloys.

It was found that the cloth could be substituted for the standard silk or nylon cloth for most metallographic samples – aluminum alloys being an exception. Polishing time was cut as much as two-thirds in some instances, for example, for high-speed steel, stainless steel, and brass. For all materials tested, the cloth was found to outwear both silk and nylon considerably. On the aluminum alloy, severe pitting occurred around inclusions, and deep scratches were produced that could not be removed entirely in the succeeding polishing steps. While the material gave good results in etch-polishing beryllium and in polishing tungsten by hand, it appears to have its greatest potential for operations involving vibratory polishing. The cloth produces undesirable edge rounding in some ceramic materials but does reduce the polishing time. It is not as universally applicable as silk or nylon but does have considerable utility.

Diallyl Phthalate Prepolymers as a Radiation-Resistant Mounting Material

E. J. Manthos

Diallyl phthalate prepolymers have been suggested for use as possible metallographic mounting material.[6] Among the advantages claimed for this material are good edge retention because of low postmold shrinkage, and good chemical resistance to etching reagents. If utilized in hot-cell metallographic work, the material must retain the above characteristics under intense radiation.

Two types of diallyl phthalate prepolymers are being tested. One is a milled glass-fiber-filled resin in powdered form, and the other is an unfilled granular resin. The unfilled granular resin is not satisfactory for hot-cell application because of its low bulk density, which makes remote mounting difficult. Both resins require molding pressures of 2500 psi at 150°C. The mounts are cured at 150°C for 6 min and then cooled under pressure to 65°C. Several unirradiated specimens were mounted in the filled and unfilled resin. These mounts appear to be as good as the standard Bakelite mounts.

In order to determine the effects of radiation on the mounting characteristics, a section of an irradiated Eu_2O_3–stainless steel absorber plate which read 20 r at 1 ft was mounted remotely in the glass-filled resin. A blank mount was also molded with the same mounting press for comparison. Hardness readings and measurements of the diameters of both mounts will be taken at various intervals.

Remote Stereomicroscope Light Source

E. J. Manthos

A new higher-intensity light source has been installed on the stereomicroscope in cell 2, Building 3025. The previous light source was unsatisfactory for photographic purposes because of the relatively low light output and short lamp life. Two quartz-halogen "Sylvania Sun Guns"[7] were adapted for use with the stereomicroscope. A removable mounting bracket was designed to permit remote replacement of the lamps. The new units have a rated lamp life of 10 to 15 hr and a light output equivalent to the output of four of the previously used 300-w reflector floods. Because of the great amount of heat generated by the lamps at full voltage, Variacs were installed so that the light intensity can be lowered when the stereomicroscope is being used for viewing instead of photography.

Ultrasonic Microchisel

G. Hallerman

The ultrasonic microchisel[8] continues to be an important tool for mechanical extraction of inclusions from metal specimens for subsequent identification by x-ray diffraction techniques. When extracted samples contain elements of low

[5] Pellon polishing cloth, manufactured by the Pellon Corp., 350 5th Ave., New York, N.Y.; distributed by Geoscience Instruments Corp., 142 Maiden Lane, New York 38, N.Y.

[6] C. A. Golden, *Metal Progr.* 79(1), 122–23 (1961).

[7] Sylvania Sun Gun Movie Light, manufactured by Sylvania Electric Products, Inc., 1740 Broadway, New York 19, N.Y.

[8] G. Hallerman, *Met. Div. Ann. Progr. Rept. July 1, 1960*, ORNL-2988, p 341.

atomic numbers, identification by this method becomes difficult. In these instances, spectrographic analysis yields good results, but only when the amount of the extracted material is on the order of 10 to 20 mg.

Low-Temperature Microscopy

G. Hallerman

A low-temperature microscope stage capable of examinations of a specimen surface during phase transformations in temperature ranges between room and liquid-helium temperatures was designed. The immediate application of the cold stage will involve optical studies of phase transformations of cerium to supplement the work done by McHargue.[9]

Delivery of the liquid-helium Dewar for the cold stage is scheduled for June.

[9]C. J. McHargue and H. L. Yakel, Jr., *Acta Met.* 8, 637–46 (1960).

Low-Level-Radiation Glove Box

E. L. Long, Jr.

Technetium and its alloys are attractive in the study of superconductivity materials. Since technetium is a low-energy-beta emitter, a Plexiglas glove box provides adequate shielding and containment. Fabrication of the glove box (96 × 41 in.) shown in Fig. 19.4 is complete, and the box is sufficiently equipped to perform all the required operations to prepare specimens for metallographic examination.

SPECIALIZED METALLOGRAPHIC STUDIES

Possible Reaction Observed Between Al_2O_3 and UO_2

C. K. H. DuBose

A sample consisting of an Al_2O_3 single crystal (synthetic sapphire) surrounded by UO_2 (sintered at 1750°C for 6 hr in hydrogen) was submitted by the Solid State Reactions Group for metallographic examination.

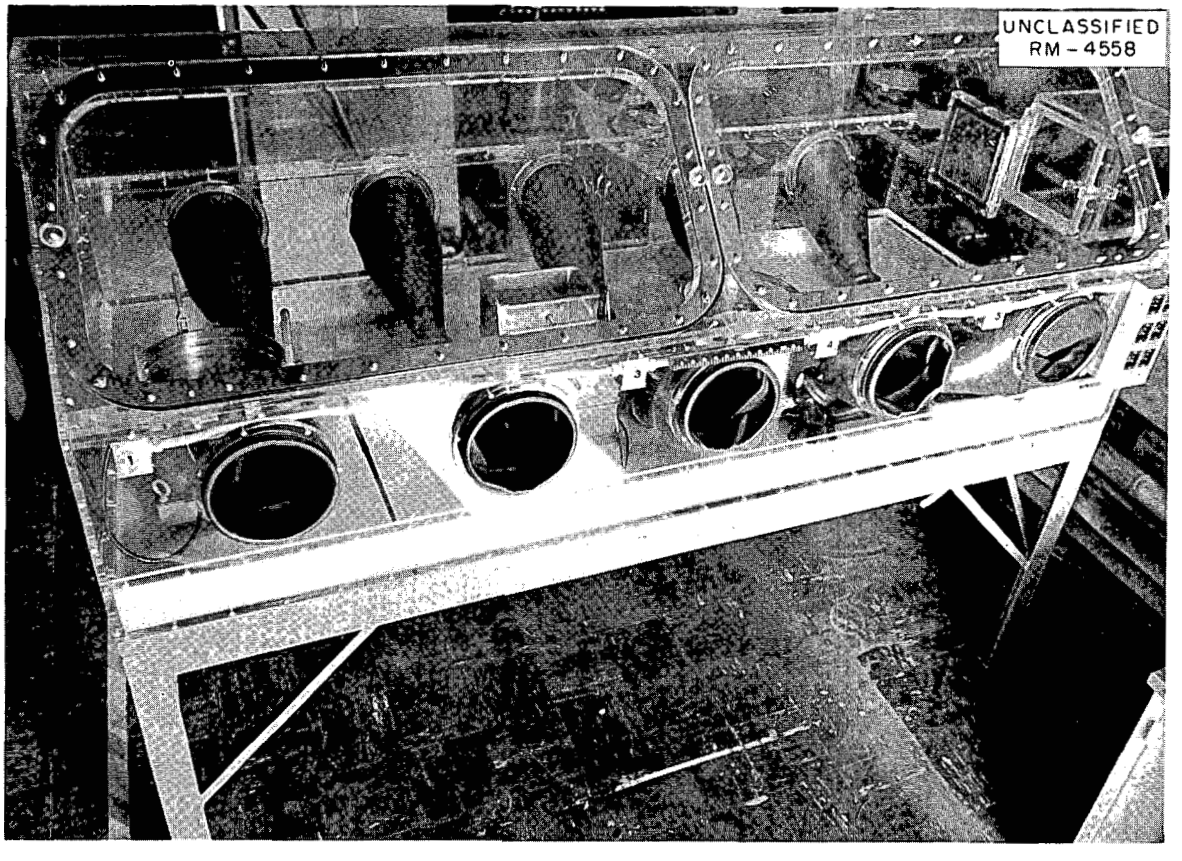

Fig. 19.4. Lucite Glove Box for Use in Preparing Metallographic Specimens of Technetium Alloys.

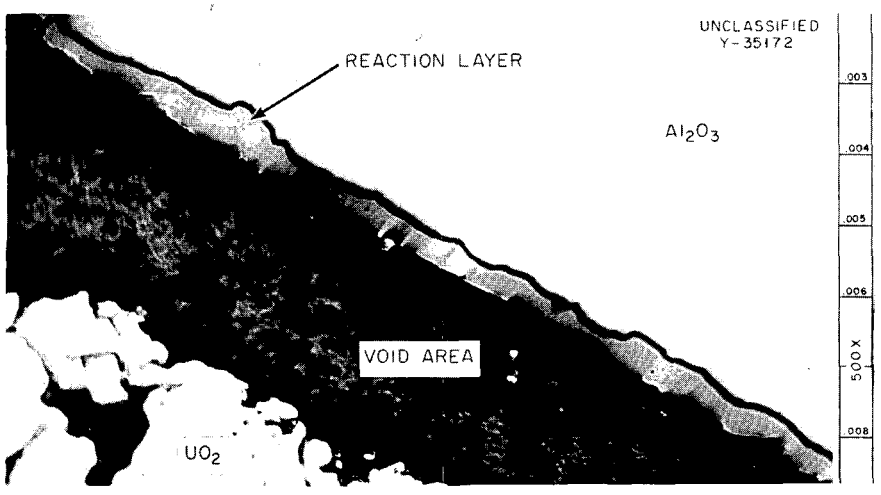

Fig. 19.5. Possible Reaction Layer Observed Between Al_2O_3 Crystal and UO_2. Sintered at 1750°C for 6 hr in hydrogen. As polished. Reduced 27.5%.

A possible reaction layer was noted between the Al_2O_3 crystal and the sintered UO_2, as shown in Fig. 19.5. A 0.003-in.-wide void area, which possibly occurred upon cooling, encircles the Al_2O_3 crystal. The UO_2 and Al_2O_3 crystal apparently were in contact during the heat treatment, since some UO_2 still remains in contact with the possible reaction layer. A second phase was found in the UO_2 adjacent to the Al_2O_3 crystal. This phase appears metallographically the same as the possible reaction layer around the Al_2O_3 crystal.

The possible reaction layer appears to be forming below the original surface of the Al_2O_3 crystal – note the straight-line outer edge of the reaction layer vs the now-irregular surface of the Al_2O_3 crystal. Before heat treatment of the UO_2-Al_2O_3, the surface of the Al_2O_3 crystal was metallographically polished, producing a flat surface.

Future studies will be made of this specimen by attempting to make an autoradiograph, using an emulsion sensitive to alpha emitters, and by x-ray diffraction studies.

Micrographic Observation of the Effect of Moisture on Arc-Cast UC and UC_2

C. K. H. DuBose

The hydrolysis of uranium carbide is of interest to nuclear-materials people because of its potential application as a fuel body in the generation of nuclear power. Hence, when metallographic mounts containing uranium carbide revealed abnormal behavior under storage conditions, this phenomenon was further explored. Some data reported in the literature support the postulate that the stability of UC on exposure to the atmosphere can be improved by the protection offered by a UC_2 shell,[10] while results of hydrolysis tests performed elsewhere[11] show UC_2 to be less stable than UC.

Microstructures have been studied for metallographically prepared specimens of two categories: (1) specimens containing a minor amount (<3.0 vol %) of α-uranium and a major amount (>97 vol %) of UC; (2) specimens containing varying amounts of UC and UC_2. Figure 19.6*a* shows the typical specimen containing 3 vol % α-uranium and 97 vol % UC after storage in a desiccator for four years but removed once or twice a month for microstructural examination. Numerous fine cracks are evident. Figure 19.6*b* illustrates the same material shown in Fig. 19.6*a* after four years' storage in a sealed desiccator. The absence of fracture is evident. Figure 19.6*c* shows a specimen containing 1 vol % α-uranium and 99 vol % UC after 15 months' exposure to the open air. Minute explosions have scattered particles over the specimen mount and surrounding

[10] A. C. Secrest, Jr., E. L. Foster, and R. F. Dickerson, *Preparation and Properties of Uranium Monocarbide Castings*, BMI-1309 (Jan. 2, 1959).

[11] L. M. Litz, *Uranium Carbides – Their Preparation, Structure and Hydrolysis*, TID-NP 1453 (1948).

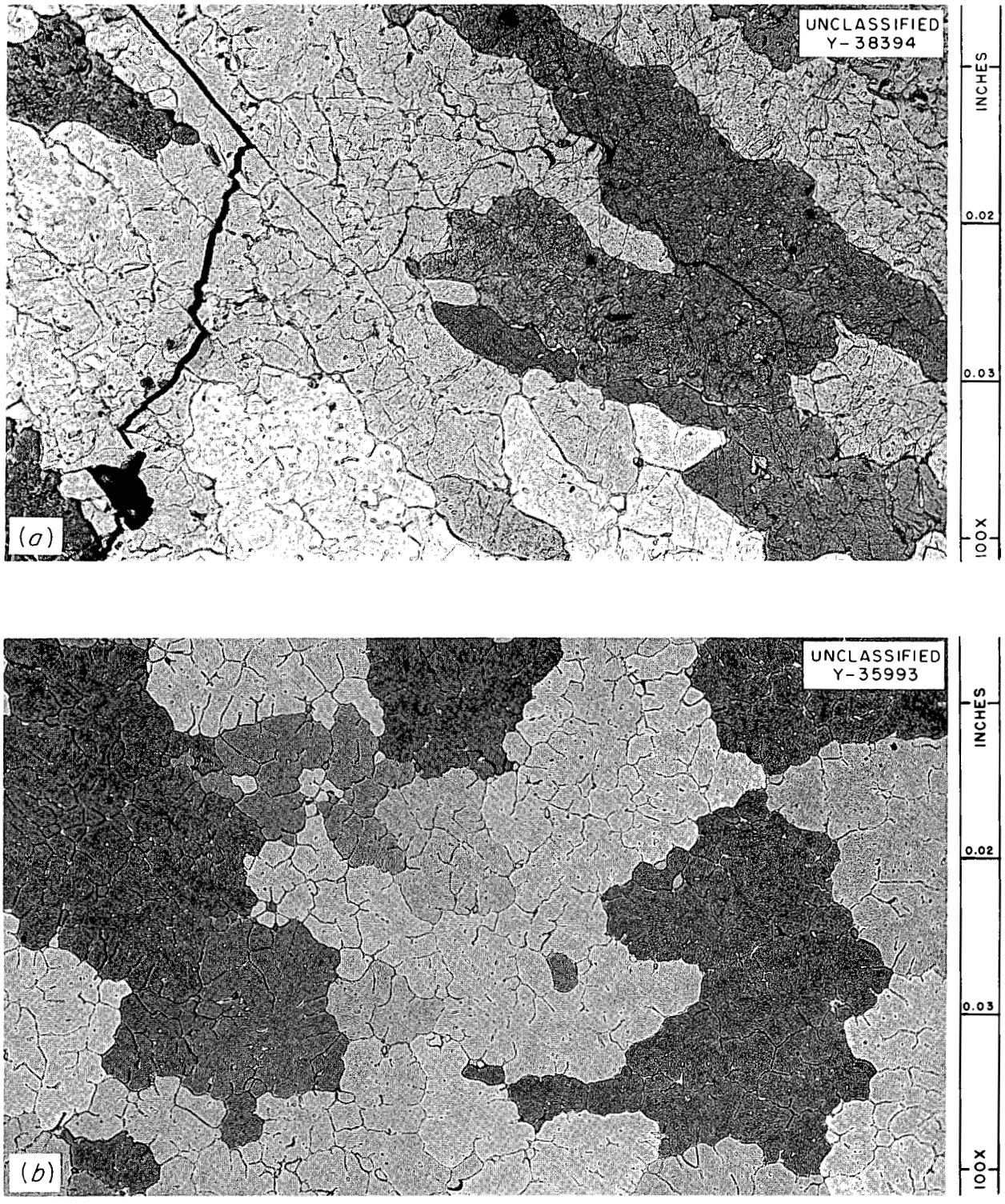

Fig. 19.6. Effect of Moisture in Room-Temperature Air on Arc-Cast UC and UC_2 over Extended Periods. Etchant: 1:1:1 H_2O, CH_3COOH, HNO_3. (*a*) Condition of microstructure after occasional removal from desiccator during four-year period. 3 vol % α-U–97 vol % UC. (*b*) Condition of microstructure after storage in sealed desiccator for four years. 3 vol % α-U–97 vol % UC.

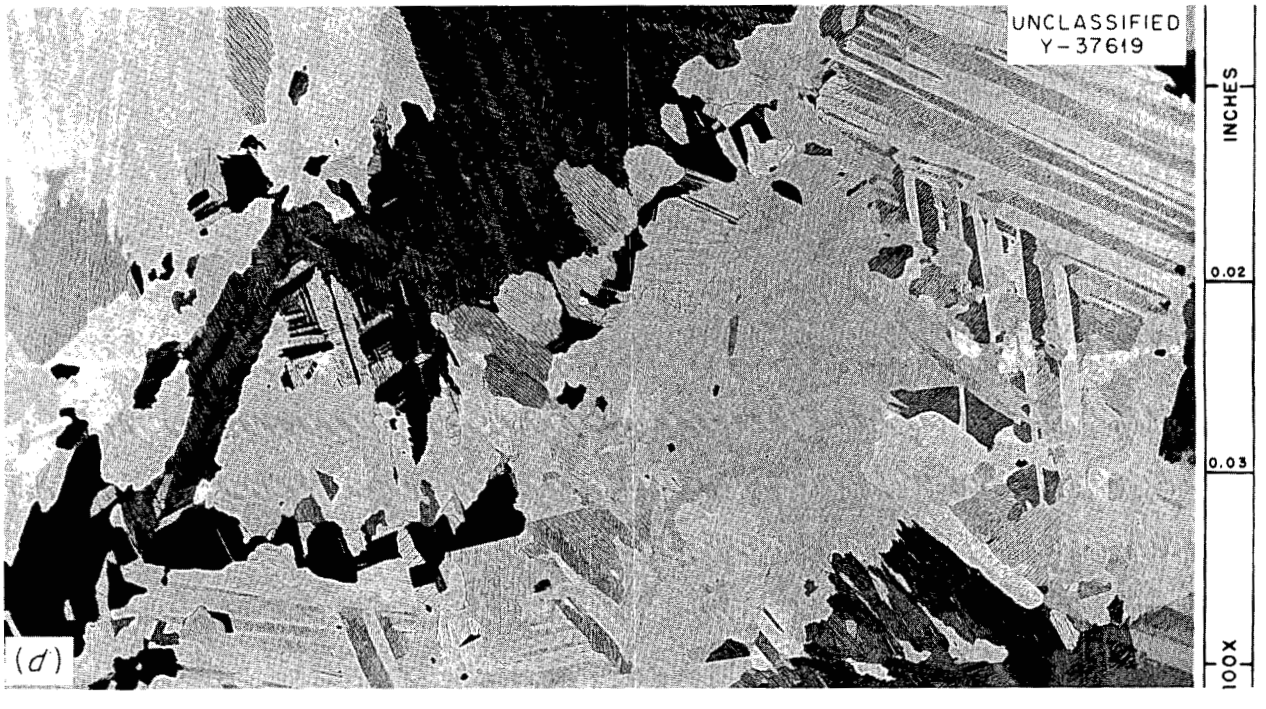

Fig. 19.6. Continued. (*c*) Condition of specimen after open exposure to air for 15 months. Specimen is shown in metallographic mount. Note minute particles scattered over metallographic mount. 1 vol % α-U–99 vol % UC. (*d*) Condition of microstructure after occasional removal from desiccator during four-year period. 20 vol % UC–80 vol % UC_2.

area. A specimen containing 20 vol % UC and 80 vol % UC_2 was stored for four years in a desiccator and removed periodically, on a schedule similar to that for the specimen shown in Fig. 19.6*a*. In contrast, however, the microstructure (Fig. 19.6*d*) exhibits no detectable change from the original as-polished condition.

It must be pointed out that the above observations are not the result of a planned experiment. The fact remains that the dicarbide appears to be the more stable of the two compounds on long exposures to room-temperature air.

Electron Metallography of Oxidized Beryllium

W. H. Bridges

During the past year many different kinds of samples have been examined by electron microscopy and electron diffraction. A typical study involving the complete utilization of the electron microscope was the characterization of the oxide of beryllium for W. J. Werner. The first operation was to mount the specimens in the electron-diffraction adapter and make a series of reflection diffractograms of the oxidized surface. The specimens were then replicated, using the two-stage technique involving a heavy plastic intermediate replica from which the palladium-shadowed carbon replica was prepared and examined. The oxide film was then removed from a portion of the specimen surface by dissolving away the beryllium substrate in dilute acid. The oxide film remaining was examined by transmission in the electron microscope. Figure 19.7 is typical of the results. The reflection diffractogram is given in Fig. 19.7*a*. Figure 19.7*b* is a photomicrograph of the replicated surface and includes some needle-like material which was determined to be beryllium oxide by selected-area diffraction. The stripped oxide film is shown in Fig. 19.7*c*.

Elevated-Temperature Hardness Testing

G. Hallerman

The preparation of test specimens and the actual creep or elevated-temperature tensile testing for evaluating the mechanical properties of materials at high temperatures are usually expensive and time consuming. Elevated-temperature hardness testing, in comparison, provides a rapid and inexpensive survey of high-temperature deformation characteristics of metals and alloys.

Elevated-temperature hardness-testing equipment, described previously,[12] is functioning properly. A topical report on elevated-temperature hardness testing is in preparation.

The hot-hardness characteristics of several metals and alloys have been investigated, and the results are summarized below.

Thorium and Thorium-Base Alloys.[13] – Thirty-six thorium alloys were tested at temperatures up to 750°C. Some of the results are shown in Fig. 19.8. Carbon is an effective strengthener of

[12] G. Hallerman, *Met. Div. Ann. Progr. Rept. July 1, 1960*, ORNL-2988, pp 342–48.

[13] See chap. 23, "Powder Metallurgy and Fuel Cycle," this report.

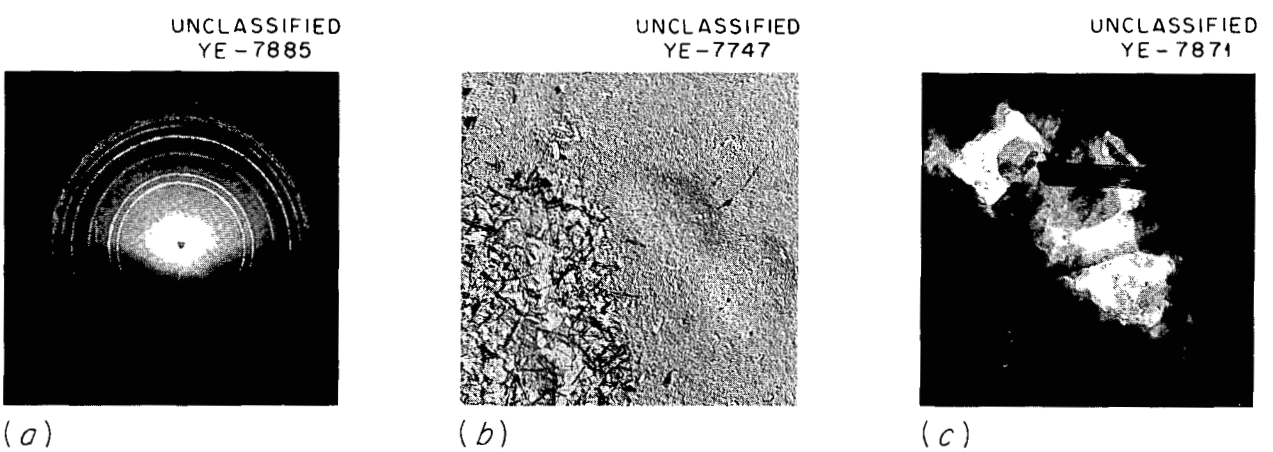

Fig. 19.7. Beryllium Oxidized in Carbon Dioxide. (*a*) Reflection diffraction; (*b*) palladium-shadowed carbon replica, 3400X; (*c*) stripped oxide, 18,500X. As polished.

thorium at lower temperatures; at higher temperatures, carbon adds very little to the hardness. As expected, hardness of the alloys increases with increasing carbon content.

Addition of 4 wt % In results in a hardness increase, especially at high temperatures. This alloy exhibited the highest elevated-temperature hardness of any of the thorium alloy samples tested. Additional Th-In alloys are being prepared in order to study the effects of indium content on elevated-temperature hardness.

Figure 19.8 also shows that the hardness of thorium alloys is additive; that is, the addition of 2 wt % In to the Th–0.2 wt % C alloy increases its hardness over the entire temperature range.

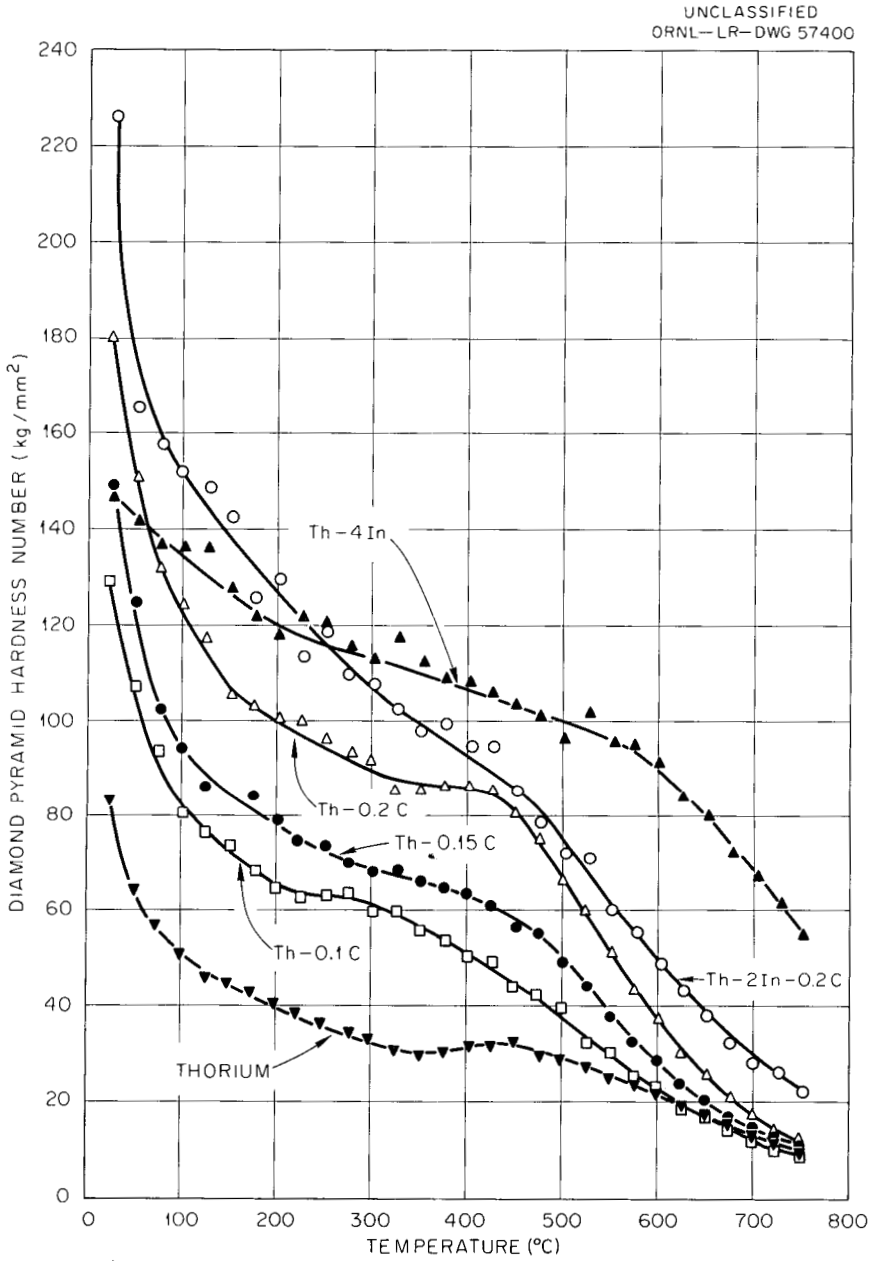

Fig. 19.8. Hot Hardness of Thorium and Thorium-Base Alloys.

Nickel–29 wt % Molybdenum Alloy. – This alloy is capable of precipitation hardening after quenching from the α region. Hardness testing at temperatures up to 900°C was made on specimens which had received one of the following heat treatments:

1. air cooled from 900°C with α phase partially retained or
2. aged at 800°C for 12 hr, furnace cooled.

Results are shown in Fig. 19.9. The hardness of the air-cooled specimen decreases up to about 600°C. Above this temperature, hardness increases rapidly to a maximum and then decreases at higher temperatures. The maximum at 775 to 800°C shows that the Ni–29 wt % Mo alloy precipitation-hardens at this temperature.

Aging of the alloy results in a substantial increase in hardness as compared with hardness of the air-cooled sample up to about 800°C. Above this temperature the hardness of both specimens is practically the same.

Type 502 Stainless Steel. – Six type 502 stainless steel specimens were given various heat treatments prior to hot-hardness testing. Figure 19.10 shows hardness as a function of temperature of three of these samples.

Aluminum Alloys. – A preliminary study was conducted to establish methods for hot-hardness testing of aluminum. Satisfactory results were obtained on the Rockwell hot-hardness tester with the $\frac{1}{8}$-in. carbide ball penetrator and a 15-kg major load. Figure 19.11 shows depth of indentation as a function of temperature for two aluminum alloys. Depth of indentation was calculated from Rockwell hardness readings to avoid the plotting of negative hardness numbers, which occur with soft materials at elevated temperatures.

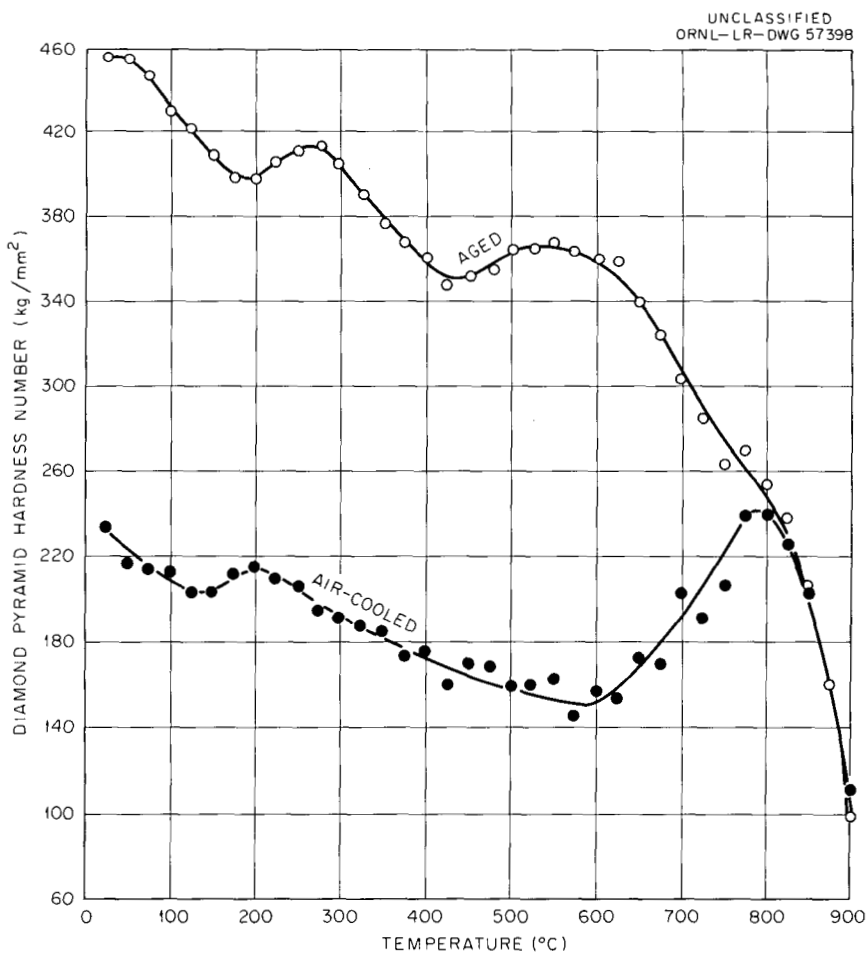

Fig. 19.9. Hardness as a Function of Temperature of Ni–29 wt % Mo Alloy.

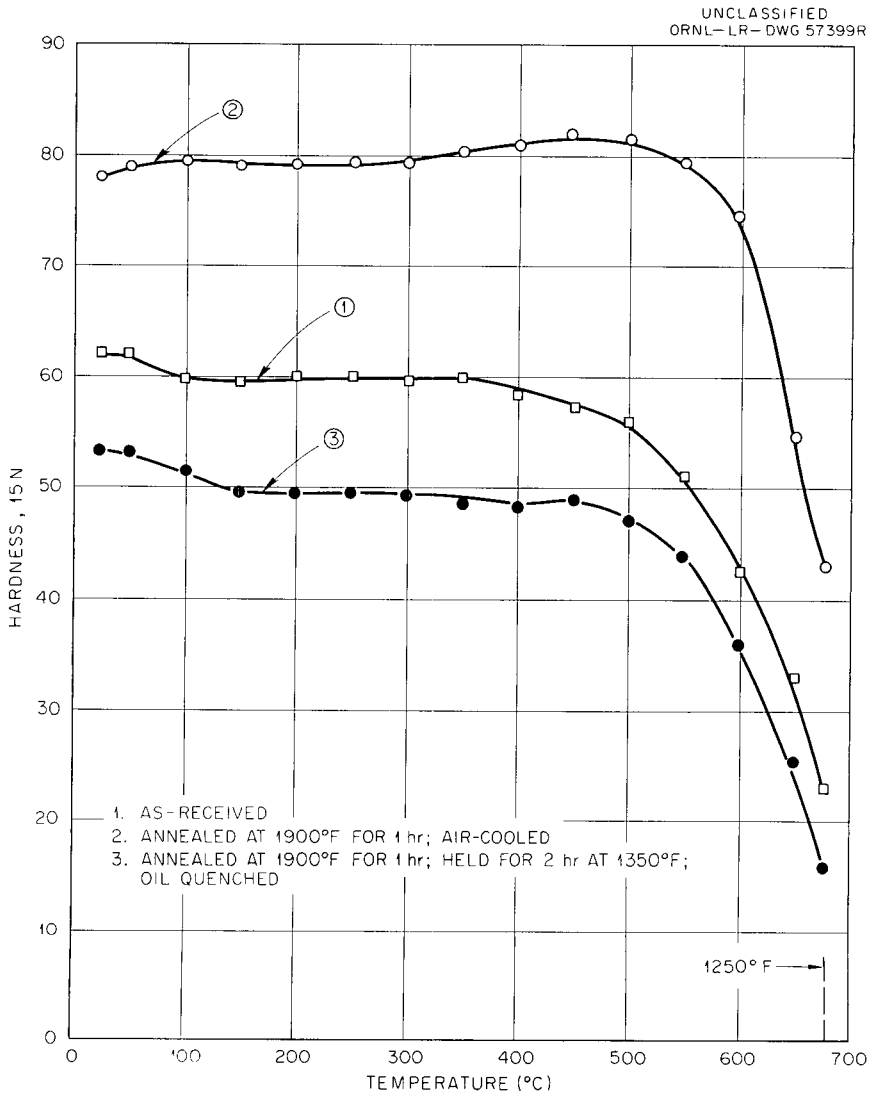

Fig. 19.10. Hardness as a Function of Temperature of Type 502 Stainless Steel.

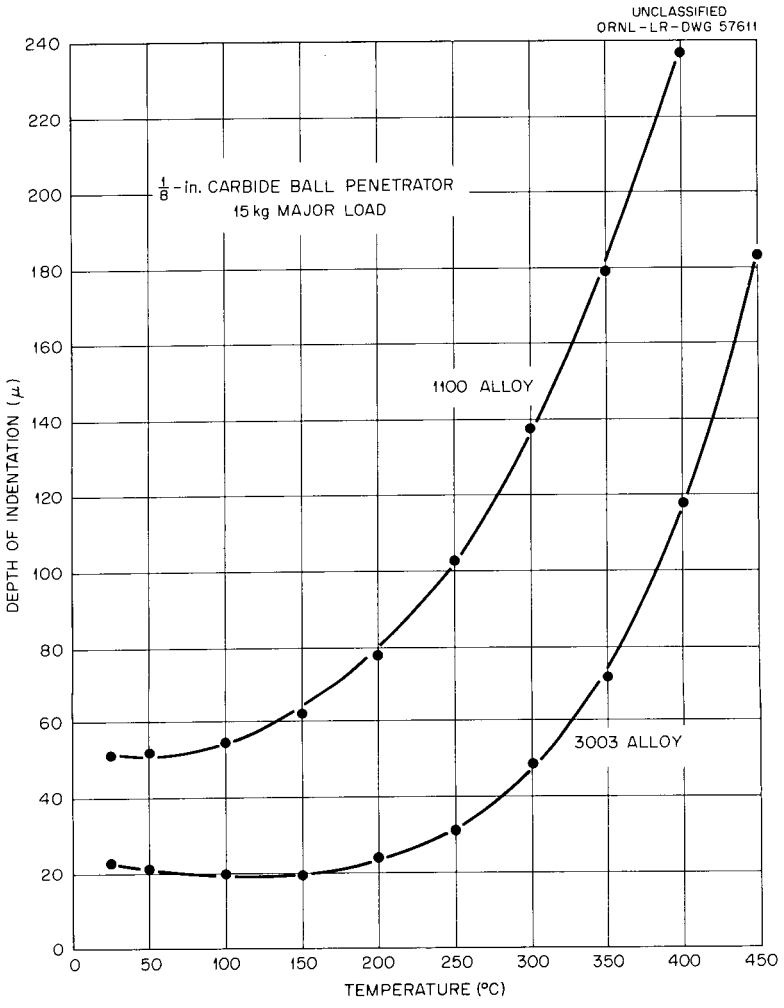

Fig. 19.11. Depth of Indentation as a Function of Temperature for Types 1100 and 3003 Aluminum Alloys.

Linear Thermal Expansion of Aluminum Powder Compacts

J. R. Riddle

The linear thermal expansion of aluminum powder compacts containing dispersions of 4.85 vol % CeO_2 and Gd_2O_3 has been determined between 25 and 600°C. This information was needed to provide preliminary information on the probable behavior of the potential target oxides of plutonium, americium, and curium. The materials were in the as-pressed condition, and a slight dimensional instability was noted on the first few thermal cycles. Typical expansion data for these composite materials in the axial and radial directions as a function of temperature are given in Table 19.1.

Table 19.1. Coefficient of Expansion for Al-CeO_2 and Al-Gd_2O_3 Compacts

Temperature Range (°C)	Average Coefficient of Expansion (μin. in.$^{-1}$ °C^{-1})			
	Al-CeO_2		Al-Gd_2O_3	
	Axial	Radial	Axial	Radial
25–100	19.2	22.5	20.5	21.6
25–200	21.3	22.9	21.2	22.3
25–300	23.0	23.5	22.1	23.2
25–400	24.4	24.6	22.9	24.3
25–500	25.5	25.7	23.9	25.4
25–600	26.5	27.0	25.2	26.5

REACTOR PROJECT SUPPORT

Examination of UC_2-Graphite Fuel Pellets

E. L. Long, Jr.

The irradiation performance is being investigated for a number of advanced fuel materials which have possible application in the Gas-Cooled Reactor. Examination of one such experiment, MTR 48-2 (ref 14), which contained unclad fuel, is complete. This capsule is one of three in this series to be examined that contained UC_2-dispersed-in-graphite fuel pellets. A photomicrograph representative of a fuel pellet of this type is shown in Fig. 19.12, which shows an area where UC_2 was formed by the reaction of UO_2 powder with the graphite matrix. A typical area revealed by the postirradiation examination is shown in Fig. 19.13. As can be seen in Fig. 19.13, the UC_2 was apparently in the molten state during irradiation. Effects from fission recoil can be seen also in the graphite surrounding the UC_2 particle.

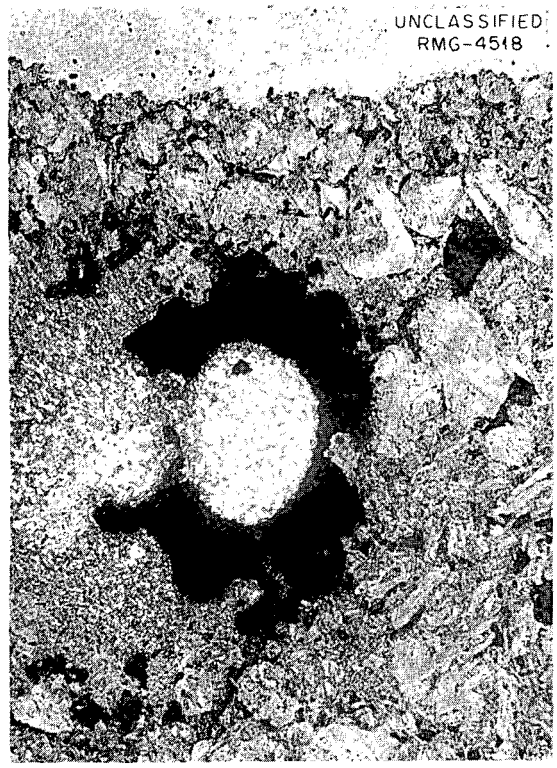

Fig. 19.13. Typical UC_2 Particle After Irradiation. The UC_2 was apparently molten during irradiation. Note fission recoil damage in graphite surrounding UC_2 particles. As polished.

[14] *GCR Quart. Progr. Rept. Mar. 31, 1961*, ORNL-3102, pp 176–78.

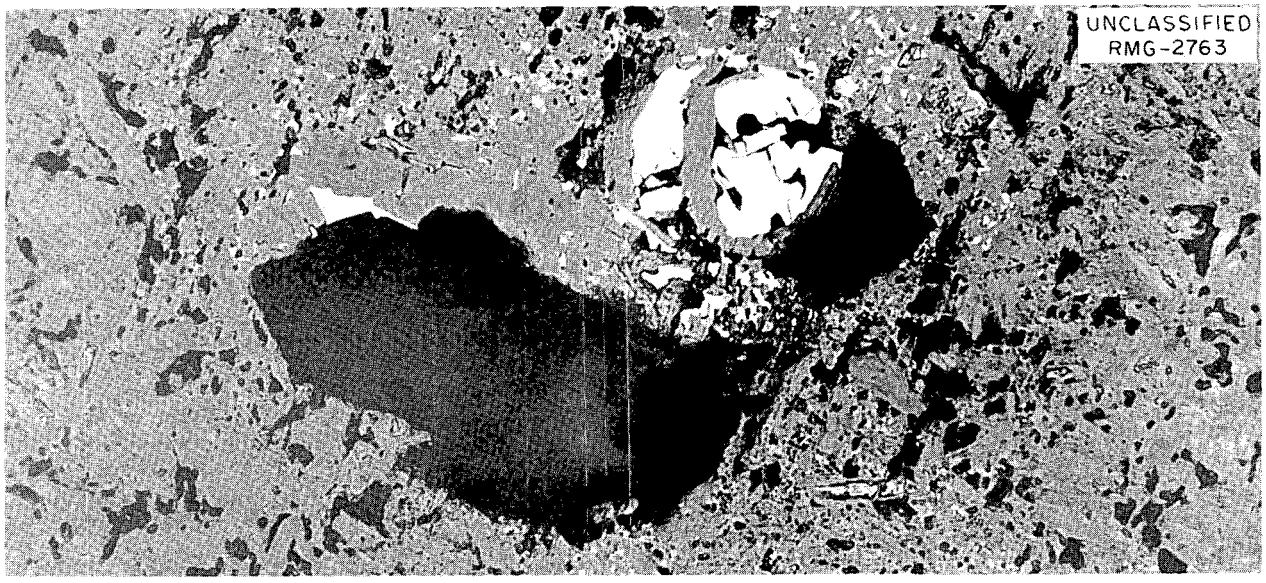

Fig. 19.12. Area Typical of an Unirradiated UC_2-Dispersed-in-Graphite Fuel Pellet. The light particles are UC_2. As polished. 250X.

Metallographic Examination of Thermocouples

D. M. Hewette II

Drift-test experiments are being performed by W. T. Rainey and R. L. Bennett[15] of the Reactor Chemistry Division to determine the long-time stability of Chromel-P–Alumel swaged thermocouples in contact with graphite in a helium atmosphere at 870°C. A swaged assembly having MgO insulation and a type 304 stainless steel protection tube drifted negatively. Metallographic examination[16] of this assembly revealed intergranular oxide attack in an area of the Chromel-P wire $9\frac{1}{2}$ to $10\frac{1}{2}$ in. from the hot junction. The resulting inhomogeneity due to the presence of the oxide could account for the error observed in the emf.

Postirradiation Examination of EGCR Prototype Capsules

E. L. Long, Jr.

Five of the eight group 1, ORR-irradiated capsules containing sintered pellets of UO_2 have been examined, and the results have been reported.[17] With the exception of one capsule, an acicular structure was found at the inside-diameter regions of the hollow UO_2 pellets (right-circular hollow cylinders). The needle-like structure is believed to be associated with the uranium nitride present in the UO_2 prior to irradiation. Less severe fracturing of the pellets and a lesser amount of the acicular structure were noted in pellets from one capsule, which contained a BeO rod that had been placed down the center of the stack of pellets.

Examination of Forced-Convection Loops (MSRP)

C. E. Zachary

Postoperational examinations were completed for INOR-8 piping exposed to molten-salt mixtures 134 (62 LiF–36.5 BeF_2–1 ThF_4–0.5 UF_4, mole %) and 135 (53 NaF–45.5 BeF_2–1 ThF_4–0.5 UF_4, mole %) in forced-circulation loops MSRP-6 and -7 respectively.[18,19] Both loops had operated for 20,000 hr at 1300°F. A surface film 2 mils thick

[15] *GCR Quart. Progr. Rept. Dec. 31, 1960*, ORNL-3049, p 312.

[16] *GCR Quart. Progr. Rept. Mar. 31, 1961*, ORNL-3102, pp 235–39.

[17] *Ibid.*, pp 163–74.

[18] *Met. Div. Ann. Progr. Rept. Sept. 1, 1959*, ORNL-2839, pp 150–53.

[19] *Met. Div. Ann. Progr. Rept. July 1, 1960*, ORNL-2988, pp 199–208.

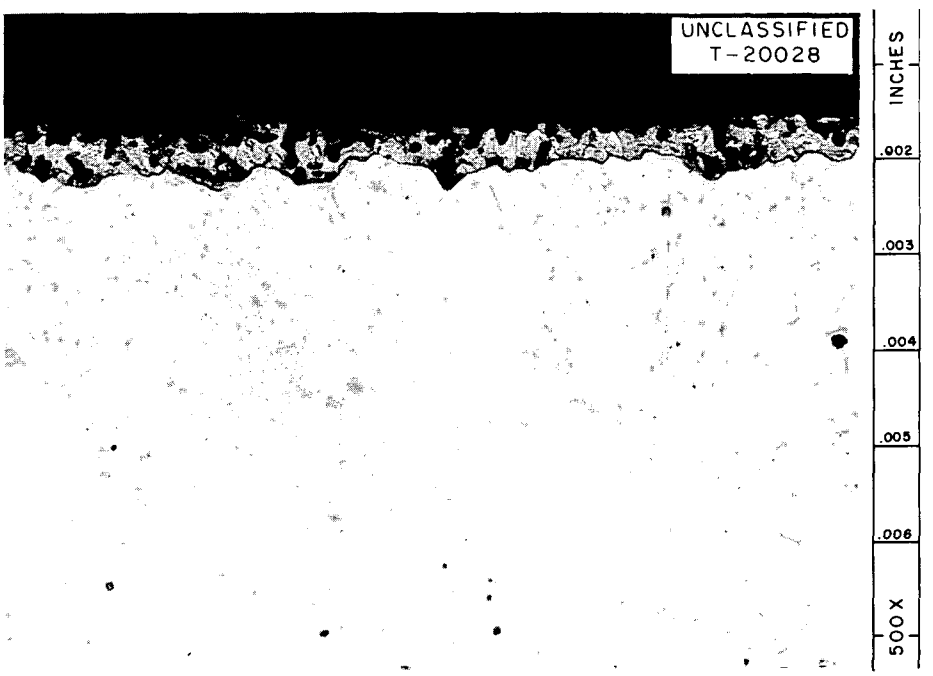

Fig. 19.14. Corrosion Product and Film Found on Inside Surface of INOR-8 Hot Zone After 20,000 hr at 1300°F with Fuel 134. As polished.

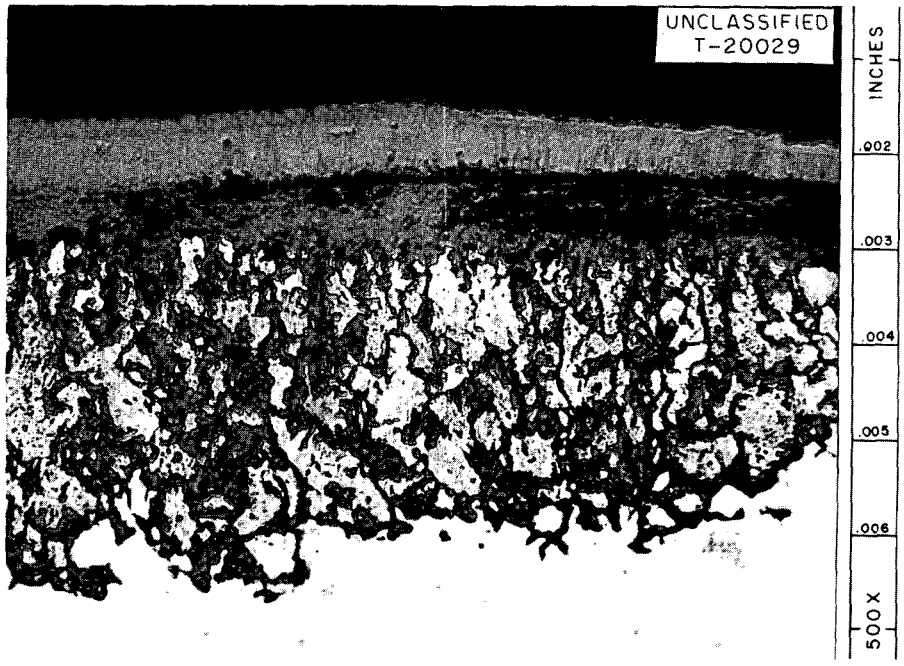

Fig. 19.15. Oxidation Found on Outside Surface of INOR-8 After 20,000 hr at 1300°F with Fuel 135. As polished.

was detected in the piping of loop MSRP-9, and a globular corrosion product was concentrated in the thicker part of the film, as shown in Fig. 19.14. Examination of the outside surfaces showed scattered areas of oxidation in some sections of the loops. The deepest oxidation noted, in loop MSRP-7, was about 5 mils and is shown in Fig. 19.15.

Examination of Heat-Flux-Corrosion-Test Samples

T. M. Kegley, Jr.

The heat-flux corrosion test was developed by the Corrosion Group of the Reactor Chemistry Division to simulate the high heat flux and corrosion conditions expected in the High Flux Isotope Reactor (HFIR). In the test, water is circulated through an aluminum flow-channel specimen which is resistance heated by means of a high-amperage current. A hindrance to the removal of heat is the formation of an oxide layer on the flow-channel specimen. Metallography provides a convenient means for the direct measurement of the oxide thickness as well as for revealing evidence of localized corrosion.[20]

Flow-channel specimens from 14 runs of the heat-flux corrosion test were examined, and the results have been reported in part.[21] To illustrate some of the data obtained, Fig. 19.16 shows a plot of the thickness of the oxide layer at the inner surface vs the distance from the flow-channel outlet for two runs of the test. The figure also indicates the decrease in the thickness of the oxide layer brought about by changing the pH of the circulating water from 7 to 5 by nitric acid addition.[22]

---

[20] *Met. Div. Ann. Progr. Rept. July 1, 1960,* ORNL-2988, pp 394–95.

[21] J. C. Griess *et al., Effect of Heat Flux on the Corrosion of Aluminum by Water. Part II. Influence of Water Temperature, Velocity, and pH on Corrosion-Product Formation,* ORNL-3056 (Feb. 1961).

[22] *Reactor Chem. Div. Ann. Progr. Rept. Jan. 31, 1961,* ORNL-3127, pp 79–80.

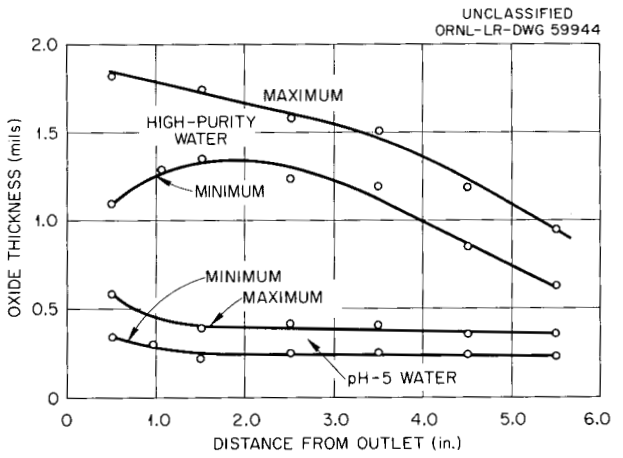

Fig. 19.16. Oxide Thickness as a Function of Distance from Outlet for Type 1100 Aluminum Flow-Channel Specimens Exposed to High-Purity Water and pH-5 Water. The average minimum and maximum thicknesses for each distance are plotted. Test conditions: duration, 240 hr; inlet water temperature, 66°C; outlet water temperature, 88°C; flow rate, 33 fps (high-purity water run) and 35.6 fps (pH-5 water run).

Examination of N.S. "Savannah" Piping

R. S. Crouse

During an in-place inspection of type 304 stainless steel piping utilized in the primary coolant system of the N.S. "Savannah" reactor at the construction site, some sections exhibited what appeared to be small cracks. The suspect areas and insulation had been wetted, due to leaks at joints and valves during hydraulic testing. Since the insulation contained leachable chlorides, responsible persons feared that chloride-induced stress-corrosion cracking might have occurred. A piece of the pipe was submitted for examination by the Metallography Group.

Two small defects were found by metallographic examination, and they appeared to be incipient stress cracks. Figure 19.17 shows a typical defect. Other fabrication defects were found and reported to be possible sites of crack initiation, since conditions existed that could promote stress-corrosion cracking.

As a result of the investigation, recommendations were reported to prevent the recurrence of

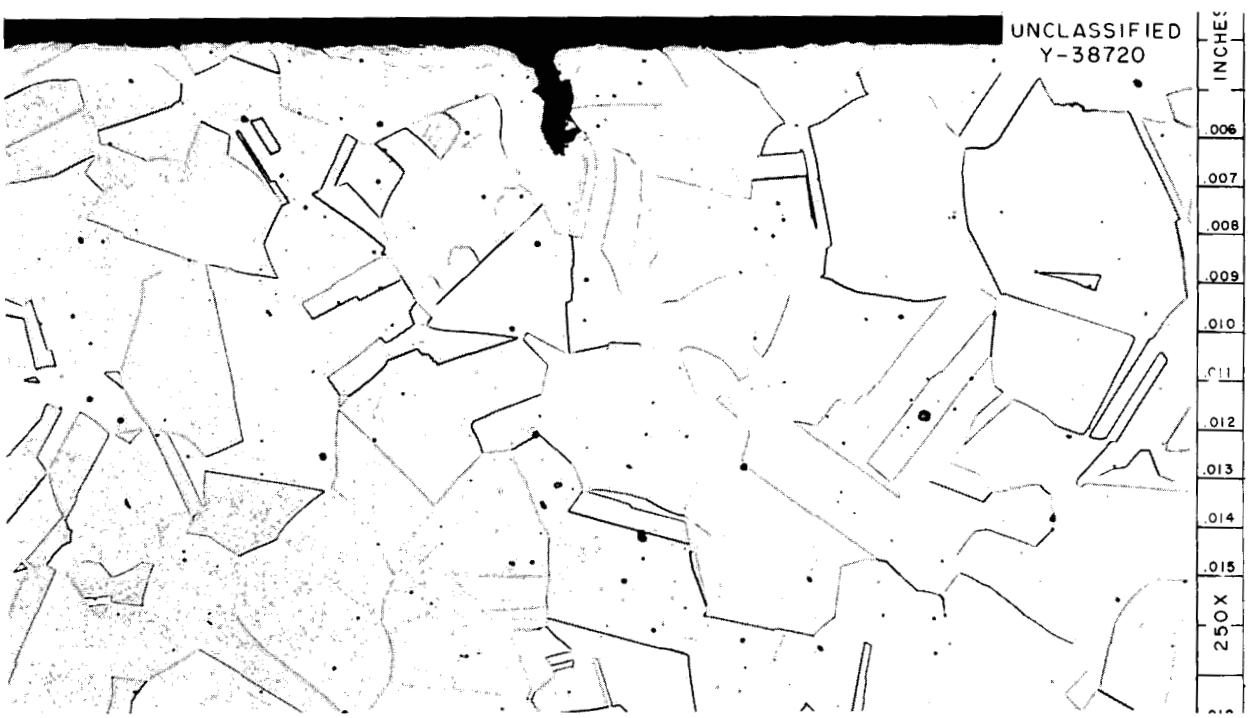

Fig. 19.17. Incipient Stress Crack in N.S. "Savannah" Piping. Etchant: aqua regia.

this situation. These data and recommendations were presented for consideration at a meeting between personnel from ORNL, Ebasco Services, AEC-MARAD, Babcock and Wilcox, and New York Shipbuilding Corporation.

An ORNL report (ORNL-3146) is to be issued in the near future. It will contain the metallographic and chemical data on the insulation and some further stress-corrosion tests on samples of the pipe.

Thermal Expansion of Uranium–10% Molybdenum Alloy

J. R. Riddle

The linear thermal expansion of a γ-quenched U–10 wt % Mo casting has been determined over the temperature range 25 to 600°C. The purpose of this study was to provide engineering data for design of the Fast Burst Reactor. The data of Fig. 19.18 show the average of ten heating and cooling curves obtained on two samples prepared from a single casting. Although the materials were in a metastable state over a portion of the temperature range, there was no indication that dimensional changes were occurring in the materials as a result of thermal cycling.

Thermal Expansion of Stainless Steel–UO_2 Compact

J. R. Riddle

For engineering design purposes, the linear thermal expansion of type 347 stainless steel containing a dispersion of 35 wt % UO_2 was determined over the temperature range 25 to 800°C to assist Atomic Power Development Associates in the design effort on core B of the Fermi Fast Breeder Reactor program. The data were obtained on two samples sectioned from fuel plate F-115 to show the expansion behavior in directions longitudinal and transverse to the rolling direction. As shown in Fig. 19.19, the expansion of this material is only slightly directional. A comparison of these curves with that for type 347 stainless steel (also shown in Fig. 19.19) indicates that the UO_2-bearing materials expand about 9% less than type 347 stainless steel.

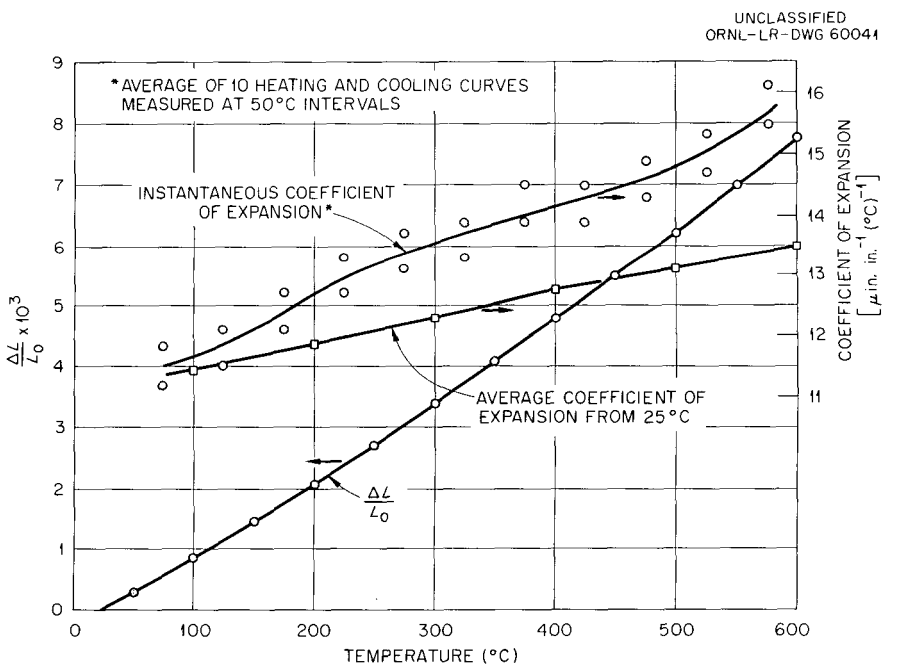

Fig. 19.18. Linear Thermal Expansion of γ-Quenched U–10 wt % Mo Casting. Aged 24 hr at 900°C in vacuum and water quenched.

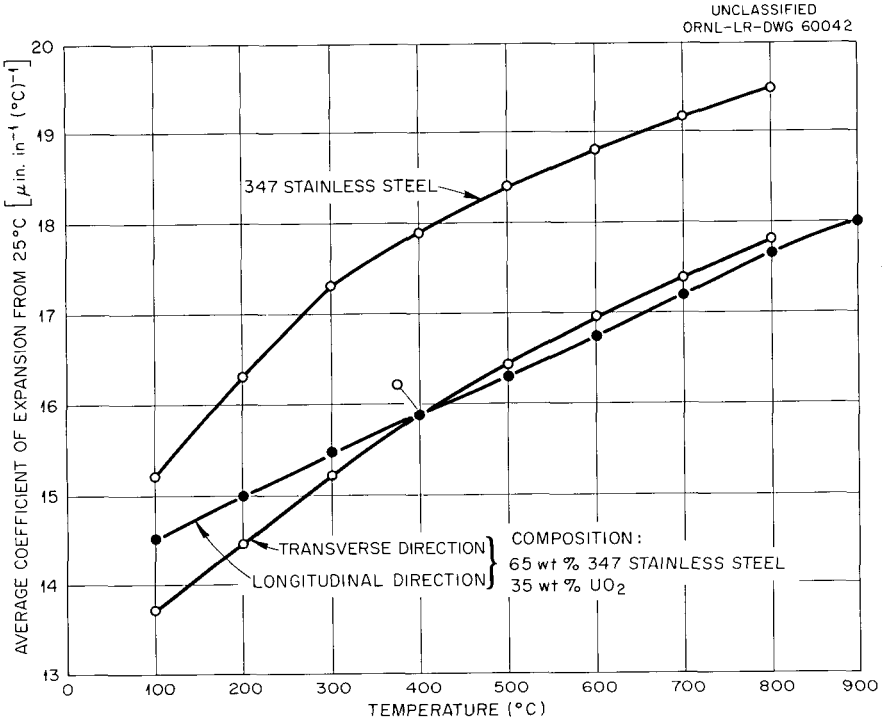

Fig. 19.19. Effect of UO_2 Dispersion on the Linear Thermal Expansion of Type 347 Stainless Steel.

Metallography of Yankee Prototype Fuel Element

R. S. Crouse

The Metallurgy Division was requested by the Chemical Technology Division to tensile test and examine metallographically a simulated Yankee prototype fuel element. The element consisted of a bundle of 36 Al_2O_3-filled type 304 stainless steel tubes brazed in a square configuration, with electroless-nickel-plated ferrules. The bundle was brazed for 3 hr at 1875 ± 25°F by Westinghouse Atomic Power Division. The Mechanical Properties and Metallography Groups collaborated in this effort.

The breaking strength of the joints was recorded in pounds pull and varied from 189 to 450 lb. The microstructures were found to be similar to those reported.[23] Figures 19.20 and 19.21 represent typical joints where failure occurred in the braze metal and in the ferrules respectively. Failure in the braze metal was due to a continuous network of a brittle nickel-phosphorus phase. Failure of a ferrule occurred when the nickel-phosphorus phase was discontinuous and a ductile nickel phase made up the center of the joint.

At a later date, two other test arrays of similar design were examined by metallography. These represented the first two attempts by Ferrotherm of Cleveland to fabricate such arrays for the Chemical Technology Division.

About half of the joints in the first array were found to be faulty, which was attributed to poor assembly for brazing. The second array was superior in number of sound joints and over-all integrity, although about one-fourth of these joints were unsound.

[23] J. T. Lamartine and W. C. Thurber, *Status Report — Application of Electroless Nickel Brazing to Tubular Fuel Elements for the N.S. Savannah*, ORNL CF-59-6-55 (June 2, 1959).

Fig. 19.20. Typical Failure in Braze Metal of Tensile-Tested Yankee Prototype Fuel Element. Etchant: 5% CrO_3, electrolytic. Reduced 21%.

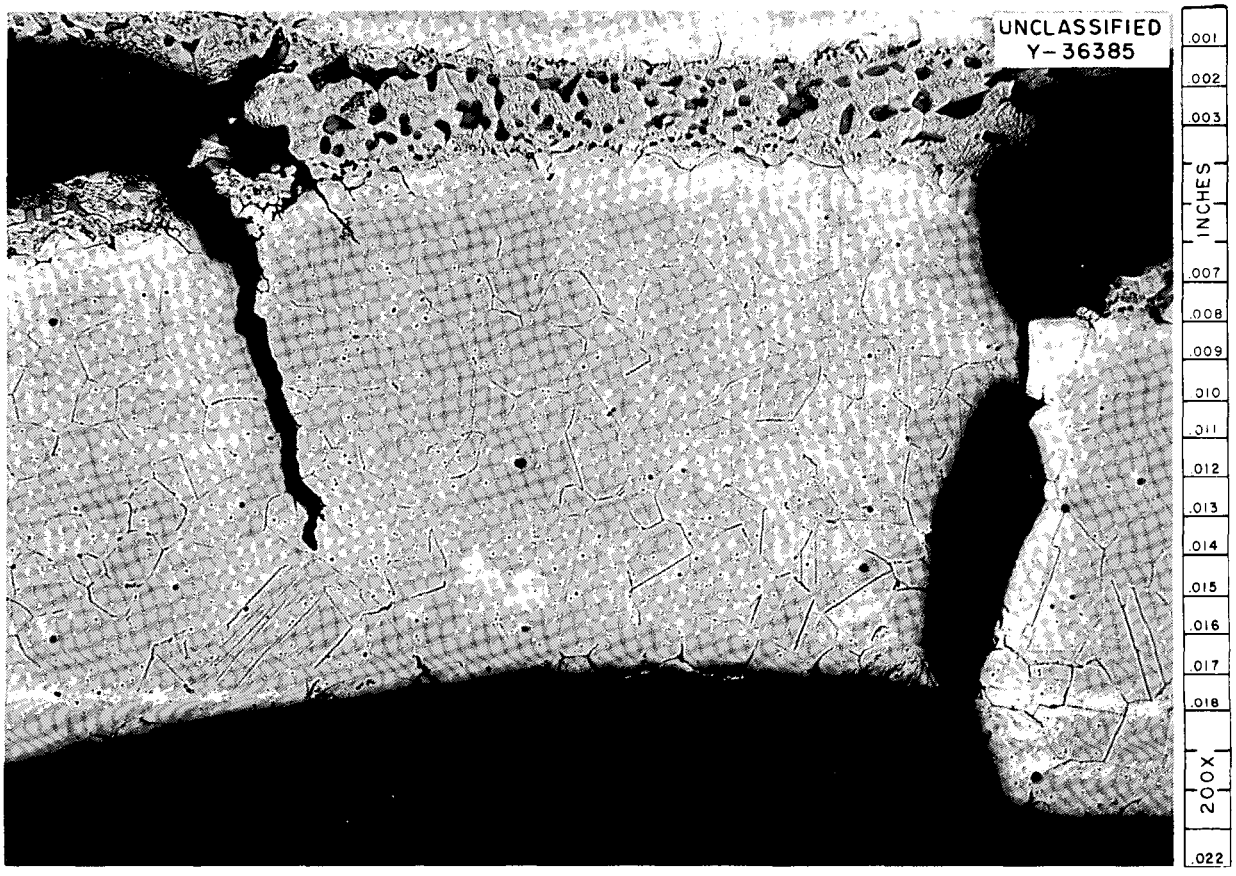

Fig. 19.21. Failure of Ferrule Tube Wall in Tensile-Tested Yankee Prototype Fuel Element. Etchant: 5% CrO_3, electrolytic.

Examination of Spherical Uranium Carbide

C. K. H. DuBose

In support of the Pebble Bed Reactor Program, as-received pyrolytic-carbon-coated and uncoated uranium carbide spheres have been examined metallographically. These two different uranium carbide products were utilized in the fabrication of two types of graphite-fuel compacts, which were also examined and compared.[24]

All samples were polished on the Syntron vibratory polisher, using a nylon cloth with a Linde A (0.3-μ alumina)-graphite-silicone oil slurry. The addition of the graphite assists in obtaining a satisfactory as-polished surface in a single-step polishing operation. The resulting structure is shown in Fig. 19.22.

Due to differences in thermal expansions, a small void was produced in the area between the UC-UC_2 particle and its coating, thus making retention of the particle quite difficult. Metallographic examination of uncoated UC-UC_2 spheres fabricated in graphite at 1000°C showed complete reaction of the UC-UC_2 along the outer edge of the pellet. This reaction is possibly caused by an oxidizing gas given off during firing, and the gas probably comes from the binder used in the graphite. The reaction product was extracted for x-ray studies and was shown to be UO_2.

No gross reaction was noted of the pyrolytic-carbon-coated UC-UC_2-graphite fuel bodies. In some few cases where the pyrolytic carbon coating had cracked open, exposing the UC-UC_2 sphere, a reaction product, $U_{0.88}O_{2.12}$, was detected.

[24]Also see J. M. Kerr, "Ceramics Technology," chap. 13, this report.

Fig. 19.22. Polarized-Light Illumination of Polished Cross Section of Pyrolytic-Carbon-Coated UC-UC_2 Spheres. The uranium carbide was etched with 1:1:1 H_2O, CH_3COOH, HNO_3. Reduced 30%.

Metallographic Examination of Oxygen-Injection Valves

T. M. Kegley, Jr.

Two valves which regulated the flow of oxygen to the HRT system became inoperable. They were examined metallographically to determine the cause of failure. One valve contained a Zircaloy-2 core and the other a tantalum core. The Zircaloy-2–stainless steel valve had operated 11 months at 360°C; the tantalum–stainless steel valve had operated six months at 400°C. Examination of both valves showed that the annulus between the valve body and the inner core was completely filled with oxide. Figure 19.23 shows the oxide-filled annulus in the tantalum–stainless steel valve and the platelets of Ta_2O_5 that extend into the tantalum core. Microhardness measurements, as plotted in Fig. 19.24, indicated that the tantalum had been hardened by oxygen diffusion to a depth of about 35 mils.

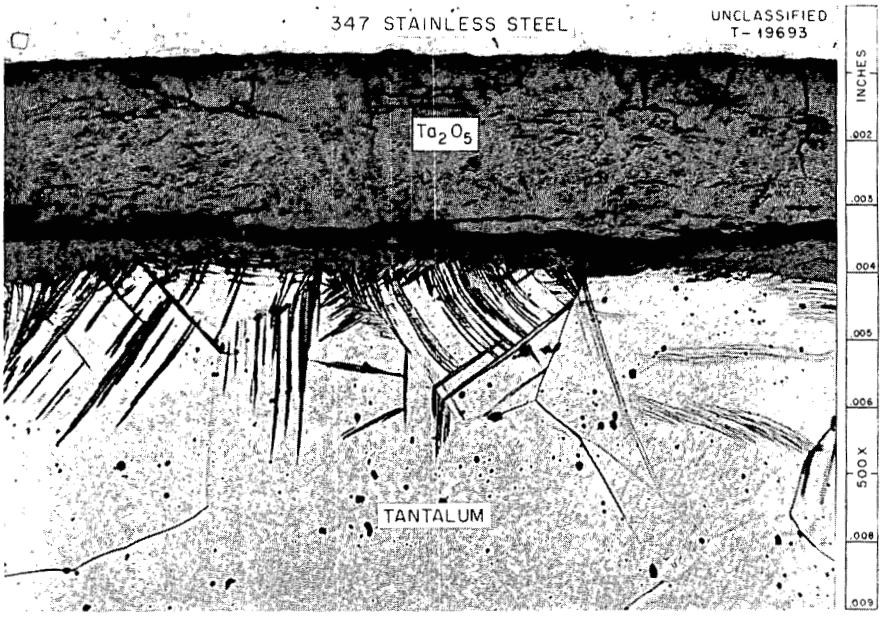

Fig. 19.23. Annulus Between Tantalum Inner Core and Stainless Steel Valve Body of Thermally Controlled Oxygen Injection Valve. Etchant: 5g NH_4F, 25 ml HF, 25 ml H_2O. Reduced 30%.

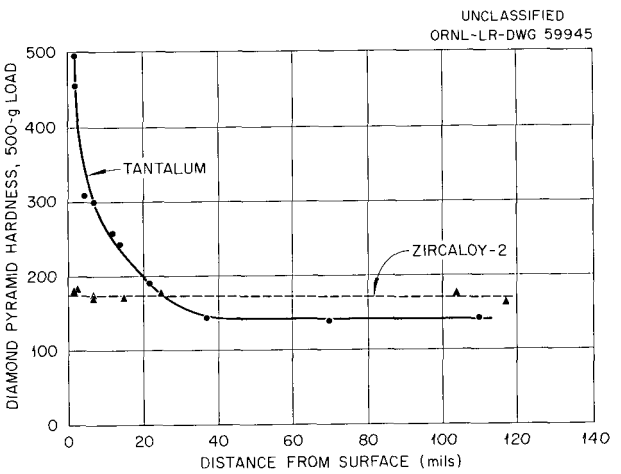

Fig. 19.24. Microhardness of Inner Cores of Thermally Controlled Oxygen Injection Valves as a Function of Distance from Surface.

Metallographic Examination of UO_2-ThO_2-BeO Pellets

C. K. H. DuBose

A pellet consisting of 13 vol % UO_2, 13 vol % ThO_2, and 74 vol % BeO and prepared by sintering at 1750°C in hydrogen for 1 hr was metallographically processed to determine optimum techniques of preparation for microstructural analysis and was examined for phase identification.[25] This material is of interest as a fuel for breeder reactors.

The purpose of the work was to obtain reference information that could be utilized during postexamination of irradiated samples. It was found that the sample could be polished successfully by remote vibratory polishing techniques. Examination of the microstructure revealed three phases: free BeO, a solid solution of ThO_2-UO_2, and a small amount of free UO_2.

[25] *GCR Quart. Progr. Rept. Mar. 31, 1961*, ORNL-3102, pp 99–104.

20. NONDESTRUCTIVE TEST DEVELOPMENT

R. W. McClung

Nondestructive test methods which have long been used by industry for routine quality control are not adequate for many inspection problems in the field of nuclear energy. For instance, industry has not been faced with the problem of inspecting the very thin sections of material such as are required by the nuclear industry for cladding material and small-diameter tubing. The extreme service conditions associated with nuclear reactors have necessitated the establishment of much tighter quality requirements on discontinuities and dimensions than are encountered in commercial practice. Further, there has been an increasing use of new and different material on which there has been little or no inspection performed. For these reasons, considerable effort has been expended toward the improvement of existing techniques and the study of other phenomena which offer developmental promise. The program includes ultrasonic and electromagnetic methods and penetrating radiation. Particular emphasis has been given to the application of these and other methods to the evaluation of such "problem" materials as beryllium and graphite and to the establishment of remote inspection techniques for use in high-level irradiation areas. In addition, applications have been made to specific problems associated with several reactor projects.

ULTRASONIC TESTING METHODS

R. W. McClung K. V. Cook

Most of the ultrasonic development work has been directed toward studies of ultrasonic testing of thin metal sections and the properties of ultrasound, with particular emphasis on the detection of nonbonded areas. This has included the evaluation of braze bonds of stainless steel tubing and sheath-to-copper disks, the inspection of flat-plate fuel elements, and the testing of the bond in duplex and triplex tubing.

Stainless Steel–to–Copper Braze Bonds

One of the items for bond evaluation was a stainless steel tube surrounded by an annular copper disk which in turn was canned in a stainless steel sheath. The copper-to-steel interfaces were braze bonded. It was determined that a Lamb-wave technique would best locate nonbonded areas in the braze between the $\frac{3}{8}$-in.-OD stainless steel tube and the large copper block. A Lamb-wave probe was constructed, and a technique was developed which was capable of detecting nonbonded areas approx $\frac{3}{16}$ in. long $\times$ $\frac{1}{16}$ in. wide. This probe was used to collect data on a number of samples. After the samples were sectioned, both frost and peel tests were applied. Correlation of the three tests was very good.

An ultrasonic "ringing" technique was established for the nondestructive inspection of the braze between the 0.065-in.-thick type 304 stainless steel "can" surrounding the copper cylinders. Calibration tests demonstrated that nonbonded areas of approx $\frac{3}{32}$-in. diam could be detected. However, when the ringing technique was applied to a large test piece, difficulties were encountered due to thickness variations of the stainless steel can. These large variations in thickness were caused by a light machining operation which was done in order to remove excess braze material from the outer surface. However, a slower ultrasonic resonance technique was successful on this test piece.

Fuel Plates

Modification of the tube-scanning tank[1] allowed the ultrasonic through-transmission detection of nonbonds in flat fuel plates. The ultrasound was beamed horizontally through the plate thickness as the chain drive moved the fuel plate past the fixed search tubes at longitudinal scanning speeds of

[1] R. B. Oliver, R. W. McClung, and J. K. White, *Immersed Ultrasonic Inspection of Pipe and Tubing*, ORNL-2254 (May 2, 1957).

150 to 200 in./min. Vertical indexing of the search tubes between successive longitudinal scans was accomplished manually by means of the cross-feed mechanism of a small lathe. The size of the index was determined in part by the size of the nonbond being sought. Design and construction of a more permanent semiautomatic facility are in progress.

Nonbond reference standards for fuel plate inspection were developed. In early attempts, Al_2O_3 and mica were introduced into the core-clad interface before fuel plate fabrication. However, small reproducible nonbonded areas were not achieved by these methods. Successful standards have been made by milling small flat-bottom holes in finished fuel plates. The holes are then plugged with a suitable material to prevent sound transmission through that area. Nonbonded areas, $\frac{1}{16}$ in. in diameter, have been readily detected on U-Al alloy plates such as are being used for the High Flux Isotope Reactor (HFIR). The localized inhomogeneities of UO_2–stainless steel cores have reduced the sensitivity to the identification of $\frac{1}{8}$-in.-diam nonbonds.

Duplex Tubing

A through-transmission ultrasonic technique was developed for the evaluation of duplex tubing. As an example, such tubing might consist of an outer layer of type 446 stainless steel 0.040 in. in thickness, a thin barrier of copper, and an inner tube of niobium some 0.030 in. in thickness. Tubing of this type was fabricated with various inside-diameter and thickness dimensions. This technique, as applied to such tubing, required the construction of a probe-type transmitting crystal which fitted into the inside diameter of the duplex tubing, and a collimated receiver crystal. Both crystals were fixed in reference to each other; however, the combination moved longitudinally along the tube as it was rotated. Areas of discontinuities were compared with indications from a $\frac{1}{16}$-in.-diam flat-bottom hole, and selected metallographic sections were taken. There was good correlation between test data and actual conditions.

EDDY-CURRENT METHODS

Spacing Measurements

C. V. Dodd R. W. McClung

The requirement for accurate measurement of the close-tolerance coolant-channel spacing in fuel elements has led to the development of new eddy-current techniques[2] to accomplish these measurements. Most of the emphasis has been on channel spacing for flat-plate fuel elements, with test systems being developed for fabrication development as well as for postirradiation hot-cell examination. However, consideration has been given to inter-rod spacing for tubular fuel elements and the measurement of tubing inner diameter. A topical report is being prepared on this development project.

Broad-Band Eddy-Current Test Equipment

C. V. Dodd

A basic eddy-current test system has been constructed. This prototype can be electrically balanced over a large range of test frequencies, and it can monitor both amplitude and phase of the output voltage. A block diagram of this system is shown in Fig. 20.1. It will be used in basic eddy-current studies and for special applications requiring a particular frequency. Most eddy-current equipment designed in the past has operated only at discrete frequencies.

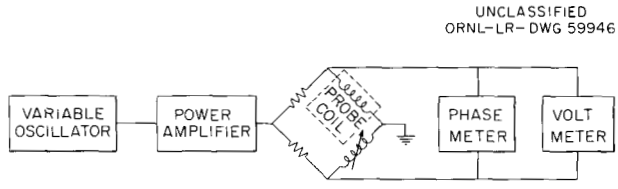

Fig. 20.1. Block Diagram of Prototype Broad-Band Eddy-Current Instrument.

Probe-Coil Field Measuring Device

C. V. Dodd

Studies are being made of the induction field of probe coils in order to improve the sensitivity of eddy-current systems for various inspection problems. The coil to be tested is clamped on a lathe bed. The pickup probe is mounted on the lathe cross feed, and the field is measured as the probe is moved in an x-y plane. The pickup probe contains two orthogonal coils to detect the axial and radial components of the magnetic field. The output of these coils is fed through two matched

[2] *Met. Div. Ann. Progr. Rept. July 1, 1960*, ORNL-2988, pp 409–11.

amplifiers to the horizontal and vertical inputs on an oscilloscope. The scale on the oscilloscope has been graduated in polar coordinates. Thus, the amplitude and direction of the magnetic field are read directly. Figure 20.2 is a block diagram of this system.

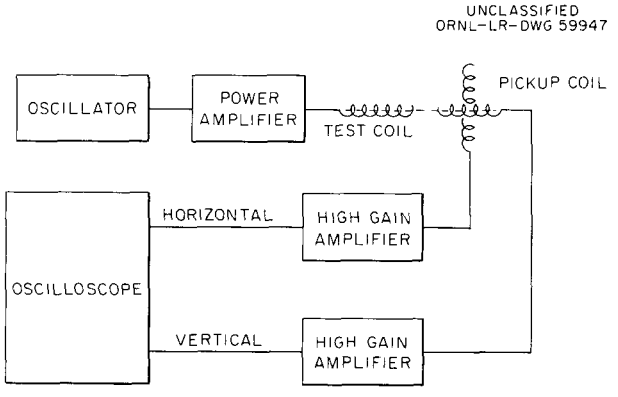

Fig. 20.2. Block Diagram of Probe-Coil Field Measuring System.

PENETRATING-RADIATION METHODS

Low-Voltage Radiography

R. W. McClung

The study of low-voltage radiographic conditions[3] has continued with exhaustive exposure data being taken on very thin sections of steel and aluminum and on thin sections of beryllium. The conditions which have been varied during this program are the input kilovoltage (energy of the x-ray beam), the specimen thickness, and the intermediate atmosphere between the x-ray tube head and the specimen. Attention has been concentrated thus far on the lower end of the 0- to 50-kvp energy band, with the specimen thickness ranging from 3 to 24 mils of type 1100 aluminum, from 1 to 6 mils of type 304 stainless steel, and from 20 to 240 mils of beryllium. The program will be extended to include graphite and thicker sections of aluminum, stainless steel, and beryllium up to the full capabilities of 50 kvp. Evaluation of the exposure data is not yet complete.

Contrast sensitivities (the ability to detect a percentage thickness change) have been considerably better than had been anticipated. For example, sensitivities as small as 0.12% were obtained on 12 mils of aluminum at an energy of 12.5 kvp, using a helium intermediate atmosphere. The poorest sensitivity noted thus far with aluminum has been 0.9% for an energy of 48.5 kvp, a 3-mil thickness, and an air atmosphere. Use of the air atmosphere results in reduced contrast sensitivity. These values have been calculated from the observed film-density change for a given specimen-thickness change. The minimum detectable film-density variation is 0.006.[4] Calculations have been made on the relative absorption of aluminum as compared with stainless steel over the 0 to 50 kvp range. Figure 20.3 shows the thickness of aluminum which has the same x-ray absorption as 1 mil of steel for different energies and both helium and air atmospheres.

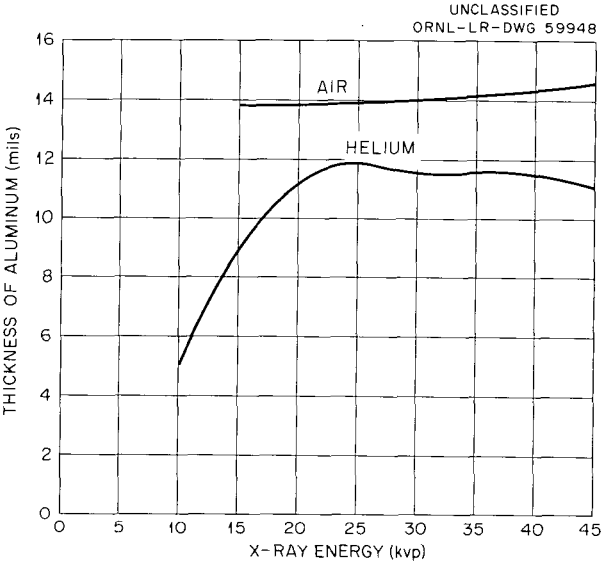

Fig. 20.3. Aluminum Thickness for X-Ray Absorption Equal to that of 0.001 in. of Type 304 Stainless Steel.

X-Ray Attenuation Coefficients

J. W. Evans[5] B. E. Foster[6]

A study of x-ray attenuation coefficients by scintillation spectrometry has been in progress on various alloy materials associated with power,

[3] R. W. McClung, *Met. Div. Ann. Progr. Rept. July 1, 1960*, ORNL-2988, pp 413–15.

[4] R. Meakin, "Scattered Radiation," *A Further Handbook of Industrial Radiology*, Edward Arnold, Ltd., London, 1957.

[5] On loan from ORINS.

[6] On loan from Instrumentation and Controls Division.

compact, and research reactors. Materials examined have been types 304 and 347 stainless steel, Zircaloy-2, 1100 aluminum, and enriched (93% U^{235}) uranium-aluminum alloys containing 7.0, 18.6, and 24.8% uranium by weight. As a result of this work, both experimental and theoretical absorption curves have been determined for the range 50 to 130 kev. These data will be useful for various thickness, density, or homogeneity measurements. A topical report is being prepared on this program.

Density Measurement of Fuel Rods by Gamma-Ray Absorption

B. E. Foster[6]

In support of the fuel-cycle program (vibratory compacted fuel rods), there is a need to observe the effect of several variables on the packing density and to correlate this with position along the fuel rods.

The likely types of rods involved are aluminum- and zirconium-base alloys and austenitic stainless steel. The individual rod sizes vary from $\frac{1}{4}$-in. OD to $\frac{3}{4}$-in. OD, with wall differences of 0.005 to 0.040 in. The rod lengths vary from 2 to 8 ft. The type of fuel to be compacted is ThO_2, UO_2, UC, and UN, with compaction resulting in densities in the range of 80 to 95% of theoretical densities.

The electronics portion of the system which has been chosen for making these density determinations consists of an NaI(Tl) crystal, photomultiplier tube, linear amplifier and pulse-height discriminator, linear count-rate meter, Brown recorder, and high-voltage supply all assembled as a conventional scintillation spectrometer (Fig. 20.4). Cesium-137 probably will be used as the gamma-ray source. The components have been purchased and the apparatus is being assembled.

The preliminary development stages will include equipment calibration and determination of equipment sensitivity, using reference standards and rods of different sizes. After preliminary development, attention will be given to the design and construction of an appropriate scanning mechanism. Consideration will be given to reasonable scanning times and the accuracy of density measurements for both experimental- and production-loaded tubes.

Gamma-Scintillation Spectrometry

B. E. Foster[6]

The work on gamma-scintillation spectrometry has been continued.[7] A calibration of the scintillation equipment was made for the assay of U^{235}

[7] *Met. Div. Ann. Progr. Rept. July 1, 1960*, ORNL-2988, pp 418–19.

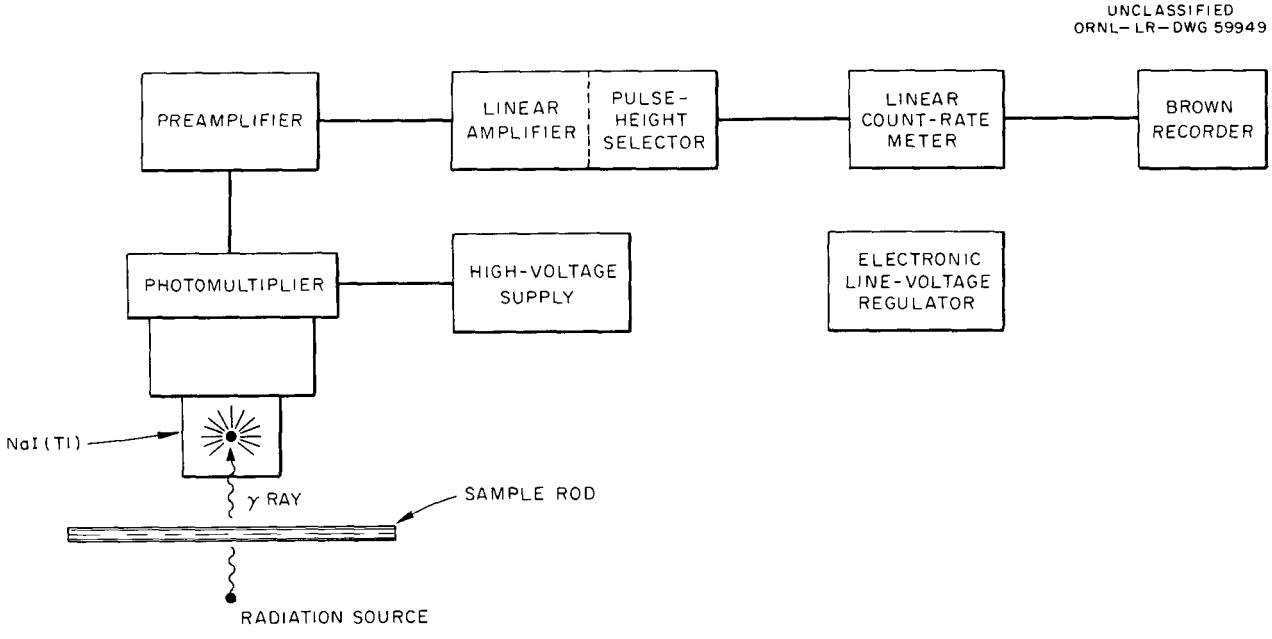

Fig. 20.4. Block Diagram of Gamma-Scintillation Spectrometer Adapted for Fuel-Rod Density Measurements.

in 18.65% U–Al alloy core blanks, using data from the Analytical Chemistry Division on a number of single core blanks. A heat of 72 cores was measured, and, from the calibration curve, it was determined that an average of 10.2 g U^{235} was present per core. This disagreed with the calculated 10.53 g per core according to the dip analysis. Studies are in progress to determine the reason for the discrepancy. A new heat of 72 cores was acquired and measured. Five of these blanks were sent to the Analytical Chemistry Division for U^{235} analysis. Four of the five blanks coincided very well with the original calibration curve. These data are being analyzed, and a determination of statistical accuracy is being made.

PROBLEM MATERIALS

R. W. McClung

Considerable effort has been directed toward the development of nondestructive tests for the evaluation of materials which are unusually difficult to inspect. Most of the attention has been directed toward beryllium, graphite, and graphite coatings.

Beryllium

Most of the inspection development for beryllium products has been limited thus far to thin-wall small-diameter tubing.[8] The developments have included techniques for low-voltage radiography, ultrasonics, penetrants, and eddy currents. Among the problems which had to be overcome were the extremely low radiation absorption and the very high velocity of ultrasound. The results of the techniques include the detection of cracks, pits, pinholes, extrusion marks, gouges, and foreign material contamination, as well as the measurement of wall thickness and inner diameter. Current work is directed toward improving the sensitivity of the preliminary techniques and developing the necessary tests for the evaluation of finned tubing.

Graphite

Preliminary tests have been developed for several different inspection problems on graphite and graphite components. Among the components have been small-diameter graphite tubing, large graphite cylinders,[9] specimens for destructive testing, uranium-bearing graphite fuels, and coatings on graphite.[10] Applicable methods thus far have been low-voltage radiography, eddy currents, and electrode potential testing. The low radiation absorption characteristics of the graphite have required the use of very low x-ray energies. The variation in the low electrical conductivity, which was intensified by changes in orientation, has created serious problems for the attainment of sensitive eddy-current inspection. However, despite these and other problems, a number of useful evaluation techniques have been developed and used in specific configurations.

REMOTE INSPECTION TECHNIQUES

R. W. McClung K. V. Cook

Measurement of Homogeneous Reactor Test Core-Vessel Wall Thickness

A survey of the wall thickness in the 90° and 30° cones beneath the spherical portion of the Homogeneous Reactor Zircaloy-2 core vessel has been made, using a pulse-echo ultrasonic technique. These measurements were made during the reactor shutdown period, with the same ultrasonic technique and instrumentation[11] that was used on the last series of measurements of the spherical vessel. A different mechanical jig had been designed which retained the transducer near the axis of the vessel. Adjustment of the crystal alignment and selection of the inspected area were accomplished by adjusting the vertical angle of the transducer, rotating the axial jig, and raising or lowering the jig. A number of measurements were made in both cones, but the uneven surfaces and the presence of screen stubs prevented a complete choice of areas to be measured. Thicknesses ranged from a low of about 0.340 in. up to about 0.358 in. in the 90° cone and from about 0.350 in. to about 0.365 in. in the 30° cone.

[8] R. W. McClung, "Development of Nondestructive Testing Techniques for Thin-Wall Beryllium Tubing," submitted to the *Journal of the Institute of Metals.*

[9] R. W. McClung and R. A. Nance, *Development of Nondestructive Tests for the Experimental Gas-Cooled Reactor Fuel Element*, ORNL-3059, pp 16–18 (Feb. 16, 1961).

[10] Will be reported in *Gas-Cooled Reactor Project Quarterly Progress Report for Period Ending June 30, 1961.*

[11] *Met. Div. Ann. Progr. Rept. July 1, 1960*, ORNL-2988, pp 416–17.

GAS-COOLED REACTOR SUPPORT PROGRAM

R. W. McClung K. V. Cook

Development work has continued on a number of varied problems in the Experimental Gas-Cooled Reactor (EGCR) Program. Among these have been inspection of coatings on graphite, remote inspection of experimental loop through-tube weldments, and nondestructive evaluation of beryllium tubing.

In addition, considerable time was spent in preparing a development report[12] and assisting in the preparation of specifications[13] for acceptance tests for the EGCR fuel assembly.

Coatings on Graphite Sleeves

The inspection problems for graphite coatings on the EGCR fuel-assembly support sleeve included the measurement of coating thickness and the evaluation of coating integrity. A tentative eddy-current technique[14] has been developed for the thickness measurement of silicon carbide or siliconized silicon carbide coatings. The accuracy of the calibration appears to be ±0.001 in. or better. A number of measurements have been made on coatings supplied by several manufacturers. Metallographic studies are in progress to determine the actual test accuracy.

An electrode-potential technique[14] has been developed for the detection of flaws in the Si-SiC coating on type 901S graphite which is being considered for the EGCR graphite sleeve. The method establishes a galvanic cell between the test specimen and a suitable electrode in the presence of an electrolyte. By monitoring the generated voltage, it is possible to determine whether or not the graphite is exposed through the coating.

Experimental Loop Through-Tube Weldments

A study was made to determine the applicability of various inspection techniques for the evaluation of the through-tube weldments. Both V-notch and fillet-weld configurations were considered, but most of the recent work has been directed toward the fillet weld because of the apparent trend toward its use. Test methods which have been considered or examined include ultrasonics,[15] radiography,[16] and gaseous leak tests. The most useful technique has been radiography. Experiments have been devised to simulate the expected radiation background at the weld position with no adverse effects.[17] The principal problem has been the poor geometrical relationship which was necessary between the radiation source, the weld, and the film.

Beryllium Tubing Evaluation

Nondestructive evaluation has continued[18–21] on the small-diameter beryllium tubing that has been received from American, British, and French sources. This tubing was manufactured by a number of different machining and extrusion techniques. The test techniques have included low-voltage radiography, penetrants, ultrasonics, eddy currents, air gaging, and helium-leak testing. The most common objectionable conditions have been excessive wall-thickness variations and the presence of foreign material contamination and of inner surface pitting. Detailed evaluation reports are being prepared on this tubing.

FERMI PROGRAM

A series of studies has been conducted to determine the applicability of nondestructive testing techniques to the measurement or evaluation of certain desired properties in the core-B Fermi fuel element.

It was demonstrated that an eddy-current technique could be used to measure the clad thickness. Core-to-clad bonding was evaluated by an ultrasonic through-transmission test. Radiography and film densitometry were shown to be capable

[12] R. W. McClung and R. A. Nance, *Development of Nondestructive Tests for the Experimental Gas-Cooled Reactor Fuel Element*, ORNL-3059 (Feb. 16, 1961).

[13] *Specifications for Fuel Assemblies for Core I of the Experimental Gas-Cooled Reactor*, ORNL CF-60-11-90 (Dec. 9, 1960).

[14] *GCR Quart. Progr. Rept. Mar. 31, 1961*, ORNL-3102, pp 115–16.

[15] *GCR Quart. Progr. Rept. Dec. 31, 1960*, ORNL-3049, pp 226–28.

[16] *GCR Quart. Progr. Rept. Mar. 31, 1961*, ORNL-3102, pp 135–36.

[17] To be reported in *Gas-Cooled Reactor Project Quarterly Progress Report for Period Ending June 30, 1961.*

[18] *Met. Div. Ann. Progr. Rept. July 1, 1960*, ORNL-2988, pp 415–16.

[19] *GCR Quart. Progr. Rept. June 30, 1960*, ORNL-2964, pp 136–38.

[20] *GCR Quart. Progr. Rept. Sept. 30, 1960*, ORNL-3015, pp 101–2.

[21] *GCR Quart. Progr. Rept. Dec. 31, 1960*, ORNL-3049, pp 230–31.

of measuring core homogeneity. A special eddy-current technique was used to measure coolant-channel spacing. A topical report is being prepared on this feasibility study.

HIGH FLUX ISOTOPE REACTOR (HFIR) SUPPORT

R. W. McClung K. V. Cook
B. E. Foster

A large number of flat fuel plates were inspected by several techniques. These plates had been fabricated for use in the first critical assembly. The tests included determinations of core homogeneity, the location of the hump or thickest portion of the irregular core, and detection of nonbonded areas. Conventional radiographic techniques were used in the study of core homogeneity. The x-ray film was evaluated by the personnel who fabricated the plates.

A through-transmission ultrasonic technique was developed and used to evaluate approx 120 HFIR plates for nonbond conditions. Most of these plates were inspected with a sensitivity capable of detecting nonbonded areas equal to a $\frac{1}{16}$-in. diam. Results on the majority of the plates were recorded in a plan view, using an electrosensitive paper recorder. Most of the plates contained a few nonbonded areas; however, a number of these areas coincided with obvious surface blisters. Every observed blister was detected as a nonbonded area; however, there were nonbonded areas that were not blistered. The greatest number of blisters and nonbonds was observed at the core ends and edges. Since it was acknowledged that fabrication difficulties caused these rather localized defects, it was requested that more inspection emphasis should be placed on the clad bonding in the central portions of the plate, away from core ends and edges, in order to detect unexpected defects. Figure 20.5 is a photomicrograph of a large nonbond which was detected.

A technique was developed for the location of the hump in the core of the HFIR plates relative to a particular plate side and edge. Three methods were initially attempted, and all met with some degree of success. The following is a comparison of these methods.

1. Autoradiography successfully located the hump relative to both particular side and edge. This was a very reliable technique but was the slowest.
2. The total gamma-counting technique located the hump quite well but, with the readily available collimation, was subject to false indications due to localized fuel segregation.
3. The eddy-current technique also located the hump relative to a particular side and edge of the plate. It proved to be the most rapid for inspection, and the equipment required was quite simple in comparison with that required for the other methods. The sensitivity to the hump curvature is due to the type 1100 aluminum filler and not to the core itself. Difficulty was encountered on some plates which had an excess of blistering on the surface. However, over 650 plates were successfully inspected by this last technique.

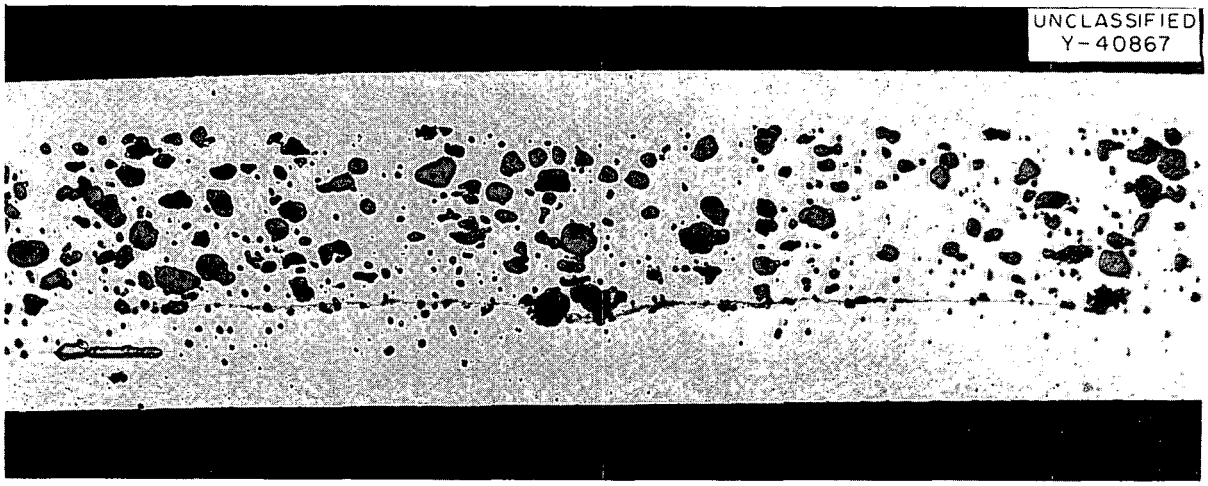

Fig. 20.5. Metallographic Section of Nonbond Detected in HFIR Fuel Plate. As polished. 32X.

21. PHYSICAL METALLURGY

H. Inouye

REACTIONS OF TYPE 304 STAINLESS STEEL WITH LOW-PRESSURE CO_2 AND CO

H. Inouye

Oxidation and carburization experiments on type 304 stainless steel were carried out as part of the Experimental Gas-Cooled Reactor (EGCR) project. This investigation is concerned with the compatibility of type 304 stainless steel in atmospheres of CO_2 and CO at temperatures up to 982°C. During this period, the factors which affect the rates of oxidation, carburization, and decarburization of the metal were determined for CO_2 + CO concentrations up to about 0.3 vol % (based on 315 psi He) in helium as a carrier gas.

Type 304 stainless steel can be considered to be a four-component alloy of Fe, Cr, Ni, and C, with each exhibiting variable degrees of reactivity with CO_2 and CO. Therefore, it was expected that variations in the gas ratios and concentrations would result in the formation of different oxides as well as affect the extent of carburization or decarburization.

With respect to the oxidizing reactions, correlations were established between the reaction rates and temperature, gas ratios, or the concentration. The effects of these variables are considered separately below.

At a particular temperature the reaction rates were found to be principally determined by the type of oxide that formed on the metal. Thus, when the oxide that formed on the metal was protective, reaction rates were insensitive to the gas ratios or their concentrations. For example, tests conducted at 760°C and at concentrations of 0.6, 6, and 2400 ppm of CO_2 resulted in weight gains of 0.28, 0.22, and 0.19 mg/cm^2, respectively, after 350 hr. The oxide in this case was $3Cr_2O_3 \cdot Fe_2O_3$. At 982°C, variations in the CO_2/CO ratios between 0.02 and 0.46 and concentration ranges of 200 to 3200 ppm resulted in weight gains of 0.75 to 1.25 mg/cm^2 after 200 hr.[1] In these tests, the principal oxides were the spinels of chromium. At both temperatures the reaction rates were parabolic. At a CO_2/CO ratio greater than 0.669, a "break-away" reaction was observed which decreased to shorter times as the CO_2/CO ratio increased.[2] The oxide associated with the break-away reaction was identified as Fe_3O_4.

The variations in the reaction rates at a constant gas composition and at various temperatures showed in each case exponential increases in the reaction rates with temperature in accordance with the Arrhenius equation. Inflections in the plots occurred when a different oxide was encountered.[1]

In general these results showed that when the oxide is protective the reaction rates are insensitive to the gas concentration or their ratios; however, when nonprotective oxides result, the reaction rates are governed by the P_{CO_2}/P_{CO} ratio.

The carburization or decarburization of type 304 stainless steel in CO-CO_2 atmospheres was determined to be dependent on the temperature and the $(P_{CO})^2/P_{CO_2}$ (ref 2). Below 650°C, changes in the carbon content of the metal (exposed to various atmospheres) were not detected for test times up to 1400 hr. Above this temperature, however, a gradual increase in the carbon content was observed. For values of $(P_{CO})^2/P_{CO_2}$ less than 0.08, the carbon content reached a maximum of about 0.15% C at about 800°C, then decreased with further temperature increases. For values of $(P_{CO})^2/P_{CO_2}$ equal to 0.363, the carbon content increased with temperature, reaching a value of 0.7 wt % C at 1000°C. The critical value of $(P_{CO})^2/P_{CO_2}$ above which serious carburization of the metal occurred is presently placed at about 0.10.

---

[1] *GCR Quart. Progr. Rept. Dec. 31, 1960*, ORNL-3049, pp 216–20.

[2] *GCR Quart. Progr. Rept. Mar. 31, 1961*, ORNL-3102, pp 127–28.

Based on the experimental evidence accumulated during this period, it is concluded that oxidation can be controlled by the P_{CO_2}/P_{CO} ratio and that carburization or decarburization can be controlled by the $(P_{CO})^2/P_{CO_2}$ ratio. The extent of uniform oxidation for test times of 1000 hr is about 0.0004 in., while the maximum depths of oxide penetration were about 0.001 in. for temperatures up to 1000°C.

The carbon in carburized specimens was in the metal and not in the oxide. Since carburization or decarburization could not be correlated with the oxide reaction product, it was concluded that the oxides were no barrier for carbon diffusion.

THE REACTIONS OF BERYLLIUM WITH GASES

W. J. Werner

Based on documented evidence,[3-6] the corrosion resistance of beryllium in high-temperature gases that are oxidizing, carburizing, and decarburizing is not predictable. The extent of this present uncertainty in its corrosion resistance prevents the use of the metal as the clad for fuel elements of a gas-cooled reactor. In particular, the problem reduces to a basic understanding of the relationships between corrosion mechanisms and the kinetics of the gas-metal reactions that lead to an accelerated corrosion rate commonly referred to as the break-away phenomenon.

The research conducted during this period was directed toward developing reliable experimental techniques that would result in reproducible data. To accomplish this the corrosion studies were for the most part performed on powders having a BET (nitrogen) surface area of 1000 to 3000 cm^2/g in order to increase the sensitivity of the reaction-rate measurements and eliminate the effects of grain boundaries and preferred orientation. The gas atmospheres used in this study were dry CO_2, wet CO_2, wet helium, and wet hydrogen. These atmospheres were selected to more clearly indicate the role of water vapor on the break-away phenomenon. The details of the research results are reported elsewhere[7] and are summarized below.

In the temperature range between 550 and 720°C, the reaction rates of beryllium with dry CO_2 were parabolic and independent of the CO_2 pressure for tests conducted at 1×10^{-3} mm Hg and 760 mm Hg. In wet CO_2 (approx 4 vol % H_2O) at atmospheric pressure, the rates were parabolic at 650°C, while at 725°C a break-away reaction commenced after 60 to 70 hr. The solid reaction products were determined to be BeO and Be_2C in both atmospheres. The carbon content of the beryllium increased with both time and temperature. This phase of the study showed that water vapor played an important role in the break-away phenomenon.

The formation of a nonprotective BeO film in water vapor was thought to be due to an intermediate oxidation stage involving the formation of $Be(OH)_2$ or $BeCO_3$ followed by their decomposition at elevated temperatures. An alternate theory was that the reaction between Be_2C with water vapor ruptured the BeO film.

To test these theories powder samples of beryllium were run in wet helium (approx 4 vol % H_2O) at 550 to 700°C. As was the case for dry CO_2, the reaction rates for high-purity Pechiney Flake were parabolic, while a commercial grade of beryllium exhibited a short period of linear oxidation followed by a parabolic rate. The linear reaction rates observed in the impure beryllium were concluded to be due to a decarburization and oxidation reaction. It is interesting to note that a polycrystalline solid sample in water vapor exhibited a break-away reaction rate at 650°C.[6] These results point out the importance of the grain boundaries and of impurities in the water vapor reactions.

The gaseous reaction products which formed between Be-H_2O were hydrogen, while CH_4 was the gas resulting from the reaction of Be_2C with H_2O or H_2. To establish the correlation between break-away and the decarburization reaction, a

[3] J. E. Antill, *The Oxidation of Beryllium in the Absence of Irradiation*, AERE-M-435 (May 1959).

[4] W. Munro and J. Williams, *Reactions of Beryllium with Carbon Dioxide in the Temperature Range 500–700°C*, AERE-M/M-108 (1956).

[5] J. E. Antill and J. K. Higgins, *Oxidation of Beryllium*, GCM/UK/15 (1959).

[6] S. J. Gregg, R. J. Hussey, and W. B. Jepson, *J. Nuclear Materials* 3(2), 190–200 (1961).

[7] W. J. Werner and H. Inouye, "Reactions of Beryllium with Wet Carbon Dioxide," submitted to the *Journal of the Institute of Metals*.

beryllium sample containing 1.65 wt % C was tested in hydrogen containing 100 ppm H_2O. At 650°C the reaction rate was parabolic up to 22 hr, after which a break-away rate occurred and continued for the duration of the test. At 700°C it required 16 hr to initiate this break-away reaction. Chemical analysis of the test specimens revealed that decarburization had occurred, while metallography showed that the corrosion path was intergranular and apparently confined to those locations initially occupied by Be_2C.

It was concluded from this study that one cause of break-away is a decarburizing reaction which removes Be_2C from the metal. The net effect of this reaction is to increase the surface area of the sample that is exposed to the oxidizing gas, thereby causing an increase in the reaction rate in proportion to the area increase.

OXIDATION OF NIOBIUM ALLOYS AT LOW PRESSURES

H. Inouye

The reactivity of niobium with oxygen restricts its use at high temperatures to short exposure times due to scaling and embrittlement by internal oxidation. Through alloying, it has been possible to reduce the oxidation rates as much as a factor of 100 at atmospheric pressures. Similarly, the reaction rates can be reduced by a factor of 400 by reducing the oxygen pressure to 1×10^{-4} mm Hg at 850 to 1200°C.[8,9] These reductions in the oxidation rates, although numerically impressive, do not provide a useful material for elevated-temperature service in air. The purpose of this study was to determine whether alloying the niobium would have the same effect at low oxygen pressures as was observed at atmospheric pressure and to provide practical information on the requirements for heat treating and high-temperature atmospheres for the alloys in the temperature range from 850 to 1200°C.

In general, alloying elements in niobium had two effects in low-pressure oxygen. In the first case, it was observed that when the alloying element forms an oxide more stable than the oxides of niobium, low concentrations of the element reduced the reaction rate below that of high-purity niobium. However, as the concentration of the element was increased, the reaction rate also increased. This behavior was characteristic for binary alloys containing up to 5 wt % Zr, 2.5 wt % Al, 1 wt % Be, and 0.5 wt % Ce. The more complex alloys, such as D-31 (10% Mo–10% Ti), FS-82 (33% Ta–0.7% Zr), F-48 (15% W–5% Mo–1% Zr), and 25% Ti–5% Al, also oxidized at a higher rate than unalloyed niobium.

The second effect of alloying elements in niobium caused little, if any, change in the oxidation rate as the alloying element was increased. In this case, the added elements formed oxides less stable than the oxides of niobium. Tin, molybdenum, tungsten, and palladium fit into this category.

The increases observed in the oxidation rates of niobium with increases in pressure suggest that chemisorption of oxygen is a preliminary reaction. It would be expected, therefore, that a foreign gas, such as nitrogen in oxygen, would influence the reaction rates due to the competition of the gases for the adsorption sites. Therefore, tests were run in low-pressure air to determine how large this effect might be.

At 1000 and 1200°C in air at an oxygen partial pressure of 1×10^{-4} mm Hg ($P_{air} = 5 \times 10^{-4}$ mm Hg), the reaction rates of unalloyed niobium were an order of magnitude lower than when the atmosphere was only oxygen. At 1200°C, measurable rates were not observed until after an incubation period of about 10 hr. The lower reaction rates in air might be due to the poisoning effect of nitrogen or the formation of a nitride layer. From contamination studies, changes in the nitrogen concentration have been determined to be insignificant and would, therefore, tend to support the idea of a poisoning effect of nitrogen.

This study showed that the oxidation rates of niobium alloys at low pressures were not improved in the same proportion that was observed when tests were run at atmospheric pressure. In fact, alloying was detrimental to the oxidation resistance in most cases. Because of the increase in reactivity promoted by alloying, heat-treating atmospheres for alloys containing elements more reactive than niobium would necessarily have to contain less oxygen.

[8] *Met. Div. Ann. Progr. Rept. July 1, 1960*, ORNL-2988, pp 428–31.

[9] H. Inouye, *The Scaling of Columbium in Air*, ORNL-1565 (Aug. 29, 1956).

CLADDING STUDIES

T. K. Roche

The objective of this research is to determine the feasibility of cladding niobium for oxidation protection in excess of 872°C. Since the aim is to develop suitable composite materials for liquid-metal-to-air radiators, emphasis has been placed on the fabrication of small-diameter composite tubing. The principal problem areas are anticipated to be (*a*) reliability, (*b*) a solution to the differential expansion of niobium and the clad, (*c*) metal-metal and metal-gas reactions, (*d*) heat transfer, and (*e*) fabrication.

With the above criteria as a basis for the study, preliminary experiments were concerned with the cladding of niobium with types 304 and 446 stainless steels, using copper and copper electroplates as an intermediate layer. Suitable tubing of the above materials was assembled, cold worked by codrawing through dies, and then vacuum annealed for 2 hr at 1010°C. In both cases (niobium clad with type 304 stainless steel and with type 446 stainless steel) metallurgical bonding was, in general, poor due either to the development of reaction layers at the niobium interface or insufficient contact pressure at the annealing temperature. Preliminary compatibility studies at 815 to 1037°C indicate that the thickness of the copper barrier layer should be more than 0.001 in.

TRIPLEX TUBING

T. K. Roche

A heat exchanger utilizing triplex tubing is designed to eliminate an intermediate heat exchanger, to incorporate into the structure a leak-detecting device, and to provide reliability. The triplex tubing consists of a porous metallic annulus which is clad both on the outside diameter and the inside diameter with selected corrosion-resistant alloys. The use of such a composite tube depends on sensing a gas-pressure change in the annulus – a pressure which is intermediate between the fluid pressures on the outside diameter and the inside diameter of the tube. The problems, therefore, reduce to the development of techniques for obtaining metallurgical bonds at the clad interfaces at the highest core densities for optimum heat transfer without destroying the interconnecting pores for leak detection.

The feasibility of fabricating a triplex tubing consisting of a porous nickel core clad with Inconel has been demonstrated.[10] During this period, the studies were concerned with the effect of process variables, such as amount of cold reduction, annealing time, temperature, and the type of core material on the bond quality and core porosity. The composite for this study was an inner and outer tube of INOR-8 separated by a porous nickel tube.

For cold reductions ranging from 9 to 17% in area and annealing times of 1 to 2 hr at 1065 to 1175°C, the bond quality, as determined by metallography and bend tests, improved with time at temperature and with the per cent reduction of the assembly.

Pore compression in the nickel core was noticeable only in the specimens cold reduced 17%, and then not to a great extent. The measured porosities of the nickel cores which decreased with increasing amounts of cold work were between 13 and 27%.

AGING PHENOMENA IN NIOBIUM-BASE ALLOYS

D. O. Hobson

This investigation is a continuation of a study directed toward obtaining a clearer understanding of the effects of oxygen, carbon, and nitrogen on the mechanical properties of FS-80 (NB–1 wt % Zr). In a previous report,[11] the aging effects at 815 and 927°C observed in several commercial heats were presented. In general, aging occurred in alloys containing low concentrations of oxygen but not at higher oxygen levels. Furthermore, it was possible to decrease the aging tendency of an alloy that aged by adding oxygen or to increase the extent of the aging reaction by increasing the annealing temperature. Because these alloys also contained nitrogen and carbon impurities, it appeared that the oxygen inhibited the precipitation of carbides or nitrides that were thought to be the phases that caused the aging response.

More recent experiments showed that aging did not occur when zirconium was absent or when the major impurity in the Nb–1% Zr alloy was carbon

[10] *Met. Div. Ann. Progr. Rept. Sept. 1, 1959*, ORNL-2839, pp 178–81.

[11] *Met. Div. Ann. Progr. Rept. July 1, 1960*, ORNL-2988, pp 431–35.

or nitrogen up to 370 ppm. The experiments clearly indicated that, for the heat treatments and compositions investigated, the phase or phases responsible for the aging reactions observed at 927°C were compounds of zirconium and oxygen. A more comprehensive summary has been reported elsewhere.[12]

The variables investigated were the aging times at 927°C, oxygen levels up to 1000 ppm, and annealing temperatures of 1600, 1800, and 2000°C. The alloys studied included thirteen heats of Nb–nominal 1 wt % Zr, as well as compositions into which were introduced controlled levels of oxygen. The aging reactions were followed by measuring the changes in the tensile properties and hardness and by metallography.

In general, a typical aging curve showed an initial small decrease in the tensile strength for about 25 hr, followed by a rapid increase for a short time. The peak strength or hardness normally was reached in about 75 to 100 hr. Additional aging times resulted in a decrease in the strength or hardness. Microstructurally, it was observed that the annealed (fast cooled in a furnace) alloy contained a second phase which disappeared in the time which corresponded to a decrease in the strength. Resolvable precipitates different in morphology from the phase observed in the annealed alloys were not observed until after the peak strength was reached. The final precipitated phase was identified as ZrO_2.

The variations in the aging response caused by different levels of oxygen depended on the annealing temperature. It has been determined that when the oxygen content was increased, the annealing temperature also had to be increased to obtain an aging curve similar to that described above. If, however, the oxygen content was increased and if the annealing was done at a constant temperature, the alloy became progressively weaker after aging. Conversely, at a constant oxygen content, a specimen that was annealed at a higher temperature showed a greater aging reaction. At the very low oxygen levels (approx 50 ppm O_2), aging reactions could not be induced under a variety of heat treatments.

[12]D. O. Hobson, "Aging Phenomena in Columbium-Base Alloys," paper presented at the AIME High-Temperature Materials Conference, Cleveland, Ohio, Apr. 26–27, 1961.

At this writing, it appears that the phase or phases observed in the annealed alloys are carbides or nitrides that precipitated on cooling at temperatures below the aging temperatures. Aging subsequently caused solution of the carbides or nitrides that was then followed by the precipitation of a coherent oxide-like phase that ultimately becomes ZrO_2 when overaged.

To thoroughly understand the aging of alloys of this type, the phase relationships of the niobium-rich corner of the Nb-Zr-O is required. Because of the variations in the aging response induced by the solution annealing temperature, it is thought that the annealing temperatures are within a two-phase field and not a homogeneous solid solution of Nb-Zr-O.

FERMI REACTOR PROJECT

H. Inouye

The utilization of all-metal alloy fuels for fast reactors of the Fermi type depends to some extent on the strength and stability of the alloy system. The high-temperature γ phase of uranium can be stabilized at room temperature by alloying with molybdenum or niobium. On heating U-Mo alloys to subcritical temperatures, the gamma phase transforms to α uranium and γ' (U_2Mo). Irradiation of these alloys at subcritical temperatures opposes the tendency for the alloys to transform due to the heat generated by thermal spikes. Thus, at a subcritical fission rate, it is thought that the sweeping action of the phase boundary and the low resistance to plastic flow during transformation aids fission-gas agglomeration. The swelling characteristics of the alloys are therefore implied to be directly related to the stability of the γ phase and the resistance of the alloy to plastic deformation (creep resistance).

The purpose of this investigation is to survey the creep resistance of γ-stabilized alloys under conditions that will reflect the effect of alloying and transformation. A second objective is to determine the effect of time, temperature, and stress on the extent of transformation.

To date, the creep properties of γ-quenched alloys have been surveyed at 550°C and at a stress of 5000 psi. Under these conditions the creep rates of the alloys ranged between 4×10^{-5} to 6×10^{-3}%/hr and increased in the order U–13%

Mo, U–15% Mo, U–10% Mo, U–10% Nb–4% Zr, and U–10% Nb.

The creep curve obtained from a U–10% Mo specimen exhibited a characteristic first-stage creep for about 50 hr, after which time a rapid linear increase was observed for the duration of the 900-hr test. Inasmuch as the time for the change in the creep rate coincided with the beginning of transformation in this alloy, it appears that transformation does decrease the resistance to plastic flow.

In opposition to this behavior, a U–13% Mo specimen exhibited a creep behavior characteristic of age-hardenable alloys. After 1500 hr, the creep rates were not measurable. On increasing the stress in 1000-psi increments to 10,000 psi, the specimen appeared to contract for 1000 additional hours. The stress-induced phenomena might be due to the transformation of γ to $\alpha + \gamma'$ (U_2Mo), which is more dense.

A hydrogen-absorption technique was used to follow the transformation kinetics in these alloys. The principle is based on the evidence that the γ and the γ' phases do not absorb hydrogen whereas the α-uranium-transformation product does. This has been substantiated by x-ray identification of the phases after transformation and hydriding.

For alloys that were γ quenched from 900°C and transformed at 500°C, the times required to transform to equivalent amounts of α uranium were calculated to be 48, 500, and 1000 hr for U–10% Mo, U–13% Mo, and U–15% Mo, respectively. Cold working the alloys prior to the transformation heat treatment increased the amount of α uranium in the alloys by a factor of about 10. Depending on the amount of hydrogen absorbed, the hydrided alloys either disintegrated to powders or could be readily pulverized.

HIGH-TEMPERATURE STABILITY OF INOR-8

T. K. Roche

INOR-8 (17% Mo–7% Cr–5% Fe–bal Ni) was selected to contain a variety of complex uranium, thorium, and alkali-metal fluoride melts up to 704°C. When the solubility limit of molybdenum, chromium, or iron in nickel is exceeded, intermetallic compounds having a high concentration of the alloying elements will precipitate, which may have adverse effects on the chemical or mechanical properties.

The purpose of this study was to determine whether undesirable phases existed in the alloy when the elements were within the established specifications and at their maximum permissible concentration of 18% Mo–8% Cr–5% Fe. Furthermore, since welds and castings represent the worst cases for alloy inhomogeneity, the study was further extended to establish an approximate solid-solution-phase boundary.

From metallographic studies and x-ray examination of extracted residues from electrolytic dissolution of the alloy, it was concluded that INOR-8 does not contain intermetallic compounds up to temperatures of 1092°C. In this temperature range, however, both $M_{23}C_6$ and M_6C types of carbides are stable phases for carbon contents of about 0.06% C. For carbon levels of about 0.01% C, carbides precipitate as a fine grain-boundary phase between 593 and 899°C. At 982°C and above, the carbides redissolve. The carbon solubility up to 899°C is therefore less than 0.01% C and increases to 0.01 to 0.06% C above this temperature.

In the ternary system Ni–20% Mo–Cr, solid solutions exist for chromium contents up to 10%. In the presence of 20% Mo and more than 5% Cr, the solubility of iron lies between 4 and 10%. At 18% Mo, an unidentified phase that appears to be an intermetallic compound was observed in an alloy containing 8% Fe and 8% Cr.

The specific heat of annealed INOR-8 as determined by direct calorimetric measurements by Stansbury and Brooks[13] was observed to increase uniformly from a value of 0.409 joule/g at 60°C to 0.483 joule/g at 540°C. At 550°C, an anomalous rise of about 20% in the specific heat was observed, reaching a maximum value of 0.586 joule/g at 610°C. Above this temperature the specific heat decreased to a value of 0.578 joule/g at 700°C. The phenomenon has been postulated to be an ordering and disordering reaction.

[13]ORNL subcontract No. 1114, with the University of Tennessee.

22. POSTIRRADIATION EXAMINATION

A. R. Olsen

The current effort of the Postirradiation Examination (PIE) Group is centered on two main activities: (1) service functions in support of various experimental and reactor projects, principally using the available facilities in Building 4501; and (2) the design, development, construction and testing of equipment, as well as the development of experimental techniques for use in both the present and the future hot-cell facilities.

Construction of the new hot-cell facility, Building 3525, is approx 50% complete. The construction is somewhat behind schedule, and the actual date for completion, some time late in 1961, is uncertain. The new facility and its functions have been described previously.[1,2]

The hot-cell facilities in Building 4501 were modified to meet the revised containment criteria for operations involving radiation and contamination hazards. These modifications were made with only a minor loss in productivity. Although the changes have not altered the facility limitations on shielding, they have increased the allowable quantity of contaminants and the number of functions which may be performed safely and economically. A change room connected to an airlock was installed at the entry to the manipulator cell operating face. The rear of this cell was provided with an airlock to aid in the charging and discharging operations.

A number of small shielded glove boxes or "caves" were installed for performing specific tasks on low beta-gamma radiation intensity materials. The caves permit better utilization of the limited cell space for higher activity level operations.

[1]A. R. Olsen and R. E. McDonald, *Met. Div. Ann. Progr. Rept. July 1, 1960*, ORNL-2988, pp 436–37.

[2]Staff of the Metallurgy Division, *Technical Function and Operation of the High Radiation Level Examination Laboratory, Bldg. 3525*, ORNL CF-61-1-75 (Jan. 31, 1961).

AQUEOUS THERMAL BREEDER PROJECT SUPPORT ACTIVITIES

R. E. McDonald

Hot-Cell Cutup and Examination of an In-Pile Solution Loop

As an integral part of an experimental program to investigate the effects of irradiation on the corrosion behavior of selected reactor structural materials in UO_2SO_4 solutions, additional hot-cell work was performed on the first in-pile loop exposed to higher neutron-flux levels in the ORR HN-1 facility. The loop design, materials of construction, and operating conditions of the in-pile test, as well as preliminary results, have been reported.[3] New findings along with a brief description of the techniques utilized and the current status of the examination are summarized below.

1. A gross-gamma-activity scan of the pump purge lines was successful in locating a plug noted during loop operation. The plug was extracted, photographed, and submitted for chemical identification. On visual examination after extraction, the plug appeared to be a collection of rust-colored corrosion products.

2. Examination at 200X of a replica taken on the interior surface of the pressurizer at the vapor-liquid interface revealed (1) the presence of two distinct scale thicknesses, one above and another below the vapor-liquid interface, and (2) that a suspect-pit area was in reality only a missing section of heavy scale. The pressurizer was subsequently sectioned to obtain samples at selected points of interest for metallographic examination.

3. A large number of the corrosion-coupon surfaces were replicated successfully, employing the

[3]A. R. Olsen and R. E. McDonald, *Met. Div. Ann. Progr. Rept. July 1, 1960*, ORNL-2988, pp 439–42.

cellulose acetate technique described in the last report.[3] Evaluation of these replicas is incomplete, although certain interesting scale topographies have been noted.

In general the examinations did not reveal any unusual behavior traceable to an increase in neutron flux. The corrosion data[4] tend to confirm previously established power density–corrosion relationships and the effect of adsorbed uranium. These findings will be reported in detail at a later date by the experimental group in charge of the over-all loop-test program.

Preliminary Examination of In-Pile Slurry Loops

After drainage of the test slurry and rinsing at the reactor site, the first in-pile slurry loop[5] was forwarded to the hot cells for examination. The loop had operated with a slurry of thoria, 1350 g of thoria per kg of D_2O, to which 0.5 wt % of enriched uranium, based on thorium, and 0.019 *m* palladium had been added. The primary objectives of the postoperational examination were to determine the distribution of any retained slurry in the loop components together with the irradiation effects on corrosion. Both the loop design, which is unique, and the residual thoria, which is contained in the loop, require special handling and examination techniques.

Two new pieces of equipment were utilized during the initial stages of the examination.

1. Before dismantling, selected sections of the loop were examined with a collimated multichannel gamma-ray spectrometer to determine the distribution of retained slurry in the relatively undisturbed portion of the loop. Similar examinations are being made on individual components or sections after removal from the loop. The spectra did show characteristic intensity peaks for such elements as Zr^{95}, Cs^{137}, Co^{60}, Co^{58}, and Cr^{51}; and the relative intensities varied from one location to another. These preliminary results are encouraging, since out-of-pile experiments have shown that both corrosion products and fission products tend to be strongly adsorbed by the slurry particles. The core section has been removed from the loop, and short sections of the core inlet and outlet piping have been examined individually for gamma spectra. A comparision of the spectral data before and after cutup does not correlate but indicates a high probability that slurry has been retained in a section of the pressurizer heater which is located in the same general loop area.

2. The corrosion specimens from the four-core arrays were removed by slitting the core pipe sections with a small milling machine, recently made remotely operable for this operation. The unit was required because the available abrasive wheel used for opening similar corrosion specimen holders was incapable of making the precision cuts required by this holder design.

Although the examination is incomplete, as-removed weight data and preliminary surface examinations indicate that irradiation has essentially no effect on the corrosion rates of the Zircaloy, titanium, and stainless steel samples under the specific test conditions. The remainder of the loop is still to be examined. The detailed findings and conclusions will be reported by the experimenter when the examination is completed.

Hot-Cell Examination of In-Pile Slurry Autoclaves

During the past year a total of four in-pile thoria-slurry autoclaves were dismantled and examined. Three of the test units were designed to study only the effect of irradiation on the ThO_2-bearing slurry,[6–8] while the fourth[9] unit included specimens to evaluate corrosion behavior as well. Samples of the solids, supernatants, and rinses were obtained and submitted for chemical analysis. Descriptions of the autoclave bodies, slurry conditions, and corrosion samples along with complete photographic coverage were obtained. Although the detailed analysis of the material examinations has been reported by the experimenter, it is of interest to note that in one autoclave a black, vitreous material was found.

---

[4] G. H. Jenks *et al.*, *HRP Quart. Progr. Rept. July 30, 1960*, ORNL-3004, pp 65–77.

[5] E. L. Compere *et al.*, *HRP Progr. Rept. Nov. 30, 1960*, ORNL-3061, pp 89–94.

[6] J. P. McBride, *HRP Quart. Progr. Rept. Nov. 30, 1960*, ORNL-3061, p 75.

[7] J. P. McBride, S. D. Clinton, and W. L. Pattison, *HRP Progr. Rept. Apr. 30, 1961* (to be issued).

[8] J. P. McBride, *Chem. Tech. Ann. Progr. Rept. FY 1961* (to be issued).

[9] E. L. Compere *et al.*, *HRP Quart. Progr. Rept. Apr. 30, 1961* (to be issued).

It had accumulated in the vapor-phase region of the autoclave. The unidentified material exhibited an apparent bulk density of about 1 (part of it floated and part sank in water). The examinations also showed that there is a significant quantity of fines produced by irradiation of thoria spheres even under static conditions. The material balances on these tests have not been completed.

DEVELOPMENT OF POSTIRRADIATION EXAMINATION TECHNIQUES

R. E. McDonald

In performing normal service functions, certain requests or needs lead to the development of new or modified equipment and techniques. The more significant of these developments are briefly described here.

Remote Viewing

R. E. McDonald

The group assisted in developing equipment and techniques for the macroscopic examination and photographing of the HRE-2 core-vessel interior.[10] Photographs giving printed magnifications of 4 and 16X were taken by utilizing an Omniscope and a Questar telescope.

A similar program was undertaken at the request of the Chemical Technology Division to view interior surfaces of the fluorinator and hydrofluorinator vessels in the Volatility Pilot Plant. In this instance the Questar telescope was used with only a mirror arrangement. A typical photograph taken with this arrangement is shown in Fig. 22.1. This technique and equipment are proving to be very versatile tools for long-range macroscopic examination. Reports on this examination and the general viewing-technique development will be published soon.

High-Level Gamma Spectrometry

R. E. McDonald J. S. Eldridge[11]

A collimator was developed that could be inserted through an existing 6-in. hole in the face of the loop dismantling cell. The collimator provided sufficient resolution and definition to identify gamma emitters retained in the first slurry loop by means of their characteristic gamma spectra.

The collimation system consisted of a 36-in. length of pipe with a 15-in.-long sliding sleeve filled with lead shot. An axially located 1-in.-diam pipe could accommodate as many as five 3-in.-long lead cylinders. These cylinders contained center-line holes of various diameters. The most effective set was an array of three cylinders containing $\frac{3}{4}$-in.-, $\frac{5}{8}$-in.-, and $\frac{1}{2}$-in.-diam holes decreasing in size toward the source. The detector crystal and preamplifier package were installed in the large pipe behind the collimator. The detector was connected to the 256-channel analyzer.

A simple camera attachment was fabricated for use with the spectrometer cathode-ray tube. The use of the attachment along with a Polaroid camera facilitated the collection of data.

The loop in the cell was loosely fitted through a 1-in.-thick lead sleeve with a 2 × 3 in. window. The window was aligned with the detector by means of a light beam through the collimator. Determinations were made by raising or lowering the loop past the window. Rotation of the loop inside the sleeve provided determinations 90° apart at each vertical position.

This installation was also used to examine sections of experimental control materials for the APPR project. A miniature composite plate containing 30 wt % Eu_2O_3 dispersed in stainless steel and clad in stainless steel was sectioned for examination with the spectrometer. Two sections, one of stainless steel frame and the other containing the Eu_2O_3, were measured. The data have not been completely analyzed; however, the findings show that this will be a reasonable method for either direct or indirect burnup analyses on such control materials. Additional experimentation will be required to determine the quantitative accuracy.

Remote Replication

R. E. McDonald B. W. McCollum G. A. Moore

The first remote replication of the interior surface on an autoclave was made during this period. The replication was produced by centrifugally casting a thin section of RTV silicone rubber

[10] S. E. Beall *et al.*, *HRP Quart. Progr. Rept. Nov. 30, 1960*, ORNL-3061, pp 3–9.

[11] J. S. Eldridge of the Analytical Chemistry Division cooperated in the design and operation of this installation.

Fig. 22.1. Interior of Hydrofluorination Vessel Taken Through A Questar Telescope. This photograph shows the diffuser plate and the wall as seen through the tilted mirror. Original magnification 2X.

UNCLASSIFIED
Y-40843

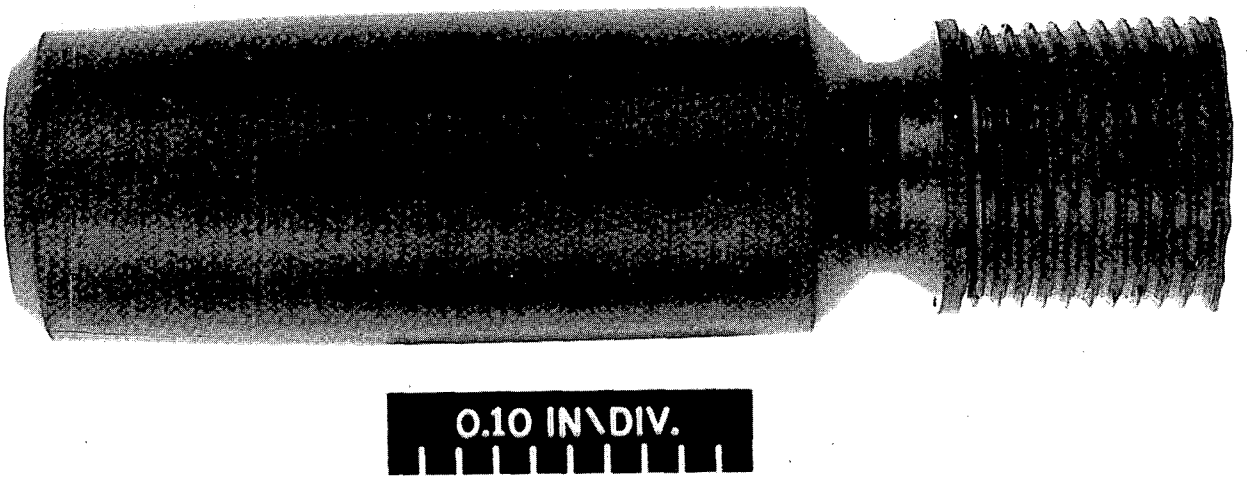

Fig. 22.2. Remotely Replicated In-Pile Autoclave Interior Surface. Centrifugally cast RTV silicone rubber used as the replicating material.

with a modified curing agent on the interior walls. Replications of this sort permit high-magnification examination of entire interior surfaces. Figure 22.2 is a photograph of this replica.

Cellulose acetate replicas[12,13] were made of the polished and etched metallographic surfaces of the sample of the HRE-2 core wall.[14] This sample was removed prior to repair of the hole in the core. Replication involved the use of cellulose acetate sheets suitable for large flat surfaces. Ultrasonic decontamination in an HNO_3-HF solution eliminated most of the occluded radioactive particles without damage to the replica.

EQUIPMENT DEVELOPMENT FOR NEW FACILITY

J. R. Parrott J. E. VanCleve

The equipment testing and development for the new facility have been broken up into two very broad areas: specific experimental equipment and facility-support equipment. Examples of specific experimental equipment are: hardness testers, impact testers, metallographic etching and polishing items, and ultrasonic inspection equipment. Facility-support equipment consists of items that will be of general application, and examples of such items are: in-cell lighting, manipulators, and service sleeves and plugs.

The following remote-metallography items were described in detail in the previous annual report:[15] microhardness tester, cathodic etcher, cutoff machine, vibratory polisher, electrolytic polisher, extended-range superficial hardness tester, mounting press, and metallographs. This equipment is all fabricated or in the final stages of fabrication. Some of it has been placed in operation in existing hot-cell facilities, and some items are undergoing testing in the cell mockup or cold laboratories.

A detailed description of all the currently proposed equipment and functions has been reported

[12] A. R. Olsen and R. E. McDonald, *Met. Div. Ann. Progr. Rept. July 1, 1960*, ORNL-2988, pp 439–42.

[13] Metallurgy Division Staff, *Technical Function and Operation of the High Radiation Level Examination Laboratory, Bldg. 3525*, ORNL CF-61-1-75, pp 49–50 (Jan. 31, 1961).

[14] M. L. Picklesimer, *HRP Quart. Progr. Rept. July 30, 1960*, ORNL-3004, pp 9–17.

[15] *Met. Div. Ann. Progr. Rept. July 1, 1960*, ORNL-2988, pp 341–405.

in the staff paper.[16] Only a few examples of specific items and their status are discussed here.

Carbon Replication

J. E. VanCleve

The purpose of the carbon-replication apparatus is to provide direct, shadowed carbon replicas of the topography of radioactive samples for examination with an electron microscope. The mechanical design is finished, and the instrumentation is well under way. One set of replicas was produced on a partially assembled unit which proved the design integrity but revealed some shortcomings in the equipment. Modifications to correct these defects are included in the instrumentation work. The quality of the replicas was good, but they lacked mechanical strength. When the modifications are complete a procedure will be developed to correct this flaw.

Bausch and Lomb Stereomicroscope

J. E. VanCleve J. R. Parrott

The first stereomicroscope specifically designed to meet the containment and maintenance features of the new facility has been received. The testing of this unit will be done in the mockup facility when the focusing stage has been completed.

The location of the in-cell air filters made necessary the design of a cantilevered focusing stage for use with the stereomicroscope. The focusing stage includes facilities for positioning the sample in addition to effecting the required three rectilinear motions, table rotation, and table tilt.

Gamma Spectrometer

J. R. Parrott

Accommodations for a through-the-wall collimated gamma spectrometer were included in the new facility. This equipment will provide gamma-spectrometer scans for nondestructive burnup analysis of irradiated fuel-element components and induced activity measurements on highly irradiated samples of structural material. The shielded crystal detector and collimator will be installed outside of the containment seal, and design of this portion of the equipment is complete. The design of the specimen positioner for use with this unit is 95% complete. The positioner will be installed inside the cell and will accommodate specimens from $\frac{1}{2}$ to 4 in. wide in any length up to 40 in., with complete surface scanning. Positions from within $\frac{1}{8}$ in. of the cell wall, where the collimation begins, to 2 ft from the wall are attainable. Features suggested by the current service-function developments are being incorporated.

Mercury-Vapor-Lamp Shrouds

J. R. Parrott

In-cell lighting and the remote servicing of such lighting has long been a problem in hot cells. During the design of the new facility this problem was deferred for thorough mockup testing. The Research Equipment Company markets a lamp shroud which has been used with some success by others. Starting with this unit, tests have been conducted to determine lighting efficiency and maintenance techniques.

Although all modifications to this fixture have not been achieved, several real improvements have been attained. A simple hanging hook has been included and the replacement of bulbs greatly simplified. The original wire screens guarding the bulb and held in place by screws have been replaced with a guard made of rods held in place by a simple spring action. This modification not only provides increased mechanical strength and easier maintenance but has increased available illumination by 50% as well. The modified unit is shown in Fig. 22.3.

Master-Slave Manipulators

J. R. Parrott J. E. VanCleve

During this period the prototype pair of sealed model A master-slave manipulators developed by Central Research Laboratories have been undergoing a thorough functional check in the mockup. Some of the gears had to be modified because of slippage, and this change has been incorporated into the production models. One unique difficulty encountered, when the slave end was removed, was a distinct tendency for

[16] *Technical Function and Operation of the High Radiation Level Examination Laboratory, Bldg. 3525,* ORNL CF-61-1-75 (Jan. 31, 1961).

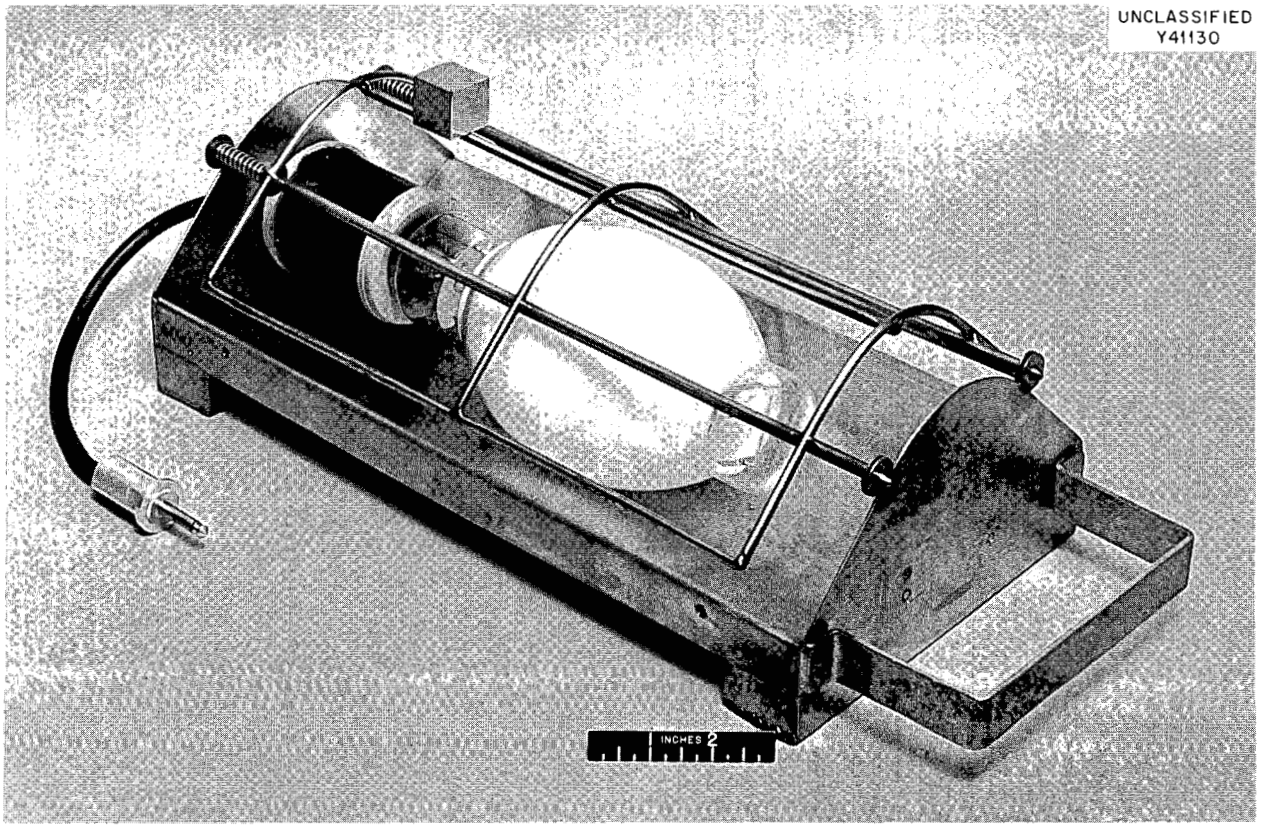

Fig. 22.3. Modified In-Cell Mercury-Lamp Shroud.

the master end to invert. Splitting the counterweight between master and slave ends only shifted the problem to the slave end, where the consequences would be more severe because, when inverted, the slave end will disengage from the seal unit and fall to the cell floor. A simple solution was found in the installation of a lock-pin mechanism on the exterior cell wall; Fig. 22.4 shows this mechanism. The findings and developments on the prototype models are being passed on to the manufacturer for inclusion or correction.

Kollmorgen Periscope

R. E. McDonald J. L. Wilson

The Kollmorgen periscope is used for general observation and photography within the cell. In order to view in some cases, it is necessary to revolve the entire mechanism around its axis. The standard periscope is equipped with a large overhead counterweight for balance. This counterweight complicates the transfer from one position

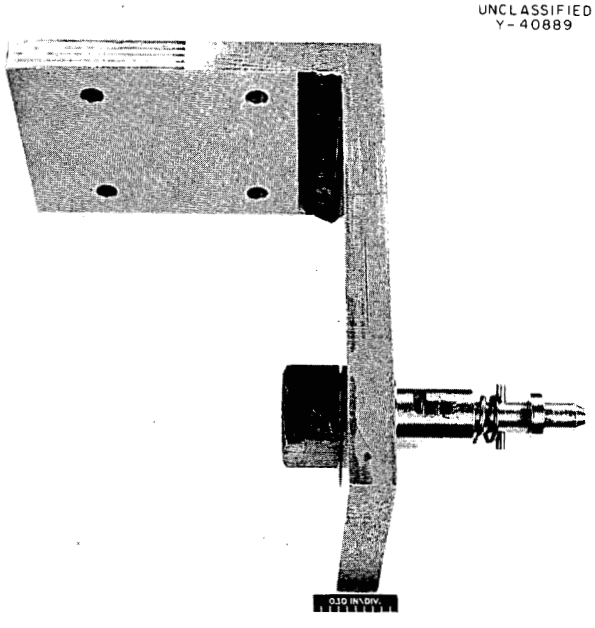

Fig. 22.4. Model "A" Manipulator Master End Locking Pin Used to Prevent Inversion During Maintenance.

to another, as it must be removed during transit. In addition, the unit was unstable during photographing operations and required frequent realignment and adjustment. To overcome these difficulties a simple mechanical expanding-shoe brake was designed. No changes to the periscope were necessary other than the removal of the weight.

The brake is shown installed on the mockup periscope in the following two pictures. Figure 22.5 is a closeup of the brake. The brake is the light-shaded material between the periscope barrel and outer tube. The brake is actuated by the light-shaded handle. Figure 22.6 is an over-all view of the installation with the periscope tilted. A camera is in place to show that the brake is capable of holding its weight.

Radioactive-Material Transport

R. E. McDonald J. R. Parrott

Transporting radioactive material outside of the cell complex, either for introducing experiments

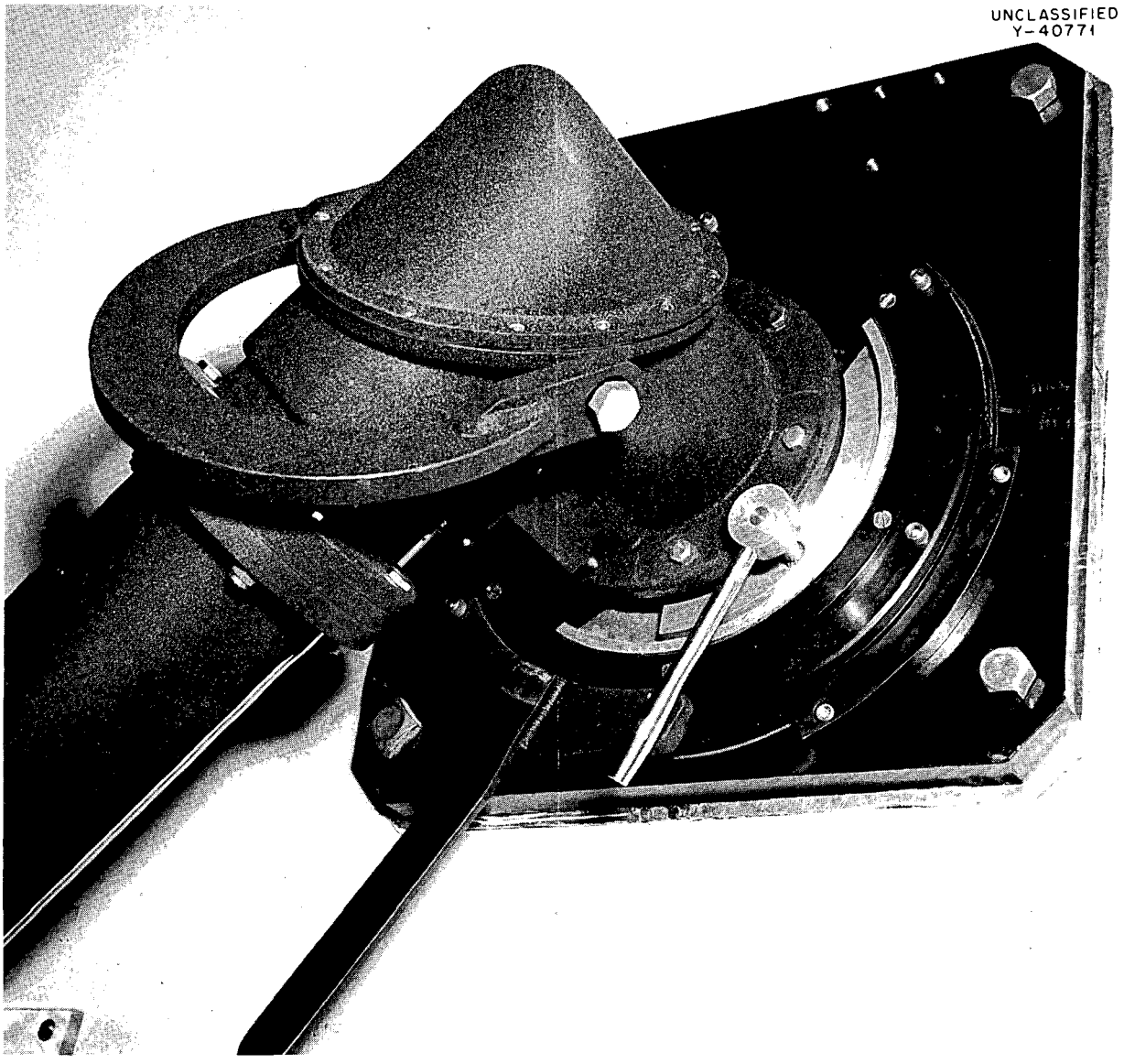

Fig. 22.5. Closeup of PIE-Designed Locking Brake Installed on a Standard Kollmorgen Periscope to Replace Counterweight.

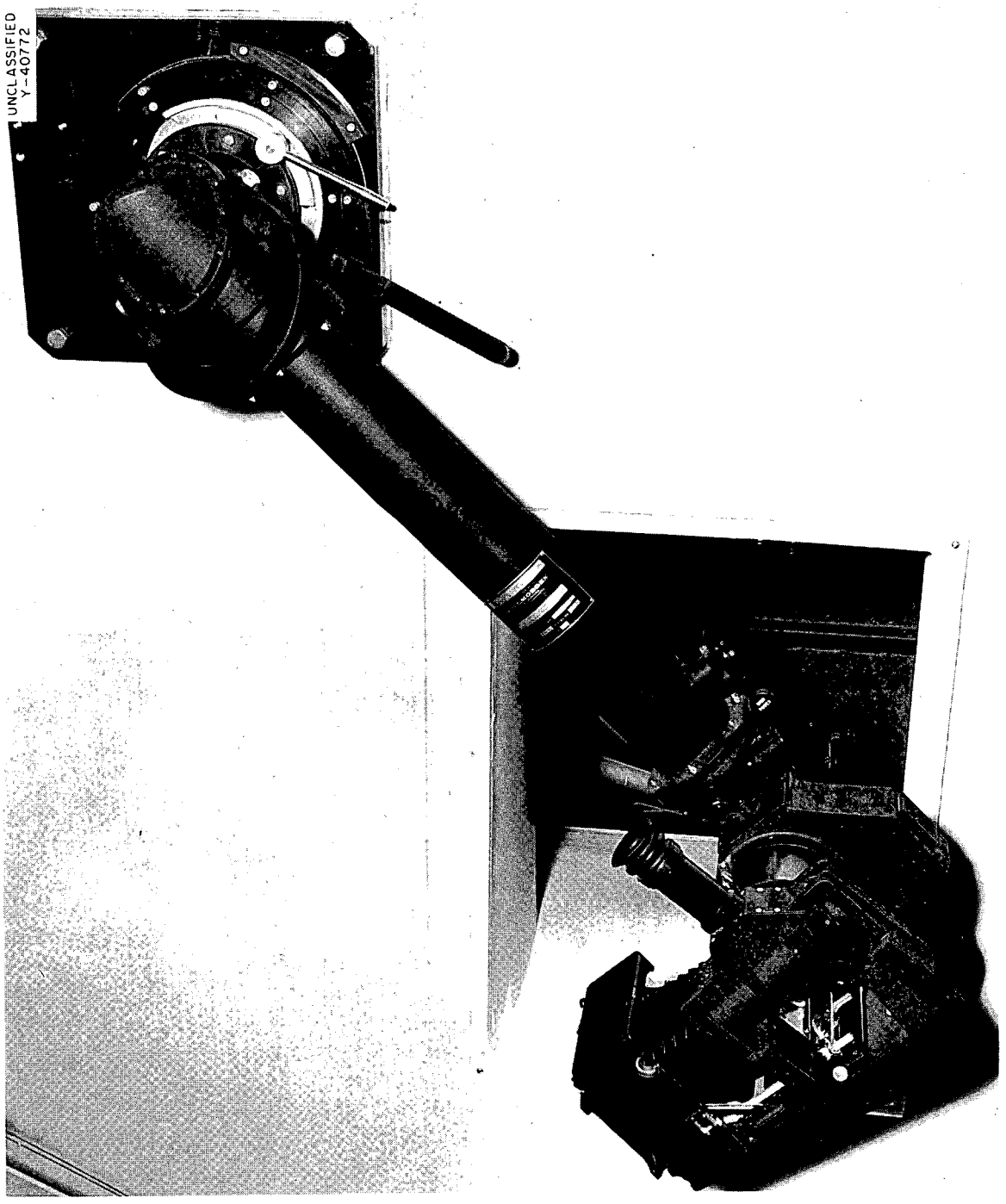

Fig. 22.6. Kollmorgen Periscope Firmly Held in an Extremely Unbalanced Condition by the PIE Locking Brake.

into the operations or removing solid waste and samples safely, is a major problem in the operation of hot cells. During this period two carriers were designed to function with the 14½-in. and 6½-in. transfer ports in the new facility. This design was coordinated with the transfer stations, the waste cans, and the decontamination equipment that will have to be installed in the cell. Since the rapid and safe conduction of these essentially nonproductive operations controls the efficiency of productive operations to a large degree, considerable attention has been and will continue to be focused on perfecting the equipment and techniques in this area.

HRLEL X-RAY DIFFRACTION APPARATUS[17]

H. L. Yakel

The period covered by this report has seen the development of a satisfactory design for the transfer mechanism and biological shield of the goniometer. This was accomplished in collaboration with the Philips Electronics Company, who will construct the instrument.

The design adopted should make this goniometer more accessible for maintenance and service than similar existing instruments, while sacrificing no radiological safety or instrumental accuracy. Tests of the assembled equipment are scheduled for June 1961. Incorporation into the cell will take place in the following few months.

HIGH RADIATION LEVEL EXAMINATION LABORATORY (HRLEL)

R. W. McClung K. V. Cook

A remote scanning tank for the ultrasonic inspection of high-level irradiated components in the HRLEL has been designed and built.[18] The system incorporates capabilities for remote movement of the ultrasonic transducer through X, Y, and Z linear directions and angular adjustment in two directions. Cylindrical specimens can be clamped and rotated by a remotely operated chuck. Wherever possible, consideration has been given to the remote maintenance of this equipment.

[17] *Technical Function and Operation of the High Radiation Level Examination Laboratory, Building 3525*, ORNL CF-61-1-75 (Jan. 31, 1961).

[18] *Ibid.*, pp 27–29.

23. POWDER METALLURGY AND FUEL CYCLE

J. P. Hammond

LIQUID-PHASE SINTERING OF URANIUM CARBIDE FUELS

J. D. Sease J. P. Hammond

Uranium carbide offers advantages over UO_2 in that it has superior thermal conductivity, a higher uranium density, and improved resistance to thermal shock. Also, it is reported to have good irradiation stability. The shortcomings of uranium carbide are its difficulty of fabrication and its hygroscopicity. Sintering temperatures as high as 2000°C are required to achieve acceptable bulk densities; storage, even as pellets, requires special measures to prevent degradation.

Under the sponsorship of the Gas-Cooled Reactor Project, liquid-phase sintering with a permanent cementing agent was investigated for overcoming the above-mentioned shortcomings cited for uranium carbide. While the details of this work are given elsewhere,[1] a summary of the results is given below.

Nickel, chromium, and the uranium intermetallics (U_2Mo, U_3Si_2, and USi_2) were investigated as cementing agents. Carbide fuels bonded with the uranium silicides gave very gratifying results. With 5, 10, and 15 wt % USi_2 as the binder, a density of 97% of theoretical was obtained with firing in a vacuum at 1650°C; 18 wt % U_3Si_2 gave 97.5% density on sintering at 1550°C. Under certain conditions of fabrication, the U_3Si_2 binder was made to assume a continuous network, significantly improving the corrosion resistance. It is to be observed that the uranium silicide-bonded carbides represent highly fabricable fuels of high uranium density and low thermal-neutron-absorption cross section.

DEVELOPMENT OF THORIUM-BASE ALLOYS WITH IMPROVED ELEVATED-TEMPERATURE STRENGTH

J. A. Burka J. P. Hammond

Besides having unique nuclear properties, thorium metal withstands high nuclear burnup while maintaining ductility and useful isotropic mechanical properties. Such attributes suggest the use of thorium where advantage is taken of its structural as well as nuclear properties. With this in mind, an exploratory study was made of thorium alloys to evaluate the effects of various elements in enhancing its elevated-temperature strength and creep properties. Hot hardness and recrystallization temperature were used as screening tests, whereas hot tensile and creep are to be employed for final evaluation.

Forty-five alloys (based on binary systems containing C, Al, Cr, U, In, Mo, Nb, Zr, Sn, Be, Ti, and V, and ternaries of these with carbon) have been examined by the preliminary tests. For temperatures in excess of 500°C, indium proved to be by far the most potent strengthener, with zirconium being the next best additive. Thorium alloyed with 4 wt % In gave a fourfold increase in hot hardness over that for unalloyed thorium at 600°C, and a 5½-fold increase at 750°C (Fig. 23.1). For these temperatures, the increase with a 5 wt % addition of zirconium was threefold and fourfold respectively. Whereas, below about 550°C the hot hardness increased with increasing zirconium content, above this temperature 5 wt % Zr was as good or superior to larger amounts (Fig. 23.1). For the most part, the other binary alloys (hatched band in Fig. 23.1) showed only nominal increases in hot hardness over the unalloyed thorium. The sharp dip in the Th-Zr alloy curves is attributed to the "scavenging" of carbon, occurring as an impurity in the thorium. The Vickers hardnesses of the same alloys (at room temperature) after cold rolling and annealing for 1 hr at temperature are shown as a function of annealing temperature in Fig. 23.2. The hatched band again represents data obtained from the remaining alloys tested. The curves indicate that softening begins at approx 530°C for the alloys containing zirconium and at 600°C for the alloy containing indium. Recrystallization curves for most of the ternary

[1] *GCR Quart. Progr. Rept. June 30, 1961*, ORNL-3166 (in press).

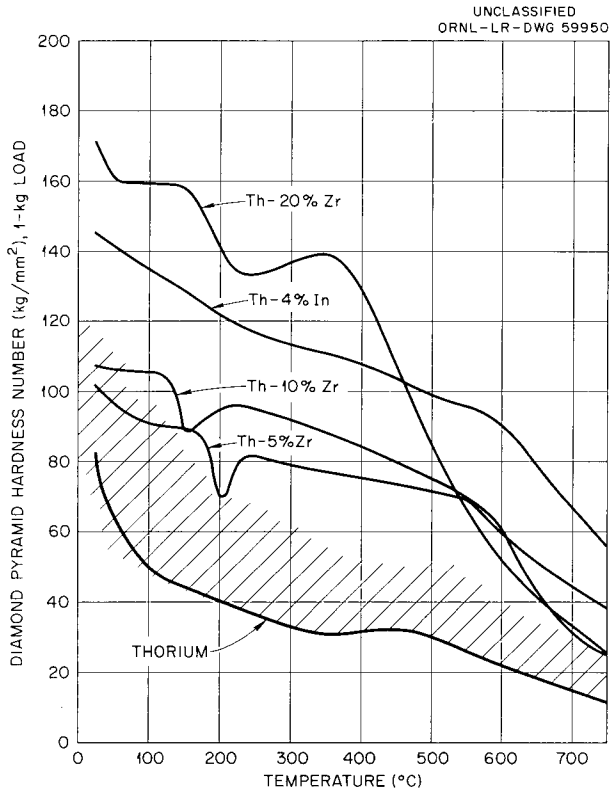

Fig. 23.1. Hot-Hardness Curves for Binary Thorium-Base Alloys. The hatched band represents results obtained on other binary alloys (C, Al, Cr, U, Mo, Nb, Sn, Be, Ti, and V incorporated as additives). Samples arc melted six times, solution annealed 8 hr at 1000°C, and hot rolled at 800°C.

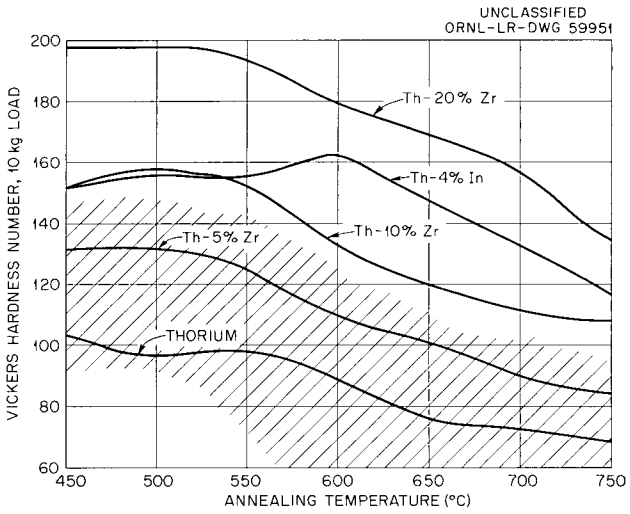

Fig. 23.2. Recrystallization Temperature Curves for Binary Thorium-Base Alloys. Hardness determinations were made on materials cold rolled to 75% reduction in area and annealed for 1 hr at temperatures shown. The hatched band represents results obtained on other binary alloys (C, Al, Cr, U, Mo, Nb, Sn, Be, Ti, and V included as additives). Samples arc melted six times, solution annealed 8 hr at 1000°C, and hot rolled at 800°C.

alloys containing carbon could not be obtained because of the embrittlement of thorium by carbon.

Figure 23.3 illustrates the effect of additions of 0.2 wt % C on hot hardness of alloys containing 0.2 wt % Be and 5 wt % U. Carbon is a very potent strengthener of thorium at room temperature, but its effect decreases rapidly with increasing temperature. For the most part, the effect of carbon in ternary alloys was additive. The Th–0.2 wt % Be–0.2 wt % C alloy has definite potential for use at temperatures up to 400°C because high hardness is produced by very small additions of elements with low thermal-neutron-absorption cross sections. The hot-hardness curve for the alloy containing 4 wt % In (alloy of the highest hardness) is inserted for comparison.

Elevated-temperature tensile tests have been performed in duplicate on hot-rolled thorium and the Th–5 wt % Zr alloy at 600°C, the results (averaged values) of which are as follows:

	Thorium	Th–5 wt % Zr
Tensile strength, psi	8600	37,500
Yield strength, psi	4700	32,500
Elongation in 1 in., %	52.8	32.0
Reduction in area, %	82.6	43.6

As indicated, the addition of 5 wt % Zr to thorium increases its tensile strength fourfold. This compares with a threefold increase in hot hardness at this temperature. The alloy containing 4 wt % In should exhibit substantially higher strength than even that shown by the Th–5 wt % Zr alloy since its hot hardness is four times that of thorium at 600°C. However, difficulties were encountered in the hot fabrication of this alloy because of its high elevated-temperature strength, and hot tensile specimens have not been obtained from it as yet.

In the future, several additional ternary alloys will be explored with the more promising materials being tested for stress rupture and long-time creep properties. In addition, methods are being developed for producing very fine thorium powders,

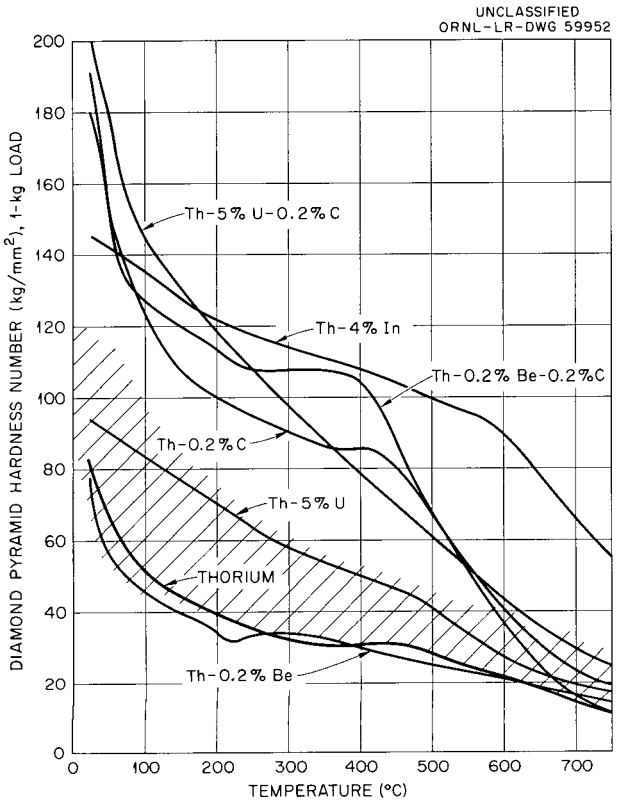

Fig. 23.3. Hot-Hardness Curves for Thorium-Base Binary Alloys and Ternary Alloys Containing Carbon. The hatched band represents results obtained on other ternary alloys; these include carbon-containing alloys with Al, Cr, Mo, Nb, Sn, Ti, and V. Samples arc melted six times, solution annealed 8 hr at 1000°C, and hot rolled at 800°C.

and later, effort will be devoted to the study of dispersion hardening in thorium, using powder metallurgy as the method of fabrication.

DISPERSION FUELS WITH UO_2 OR UC IN DEPLETED URANIUM–10 TO 15 wt % MOLYBDENUM MATRIX

S. A. Rabin M. M. Martin[2]
A. L. Lotts J. P. Hammond

Fabrication of dispersion fuels using UO_2 and UC as the dispersoid and U-Mo (10 to 15 wt % Mo) γ-phase alloy as the matrix, has been investigated in connection with the ORNL Fast Breeder Assistance Program (a report is in preparation). Two main areas of investigation were successfully covered:

1. fabrication development of the dispersion fuel elements, using the conventional picture-frame, roll-cladding technique, and
2. rotary swaging development on U–10 to 15 wt % Mo powders.

Cores containing 17.8 wt % (25.0 vol %) UO_2 dispersed in a U-Mo alloy (15% Mo) were successfully fabricated, using a procedure of cold pressing at 50 tsi, 1100°C sintering, and cold coining at 50 tsi. Fabricability of these dispersions was shown to be a function of the type of matrix powder. Cores of good strength and with densities 81% of theoretical or higher were obtained by using prealloyed powder that had been prepared by bomb reduction with calcium. However, to prevent swelling, a vacuum degassing of the prealloyed powder was necessary prior to fabrication. Suitable compacts were also obtained with UO_2 dispersed in elemental molybdenum and uranium powders that had been made by calcium reduction. Hydride uranium, owing to its voluminous quality, gave poor compactibility. The pressing of compacts containing as-received prealloyed U–10 wt % Mo and U–14 wt % Mo shot was successful only after the addition of large quantities of organic binder, apparently necessary because of surface oxide on the powder. Chemically cleaning the surface of such particles enhanced compatibility, but bonding during sintering was still not achieved.

Dispersion cores also were prepared with UC as the dispersoid. Fabrication of these compacts resulted in products similar to those containing UO_2.

Compacts were assembled into billets and hot rolled at various temperatures. The effects of core composition, sheathing materials, rate of reduction, and rolling temperature on density and microstructure were determined. Cladding materials evaluated were: (1) molybdenum, (2) Zr–3 wt % Al, (3) Fansteel 82, (4) Nb–1.8 wt % Cr, and (5) Inconel-clad molybdenum. After completing screening tests, cylindrical cores of 17.8 wt % (25 vol %) UO_2 dispersed in a matrix of elemental U–15 wt % Mo alloy were clad with either molybdenum or Zr–3 wt % Al and then rolled at 1150 and 910°C respectively.

Very promising results were obtained with the molybdenum cladding. Metallurgical bonding between both the core and clad and the frame and

[2]Metal Forming and Casting Group.

clad were achieved, as determined by metallography, mechanical-peel, and thermal-shock tests. A density of 99% of theoretical was obtained in the rolled dispersion. Representative microstructures of the core and bonding at the core-clad interface are shown in Fig. 23.4*a* and 23.4*b* respectively. It may be noted that the structure of the molybdenum is finer near the core-clad interface, and, that while the UO_2 has stringered, it has not broken up. Nonbonding between the

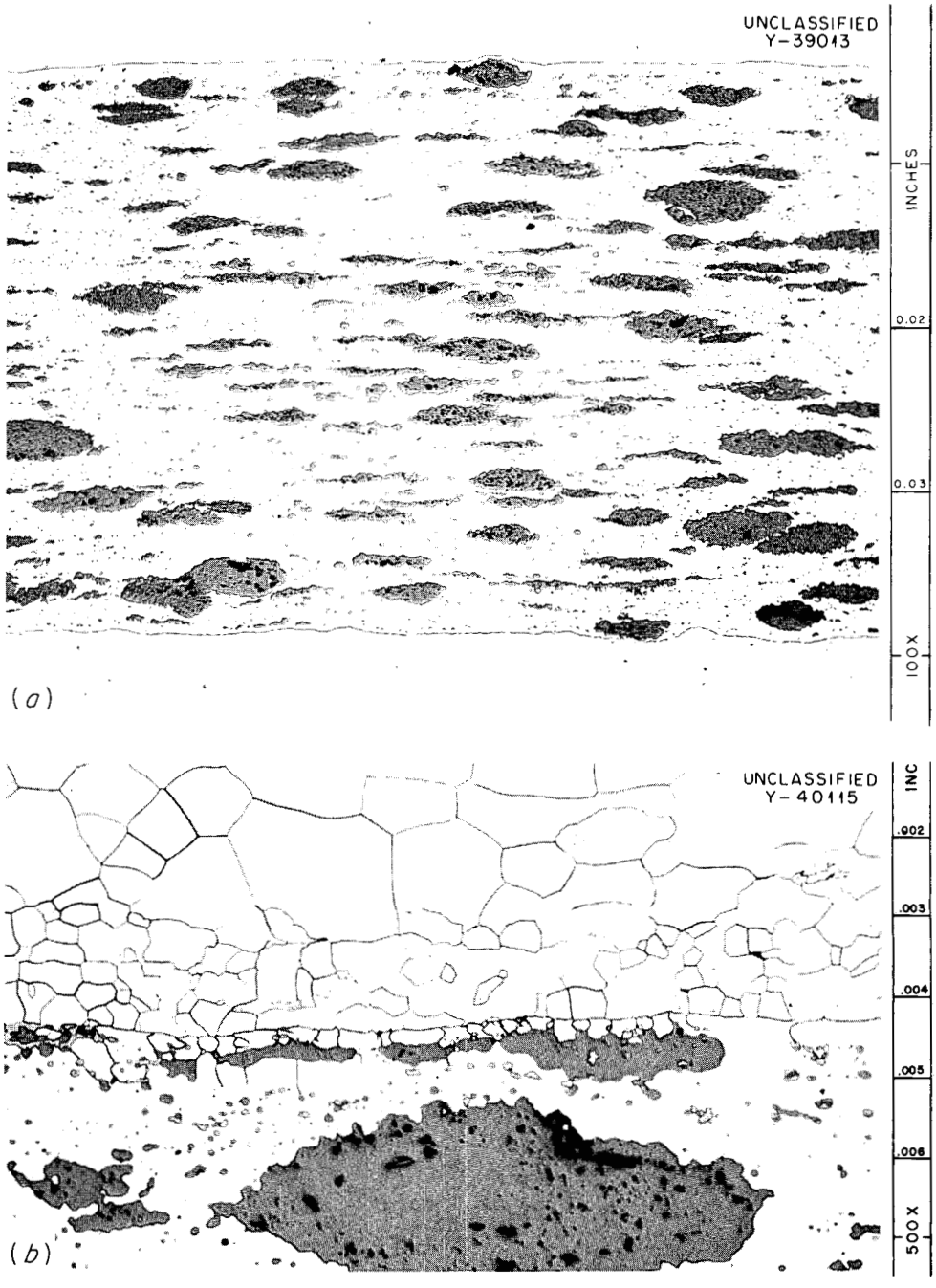

Fig. 23.4. Transverse Section from Plate 2A Showing Core, Containing 17.8 wt % (25 vol %) UO_2 Dispersed in U–15 wt % Mo, and Molybdenum Clad. (*a*) As polished; (*b*) core-clad bond in greater detail. Etchant: 1 NH_4OH–1 H_2O_2. Reduced 13%.

stainless protective sheath and the molybdenum clad permitted ready stripping of the sheathing from the molybdenum clad. Examination of the rolled plates indicated differences in thicknesses over the frames and cores, undoubtedly caused by too high a rolling temperature.

With the Zr–3 wt % Al cladding, excellent self-bonding was achieved to the frames, but the bonds to the cores were very poor. An apparently brittle diffusion layer was present in the interface. Also, the UO_2 was badly stringered and fractured.

Swaging parameters studied included alloy composition, types of powder, swaging temperature, reduction in area, and post-heat treatment. Elemental powders could be swaged at 1050 and 1100°C to greater than 95% of theoretical density. Good interparticle bonding was obtained, and $^3/_{16}$-in.-diam specimens were machined from the swaged rods. Internal oxidation and inhomogeneity were the primary problems encountered.

The as-received prealloyed shot could be swaged to densities comparable to those for elemental powders, but interparticle bonding was not achieved. Acid cleaning the uranium-molybdenum shot prior to swaging resulted in marked improvement in the quality of interparticle bonding for swaging at 1050°C.

Factors proving important in achieving good swaging results include: (1) purity of powders, (2) high tap density, (3) swaging temperature of at least 1050°C, and (4) maintenance of a good atmosphere in the capsule during processing. It also was indicated that a prolonged annealing treatment prior to swaging is advantageous, especially to achieving homogeneity.

EVALUATION OF BOROSILICATE GLASS AS A BURNABLE POISON

T. D. Watts

To evaluate borosilicate glasses as potential burnable poisons for use in Army Package Power Reactors (APPR), fabricability and compatibility studies have been made on a variety of glasses. The glass particles are attractive as poisons since they have the ability to retain fission gases and should be stable under reactor conditions.[3] They should also minimize the boron-loss problems encountered with most other boron compounds.

It has been shown that a refractory grade of glass containing 4 wt % B_2O_3 may be added to APPR-type fuel elements (type 347 stainless steel–UO_2 dispersions) and then be roll clad into miniature fuel plates. The glass remained spherical, with no evidence of stringering or reactions with the matrix material or fuel (see Fig. 23.5).

[3] W. K. Anderson, "Nuclear Applications of Yttrium, Scandium, and Lanthanons," *Rare Earths and Related Metals*, American Society for Metals, Cleveland, Ohio (in press).

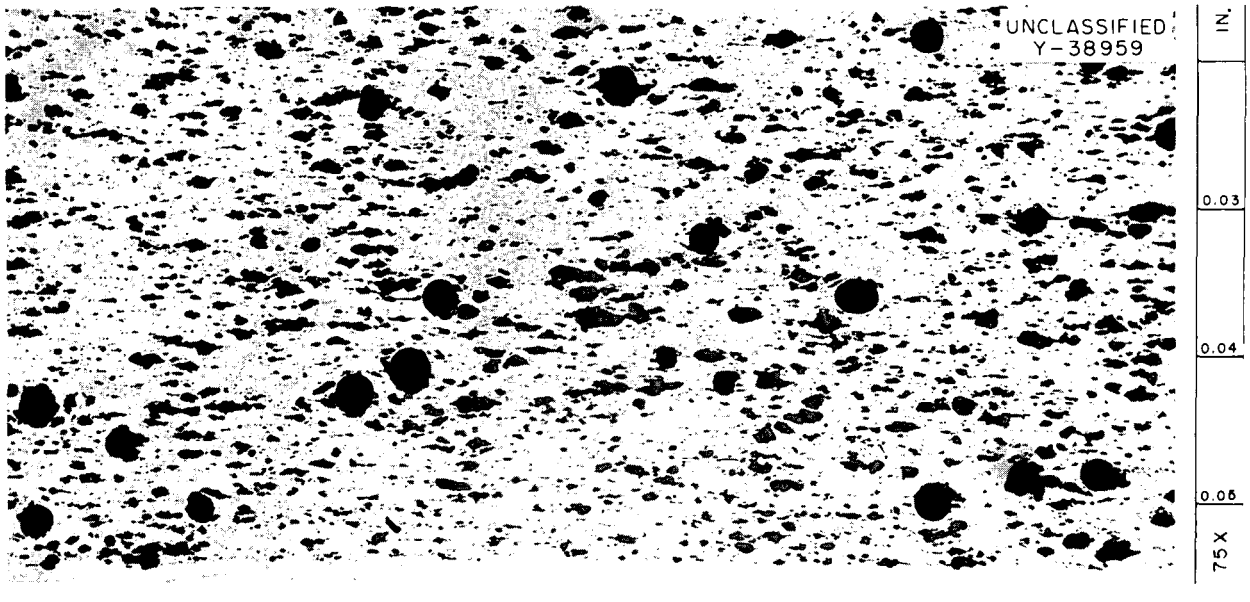

Fig. 23.5. Longitudinal Cross Section of Miniature Plates Containing Hydrogen-Reduced UO_2 and Refractory Borosilicate Glass Beads. Uranium and boron are of SM-2 concentration (21.19 wt % U^{235}, 0.06 wt % B^{10}), and rolling was at 1050°C. The round particles are glass; the irregular particles are UO_2. As polished.

In preliminary tests, a number of borosilicate glasses of selected grades (refractory-type beads, Pyrex beads, enriched Pyrex, etc.) were pressed with type 347 stainless steel powder, sintered, and cold coined. Compacts were roll clad in type 347 stainless steel to evaluate the resistance of the glasses to stringering. These glasses varied in B_2O_3 content and softening points. The volume fraction of glass was adjusted to maintain a uniform boron content. After hot rolling, metallography showed that all glasses, with the exception of the refractory glass, were badly stringered.

The refractory-type glass was then evaluated for compatibility in plates containing UO_2. Compacts were made with 21.19 wt % U and 0.06 wt % B (the SM-2 concentration). All pressed compacts were dense and strong, with no evidence of reactions after sintering and coining. Roll cladding in type 347 stainless steel yielded well-bonded plates with good surfaces and no evidence of reactions or stringering.

Boron retention was evaluated by conducting chemical analyses on samples taken at each step in the fabrication process. Within the accuracy of the method, no boron was lost. All boron-bearing poisons previously examined were subject to considerable boron loss during fabrication. Thus, the borated glass shows great merit in this respect.

OPTIMIZATION OF UO_2–STAINLESS STEEL DISPERSION FUELS

S. A. Rabin J. H. Cherubini

A project is being conducted in conjunction with the APPR Program to develop optimum UO_2–stainless steel dispersions, using the hot-roll cladding method of fabrication. The objective is to improve the properties of UO_2–stainless steel dispersion fuels at reasonable cost. Special emphasis has been given to initial distribution of the dispersoid and its stringering during rolling. While not readily attainable, the ideal fabricated structure would be one with spherical UO_2 positioned in close-packed array in the matrix.

The most outstanding finding of the study to date has been the discovery that very good plate-fabrication results can be obtained with green compacts. In the investigation of the effects of compact condition and density on plate-fabricating characteristics, varying of the initial state was achieved by using (1) cold-pressed condition with increasing pressing pressure, (2) sintered condition with increasing sintering time at a given temperature, and (3) sintered and coined condition. Examination of the rolled composites indicated that green compacts yield equal or better core structure (less stringering and fragmentation of the UO_2) than their sintered or sintered and coined counterparts (see Fig. 23.6). This is most encouraging, since reducing the processing steps will result in a significant cost reduction. Present work is directed at reproducibility of results and the question of whether the improvement in fabrication stems from the elimination of the sintering and/or coining steps or from a lower initial core density.

Blending studies, using 33 wt % (25 vol %) UO_2 (–100 +140 mesh) in –325 mesh stainless steel powder, have shown that the Fermi paste-blending technique[4] produces the most homogeneous cores. However, a technique that includes precoating of the UO_2 particle with camphor and blending with dry stainless steel powder gave good preliminary results, warranting further investigation.

The effect of dispersoid volume fraction on sintered and coined compact density, homogeneity, and the density of the core after rolling was determined and is illustrated in Table 23.1. Although the absolute densities (g/cc) of the compacts increase with increasing UO_2 loading, significantly, the theoretical densities remain fairly constant. For this paste-blending procedure, homogeneity varied with the UO_2 loading, giving the best results at around 25 vol % loading. It was observed with roll cladding at 1200°C that the fuel densities generally decreased with increasing fuel loading (Table 23.1). The seemingly anomalous result at the 20 wt % UO_2 loading is being reexamined.

Allied to this and other dispersion-fuel projects, a program is being conducted with the objective of evaluating the effects of important factors on irradiation damage and elucidating the mechanism of failure.[5] In this connection fabrication development is in progress to prepare irradiation

[4] J. H. Cherubini, R. J. Beaver, and C. F. Leitten, Jr., *Fabrication Development of UO_2-Stainless Steel Composite Fuel Plates for Core B of the Enrico Fermi Fast Breeder Reactor*, ORNL-3077 (Apr. 4, 1961).

[5] J. R. Weir, *A Failure Analysis for the Low-Temperature Performance of Dispersion Fuel Elements*, ORNL-2902 (May 27, 1960).

Fig. 23.6. Transverse Section of Fabricated Plate Containing 35 wt % UO_2 in Stainless Steel Green Compact, Hot Rolled at 1200°C. As polished.

Table 23.1. Stainless Steel Compact Density and Homogeneity as a Function of UO_2 Loading

Uranium Dioxide[a] (wt %)	Sintered[b] (g/cc)	Sintered[b] (% TD)	Coined[c] (g/cc)	Coined[c] (% TD)	Estimate of Homogeneity[d]	Density of Roll-Clad Fuel Section[e] (% TD)
10	5.97	73.5	6.54	80.5	Poor	99
20	6.15	73.5	6.74	80.6	Fair	94.8
25	6.25	73.6	6.84	80.5	Good	97.9
30	6.34	73.6	6.96	80.8	Fair	96.8
40	6.54	73.7	7.18	80.9	Poor	95.8

[a]Mixed −100 +140 (J-03-HA) UO_2 and −100 mesh prealloyed stainless steel.
[b]Cold pressed at 33 tsi; sintered at 1215°C for 1¼ hr.
[c]Coined at 33 tsi.
[d]Paste blending was used.
[e]Rolled at 1200°C.

samples which will incorporate the quantity, size, and porosity of the dispersoid as variables.

Spherical boron carbide is used as the dispersoid constituent and copper for the matrix. By using B_4C instead of a uranium compound, the following experimental advantages will be gained.

1. Consistent with high burnup (gas generation), lower flux positions and/or shorter exposure times can be used.

2. Better experimental control is permitted since less heat is generated.

3. After exposure, samples will be less radioactive.

To ensure close-packed positioning of the dispersoid, the matrix material (copper) is being coated on the B_4C prior to consolidation by hot-die pressing. Densities to 95% of theoretical have been obtained by hot pressing and coining spheroidal copper powder, with higher densities anticipated.

ALUMINUM-MATRIX Al-U_3O_8-B_4C PRESSINGS WITH SYMMETRICAL, STRAIGHT-TAPER GEOMETRY

T. D. Watts A. L. Lotts

The design of the High Flux Isotope Reactor (HFIR) fuel element requires powder metallurgy cores containing U_3O_8, B_4C, and Al for the inner annulus.[6] The original cores were to be 3 in. wide, 2 in. long, and have a linear thickness variation from 0.050 in. to 0.200 in. along the 3-in. width. Plate fabrication called for incorporating the core, together with complementing inserts, to produce a rectangular assembly, in an aluminum alloy frame, and roll cladding along the 2-in. dimension.

Development showed that a tapered die top was required for loading the die in order to obtain a proper distribution of powder. To determine what the powder distribution should be, a statistical analysis was made of as-poured loose-powder tapers (hand graded) vs final pressed taper for a sample of over 100 pressings of various hand-graded tapers. A die top was then designed to conform to the near-optimum graded taper, resulting in a total die configuration which reproducibly gave cores of the desired taper and uniformity of density. A similar die configuration was developed for pressing the matching inserts (B_4C in aluminum).

A number of pressed cores and inserts were sectioned and chemically analyzed for uranium and boron content, respectively. A summary of the chemical analyses along with the densities and configurational tolerances obtained are given in Table 23.2.

All the conditions shown in the table (dimensional as well as chemical) have a bearing on the amount of fuel or poison which will be present through any section normal to the taper. It is the variation in fuel and poison content in relation to the taper direction that is important to control. The values for these factors (with the tolerances shown) gave the fuel content through any section (normal to the taper) within 5% of that specified by the fuel design. This variation was within specified tolerance. These cores were successfully rolled into composite plates while maintaining tolerances.

[6] R. J. Beaver, "Metal Forming and Casting," chap. 18, this report.

Table 23.2. Variations in Homogeneity and Other Properties in HFIR Fuel Cores and Inserts

	U_3O_8-B_4C-Al Fuel Cores		
	Thin Side of Core	Center of Core	Thick Side of Core
Thickness, in.	0.050 ± 0.001	0.125 ± 0.002	0.200 ± 0.002
Density, g/cc	3.784 ± 0.055	3.782 ± 0.057	3.785 ± 0.053
Uranium, %	32.56 ± 0.3	32.57 ± 0.3	32.59 ± 0.3
Boron, %	0.051 ± 0.0015	0.050 ± 0.0013	0.052 ± 0.0014
	B_4C-Al Inserts		
	Thin Side of Insert	Center of Insert	Thick Side of Insert
Thickness, in.	0.020 ± 0.001	0.057 ± 0.001	0.095 ± 0.002
Density, g/cc	2.645 ± 0.048	2.640 ± 0.053	2.642 ± 0.051
Boron, %	0.045 ± 0.0016	0.047 ± 0.0015	0.046 ± 0.0012

While this core design will not be used in the HFIR (the design was subsequently changed), this method of cold pressing mixed powders to a symmetrical, straight-taper geometry nevertheless is novel and represents an advance in the art. Powder fabrication of the new HFIR design was done in conjunction with the Metal Forming Group and is reported in Chap. 18 of this report.

FABRICATION OF HFIR TARGET

E. S. Bomar T. D. Watts

The heart of the HFIR reactor is the target array containing the materials being irradiated to produce the desired transuranic isotopes. While the final design of the target has not been determined, it will consist of approx 31 tubes $\frac{3}{8}$ in. in diameter, each with an active length of 20 in. and a total length of 29 in. Because of the intense radioactivity of many of the heavier isotopes, it will be necessary that all fabrication be done by sealed, remote operations. The fabrication sequence for producing these tubes will consist of pressing pellets of the transuranium oxides dispersed in aluminum, inserting the pellets into an aluminum tube, and then seal welding, followed by collapsing the tube firmly against the pellets.

The HFIR target problem is complicated by the fact that the target materials are not available for large-scale development work. Also, their extremely high radioactivity require that studies be done remotely. Therefore, substitute materials, CeO_2 and Gd_2O_3 (materials chemically similar to the actual target oxides), were used in the preliminary tests.

Pressed pellets of CeO_2 and Gd_2O_3 in aluminum showed only slight density decreases (<3%) in compatibility tests at 600°C. No evidence of any reaction between CeO_2 and aluminum was found metallographically in the 600°C-aged samples. While half the Gd_2O_3 had reacted in the 600°C samples, it was shown to be stable at 500°C. This work was followed by a compatibility test with PuO_2 in aluminum, conducted by the Chemical Technology Division,[7] which confirmed these results. As a portion of this problem, equipment was developed for performing remote metallographic operations with these dispersions.[8]

To permit the architect to proceed with the design of the target-fabrication facility, the manufacturing process indicated above was examined in detail. Tentative items of equipment were selected and have been fitted into the proposed hot cells. Laboratory development has been started on the remote steps considered most likely to cause trouble. At present, emphasis is on the lubrication of the walls of the pressing die and the removal of any lubricant transferred to pellets before incorporating them in tubes.

A second part of the target program has entailed the fabrication of a mockup assembly for the critical experiment. This mockup possessed the same aluminum-to-water ratio as the final element; however, to facilitate criticality testing, a slightly different configuration was used. This target incorporates 30 pellet-containing tubes together with 78 empty tubes. The composition of the pellets was selected to simulate the nuclear characteristics of a target after three months of irradiation. Each of the 30 rods assigned for pellets contained 5.219 g of UO_2 and 3.587 g of silver in an aluminum matrix. The compacts were 0.2375 ± 0.005 in. in diameter and stacked to a length of $20 \pm \frac{1}{8}$ in.

It was determined by radiographic, metallographic, and electron reflection studies that segregation could be minimized by using a binder of 5% paraffin in CCl_4 ($\frac{1}{2}$ wt % paraffin, based on total weight of constituents present in the compact). This combination produced pellets much more homogeneous (see Fig. 23.7) than those obtained by using any other binder. After overcoming difficulties due to entrapped binder and die lubricant, pellets were pressed to the required dimensions and uniformity. Then they were incorporated into rods and the target successfully fabricated.

[7] *Oak Ridge National Laboratory Status and Progress Report*, ORNL-3097, p 26 (Mar. 9, 1961) (Official Use Only).

[8] "Metallography," chap. 19, this report.

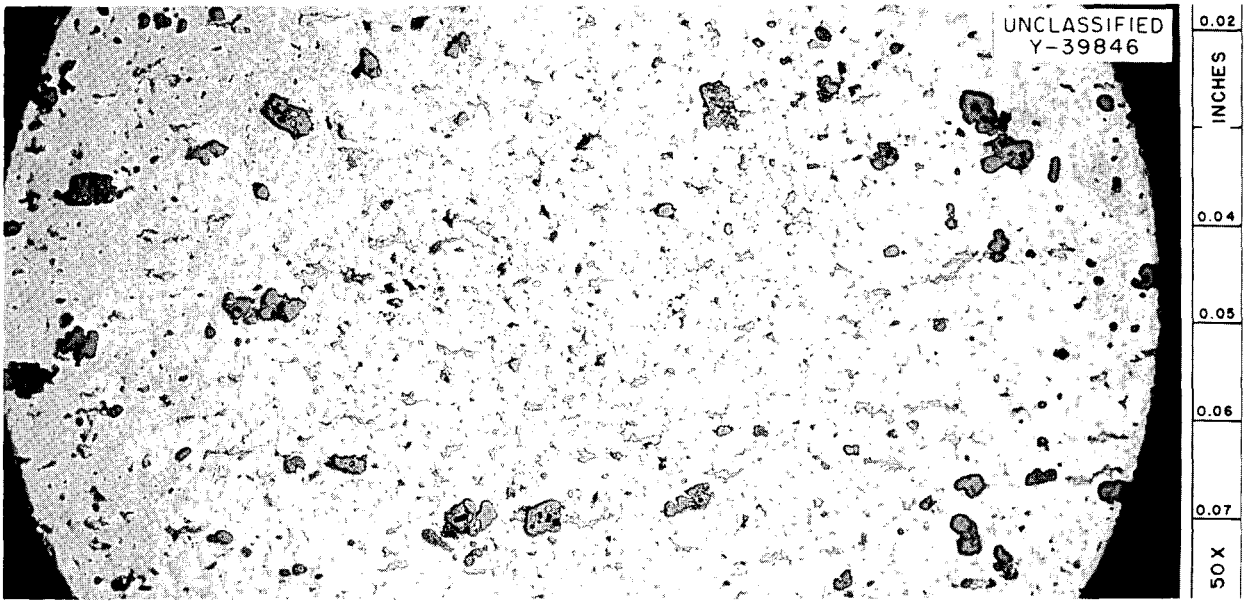

Fig. 23.7. Microstructure of Matrix of Target Rods Prepared for HFIR Critical Experiments. The dark gray phase is UO_2; the light gray phase is silver; the matrix is aluminum. As polished.

COMPATIBILITY OF MATERIALS OF INTERMEDIATE NEUTRON CROSS SECTION WITH ALUMINUM

T. D. Watts

A formidable area of development is concerned with the "gray" section of the HFIR control element. One control-element concept calls for the use of absorber elements of varying cross section dispersed in a matrix of aluminum. Elements considered suitable in neutron-absorption cross section for the gray section are manganese, tantalum, or tungsten. The study herein reported deals specifically with the pressing behavior of the gray absorber elements in aluminum and whether these elements will be chemically compatible.

A series of pressings were made on equivalent concentrations of manganese (51 at. %), tantalum (37 at. %), and tungsten (43 at. %) in aluminum. These amounts constitute estimates of concentrations required for the gray section. For ½-in.-diam manganese-aluminum compacts, the pressed density ranged from 64.31 to 85.95% of theoretical, for pressures varying from 3 to 33 tsi. Under similar conditions, the tantalum-aluminum compacts had densities ranging from 61.06 to 89.25%. Tungsten-aluminum compacts pressed at pressures less than 20 tsi cracked or broke when ejected from the pressing die, and the highest density achieved was 74.71% of theoretical.

Heat treatments for 100 and 500 hr at 500 and 600°C were conducted on aluminum-matrix compacts containing manganese, tantalum, or tungsten. These samples were pressed at 33 tsi and had the concentrations given earlier. The manganese and tungsten samples showed severe cracking and expansion as a result of reactions. The microstructure of the tantalum-aluminum compacts showed evidence of considerable reaction, but the pellets remained sound, with no appreciable changes in dimensions.

Compacts also were pressed by using TaC or WC as the dispersoid, maintaining the same atom percentages of tantalum and tungsten. With these materials, a binder (dodecyl alcohol) was required to achieve a compact with sufficient strength for handling. Heat treatment of these compacts resulted in a small amount of reaction but no deleterious dimensional effects.

Additional pressing and heat-treating studies were made on the tantalum-aluminum system, with the tantalum content ranging from 37.36 to 73.91 at. % (80 to 95 wt %). The bulk densities and structures at each step were not noticeably affected by increasing the quantity of tantalum.

It was shown also to be possible to hot roll-clad the small tantalum-aluminum compacts by using high-strength type 6061 aluminum as cladding. Full-size plates remain to be tried.

24. WELDING AND BRAZING

G. M. Slaughter

MATERIALS-JOINING DEVELOPMENT

Beryllium

R. G. Gilliland

The unique properties of beryllium, such as its low neutron-absorption cross section, make it extremely attractive as a cladding material for advanced fuel elements. The obvious lack of suitable joining procedures, however, has been a major obstacle in the consideration of this metal for high-temperature nuclear applications. Serious weld-metal and heat-affected zone-cracking difficulties have been encountered by several investigators, and gross weld-metal porosity and brittle joints are other common salient defects. The development of brazing alloys for joining beryllium has been hindered by the generally poor wettability of this material and the rapid formation of brittle intermetallics along the base metal–braze metal interface. The development of suitable joining techniques for beryllium is therefore in progress, under Gas-Cooled Reactor Program support, in an effort to improve the over-all technology of fabricating advanced fuel elements.

As a result of these studies, two beryllium-clad capsules containing UO_2 were successfully fabricated for irradiation investigations in the ORR poolside facility.[1] In addition, the fabrication of over 200 beryllium tube-burst specimens for use in high-temperature in- and out-of-pile testing was completed.[2] No failures have occurred thus far in either the welded or brazed joints. The detailed determination of optimum values of the important welding variables such as welding current, inert-gas flow rate, and preheat permitted the production of very sound, high-integrity, tube-to-end-cap welds.

Significant differences in the weldabilities of beryllium tubes made by different vendors by various fabrication processes were also observed, and modifications in procedures for producing sound welds in each type of material were successfully developed.

Stainless steel capillary tubes were successfully brazed into the aforementioned beryllium tube-burst specimens with an experimental Ti-Cu-Be (49-49-2 wt %) experimental alloy. This alloy, although adequate for applications where induction brazing (with consequent short brazing times) can be used, forms brittle intermetallics when the time at brazing temperature is increased. The longer-range studies have therefore been associated with the development of more versatile alloys.

Niobium

Welding (E. A. Franco-Ferreira). – The excellent elevated-temperature mechanical properties of niobium and its alloys cause them to be of major interest as structural materials for high-temperature reactor systems. An extensive program was conducted to study the aging reaction that has been observed to occur in welds in the Nb–1% Zr alloy, an alloy exhibiting a particularly good compromise in properties for liquid-metal systems. Although the binary phase diagram for the niobium-zirconium system indicates that a solid solution should exist at this composition, interstitial impurities cause another phase (or phases) to precipitate in the 1500 to 1800°F range, which results in serious embrittlement in welds. It was therefore felt that the investigation of this phenomenon and methods for minimizing it was of prime importance.

A study was made of various post-weld annealing treatments as a possible method of circumventing the aging reaction. Hardness studies indicated that annealing for approx 1 hr at 1900 to 2200°F is very effective in preventing the

[1] *GCR Quart. Progr. Rept. Sept. 30, 1960*, ORNL-3015, pp 102–6.

[2] *GCR Quart. Progr. Rept. Dec. 31, 1960*, ORNL-3049, pp 231–35.

aging reaction and its consequent weld embrittlement. However, the annealing range 2000 to 2200°F produces a significant reduction in hardness values when compared with an annealing temperature of 1900°F. A metallographic survey was also made of the welds in this study and composite photographs are shown in Fig. 24.1. As the annealing temperature is raised, a heavy precipitate appears as a network throughout the matrix. Further, there is very little change in appearance after aging. X-ray diffraction and microprobe-analysis techniques are being utilized in an attempt to determine the nature of the precipitate.

The use of the Rockwell-B hardness test to evaluate the aging behavior of welds was also studied, and the results were compared with previous bend-test results.[3] Although this test is useful for following the aging phenomenon as it occurs in welds, it is not reliable for determining the absolute extent of aging that has occurred. Some points associated with brittle and borderline behavior have, in some cases, lower hardness values than points associated with ductile behavior. Thus, it is impossible to predict from mere knowledge of the hardness of an aged weld whether or not it will be brittle.

Brazing (C. W. Fox). – In view of the extreme interest in niobium and its alloys for a variety of high-temperature reactor applications, a program has been initiated to develop suitable brazing alloys and brazing procedures for attaching niobium to itself and to stainless steels. The conventional commercial nickel-base and precious-metal-base high-temperature brazing alloys are not suitable for brazing niobium because of their poor flowability and joint strength or because of their poor corrosion resistance to liquid metals (an environment of particular interest to high-temperature refractory-metal systems).

The alloy development program has consequently been concentrated on systems which are based on corrosion-resistant refractory metals such as titanium and zirconium. Several experimental brazing alloy compositions were formulated from a study of the applicable phase diagrams, and the more promising were used to make niobium-to-niobium and niobium–to–stainless steel T-joints.

Preliminary studies, the results of which are shown in Table 24.1, revealed that all these alloys readily wet and flowed on niobium, and several appeared promising for joining niobium to stainless steel. In view of the very promising nature of this initial work, an extensive program

[3] *Met. Div. Ann. Progr. Rept. July 1, 1960*, ORNL-2988, pp 456–58.

Table 24.1. Results of Brazing Studies on Niobium-to-Niobium and Niobium–to–Stainless Steel T-Joints

Brazing Alloy (wt %)	Flow Point (°C)	Flowability on	
		Niobium-to-Niobium	Niobium–to–Stainless Steel
67 Zr–29 V–4 Fe	1300	Excellent	Extreme stainless steel dilution – poor flow
60 Zr–25 V–15 Nb	1280	Excellent	Severe stainless steel dilution – fair flow
48 Zr–48 Ti–4 Be	1050	Excellent	Good flow
63 Ti–27 Fe–10 Mo	1250	Excellent	Good flow
63 Ti–27 Fe–10 V	1280	Excellent	Severe stainless steel dilution – very poor flow
68 Ti–28 V–4 Be	1250	Excellent	Poor flow – joint separated on cooling
45 Ti–40 Zr–15 Fe	1050	Excellent	Good flow
75 Zr–19 Nb–6 Be	1050	Excellent	Good flow
80 Zr–17 Fe–3 Be	1000	Excellent	Very poor flow – joint separated on cooling
46 Ti–46 Zr–4 V–4 Be	1000	Excellent	Very poor flow
95 Zr–5 Be	1000	Excellent	Good flow
62 Ti–26 Fe–8 Mo–4 Zr	1250	Excellent	Fair flow – joint separated on cooling

has been outlined to further evaluate these alloys. It will include tests of joint aging, mechanical properties, effects of thermal cycling, and liquid-metal corrosion.

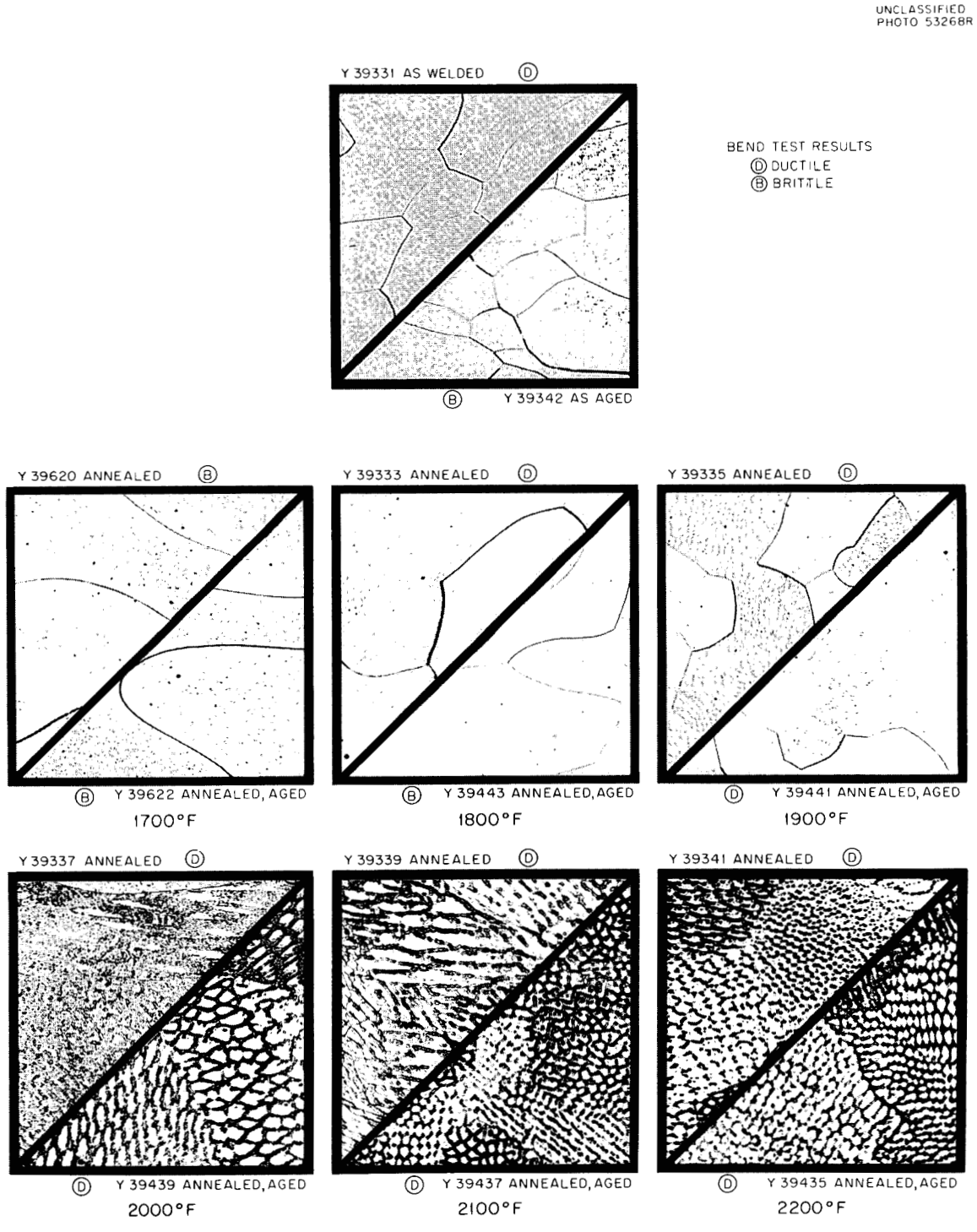

Fig. 24.1. Nb–1% Zr Welds Annealed at Various Temperatures for 2 hr (Upper Left); Aged 100 hr at 1500°F After Annealing (Lower Right). Photograph at top is a control. Reduced 54%.

INOR-8

R. G. Gilliland

INOR-8, an Ni-Mo-Cr alloy, will be used as the structural material for the Molten-Salt Reactor. Extensive studies[4] on this material indicated that it possessed generally good weldability and that no cracking difficulties should be encountered even when welding under conditions of high restraint. However, during the routine qualification of welders at the Y-12 plant, a possible weld-cracking problem was detected. The incidence of cracking of this heat was demonstrated in bend tests and metallographic examination. A cursory examination of the welding procedures indicated no obvious remedy, but it did reveal that all the material came from a single heat. In view of the importance of this problem, an investigation was immediately initiated to determine its seriousness and to develop methods for circumventing it.[5]

Welding tests were performed with a variety of heats of parent metal and weld metal and with different plate thicknesses. Detailed examination, including extensive metallography, of the numerous test weldments was performed. The principal reason for the INOR-8 cracking difficulty seemed to result from improper melting practice at the vendor's plant, and, consequently, special heats of material made with improved practices were obtained. Welding tests conducted at the vendor's plant and at ORNL indicated that these special heats possess good weldability. The information obtained from these tests will be utilized to advantage in the purchase of the INOR-8 for the actual reactor applications.

As a means of overcoming the weld-cracking difficulties, a slightly modified experimental INOR-8 filler wire composition containing 2 wt % niobium also was found to be adequate. This filler metal was developed in the course of the INOR-8 welding program previously conducted by the Welding and Brazing Laboratory and was considered to be exceptionally promising, in view of its excellent elevated-temperature mechanical properties.[6] Despite its somewhat increased cost, this filler wire is a definite alternative solution to the problem, since no evidence of weld-metal cracking was observed either in bend tests or in metallographic sections. Its use would serve also as a safety factor, since parent materials of marginal weldability can also be welded with filler wire of this composition.

Studies to evaluate the microfissuring tendencies of INOR-8 have been performed by using the hot-ductility test developed and carried out at Rensselaer Polytechnic Institute. To date, it has been demonstrated that the particular heat of parent material exhibiting the cracking tendencies in the Y-12 qualification work possesses extremely poor ductility at high temperatures. The ductility test may serve as a rapid definitive measure of the weldabilities of specific heats of INOR-8, since compositions possessing good known weldability have also exhibited good hot ductility in this test.

Welding of Ferritic Steels to Stainless Steels

G. M. Slaughter

From an economic standpoint, it is often desirable to use ferritic carbon or low-alloy steels for pressure vessels and steam generators. Studies were continued to determine the best methods for joining these ferritic steels to austenitic stainless steels for such critical applications as the primary coolant piping for the Experimental Gas-Cooled Reactor.[7,8] The experience of the steam-power industry indicated that cracks in dissimilar welds could be expected after repeated thermal cycling, as a result of the differing thermal expansion coefficients of the two materials. A nickel-base alloy electrode, INCO BP-85,[9] was determined to be a satisfactory filler metal because of its intermediate thermal expansion coefficient, excellent mechanical properties, and its good capability for depositing sound weld metal.

---

[4] G. M. Slaughter, P. Patriarca, and R. E. Clausing, "Welding of Nickel-Molybdenum Alloys," *Welding J.* 38(10), 393s (1959).

[5] *MSR Quart. Progr. Rept. Jan. 31, 1961*, ORNL-3122 (in press).

[6] *MSR Quart. Progr. Rept. July 31, 1959*, ORNL-2799, p 72.

[7] *GCR Quart. Progr. Rept. Sept. 30, 1960*, ORNL-3015, pp 95–96.

[8] *GCR Quart. Progr. Rept. Dec. 31, 1960*, ORNL-3049, pp 224–27.

[9] International Nickel Co., New York, N.Y.

Transverse tensile specimens were machined from carbon steel [ASTM designation: A212 – 57T (grade B)]–to–type 304 stainless steel welds and from 2¼ Cr–1 Mo steel–to–type 304 stainless steel welds. These were tested at room and elevated temperatures, and in every case the specimens failed in the base metal with the tensile strength at failure essentially that reported for the base material.

The thermal cycling of large pipes (14 in. in diameter, 1-in.-thick wall) containing these ferritic steel–to–stainless steel welds is also in progress, and no evidence of cracking was found in the joints after 50 cycles between 1050°F and room temperature.

A subcontract to study the diffusion of carbon in dissimilar-metal welds at elevated temperature is in effect at Virginia Polytechnic Institute.[10] The results to date indicate that when carbon diffuses into the type 304 stainless steel side of the joint, the type 304 stainless steel adjacent to the original interface becomes saturated with carbon and no further diffusion can occur until the area again becomes unsaturated in carbon. The only way this can occur is for the carbon to diffuse farther into the type 304 stainless steel. It is generally accepted that the diffusion rate of carbon is more rapid in ferrite than in austenite, so the diffusion of carbon from the ferrite to the austenite will be slowed down somewhat by the slower diffusion rate in the austenite. Examination of the type 304 stainless steel side of the interface shows that diffusion is more rapid along the austenite grain boundaries than within the austenite grains.

From the calculations, it seems that the major part of carbon diffusion occurs in the early stages of exposure at the temperature investigated, and that after prolonged exposures, the width of the decarburized zone changes very little. This indicates that the major portion of the property changes in welds between type 304 stainless steel and SA-212 (grade B) would occur after relatively short times. These changes are caused by the diffusion of carbon from SA-212 (grade B) into the type 304 stainless steel. It would also be expected that little change in the properties would occur after the first few years of exposure.

[10] Progress Report on Diffusion of Carbon in Dissimilar-Metal Welds to Union Carbide Nuclear Co., Subcontract No. 1444, Feb. 20, 1961, private communication.

Zircaloy-2

J. W. Tackett

Welding Misaligned Components. – The present HRT core vessel was fabricated by welding together a network of preformed spherical sections by the Newport News Shipbuilders and Drydock Company under Subcontract No. W40X-31990.[11] If hot spinning were to be used to fabricate the replacement-vessel components, it might be extremely difficult and expensive to obtain a perfect preweld fitup for the single-girth weld.

Therefore, an investigation was conducted to determine the amount of misalignment which could be allowed in the preweld fitup to permit a sound, uncontaminated root pass with a hydrodynamically acceptable contour.[12] Zircaloy-2 plate, 0.317 in. thick, was utilized for the complete study. The results indicated that the production of satisfactory welds is feasible where the joint components are misaligned as much as 0.090 in., an amount which should be reasonable to meet in fabrication.

Attachment of Inlet Orifice Vanes. – Possible designs of HRT replacement core tanks called for a double-walled Zircaloy-2 inlet region, with closely spaced vanes located in the annulus in order to direct the inlet fuel stream tangentially against the outer core-vessel wall. The vanes would probably have a contoured shape, with a maximum thickness of 0.1 to 0.2 in. and a length of 0.5 to 1 in., spaced at intervals of twice the vane thickness. Studies were therefore conducted to determine suitable methods of fabricating vaned inserts.[13]

A very promising method consisted of machining the vanes so as to be integral with the outer wall. These vanes were subsequently welded to the inner wall in an inert-atmosphere chamber by the inert-arc process. A mockup assembly was successfully fabricated involving this joint design.

[11] D. E. Tackett, *Fabrication History of HRT Core Tank*, ORNL CF-58-12-6 (Dec. 1, 1958).

[12] *HRP Quart. Progr. Rept. Nov. 30, 1960*, ORNL-3061, pp 104–8.

[13] *HRP Quart. Progr. Rept. Nov. 30, 1960*, ORNL-3061, pp 102–6.

COMPONENT FABRICATION DEVELOPMENT

Aluminum-Alloy Fuel Element Development

J. W. Tackett

The welding development studies over the past year for the High-Flux Isotope Reactor (see Chap. 18) have consisted primarily of determining suitable procedures for fabricating a prototype fuel element for criticality studies.[14,15]

A joint design (see Fig. 18.8, Chap. 18) was selected which permitted the welding of the outer trailing edges of the fuel plates to each other with a minimum of effect on the water gap or plate-to-plate spacings. Several subsize mockup assemblies were then constructed to determine suitable values for the welding current, travel speed, and other welding variables. Welder qualification tests were conducted in order to thoroughly familiarize the assigned welder with the problems peculiar to the fabrication of the critical assembly.

The fabrication of the outer and inner annuli were undertaken separately in a special temporary weld shop set up for this purpose. The fuel plates were held rigidly in position for welding by a number of circumferential steel bands. Short longitudinal weld beads were randomly deposited between the steel bands in the first step. The steel bands were then removed and the outer annulus completely sealed around the circumference by welding, as shown in Fig. 24.2. Some difficulty with excessive shrinkage was encountered while making the final tie-ins of the outer element; therefore, the inner element was left

[14] C. A. Burchsted, *High Flux Isotope Reactor Critical Experimental Equipment*, ORNL CF-60-4-120 (Apr. 20, 1960).

[15] P. R. Kasten and R. D. Cheverton, *Revised Version of HFIR Critical Experiment-2 (HFCE-2)*, ORNL CF-61-1-42 (Jan. 16, 1961).

UNCLASSIFIED
PHOTO 53466

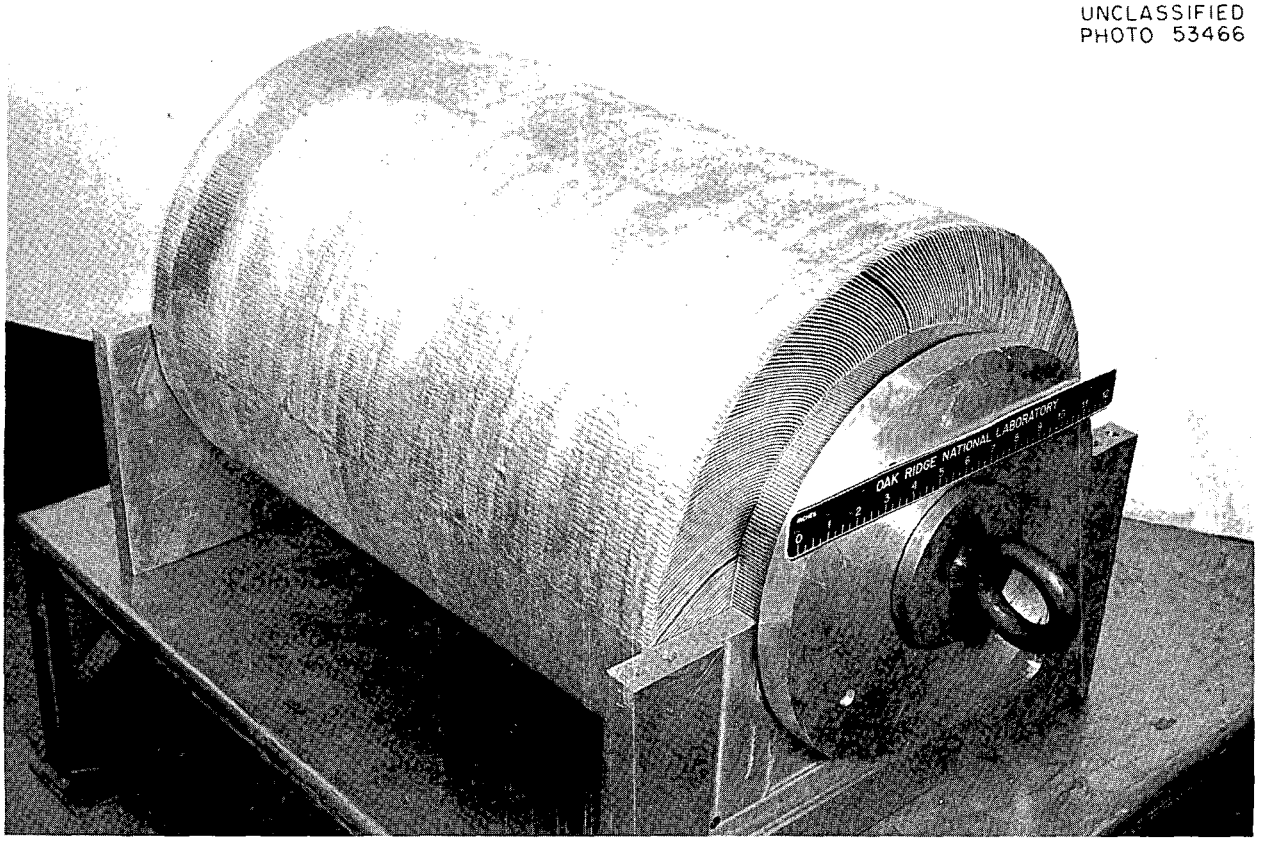

Fig. 24.2. Outer Annulus of HFIR Critical Assembly After Completion of Welding.

with short welds covering about half the total length. After completion of each annulus, the two were assembled (see Fig. 18.5) and delivered for criticality tests.

The welding operations performed on the inner annulus were conducted subsequent to the operations on the outer annulus and incorporated several corrective steps for improved dimensional control. Teflon spacers were placed near the outer edges of the water channels and extended in one-third of the distance from each end. The plate spacings obtained on this element are summarized in Table 24.2. While the outer annulus was welded successfully and will serve for the critical test, sufficient deformation of the plates occurred in reducing the diameter to size to make invalid any comparison of plate spacing. However, achieving such control on the first element assembled by this technique is a significant achievement and demonstrates that fabrication of such a unit is technically feasible.

Table 24.2. Spacing Measurement on Inner Annulus of HFIR Critical Element

Channels	
Number measured	159
Per cent within 0.005-in. tolerance[a]	883.0
Per cent within 0.003-in. tolerance[b]	76.7
Channel cross sections	
Number measured	1113
Per cent with 0.005-in. tolerance[a]	99.3
Per cent within 0.003-in. tolerance	94.9
Per cent of individual measurements outside ±0.010 in.	98.2

[a]HFIR critical element tolerance – average for each channel cross section is ±0.005 in., with no individual measurement greater than ±0.010 in.

[b]Reactor element tolerances – average for each channel cross section is ±0.003 in., with no individual measment greater than 0.010 in.

Stainless Steel Flat-Plate Fuel Element Development

R. G. Donnelly

At the request of Atomic Power Development Associates in Detroit, Michigan, the ORNL Metallurgy Division was given the responsibility for materials development of the Enrico Fermi Reactor core B fuel element. The Welding and Brazing Laboratory undertook the development of satisfactory procedures for assembling the individual fuel plates into a rigid bundle, a schematic drawing of which is shown in Fig. 24.3. The difficulty of the task is illustrated by the required tolerances, listed below.

	Nominal Dimensions (in.)	Tolerance (in.)
Element height	2.398	±0.005
Plate-to-shroud spacing	0.035	±0.0015
Plate-to-plate spacing	0.054	±0.002

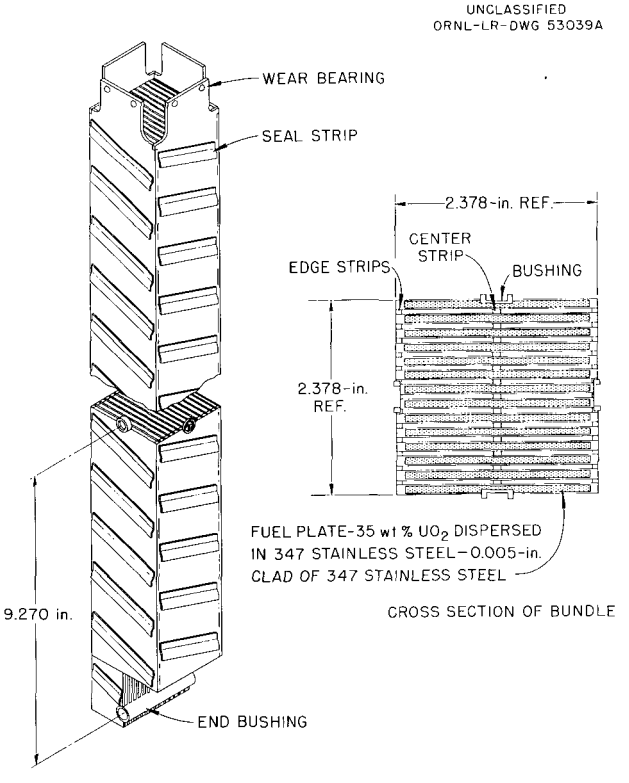

Fig. 24.3. Schematic Drawing of Core B Fuel Bundle for the Enrico Fermi Reactor.

The development program was concentrated on a brazed fuel bundle, since preliminary experiments indicated that the welding created excessive distortion. Several subsize mockup assemblies were constructed in order to determine the correct amount of brazing alloy and the optimum brazing cycle and to determine suitable jigging procedures

for attaining the desired tolerances. A low cross section, commercial, high-temperature brazing alloy, Ni-Cr-Se-Fe, was selected on the basis of mechanical properties, cross section, and sodium-corrosion resistance.

Three full-size assemblies with nonfuel-containing plates were then successfully fabricated at ORNL. Excellent flow of the braze was obtained, and the over-all appearance was excellent. These bundles also included the attachment of the necessary spring fingers, wear balls, and center and side bushings. A photograph of a completed dummy bundle is shown in Fig. 24.4. Typical frequency-vs-distribution plots of the type shown in Fig. 24.5 were made for each bundle, and the results indicated excellent control of the channel-spacing measurements. This dummy bundle exhibited a very even distribution and a peak on the nominal spacing of 54 mils. Only two of the 442 measurements taken were out of tolerance, and then by only $\frac{1}{2}$ mil.

The fabrication of similar assemblies with fuel-containing plates is in progress in view of the success obtained with the work to date.

Solidified-Metal Seal Development

R. G. Donnelly

The use of solidified-metal seals for elevated-temperature, leak-tight, quick-disconnect joints has been considered for a number of applications, including high-vacuum valve and flange studies for the Sherwood Project.[16] Such seals appear to be especially suitable for molten-salt reactor application since they are readily applicable for remote handling and since relatively simple equipment may be used for making and breaking the joint.

To demonstrate the feasibility of these types of solidified-metal seals, several small components have been constructed and evaluated.[17,18] A sump-type seal, fabricated from INOR-8 and sealed

[16] J. W. Tackett, *Progress Report — Bakable High-Vacuum Valve and Flange Studies*, ORNL CF-59-2-3 (Feb. 6, 1959).

[17] *MSR Quart. Progr. Rept. July 31, 1960*, ORNL-3014, pp 58–61.

[18] *MSR Quart. Progr. Rept. Jan. 31, 1961*, ORNL-3122 (in press).

UNCLASSIFIED
PHOTO 52673

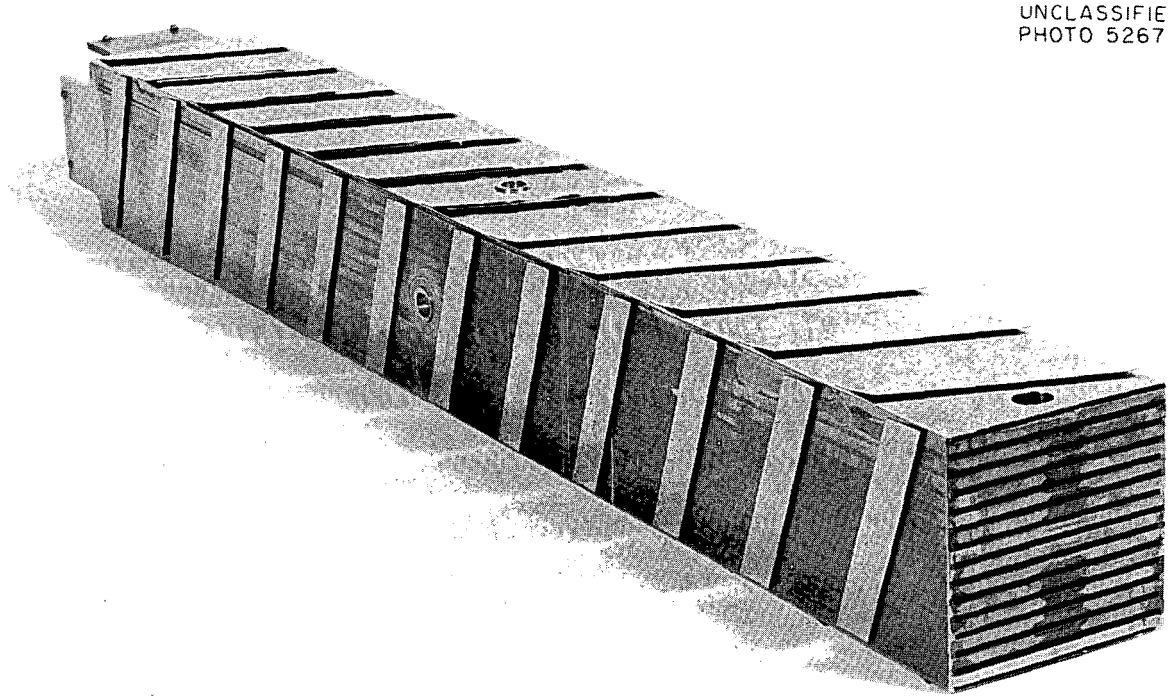

Fig. 24.4. Completed Full-Size Core B Mockup Fuel Assembly for the Enrico Fermi Reactor.

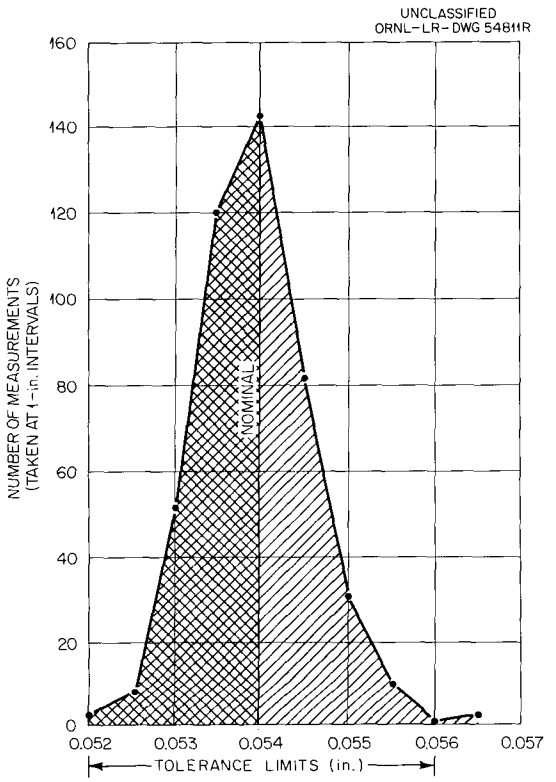

Fig. 24.5. Dermitron Data of Channel Spacing in Fermi Core B Dummy Element No. 1.

with 80 Au–20 Cu (wt %), has been operated and found to be helium leak-tight after each of ten cycles of breaking and sealing.

Unsintered molybdenum-fiber compacts impregnated with gold-copper are also being investigated for use as potential seal materials. Demonstration assemblies have been operated, and it appears that impregnated fiber compacts of this type can be operated successfully for several sealing operations. However, since slight oxidation of the mating components will prevent adequate sealing, these components must either be brightened in hydrogen or replaced.

Instrumented Fuel-Capsule Fabrication

E. A. Franco-Ferreira

Developmental work is being carried out in an effort to improve the methods of attaching thermocouples for measuring temperatures in gas-cooled reactor irradiation test capsules.[19,20] This work also is directly applicable to the fabrication of instrumented fuel assemblies for the EGCR.

One of the most difficult problems is that of joining refractory-metal (tungsten or molybdenum) tubular thermocouple wells to stainless steel end caps of irradiation test capsules. The wide differences in thermal expansion coefficients and variations in wetting and alloying behavior require special brazing techniques to obtain leak tight, high-melting seals. The use of copper as a brazing alloy was found to be suitable for brazing these wells in the end caps of irradiation test capsules since it wets both the refractory metals and stainless steel and is very ductile.

Another problem of prime importance is associated with the fabrication of tungsten-rhenium thermocouples for the measurement of very high temperatures in the interior of the fuel pellets. Extreme care in fitup of the joint and close control over the welding current are necessary for joining these fine-wire thermocouples. However, the reliability of the over-all assembly is reduced by the inherent low ductility of tungsten wire and the added embrittlement of the tungsten that results from recrystallization during welding. One approach for solving this problem, which has been investigated and appears promising, was suggested by investigators at the General Electric Company[21] and involves the use of stranded small-diameter tungsten wires. Typical assemblies have been made and are highly flexible, but difficulties associated with obtaining such composites from industrial sources have prevented their use in actual capsules. Procedures have also been developed which appear entirely satisfactory for attaching thermocouples to the stainless steel fuel element tubes for the measurement of surface temperatures. Special electrodes were required in order to resistance-tack-weld the thermocouples to the interior of the tube walls in the exact desired location prior to brazing. Some modifications in welding procedure were also necessary for making the end-closure weld with a thermocouple penetration immediately adjacent to the joint. Sections taken through the thermocouple and end cap at the place where the thermocouple is brazed to the end cap have revealed excellent brazing-alloy flowability.

[19] *GCR Quart. Progr. Rept. Dec. 31, 1960*, ORNL-3049, pp 220–25.

[20] *GCR Quart. Progr. Rept. Mar. 31, 1961*, ORNL-3102, pp 131–33.

[21] Private communication from General Electric Co.

PAPERS, ORAL PRESENTATIONS,

AND

OPEN-LITERATURE PUBLICATIONS

PAPERS AND ORAL PRESENTATIONS GIVEN AT SCIENTIFIC AND TECHNICAL MEETINGS JULY 1, 1960–MAY 31, 1961

Tenth High-Temperature Fuels Committee Meeting, Atomics International, Canoga Park, California, Aug. 9–10, 1960

J. E. Cunningham, "Fuels Studies"
J. L. Scott, "The Development of Fuel Element Materials for Gas-Cooled Reactors"

Fifth General Assembly of the International Union of Crystallography, Cambridge, England, Aug. 15, 1960

H. L. Yakel, "Erbium Manganite – A New ABO_3 Structure"
H. L. Yakel, "A Structural Study of Transformations in Metastable Body-Centered-Cubic Alloys"

VII International Conference on Low Temperature Physics, University of Toronto, Canada, Aug. 29–Sept. 3, 1960

J. O. Betterton, Jr.,* and D. S. Easton, "Effects of Alloying Elements on the Electrical Resistivity of Zirconium"
G. D. Kneip, Jr.,* and J. O. Betterton, Jr., "The Specific Heats of Some Zirconium Alloys"

Symposium on the Environmental Factors Influencing Optimum Operations of Ordnance Materiel, San Antonio, Texas, Sept. 27–30, 1960

H. E. McCoy* and J. R. Weir, "Effect of Environment on the Mechanical Properties of Metals"

1960 Annual Meeting of the AEC Welding Forum, San Antonio, Texas, Oct. 3–6

G. M. Slaughter, "Resumé of Welding and Brazing Developmental Work Under Way at the Oak Ridge National Laboratory"
G. M. Slaughter* and T. R. Housley, "Welding of Ferritic Steels to Austenitic Stainless Steels"
E. A. Wick* and R. L. Heestand, "Fabrication of Fuel Assemblies for the Experimental Gas-Cooled Reactor"

Refractories Division Meeting of the American Ceramic Society, Bedford Springs, Pa., Oct. 7, 1960

A. T. Chapman,* W. R. Foster, and T. S. Shevlin, "An Investigation of the Compatibility Relationships and Kinetics of Selected Reactions in the Si-O-C System"

Metallurgy Society of the AIME, Philadelphia, Pa., Oct. 17–20, 1960

G. F. Bolling, T. B. Massalski, and C. J. McHargue,* "An X-Ray Study of Deformation Stacking Faults at Low Temperatures in Lead, Some Lead Alloys, and Aluminum"

Fall Meeting of the Electrochemical Society, Houston, Texas, Oct. 9–13, 1960

R. E. Pawel,* J. V. Cathcart, and J. J. Campbell, "Microtopography of Oxide Films Formed on Tantalum"

First Conference on Nuclear Reactor Chemistry, Gatlinburg, Tennessee, Oct. 12–14, 1960

J. H. DeVan, "Corrosion of EGCR Structural Materials by Contaminants Desorbed from Moderator Graphite"

*Speakers.

American Society of Metals, Chattanooga Chapter, Chattanooga, Tennessee, Oct. 28, 1960

D. A. Douglas, "Mechanical Properties Studies for Design and Construction of Reactors"

Annual Meeting of the Geological Society of America, Denver, Colo., Nov. 3–5, 1960

Otto C. Kopp,* L. A. Harris, and G. W. Clark, "The Hydrothermal Conversion of Muscovite to Kalsilite and an Iron-Rich Mica"

Franklin Institute Weekly Seminar, Philadelphia, Pa., Nov. 7, 1960

Bernard Borie, "An X-Ray Diffraction Study of the Oxidation of Copper"

Dispersions Fuel Elements Meeting, AEC, Washington, D.C., Nov. 9, 1960

G. M. Adamson, Jr., "Progress in the Technology of Dispersion Fuel Elements at the Oak Ridge National Laboratory"

J. L. Scott, "Analytical Work on the Failure of UO_2–Stainless Steel Dispersion Fuels"

The Aluminum Task Force Meeting, AEC, Washington, D.C., Nov. 10, 1960

G. M. Adamson, Jr., "Summary of Aluminum-Base Fuel Element Development at the Oak Ridge National Laboratory

1960 Annual Winter Meeting of the ASME, New York, N.Y., Nov. 27–Dec. 2

D. L. McElroy, Discussion of paper, "Thermal Conductivities of Some Commercial Iron-Nickel Alloys," by T. W. Watson and H. E. Robinson

C. R. Kennedy, Discussion of paper, "Effect of Combined Stress on Yield and Fracture of Zircaloy-2," by R. L. Mehan

M. L. Picklesimer* and P. L. Rittenhouse, Discussion of paper, "Effect of Combined Stress on Yield and Fracture of Zircaloy-2," by R. L. Mehan

AEC/AECL Meeting on Uranium Dioxide Information Meeting, Savannah River Laboratory, Aiken, S.C., Nov. 30–Dec. 1, 1960

W. C. Thurber, "UO_2 Fuel Elements for the Maritime and Fermi Reactors"

D. F. Toner* and J. L. Scott, "Study of the Factors Controlling the Release of Xe^{133} from Bulk UO_2"

First AEC Beryllium Oxide Meeting, Oak Ridge National Laboratory, Oak Ridge, Tenn., Nov. 30, 1960

W. O. Harms, "Research on Beryllium Oxide and Fueled Beryllium Oxide at Oak Ridge National Laboratory"

Third AEC Uranium Carbide Meeting, Oak Ridge National Laboratory, Oak Ridge, Tenn., Dec. 1–2, 1960

T. Hikido, "Uranium Carbide Research at the Oak Ridge National Laboratory"

AEC-NASA Liquid Metals Corrosion Meeting, Washington, D.C., Dec. 7–8, 1960

E. E. Hoffman, "Summary of Boiling Alkali Metal and Related Studies at Oak Ridge National Laboratory"

1960 Annual American Nuclear Society Meeting, San Francisco, Calif., Dec. 11–14

W. R. Martin, "Dimensional Studies of Simulated EGCR Fuel Capsule at Elevated Temperature"

Eleventh High-Temperature Fuels Committee Meeting, General Atomic, San Diego, Calif., Jan. 10–12, 1961

J. L. Scott, "Advances in the Development of Fuel Element Materials for Gas-Cooled Reactors"

W. C. Thurber, "Fuel Element Development for Maritime and Army Reactors"

Fourth Semiannual Meeting on the ORNL Fast Breeder Assistance Program, Detroit, Mich., Jan. 31, 1961

J. H. Cherubini,* J. M. Robbins, and A. J. Taylor, "Fuel Plate Development"

R. G. Donnelly, "Subassembly Fabrication"

S. A. Rabin,* H. Inouye, and M. M. Martin, "Development of Uranium-Molybdenum-Base Cermets"

R. W. Swindeman, "The Mechanical Properties of the UO_2–Type 347 Stainless Steel Cermet Proposed for Core B of the Fermi Reactor"

W. C. Thurber, "Irradiation Testing of Core B Fuel Specimens"

W. C. Thurber* and R. W. McClung, "Nondestructive Testing of Core B Fuel Plates and Subassemblies"

Symposium on Quantitative Metallography, University of Florida, Gainesville, Fla., Feb. 1–3, 1961

M. L. Picklesimer, "Theory and Practice of the Selection of the Plane of Examination"

ASME High-Temperature Materials Course, Cincinnati, Ohio, Feb. 7, 1961

E. E. Hoffman, "Liquid Metal Cooled Reactors"

ASM Technical Meeting, Wilmington, Del., Feb. 8, 1961

E. E. Hoffman, "Liquid Metals as High-Temperature Nuclear Reactor Coolants"

University of Virginia Crystal Conference, Charlottesville, Va., Feb. 9, 1961

B. S. Borie, "X-Ray Diffraction Studies on Cu_2O Films Grown on Copper"

J. V. Cathcart, "Optical Anisotropy of Thin Oxide Films on Copper"

R. E. Pawel,* J. V. Cathcart, and J. J. Campbell, "Oxide Formation in Tantalum Single Crystals"

ASM Educational Series, Long Island Chapter, Long Island, N.Y., Feb. 14, 1961

J. V. Cathcart, "Gaseous Oxidation of Metals"

1961 Annual Meeting of the Metallurgy Society of the AIME, St. Louis, Mo., Feb. 19–23

J. O. Betterton, Jr.,* and D. S. Easton, "Lattice Constants of Alpha-Zirconium Alloys with Additions of Ag, Cd, In, Sn, and Sb"

AEC-AECL Conference on Zirconium-Base Alloys, Savannah River Laboratory, Aiken, S.C., Mar. 1–2, 1961

M. L. Picklesimer, "Activities in the Zirconium Metallurgy Group, Metallurgy Division of the Oak Ridge National Laboratory"

Technical Meeting, Metropolitan Section of the SNT, New York City, Mar. 8, 1961

R. W. McClung, "Ultrasonic Testing"

Third Symposium on Temperature, Its Measurement and Control in Science and Industry, Columbus, Ohio, Mar. 27–31, 1961

D. L. McElroy* and J. F. Potts, Jr., "Thermal emf Stability of Nickel-Base Alloys in the Temperature Range 150 to 1000°C"

D. L. McElroy* and J. F. Potts, Jr., "The Effects of Cold Working, Heat Treatment, and Oxidation on the Thermal emf of Nickel-Base Thermoelements"

ASM Educational Lectures on Refractory Metals, Philadelphia Chapter of ASM, Philadelphia, Pa., Mar. 28, 1961

M. L. Picklesimer, "Metallurgy of Zirconium Alloys"

ASM Educational Series, Oak Ridge Chapter, Oak Ridge, Tenn., Apr. 5, 1961

W. O. Harms, "Oxide Ceramics"

April 1961 National Aeronautic Meeting of the Society of Automotive Engineers, New York, Apr. 4–7, 1961

G. M. Slaughter, "Welding and Brazing of Refractory Metals"

Fifth National Meeting, Institute of Environmental Sciences, Washington, D.C., Apr. 5–7, 1961

H. E. McCoy,* W. R. Martin, and J. R. Weir, "Effect of Environment on the Mechanical Properties of Metals"

Annual Spring Meeting of the American Welding Society, New York, Apr. 17–21, 1961

R. G. Donnelly* and G. M. Slaughter, "The Brazing of Graphite"

Symposium on Ceramics in Nuclear Energy at the Annual Meeting of the American Ceramic Society, Toronto, Canada, Apr. 23–27, 1961

L. A. Harris* and A. J. Taylor, "A Pressure Induced Phase Transformation in a UO_3 Monohydrate"

A. J. Taylor, R. A. McNees,* and A. J. Caputo, "Precision Sintering of Uranium Dioxide"

A. T. Chapman* *et al.*, "Silicon Monoxide: Its Stability Between 1555°K and 1875°K and Behavior During Condensation"

American Physical Society Meeting, Washington, D.C., Apr. 24–27, 1961

G. D. Kneip* *et al.*, "Hysteresis Effects in the Nb_3Sn Superconducting Transition"

Southern Metals Conference of the American Society for Metals, Atlanta, Ga., Apr. 24–26, 1961

Warren H. Bridges, "Electron Metallography at the Oak Ridge National Laboratory"

J. V. Cathcart, "The Role of Strain in the Oxidation Process for Metals"

J. H. DeVan, "Corrosion Properties of High-Temperature Fused-Salt Mixtures"

ASME Conference on Tailoring Materials to Engineering Design, Philadelphia, Pa., Apr. 24–26, 1961

D. A. Douglas, Jr., "Current Styles in Tailoring Materials for Nuclear Technology"

Fifth Meeting of Sodium Reactor Fuel Element Design Group, Atomic Power Development Associates, Inc., Detroit, Mich., Apr. 25–26, 1961

W. C. Thurber, "Development of Fuel Elements for Core B of the Enrico Fermi Fast Breeder Reactor"

W. C. Thurber, "Development of a Fertile-Matrix Dispersion Fuel for the Fermi Reactor"

W. C. Thurber, "Irradiation Testing of Fermi Core B Miniature Fuel Specimens"

AIME/IMD High-Temperature Materials Conference, Cleveland, Ohio, Apr. 26–27, 1961

E. A. Franco-Ferreira* and G. M. Slaughter, "Welding of Columbium and Its Alloys"
D. O. Hobson, "Aging Phenomena in Columbium-Base Alloys"

Space-Nuclear Conference of the American Rocket Society, Gatlinburg, Tenn., May 3–5, 1961

E. E. Hoffman, "Corrosion of Materials by Liquid Metals at Elevated Temperatures"
J. L. Scott, "High-Temperature Fuel Element Development"
G. M. Slaughter* and P. Patriarca, "Fabrication of High-Temperature Heat Exchangers and Radiators"

Tenth Annual AEC Corrosion Symposium, San Diego, Calif., May 9–11, 1961

E. E. Hoffman, "Stainless Steel-Lithium Corrosion Studies at Elevated Temperatures"
W. R. Martin,* H. E. McCoy, Jr., and J. R. Weir, Jr., "Effect of CO_2 Environment on the Mechanical Properties of Stainless Steels"
H. E. McCoy, Jr., W. R. Martin,* and J. R. Weir, Jr., "Effect of Hydrogen on the Mechanical Properties of High-Temperature Alloys"
R. C. Schulze, "Corrosion of Nickel-Base Alloys in Contact with Molten Fluoride Salts"
W. J. Werner* and H. Inouye, "The Reactions of Beryllium with Wet Carbon Dioxide"

Society for Nondestructive Testing Conference, Montreal, Canada, May 17–19, 1961

R. W. McClung, "Development of Nondestructive Tests for the EGCR Fuel Element"

Fifteenth AEC Metallography Group Meeting, Savannah River Laboratory, Aiken, S.C., May 17–18, 1961

R. S. Crouse, "Preliminary Evaluation of a New Type of Polishing Cloth"
C. K. H. DuBose* and R. J. Gray, "Metallography of Pyrolytic-Carbon-Coated Uranium Carbide Spheres"
R. J. Gray* and C. K. H. DuBose, "A Micrographic Study of the Effect of Moisture in the Air on Arc-Cast UC and UC_2 at Room Temperature over Extended Periods"
E. L. Long, Jr., J. T. Meador, and R. J. Gray,* "Status of Vibratory Polishing at Oak Ridge National Laboratory"
A. E. Richt* *et al.*, "A Remote Metallographic Specimen Grinder"
A. E. Richt,* E. J. Manthos, and E. D. Sims, "Metallography of Irradiated Dispersion Type Fuel Elements"

Twelfth High-Temperature Fuels Committee, Battelle Memorial Institute, Columbus, Ohio, May 23–25, 1961

J. E. Cunningham, "Various Fuel Studies at Oak Ridge National Laboratory"
J. L. Scott, "High-Temperature Fuel Development at the Oak Ridge National Laboratory"

PUBLICATIONS

Adamson, G. M., R. S. Crouse, and W. D. Manly, *Interim Report on Corrosion by Zirconium-Base Fluorides*, ORNL-2338 (Jan. 3, 1961).

Beaver, R. J., and T. E. Cole, "Puerto Rico Nuclear Reactor Uses New Type Fuel Elements," *Research Reactor J.* 1(2), 8–12 (1961). Published quarterly by AMF Atomics, a division of American Machine and Foundry Co., Greenwich, Conn.

Betterton, J. O., Jr., and D. S. Easton, "Electrical Resistivities of Zirconium with Dilute Additions of Ag, Co, In, Sn, and Sb," pp 270–73 in *Proceedings of the VII International Conference on Low Temperature Physics*, ed. by G. M. Graham and A. C. Hollis Hallett, University of Toronto Press, 1961.

Betterton, J. O., Jr., R. W. Boom, G. D. Kneip, R. E. Worsham, and C. E. Roos, "Superconductivity of Nb_3Sn in a Pulsed Magnetic Field," *Phys. Rev. Letters* **6**(10), 532–34 (May 15, 1961).

Borie, Bernard, "The Separation of Short Range Order and Size Effect Diffuse Scattering," *Acta Cryst.* **14**(5), 472–74 (May 1961).

Cardwell, Roy G., "Principles of Fuel Element Fabrication," chap. 7, pp 179–215 in *Management of Nuclear Materials*, ed. by R. F. Lumb, Van Nostrand, Princeton, N.J., 1960.

Cathcart, J. V., R. Bakish, and D. R. Norton, "Oxidation Properties of Tantalum Between 400 and 530°C," *J. Electrochem. Soc.* **107**(8), 668–70 (1960).

Cathcart, J. V., and F. W. Young, Jr., "Influence of Reactor Radiation on the Oxidation of Niobium," *Corrosion* **17**, 77–79 (February 1961).

Cathcart, J. V., "Oxidation of Metals and the Effect of Radiation," *Proceedings of the US/UK Meeting on the Compatibility Problems of Gas-Cooled Reactors, Held at Oak Ridge National Laboratory, February 24–26, 1960*, TID-7597, book 2, pp 612–32 (Mar. 3, 1961).

Cherubini, J. H., R. J. Beaver, and C. F. Leitten, Jr., *Fabrication Development of UO_2-Stainless Steel Composite Fuel Plates for Core B of the Enrico Fermi Fast Breeder Reactor*, ORNL-3077 (Apr. 4, 1961).

DeVan, J. H., *et al.*, *Self-Diffusion of Chromium in Nickel-Base Alloys*, ORNL-2982 (Jan. 20, 1961).

DeVan, J. H., *et al.*, "Radiotracer Techniques in the Study of Corrosion by Molten Fluorides" (Abstract), *Intern. J. Appl. Radiation and Isotopes* **9**(1–4), 170 (1960).

DeVan, J. H., "Reactions of Reactor Materials with Contaminants Outgassed from Graphite," *Proceedings of the US/UK Meeting on the Compatibility Problems of Gas-Cooled Reactors, Held at Oak Ridge National Laboratory, February 24–26, 1960*, TID-7597, book 2, pp 698–732 (Mar. 3, 1961).

Douglas, D. A., Jr., "Materials Research on Cladding for a Gas-Cooled Fuel Element," pp 157–78 in *Fuel Element Fabrication Symposium*, Academic Press, London, 1961.

Dragoumis, P., J. R. Weir, and G. W. Leddicotte, *Fast-Flux Measurements in the ORR Core*, ORNL-3028 (Jan. 16, 1961).

Harms, W. O., "Research on Beryllium Oxide and Fueled Beryllium Oxide at the Oak Ridge National Laboratory," *Proceedings of the Beryllium Oxide Meeting, Held at Oak Ridge National Laboratory, Oak Ridge, Tennessee, December 1–2, 1960*, TID-7602, part 1, pp 29–38 (1961).

Harris, L. A., *et al.*, "The Compounds $NaF \cdot BeF_2 \cdot 3ThF_4$ and $NaF \cdot BeF_2 \cdot 3UF_4$," *J. Am. Ceram. Soc.* **43**(11), 608 (1960).

Hikido, T., "Uranium Carbide Research at the Oak Ridge National Laboratory," *Proceedings of the Uranium Carbide Meeting, Held at Oak Ridge National Laboratory, Oak Ridge, Tennessee, December 1–2, 1960*, TID-7603, pp 107–13 (1961).

Hobson, D. O., *A Preliminary Study of the Aging Behavior of Wrought Columbium–1% Zirconium Alloys*, ORNL-2995 (Jan. 6, 1961).

Hoffman, E. E., *Corrosion of Materials by Lithium at Elevated Temperatures*, ORNL-2924 (Oct. 3, 1960).

Hoffman, E. E., "Solubility of Nitrogen and Oxygen in Lithium and Methods of Lithium Purification," pp 195–206 in *Symposium on Newer Metals*, Spec. Tech. Publ. No. 272, American Society for Testing Materials, Philadelphia, Pa., 1960.

Kennedy, C. R., W. O. Harms, and D. A. Douglas, "Multiaxial Creep Studies on Inconel at 1500°F," *J. Basic Eng.*, series D, No. 4, 599 (1959).

Kennedy, C. R., and D. A. Douglas, "Relaxation Characteristics of Inconel at Elevated Temperatures," *Am. Soc. Testing Materials, Proc.* 60 (1960).

Kneip, G. D., and J. O. Betterton, Jr., "The Specific Heats of Some Zirconium Alloys," pp 357–58 in *Proceedings of the VII International Conference on Low Temperature Physics*, ed. by G. M. Graham and A. C. Hollis Hallet, University of Toronto Press, 1961.

Leitten, C. F., Jr., *The Stability of Europium Oxide in Silicon-Bearing Stainless Steel*, ORNL-2946 (Aug. 9, 1960).

Leonard, W. J., *et al.*, "Titanium and Titanium Alloys," chap. 73 in *Welding Handbook*, 4th ed., ed. by A. L. Phillips, American Welding Society, New York, 1960.

Litman, A. P., and A. E. Goldman, *Corrosion Associated with Fluorination in the Oak Ridge National Laboratory Fluoride Volatility Process*, ORNL-2832 (June 5, 1961).

Long, E. L., Jr., J. T. Meador, and R. J. Gray, "Experience with Vibratory Polishers and Design for Hot Cell Application," pp 79–89 in *Symposium on the Preparation of Metallographic Specimens*, Spec. Tech. Publ. No. 285, American Society for Testing Materials, Philadelphia, Pa., 1960.

Martin, W. R., and J. R. Weir, *A Device to Simulate the Service Thermal Conditions in EGCR-Type Fuel Elements*, ORNL-3032 (Dec. 28, 1960).

McClung, R. W., "Ultrasonic Techniques," *Symposium on Nondestructive Testing Trends in the AEC Reactor Program*, TID-7600, pp 20–54 (March 1961).

McClung, R. W., and R. A. Nance, *Development of Nondestructive Tests for the EGCR Fuel Element*, ORNL-3059 (Feb. 16, 1961).

McCoy, H. E., "Reaction of Uranium in Bromine Trifluoride Solutions," pp 14–15; "Graphite and Control-System Poisons," p 17; "Pyrophoricity of Uranium and Zirconium," pp 17–18, *Nuclear Safety* 2(2) (December 1960).

McCoy, H. E., and J. R. Weir, "Effect of Environment on the Mechanical Properties of Metals," pp 115–48 in *Proceedings of the Symposium on the Environmental Factors Influencing Optimum Operation of Ordnance Materiel, September 27–30, 1960*, Southwest Research Institute, San Antonio, Texas, 1961.

McCoy, H. E., W. R. Martin, and J. R. Weir, "Effect of Environment on the Mechanical Properties of Metals," pp 163–76 in *1961 Proceedings of the Institute of Environmental Sciences National Meeting, April 5–7, 1961, Washington, D.C.*, Institute of Environmental Sciences, Mt. Prospect, Illinois, 1961.

McHargue, C. J., and H. L. Yakel, Jr., "Phase Transformation in Cerium," *Acta Met.* 8(9), 637–46 (1960).

McHargue, C. J., *et al.*, "An X-Ray Study of Deformation Stacking Faults at Low Temperatures in Lead, Some Lead Alloys, and Aluminum," *Phil. Mag.* 6, 491 (1961).

McHargue, C. J., *et al.*, "Neutron Diffraction Investigations of Metallic Cerium at Low Temperatures," *Phys. Rev.* 122, 1409 (1961).

McHargue, C. J., and C. G. Dunn, "On a Complex Recrystallization Texture in 3% Silicon Iron," *J. Appl. Phys.* 31(10), 1767–70 (1960).

McHargue, Carl. J., "Twinning of Vanadium," *Acta Met.* 8(12), 900 (1960).

Patriarca, P., *et al.*, "Nickel and High-Nickel Alloys," chap. 67 in *Welding Handbook*, 4th ed., ed. by A. L. Phillips, American Welding Society, New York, 1960.

Pawel, R. E., J. V. Cathcart, and J. J. Campbell, "Microtopography of Oxide Films Formed on Tantalum," *J. Electrochem. Soc.* **107**(12), 956–60 (1960).

Rittenhouse, P. L., and M. L. Picklesimer, *Metallurgy of Zircaloy-2 Part I. The Effects of Fabrication Variables on the Anisotropy of Mechanical Properties*, ORNL-2944 (Oct. 13, 1960).

Rittenhouse, P. L., and M. L. Picklesimer, *Metallurgy of Zircaloy-2 Part II. The Effects of Fabrication Variables on the Preferred Orientation and Anisotropy of Strain Behavior*, ORNL-2948 (Jan. 11, 1961).

Schulze, R. C., R. B. Evans III, J. L. Crowley, and W. H. Cook, *INOR-8–Graphite–Fused Salt Compatibility Test*, ORNL-3124 (June 1, 1961).

Scott, J. L., *et al.*, *Fission-Product Release from* UO_2, ORNL-2935 (Sept. 13, 1960).

Slaughter, G. M., "Welding and Brazing of Refractory Metals," *SAE Trans.* **69**, 52–5 (1961).

Smith, G. P., and C. R. Boston, "$n \rightarrow \pi^*$ Electron Transition in Pure Alkali Nitrate Melts," *J. Chem. Phys.* **34**(4), 1396–1406 (1961).

Swindeman, R. W., and D. A. Douglas, *Mechanical Properties of INOR-8*, ORNL-2780 (Jan. 10, 1961).

Wick, E. A., *Assembly of Fifty Prototype Fuel Elements for the Experimental Gas-Cooled Reactor*, ORNL-2936 (Dec. 12, 1960).

Williams, R. O., "A Deformation Calorimeter," *Rev. Sci. Instr.* **31**(12), 1336–41 (1960).

Williams, R. O., "Effect of Strain Rate and Temperature on the Compression Texture of Aluminum," *Trans. Met. Soc. AIME* **218**, 1133 (December 1960).

Wodtke, C. H., "Constricted-Arc Process Cuts Metal Under Water," *Metal Progr.* **78**(6), 91–3 (1960).

Wodtke, C. H., "Cooling Off a Hot Plate," pp 12–13 in *Metalworking Bulletin* vol 12, No. 2, Linde Company, Long Island, N.Y., 1961.

Yakel, H. L., E. W. Hughes, and H. C. Freeman, "The Crystal Structure of Biuret Hydrate," *Acta Cryst.* **14**, 345 (1961).

ORNL-3160
UC-25 – Metals, Ceramics, and Materials
TID-4500 (16th ed.)

INTERNAL DISTRIBUTION

1. Biology Library
2-4. Central Research Library
5. Reactor Division Library
6. ORNL-Y-12 Technical Library, Document Reference Section
7-26. Laboratory Records Department
27. Laboratory Records, ORNL-RC
28. G. M. Adamson, Jr.
29. R. J. Beaver
30. J. O. Betterton, Jr.
31. D. S. Billington
32. A. L. Boch
33. E. G. Bohlmann
34. B. S. Borie
35. R. B. Briggs
36. J. V. Cathcart
37. C. E. Center
38. R. A. Charpie
39. G. W. Clark
40. R. E. Clausing
41. J. H. Coobs
42. J. A. Cox
43. F. L. Culler
44. J. E. Cunningham
45. J. H. DeVan
46. D. A. Douglas
47. J. H. Erwin
48. J. H. Frye, Jr.
49. J. H. Gillette
50. R. J. Gray
51. W. R. Grimes
52. J. P. Hammond
53. W. O. Harms
54. C. S. Harrill
55-59. M. R. Hill
60. N. E. Hinkle
61. E. E. Hoffman
62. A. Hollaender
63. A. S. Householder
64. A. P. Huber (K-25)
65. H. Inouye
66. R. G. Jordan (Y-12)
67. W. H. Jordan
68. M. T. Kelley
69. R. B. Korsmeyer
70. J. A. Lane
71. R. S. Livingston
72. T. S. Lundy
73. H. G. MacPherson
74. W. D. Manly
75. R. W. McClung
76. D. L. McElroy
77. C. J. McHargue
78. A. J. Miller
79. E. C. Miller
80. C. S. Morgan
81. K. Z. Morgan
82. J. P. Murray (K-25)
83. M. L. Nelson
84. A. R. Olsen
85. P. Patriarca
86. D. Phillips
87. M. L. Picklesimer
88. H. W. Savage
89. A. W. Savolainen
90. J. L. Scott
91. H. E. Seagren
92. M. J. Skinner
93. G. M. Slaughter
94. C. O. Smith
95. G. P. Smith, Jr.
96. J. A. Swartout
97. A. Taboada
98. E. H. Taylor
99. W. C. Thurber
100. M. S. Wechsler
101. A. M. Weinberg
102. J. R. Weir
103. R. O. Williams
104. J. C. Wilson
105. C. E. Winters
106. H. L. Yakel, Jr.
107. A. A. Burr (consultant)
108. C. S. Smith (consultant)
109. R. Smoluchowski (consultant)

110. D. E. Baker, GE, Hanford
111-112. D. F. Cope, Reactor Division, ORO
113. Ersel Evans, GE, Hanford
114. J. L. Gregg, Cornell University
115-118. J. Pheline, Saclay
119. J. Simmons, DRD, AEC, Washington, D.C.
120. L. M. Slifkin, Department of Physics, University of N. Carolina
121. E. E. Stansbury, University of Tennessee
122. D. K. Stevens, Metallurgy and Materials Branch Division of Research, AEC, Washington, D.C.
123. Watt Webb, Union Carbide Metals
124. Division of Research and Development, AEC, ORO
125-701. Given distribution as shown in TID-4500 (16th ed.) under Metals, Ceramics, and Materials category (75 copies – OTS)

Reports previously issued in this series are as follows:

ORNL-28	Period Ending March 1, 1948
ORNL-69	Period Ending May 31, 1948
ORNL-407	Period Ending July 31, 1949
ORNL-511	Period Ending October 31, 1949
ORNL-583	Period Ending January 31, 1950
ORNL-754	Period Ending April 30, 1950
ORNL-827	Period Ending July 31, 1950
ORNL-910	Period Ending October 31, 1950
ORNL-987	Period Ending January 31, 1951
ORNL-1033	Period Ending April 30, 1951
ORNL-1108	Period Ending July 31, 1951
ORNL-1161	Period Ending October 31, 1951
ORNL-1267	Period Ending January 31, 1952
ORNL-1302	Period Ending April 30, 1952
ORNL-1366	Period Ending July 31, 1952
ORNL-1437	Period Ending October 31, 1952
ORNL-1503	Period Ending January 31, 1953
ORNL-1551	Period Ending April 10, 1953
ORNL-1625	Period Ending October 10, 1953
ORNL-1727	Period Ending April 10, 1954
ORNL-1875	Period Ending October 10, 1954
ORNL-1911	Period Ending April 10, 1955
ORNL-1988	Period Ending October 10, 1955
ORNL-2080	Period Ending April 10, 1956
ORNL-2217	Period Ending October 10, 1956
ORNL-2422	Period Ending October 10, 1957
ORNL-2632	Period Ending October 10, 1958
ORNL-2839	Period Ending September 1, 1959
ORNL-2988	Period Ending July 1, 1960